Department of Chemical Engineering

# Experimental Kinetics Studies and Wavelet-based Modelling of A Reactive Crystallisation System

Johan Utomo

This thesis is presented for the Degree of
Doctor of Philosophy
of
Curtin University of Technology

February 2009

# *Declaration*

To the best of my knowledge and belief this thesis contains no material previously published by any other person except where due acknowledgement has been made.

This thesis contains no material which has been accepted for the award of any other degree or diploma in any university.

Signature : ……………

Date : ……………

# *Abstract*

This thesis has made two significant contributions to the field of reactive crystallisation. First, new data from batch cooling crystallisation and semi-batch reactive crystallisation experiments of mono-ammonium phosphate (MAP) were obtained to describe the key factors that influence crystal nucleation and growth rates, crystal size distribution (CSD), and crystal shape. The second contribution is the development of a numerical scheme for solving the population balance equations, which can be used to describe the evolution of CSD during the crystallisation process. This scheme combines the finite difference method with a wavelet method, and is the first reported application of this approach for crystallisation modelling and simulation.

Experiments into the batch cooling crystallisation of MAP were conducted both with and without seed crystals. The effects of key factors such as cooling rate, initial level of supersaturation and seeding technique, including seed concentration and seed size, on the real time supersaturation, final CSD, crystal yield and crystal shape were investigated. It was found that a seed concentration of 20-30% effectively suppressed nucleation. The growth and nucleation rate were estimated by using an isothermal seeded batch approach and their parameters were calculated by non-linear optimisation techniques.

The second series of experiments involved the semi-batch reactive crystallisation of MAP. Both single-feed and dual-feed systems were investigated. In the single-feed arrangement, an ammonia solution was fed into a charge of phosphoric acid. In the dual-feed system, phosphoric acid and ammonia solution were fed into a charge of saturated MAP solution. The molar ratio of the reactants, initial supersaturation, presence or absence of seed crystals, initial MAP concentration, reactants' flow rate, feeding time and stirring speed were varied, and the effects upon the real time supersaturation, final CSD, crystal yield, crystal shape and solution temperature were measured. X-ray diffraction analysis showed that MAP can be produced in both the single-feed and dual-feed arrangements. For the single feed system, the N/P mole ratio controlled the degree of reaction and the CSD of the product. Di-ammonium phosphate (DAP) was not be observed in the single-feed system due to its high solubility. In the dual-feed system, a seeded solution with slow feed addition, moderate stirring speed and a low initial supersaturation provided the most favourable conditions for generating a desirable supersaturation profile, and thus obtaining a product with good CSD and crystal shape.

A comparative numerical study was undertaken in order to evaluate the existing numerical schemes for solving the population balance equations (PBE) that describe crystallisation. Several analytical solutions to the PBE were used to benchmark the following numerical schemes: Upwind Finite Difference, Biased Upwind Finite Difference, Orthogonal Collocation with Finite Elements, and Wavelet Orthogonal Collocation. The Wavelet Finite Difference (WFD) method has been applied here for the first time for solving PBE problems. The WFD scheme was adapted to solve the batch cooling and the semi-batch reactive crystallisation models, and the solutions were validated against experimental data that we obtained.

In summary, the experimental data provide an improved understanding of MAP reaction and crystallisation mechanisms. The adaptability of the WFD method has been demonstrated validating the two crystallisation systems, and this should help extend the application of wavelet-based solutions beyond crystallisation processes and into more diverse areas of chemical engineering.

# *Acknowledgement*

This thesis would not have been finished without the support, help, and love from many people who have enriched my life and added so much joy to it. First of all, I would like to thank my supervisor, Professor Moses Tadé, who has taught me so much about academic life. Secondly, I would like to thank my co-supervisor, Dr. Nicoleta Balliu, who has motivated and fully supported me throughout the last four years. Their constant support and direction are really helpful, especially in the difficult times of performing research. Dr Budi H. Bisowarno as my colleague and superior at Parahyangan Catholic University (UNPAR), for his continuous support is greatly appreciated. I would also like to thank Dr Tonghua Zhang, who helped me a lot in understanding the mathematical background of the wavelet method and gave me continuous encouragement throughout my studies.

This work was supported by several parties to whom I would like to acknowledge my highest gratitude. I thank my first sponsor, the Australian government through the Australian Development Scholarships (ADS) from 2005-2007. I also thank Curtin University of Technology who supported me with a full scholarship from 2007-2008 with the Curtin International Research Tuition Scholarships (CIRTS). Finally, I would also like to make particular thanks to the Department of Chemical Engineering, Curtin University of Technology, and Parahyangan Catholic University as my home institution who fully supported the last year of my study.

I am also thankful to Professor Keisuke Fukui, Assoc. Professor Kouji Maeda, and Dr. Yusuke Asakuma of the University of Hyogo, who accommodated me for almost seven months in Japan while performing my experimental work. They were very helpful and provided essential resources, and without their help, the experimental parts of my thesis would not have been completed on schedule. I have gained extensive knowledge and experience that goes beyond the scope of this thesis. I also acknowledge the financial support from the University of Hyogo through the HUMAP scholarship from November 2007 – June 2008.

Thanks are also due to my officemates: Kailash Singh, Abid Akhtar, Owen Kruger, Ganesh Veluswamy, Tejas Bhatelia, and Millin Kumar, with whom I have shared treasured moments. I also thanks my best friends, Richard Gunawan and family, Iwan Harsono and family, Agus and family, Justy Siwabessy and family, for the enjoyable moments spent with them during the time in Perth. I greatly appreciate the support from Karen Haynes, Jann Bolton, and all the staff and ex-staff of the Department of Chemical Engineering.

Finally, I wish to thank my family, especially remembering my late Dad, without him, I may not be as I am today. I will never forget his loving care, with whom I spent cherished moments as a child and teenager. Thank you to my Mom, sister and brother for their everlasting love and care. Last but not least, thanks to my wife, Fonny, for her constant love, patience and understanding.

# *Brief Biography*

Johan Utomo graduated in Chemical Engineering (S.T. – Bachelor of Engineering) degree from Parahyangan Catholic University (UNPAR), Indonesia in August 2001. He has almost four years teaching experience in Department of Chemical Engineering – UNPAR. He commenced his PhD studies in February 2005 with support from the Australian government through an Australian Development Scholarships (ADS) and then continued under a Curtin International Research Tuition Scholarships (CIRTS) from 2007-2008. He also secured sponsorship from a Hyogo University Mobility in Asia and Pacific (HUMAP) scholarship to undertake research work at the University of Hyogo, Japan from December 2007 to June 2008. He was also a teaching assistant in Process Heat Transfer, Reaction Engineering, Process Plant Engineering, Process Analysis, and Chemical Engineering Laboratory unit from February 2005 to November 2007. He was nominated for a Guild Excellence in Teaching Award in 2006, and later he was involved in the Workshops for Engineering Tutors as a presenter in 2007 and 2008.

## Publications written in support of this thesis

1. Zhang, T., Y.C. Tian, M.O. Tade, and **J. Utomo** (2007). *Comments on "The Computation of Wavelet Galerkin Approximation on a Bounded Interval"*, I. J. Numerical Methods in Engineering, Volume 72, Issue 2, pp 244-251, John Wiley & Sons, Ltd, DOI 10.1002/nme.2022.
2. Tonghua Zhang, Moses O. Tade, Yu-Chu Tian, Yanduo Zhang, **Johan Utomo** (2008). "*Wavelet approach incorporated with optimization for solving stiff systems"*, Journal of Mathematical Chemistry, 43, pp. 1533-1548, Springer Netherlands, DOI 10.1007/s10910-007-9282-2.
3. **Johan Utomo**, Yusuke Asakuma, Kouji Maeda, Nicoleta Balliu, Keisuke Fukui, Moses O. Tade. "*Semi Batch Reactive Crystallisation of Mono Ammonium Phosphate: An Experimental Study"*. Chemical Engineering Journal, Elsevier (Accepted – 14 April 2009).
4. **Johan Utomo**, Nicoleta Balliu, Moses O. Tade, "*Challenges of Modelling A Population Balance using Wavelet",* International Symposium on Advanced Control of Chemical Processes, ADCHEM 2006, Gramado, Brazil. (Accepted for oral presentation)

5. **Johan Utomo**, Kailash Singh, Nicoleta Balliu, Moses O. Tade, "*Control of Continuous Crystallizer*", CHEMECA 2006, Auckland, NEW ZEALAND. Edited by Young, B.P., Patterson, D.A. and Chen, X.D.; ISBN 0-86869-110-0
6. **Johan Utomo,** Yusuke Asakuma, Kouji Maeda, Nicoleta Balliu, Keisuke Fukui, Moses O. Tade, "*Challenges of Wavelet-Based Population Balance Solutions in Crystallization Modelling*"**,** SCEJ Spring Conference, April 2008, Hamamatsu, JAPAN.
7. **Johan Utomo,** Yusuke Asakuma, Kouji Maeda, Nicoleta Balliu, Keisuke Fukui, Moses O. Tade, "*Semi Batch Reactive Crystallisation of Ammonium Phosphates*", SSPE Conference, June 2008, Tokyo, JAPAN.
8. **Johan Utomo,** Yusuke Asakuma, Kouji Maeda, Nicoleta Balliu, Keisuke Fukui, Moses O. Tade, "*Semi-Batch Reactive Crystallization of Ammonium Phosphates: An Experimental Study*", APCChE 2009 conference, August 2008, Dalian, P.R.CHINA.
9. **Johan Utomo,** Yusuke Asakuma, Kouji Maeda, Nicoleta Balliu, Keisuke Fukui, Moses O. Tade, "*Seeded Batch Crystallisation of Mono Ammonium Phosphate*", SCEJ Autumn Conference, September 2008, Sendai, JAPAN.
10. **Johan Utomo,** Tonghua Zhang, Nicoleta Balliu, Moses O. Tade, "*Numerical Studies of Wavelet-based Method as an Alternative Solution for Population Balance Problems in a Batch Crystalliser*", International Symposium on Advanced Control of Chemical Processes, ADCHEM 2009, TURKEY – (Accepted).

# *Table of Contents*

# *List of Figures*

# *List of Tables*

# 1. Introduction and Research Overview

## 1.1 Background Information

Crystallisation is defined as a process in which crystal products are obtained from a solution by mass and heat transfer operations. Applications for crystal products are often determined by several factors, such as particle size, particle size distribution, morphology, specific surface area, and degree of agglomeration. Crystallisation is one of the oldest separation technologies and plays an essential role in the continuous manufacture of many of our daily basic materials such as sodium chloride, sucrose, urea, potassium chloride, ammonium phosphate, ammonium nitrate, etc. Furthermore, batch crystallisation technology plays an important role for many high-purity products, especially in the pharmaceutical, biotechnology, food and photographic industries. Despite a substantial increase in research activity related to crystallisation processes over recent decades, the process remains one of the most difficult to operate and control. The control of the crystal size distribution (CSD), crystal shape, and crystal purity are all challenging due to the complexity and non-linearity of the process parameters, as well as a general lack of reliable on-line instrumentation for measurement (Rohani et al. 1999; Braatz 2002). Therefore, crystallisation is an opportune area for research. A better understanding of the complexities is essential for increasing process efficiency, improving product quality, and ensuring the stability of the process.

Reactive crystallisation is often called a “precipitation” process because it is a combination of both crystallisation and chemical reaction mechanisms. The driving force for reactive crystallisation is different from traditional crystallisation. In reactive crystallisation, supersaturation is caused not only by changes to the physical properties of a solution, but it is also influenced by a chemical reaction between two soluble components leading to a less soluble product which then crystallises. Reactive crystallisation is more difficult to study than classical crystallisation because the crystal generation depends on various factors, all of which have their own kinetics, such as chemical reaction kinetics, crystallisation kinetics, and mixing mechanisms. The kinetics of a chemical reaction are often very fast, and in some cases very complex so they can only be identified by rigorously defined and performed experiments. The crystallisation kinetics, which include nucleation, growth, agglomeration and breakage, are considered during the precipitation of very small particles. Micro-mixing and macro-mixing should also be considered since they can affect both the reaction and the crystallisation steps. In the modelling of a reactive crystalliser, the above factors and their interactions need to be considered. A few well known and researched examples of reactive crystallisation applications are the precipitation of calcium carbonate ($CaCO_3$), calcium oxalate, barium carbonate ($BaCO_3$), barium sulphates ($BaSO_4$), potassium dihydrogen phosphate (KDP) and calcium phosphates ($CaHPO_4$).

Many crystallisation studies have concentrated on obtaining experimental data in order to determine the crystallisation kinetics. Other researchers have focussed on modelling the process and finding a solution to the population balance problem, others have addressed process control and optimisation. In summary, the general challenge of crystallisation research is how to control the crystal size distribution (CSD) of the product. This is related to the difficulty of predicting and controlling the supersaturation conditions in the system. An advanced crystallisation model is believed to be able to provide an answer; however, the complexity of finding a solution and the required computational effort are significant. Hence, there is a need to find a new computational method which can offer a fast, general applicability, and robust model solution for both academic research and industrial applications.

## *1.2 Research Direction and Overall Objectives*

Mono-ammonium phosphate (MAP) and di-ammonium phosphate (DAP) are the most popular phosphate fertilisers. Statistics show that, in 2004, the United States produced more than 10 million tonnes of DAP and 5.3 million tonnes of MAP, compared to 9.1 million tonnes of ammonia fertiliser and 1.3 million tonnes of potassium chloride (KCl). The trend of US fertilizer production from 1994 to 2004 is shown in Figure 1-1.

In Australia, Southern Cross Fertilizer produced around 1 million tonnes of MAP and DAP annually (Campbell et al. 2006). MAP and DAP have become the leading products of water-soluble phosphate fertilizers in the world market. They have good storage and handling properties in the granular form ,with low moisture content. In addition, DAP is also widely used as a source of nitrogen in both dry and fluid fertilizers. Despite huge production and demand for these products, no studies have been done on the kinetics and crystallisation mechanisms of the MAP/DAP system. The published work on reactive crystallisation of ammonium phosphates has been limited to the effects of impurities. Recently, Campbell et al. (2006) indicated that a mixing and pumping problem in a DAP plant was due to the properties of the particles and the slurry rheology. This behaviour has led to plant shutdowns and has significantly reduced profits. The effects of impurities on the rheology of the slurry were also thoroughly investigated by Campbell et al. The conventional process of producing ammonium phosphates from phosphoric acid was modified by Zhong and co-workers (1999). A high impurity content, which can cause scaling and blocking problems, may be avoided by adopting this modified process. These two studies are the only recent work on ammonium phosphate reactive processes.

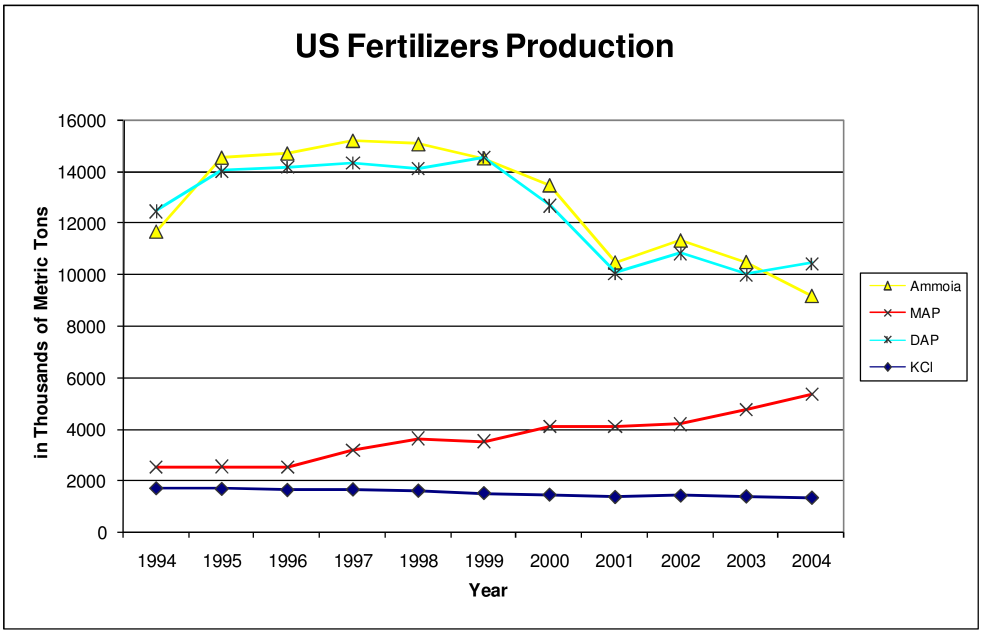

**Figure 1-1. Fertilizer Production Statistic (2006)**

In order to understand the reactive system, it is important to first investigate the non-reactive system of ammonium phosphates. The earliest information on solubility of ammonium phosphates was published by Buchanan and Winner (1920). This provided a solid framework for further studies on manufacturing mono-, di- and tri- ammonium phosphates. The majority of the non-reactive research studies was due to Mullin and co-workers (Mullin et al. 1967; Mullin et al. 1970). The information obtained from these studies does indeed provide valuable guidelines for a specific problem, but may not be useful for wide-ranging industrial applications. Therefore, it is important to conduct studies on suspension crystallisation in non-reactive and reactive systems.

Based on this background review, the two main objectives of this research have been identified. The first objective is to develop a general methodology to analyse and solve various operational challenges in crystallisation processes. This is in order to improve the process efficiency and the quality of the product, and increase revenues. The second objective is to contribute to the research studies published in crystallisation concerning the kinetics and thermodynamic data for the MAP system which are not available in the open literature.

## *1.3 Specific Research Objectives and Contributions*

The main objective of this research is to model and design a crystallisation system by using a wavelet-based model. Two case studies of mono ammonium phosphates (MAP) crystallisation were examined. The experimental data for the two cases were validated, and these results were used to confirm the general application of the wavelet-based model. This model was then analysed in order to solve the common problems that occur in MAP/DAP processes, and hence address the generic challenges in other crystallisation applications. The challenges encountered are usually due to the product requirements and specifications, and operational issues. Therefore, this thesis will make a significant contribution by:

- Development of wavelet-based numerical methods for solving the partial differential equation system.
- Development and set up of an appropriate experimental system to investigate various parameters of mono-ammonium phosphate crystallisation.
- Modelling, analysis and validation of the simulation results by using the experimental data for the crystallisation of mono-ammonium phosphate.

## *1.4 Thesis Overview*

**Chapter 2** presents a general overview of particulate processes, including challenges associated with the reactive crystallisation process. A summary of the published work on reactive crystallisation is presented chronologically, and categorised based on the type of products. In reactive crystallisation, several important aspects are covered such as the reaction engineering, crystallisation kinetics, mixing, and mass transfer, which are different from conditions in the more common crystallisation processes. Challenges in the modelling of the crystallisation process are due to the complexity of the nature of the process which is described by a population balance equation, significant non-linearity of the kinetics, lack of an existing analytical solution, and the unavailability of experimental results which can be tested in the model. In crystallisation operations, the instability of a continuous crystalliser is a major challenge, and optimization of a batch crystalliser is still a focus for many researchers. These problems were also considered in Chapter 2. An industry goal with crystallisation is to achieve a stable and controlled operation in order to produce a high purity and a specified crystal size with an economical yield. Therefore, an appropriate control system should be applied which optimises all areas of the process. To make Chapter 2 more complete, a brief review of crystallisation control is presented to build a comprehensive understanding of the challenges faced with a reactive crystallisation process.

**Chapter 3** introduces the MAP system, and defines the modelling problem. Controlling factors and model assumptions were stated. Property data of the MAP system, including the reactants, were listed from various literature sources. A crystallisation model starts with the population balance equation, combined with the component mass balances, solubility, supersaturation, and the energy balance. A reaction rate needs to be included in the reactive system as well as the crystallisation kinetics. All of these aspects were then incorporated to provide the complete crystallisation model for the MAP system. Two simulation studies were completed in order to demonstrate the applicability of the developed models, and the sensitivity analysis of key variables in the models was performed. The first simulation case was a non-reactive system, and the second was a reactive system.

**Chapter 4** commences with a brief review of wavelet applications in science and engineering fields and particularly in numerical analysis research area. This chapter then outlines the mathematics of wavelet transforms. To make this understanding complete but concise, this continued by introducing the Wavelet Galerkin (WG) method, Wavelet Orthogonal Collocation (WOC) method and finally the Wavelet Finite Difference (WFD) method. This method combines the finite difference technique and the advantages of the properties of wavelets to refine the grid and to adjust the wavelet order in the discretisation step. To date, no one has attempted to adapt this method in the chemical engineering area and or in crystallisation modelling. The Wavelet Finite Difference method was first developed by Jameson (1988) and he later applied it to an ocean modelling study. The significance of our research can be seen when benchmarking between this proposed method, the previous commonly used finite difference methods, and the wavelet collocation method. All three approaches attempted to solve several standardised population balance problems. MATLAB® codes were written for Finite Difference-based methods, Wavelet Collocation (WCO) method, and Wavelet Finite Difference (WFD) methods for our research study. The numerical solutions were then simulated in the MATLAB® software environment. The numerical results from the alternative methods were compared in order to demonstrate insight and discuss the performance of the model and its limitations as the alternative numerical solution method for PBE systems.

**Chapter 5** presents experimental studies from a MAP cooling batch crystalliser. MAP can be produced by generation of supersaturation in a batch cooling crystalliser. The inclusion of seeds crystals was studied, and compared to the non-seeded situation. Finally, the crystallisation kinetics of MAP, which are not available in the literature, were determined by using an isothermal seeded batch crystalliser modelling and a non-linear optimisation technique was utilised to postulate crystallisation kinetics parameters.

**Chapter 6** evaluates the experimental studies and data from reactive crystallisation of MAP in a semi-batch crystalliser. MAP was produced by a reaction between a concentrated phosphoric acid and ammonia solution. The reactions can produce either MAP or the other phosphates. In this chapter, our focus was on MAP only. The reaction kinetics and crystallisation kinetics for our systems have not previously been published in the literature; therefore, this research was undertaken in order to make significant contribution in this area. **Chapters 5** and **6** presents all the details of the experimental work for both systems, including the results obtained. This includes the experimental design, and the experimental methodology used to study the reaction and the crystallisation kinetics of the system. A summary of the analytical methods used was included to provide a better understanding of the validity of the results. These results were discussed and compared in order to present a reflection on the experiments and their limitations. The reaction kinetics and crystallisation kinetics gathered from this work are believed to be novel contributions to the published knowledge in this important area of study.

**Chapter 7** combines and discusses the two main areas of this research study. The first part is the determination of crystallisation and reaction kinetics from experimental data, and the other part is the model validation by using wavelet-based models. The experimental data on the MAP batch cooling crystalliser, and data from MAP reactive crystallisation in a semi-batch system presented in **Chapters 5 and 6**, were used to validate the wavelet-based solution models. The experimental results were used to benchmark the models and lead to necessary refinements, in order to develop generalised reactive and non-reactive crystallisation models for each system.

**Chapter 8** presents the conclusions from this research study, the practical implication from the results, the recommendations, and the proposed future directions for research in this area. Appendices include supplementary information in the MAP experiment works, the related mathematical derivation, and main program codes used in the thesis. The thesis structure is shown in Figure 1-2.

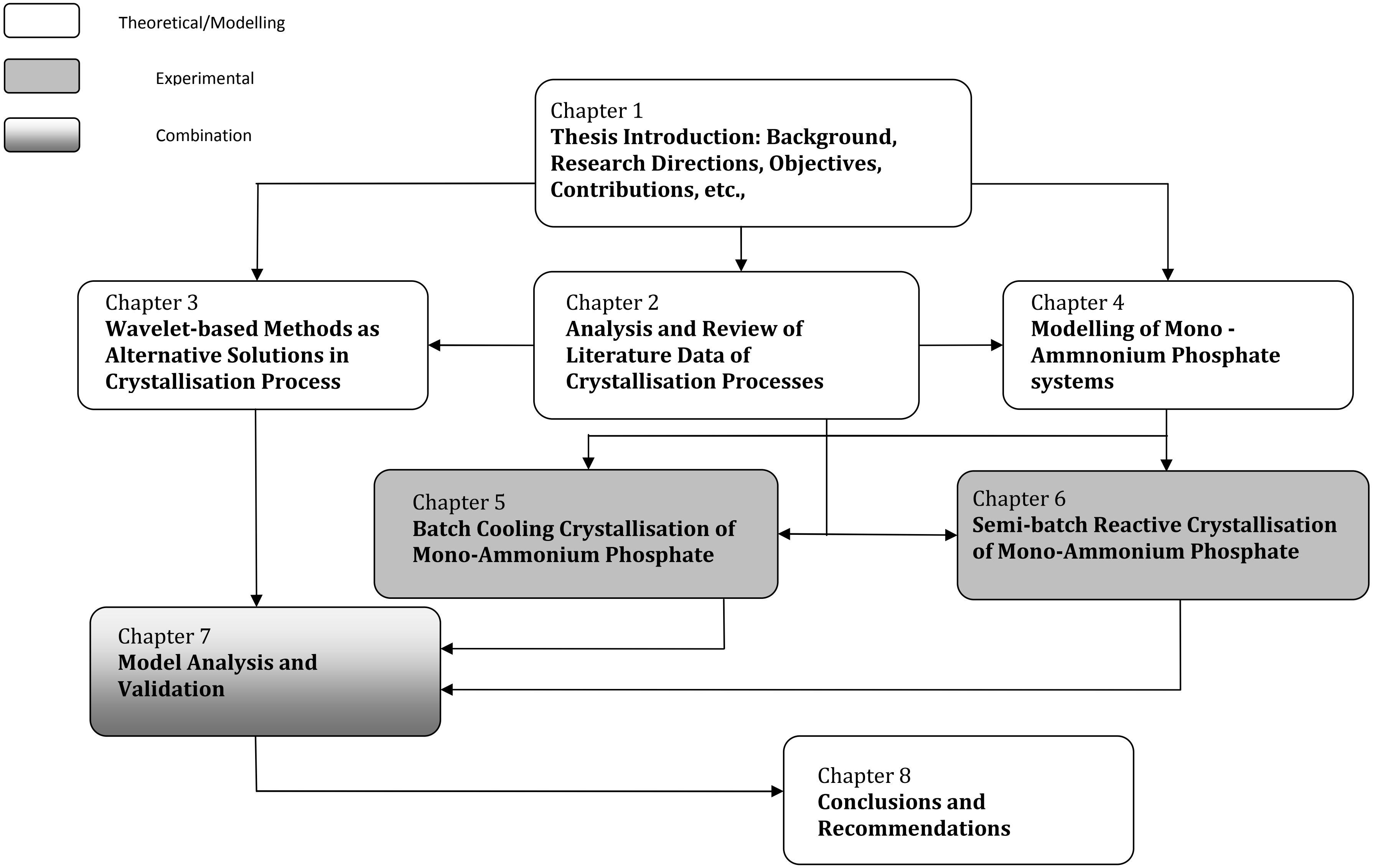

**Figure 1-2. Thesis structure**

## 1.5 References

Anon. (2006). US fertilizers. Chemical & Engineering News. **84:** 68.

Braatz, R. D. (2002). Advanced control of crystallization processes. *Annual Reviews in Control*, 26(1), 87-99.

Buchanan, G. H. and G. B. Winner (1920). The solubility of mono-and diammonium phosphate. *Industrial & Engineering Chemistry*, 12(5), 448-451.

Campbell, G. R., Y. K. Leong, C. C. Berndt and J. L. Liow (2006). Ammonium phosphate slurry rheology and particle properties - --the influence of Fe(iii)fe(iii) and Al(iii)al(iii) impurities, solid concentration and degree of neutralization. *Chemical Engineering Science*, 61(17), 5856-5866.

Mullin, J. W. and A. Amatavivadhana (1967). Growth kinetics of ammonium and potassium dihydrogen phosphate crystals. *Journal of Applied Chemistry*, 17, 151-156.

Mullin, J. W., A. Amatavivadhana and M. Chakkraborty (1970). Crystal habit modification studies with ammonium and potassium dihydrogen phosphate. *Journal of Applied Chemistry*, 20, 153-158.

Rohani, S., M. Haeri and H. C. Wood (1999). Modeling and control of a continuous crystallization process Part 1. Linear and non-linear modeling. *Computers & Chemical Engineering*, 23(3), 263-277.

Zhong, B., J. Li, Y. X. Zhang and B. Liang (1999). Principle and technology of ammonium phosphate production from middle-quality phosphate ore by a slurry concentration process. *Industrial & Engineering Chemistry Research*, 38, 4504-4506.

# 2. Analysis and Review of Literature Data for Crystallisation Processes

## 2.1 Introduction

The consumption of nitrogen, phosphate and potash fertilisers in 2007/2008 worldwide was projected at 92 million, 37 million and 25 million tonnes respectively, as reported by Food and Agriculture Organization (FAO), the United Nations (2003). Crystallisation is an indispensable processing step in manufacturing these basic commodities. Shi et al. (2006) reported that 60% of products in the chemical industry are manufactured as particulate products (solids), and another 20% use powders as ingredients. In addition, many high-added-value products such as pharmaceuticals, dyestuffs, catalysts and proteins also utilise crystallisation in their manufacturing paths. Crystallisation is a core technology in the formation, separation, and purification of many basic and specialty chemicals.

Crystallisation is defined as a multiphase process in which solid crystals as product are obtained from a solution by mass transfer operations. A solution can also be solid (melt), liquid or gaseous. Various types of crystallisation processes were established based on operational characteristics, such as fractional crystallisation, freeze crystallisation, extractive crystallisation, etc. Crystallisation from solution can be performed based on various mechanisms, such as cooling, evaporation, salting out, stream combination, splitting, and by reaction mechanisms. Batch or continuous mode of operation can be applied to crystallisation. Crystallisation from a solution is used, and also discussed extensively in the academic and industrial literature. Crystallisation can be a preferred separation technique over other conventional methods such as distillation, particularly for the case of heat-sensitive and/or high boiling point compounds, and for difficult separations of low relative volatility mixtures. Crystallisation processes offer substantial savings in energy compared with distillation. In the biotechnology industries, crystallisation is also often applied as an intermediary process for the purification or recovery stages. Crystallisation is also often called a precipitation process having similar characteristics to crystallisation and can be used as an alternative process to deal with bio-molecules that are highly sensitivity to temperature, e.g. proteins and enzymes. Precipitation uses a mechanism to form crystals by chemical reaction through adding chemical agents in the solution.

Crystals are defined as solids in which atoms are constructed in an organised pattern that extends in three dimensions (Myerson et al. 1993; Mullin 2001). The crystal characteristic that is usually considered to be the most important factor in practice is particle size. Crystal sizes can range over several orders of magnitude from nanometres to millimetres. The crystal dimension is mainly defined in terms of its length, although it can also be described in relation to the volume of crystal. As well as the crystal dimension, the shape of the crystal can be defined in order to analyse the particulate system. Shape factor can be described according to the characteristic dimension of a particle and its surface area or volume. Two types of crystal size distribution are commonly considered, the density distribution and the cumulative distribution. The density distribution has arbitrary units of number of crystals/(size x volume) while the cumulative distribution has arbitrary units of number of crystals/volume. It is usually more convenient to represent the distribution by the mean and the width of the distribution. Therefore, the mean crystal size enables a distribution to be represented by a single dimension, while its standard deviation indicates its variation from the mean (Myerson et al. 1993).

Crystallisation equipment does not operate in isolation in a plant, and is often part of a particulate processing system. The crystallisation circuit usually consists of several sections such as the feed preparation, feed purification, crystallisation unit, solid-liquid separation, drying, and solids handling sections. The feed preparation stage, for example, can be by extraction and evaporation or by chemical reaction. The solid-liquid separation units used are filtration, sedimentation, centrifugation, etc. Finally, the solids handling units are screening, milling, mixing, granulating, tableting, bagging and packaging. There are significant interactions among unit operations in crystallisation circuit. Various problems occur which are related to the quality of the crystal products such as particle size distribution, crystal composition, shape, and many others. The main problem is the crystal size distribution (CSD), since it affects the downstream processes and the product specifications. For example in a batch crystallizer, the CSD affects the filtration time; for the continuous crystallizer, the CSD influences the required filter area. The CSD may contain excessive fines, too broad, or too narrow size distribution, and the average particle size may be too large or small. Table 2-1 shows comprehensive results for the potential problems in various downstream processing units which can be due to an undesirable crystal size distribution. The downstream processing units are filtration, washing, re-crystallisation, de-liquoring, drying, dissolution, and the mechanical solids handling processes are typically compaction and pneumatic transport. (Wibowo et al. 2001).

The crystal size distribution also affects the product specifications such as dissolution rate, crystal stability, compressibility, transport properties, and aesthetics (colour, smoothness, etc.). For pharmaceuticals, CSD and other crystal characteristics such as crystal shape are important for determining the drug dissolution rate, compressibility (for tableting) and its stability (for shelving time). Skin cream, which is a personal care product, can be felt as a gritty cream if the crystal size is greater than a critical size. Finally, the colour shading given to food is determined by a narrow size distribution which must be in the submicron range (Villadsen 1997).

**Table 2-1. Potential problems in various downstream crystallisation processing units due to CSD issues (Wibowo et al. 2001)**

| **CSD issues** | **Affected downstream processes** | | | | | | | |
|---|---|---|---|---|---|---|---|---|
| | **Filtration** | **Washing** | **Recrystallisation** | **De-liquoring** | **Drying** | **Dissolution** | **Compaction** | **Pneumatic Transport** |
| **Too much fines** | X | | | X | X | | | X |
| **Broad CSD** | X | X | | X | X | X | | X |
| **Narrow CSD** | | | | X | | | X | |
| **Small average size** | X | X | | X | X | | | X |
| **Large average size** | | | X | | | X | | |

A generalized theory for CSD analysis of a particulate system is available. Randolph and Larson (1988) gave a fundamental and comprehensive discussion for diverse particulate systems, including crystallisation. However, the mechanisms on how the crystal can grow and die, agglomerate with others and then break are still poorly understood. General predictions about the agglomeration, breakage and nucleation rates cannot be made due to the complexity of the experimental procedure. Therefore, crystallisation is considered to be a complex process concerning its mechanisms, kinetics, solute-solvent interactions and the internal properties of each component involved. The process combines the mass, energy and population balances, as well as incorporating the kinetics, fluid dynamics and particle mechanics. Because all these effects can occur in multiphase and multi-component systems, this process is very difficult to model and control although it often catches the curiosity of many researchers from diverse backgrounds. There are a number of excellent books and reviews which thoroughly described developments in crystallisation to date and can be found in various sources (Garside 1985; Marchal et al. 1988; Myerson et al. 1993; Tavare 1995; Mullin 2001; Jones 2002; Jones et al. 2005).

## *2.2 Reactive Crystallisation*

Crystallisation occurs in a solution which is thermodynamically unstable and where the driving force for particle formation is the chemical potential in excess of its equilibrium value. This can be achieved through different techniques, e.g. cooling, evaporation or chemical reaction. The main difference between crystallisation and reactive crystallisation is the means of attaining supersaturation which produces solid phase to come out of the solution. In a reactive crystallisation, the driving force depends upon the extent of chemical reaction. However for a non-reactive crystallisation, it is only the change in solubility that drives the crystallisation process. There are two possibilities which can drive the process. First, it is the chemical reaction which leads to a more, or less, soluble product which then crystallises. Second, the chemical reaction does not lead to any intermediate soluble species, and the solid product crystallises directly from reactants. The second case applies to many ionic reactions leading to a sparingly soluble salt.

Reactive crystallisation can be divided into several stages: generation of supersaturation (by chemical reaction), nucleation (primary/secondary), growth, and decay of supersaturation. Crystal agglomeration and aggregation typically accompany the primary nucleation and crystal growth and attrition and breakage, due to mechanical interaction, also occur in the suspension. The literature reports that the reaction crystallisation process is significantly affected by the hydrodynamic conditions within the crystalliser (Abbasi et al. 2007).

### *2.2.1 Solubility and supersaturation*

As stated above, in the reactive crystallisation process, there are two possible explanations for chemical reaction providing crystallisation mechanisms:

1. $A + B \leftrightarrow P \leftrightarrow S$ (solid)
2. $x\,A^{+} + \, y\,B^{-} \leftrightarrow A_xB_y$ (solid)

The first possibility is that chemical reaction leads to a more or less soluble component P, which then crystallises. The reaction can either be at equilibrium, or with finite rates in both directions. The solubility of component P can be described as the molar concentration of P in the solution at solid-liquid thermodynamic equilibrium. The solubility of P (i.e. $c^{*}$*) is a function of temperature. The supersaturation can be defined as the concentration difference between the concentration of P in the solution, $c$, and the solubility of P at certain temperature.

$$\Delta c = c - c^{*} \tag{2-1}$$

The second possibility is that chemical reaction does not lead to any intermediate soluble species, and the solid crystallises directly from the reactants. This is the case of many ionic reactions between a cation and an anion, leading to a sparingly soluble salt. For an ionic solid, the chemical potential can be written as:

$$\mu = x\mu_A + y\mu_B \tag{2-2}$$

where:

$$\mu_A = \mu_{A0} + RT\ln(a_A) \tag{2-3}$$

$$\mu_B = \mu_{B0} + RT\ln(a_B) \tag{2-4}$$

The driving force can then be written as:

$$\Delta\mu = x(\mu_A - \mu_A^{*}) + y(\mu_B - \mu_B^{*}) = RT\ln\left(\frac{a_A^{x}a_B^{y}}{a_A^{*x}a_B^{*y}}\right) = RT\ln\left(\frac{a_A^{x}a_B^{y}}{K_a}\right) \tag{2-5}$$

Supersaturation can be defined as the relative supersaturation by:

$$S_a = \frac{a_A^{x}\,a_B^{y}}{K_a} = \frac{c}{c^{*}} \tag{2-6}$$

### *2.2.2 Crystallisation kinetics (1): nucleation*

In reactive crystallisation processes, the primary nucleation is normally the predominant mode of nucleation. Nucleation is the initial step of stable nuclei generation. In general, there are three modes of nucleation, namely primary homogeneous nucleation, primary heterogeneous, and secondary nucleation. Various expressions are available to describe the primary nucleation step as follows:

$$B_{pri} = k_p \, \Delta c^p \tag{2-7}$$

$$B_{pri} = B^0 \exp(-K/(\ln S_a)^2) \tag{2-8}$$

The simple power law describes the primary nucleation rate as a function of supersaturation Δc as described by equation (2-7), where $k_p$ is the nucleation rate constant and $p$ is the nucleation exponential constant for supersaturation. A theoretical equation is described in (2-8), where $B^0$ is the pre-exponential constant, $K$ is given for a spherical nuclei (David et al. 2001), $S_a$ is the supersaturation ratio ($c/c^*$). Primary homogeneous nucleation is highly nonlinear and the nucleation kinetics are very slow for small values of supersaturation, $S_a$. In reactive crystallisation, $S_a$ can exceed a critical supersaturation value, $S_{crit}$, which is different from the crystallisation process where $S_a$ is always lower than the critical value. This is because rapid reaction generates a highly localised region of supersaturation. Therefore, it is necessary to take into account the mixing effect due to both macro- and micro-mixing levels when modelling the reactive crystalliser, in order to obtain a representative crystal size distribution.

Secondary nucleation takes place during reactive crystallisation, but it only becomes important in the low supersaturation condition, especially in a continuous crystalliser. The proposed mechanisms result from collision between two crystals, or between a crystal and a part of the crystalliser, generally the stirrer or baffles. Kinetics is described by an empirical expression such as:

$$B_{sec} = k_{sec} \, \sigma^n \, m_T^l \, \varepsilon^r \tag{2-9}$$

where $\sigma$ is the relative supersaturation; $m_T$ is the suspension density (kg/m$^3$); and $\varepsilon$ is the local specific power input (W/kg). It is believed that secondary nucleation is not as important as primary nucleation in this case. This empirical relationship for secondary nucleation is sufficient for our model development.

During the initial period when the crystallisation starts at an observable level, generally after primary nucleation and a certain period of growth, this is called an induction time. The induction time depends upon the kinetics and hydrodynamics of the various processes involved: mixing behaviour, the chemical reaction kinetics, the nucleation rate (primary), and the growth rate. The induction time then consists of two parts if we assume the reaction and the mixing are instantaneous, time $t_n$ needed for nucleation and time $t_g$ needed for sufficient growth for the crystals to become visible and have sufficient surface area for further growth. During the induction period, the supersaturation will not decrease and the suspension has not started to form. Figure 2-1 presents a typical supersaturation profile during a batch crystallisation process. It indicates that the supersaturation is constant over the induction time, and then decreasing in the next phase which may consist of crystal growth, secondary nucleation, agglomeration, attrition and breakage.

$$t_{ind} = t_n + t_g \tag{2-10}$$

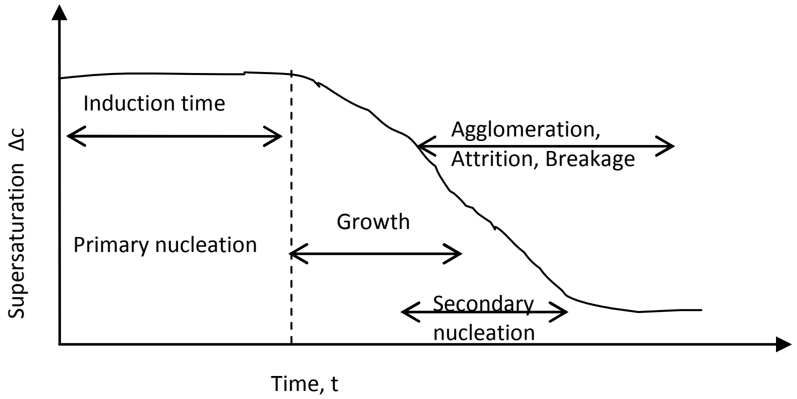

**Figure 2-1. Supersaturation profile during a batch reactive crystallisation with premixed reactants, induction time, and relevant mechanisms**

### 2.2.3 Crystallisation kinetics (2): Ostwald ripening

Ostwald ripening is the process of particle growth, whereby the large crystals grow at the expense of the small ones which then dissolve and disappear completely. Ostwald ripening is important in many reactive crystallisation processes because the solubility is also a function of crystal size and temperature when the crystal size is smaller than 1 µm. The result of Ostwald ripening is that small particles dissolve and large ones grow; this can lead to a narrower CSD of the product. This mechanism reaches thermodynamic equilibrium when a minimum total surface free energy has been achieved. As a consequence, the solubility of the crystal product should be redefined as a function of crystal size by:

$$c^* = c_0^* \exp\left(\frac{\lambda}{L}\right) \tag{2-11}$$

where $c_0^*$ is the solubility of crystal product when $L \to \infty$; λ is the Ostwald diameter; and $L$ is the diameter of the particle. More detailed explanation of this concept can be found in (Matz 1985).

### *2.2.4 Crystallisation kinetics (3): growth*

The growth model for reactive crystallisation is different from ordinary crystallisation processes. To date, numerous growth models have been proposed (Davies et al. 1955; Doremus 1958; Chiang et al. 1988), Chiang et al. proposed a combined growth model based on chemical reaction engineering and crystallisation theory, three growth mechanisms have been introduced and discussed their applicability in reactive crystallisation processes. The first mechanism is based on the surface-reaction and molecular integration; the second mechanism is based on sequential ionic integration; and the third mechanism is based on molecular growth.

**Mechanism I:**

$$A^{+}(sol.) \leftrightarrow A^{+}(ads.)$$

$$B^{-}(sol.) \leftrightarrow B^{-}(ads.)$$

$$A^{+}(ads.) + B^{-}(ads.) \leftrightarrow AB(ads.)$$

$$AB(ads.) \leftrightarrow AB(lattice)$$

**Mechanism II:**

$$A^{+}(sol.) \leftrightarrow A^{+}(ads.) \leftrightarrow A^{+}(lattice)$$

$$B^{-}(sol.) \leftrightarrow B^{-}(ads.) \leftrightarrow B^{-}(lattice)$$

**Mechanism III A:**

$$A^{+}(sol.) + B^{-}(sol.) \leftrightarrow AB(sol.)$$

$$AB(sol.) \leftrightarrow AB(lattice)$$

**Mechanism III B:**

$$A^{+}(sol.) + B^{-}(sol.) \leftrightarrow AB(sol.)$$

$$AB(sol.) \leftrightarrow AB(ads.) \leftrightarrow AB(lattice)$$

For reactive crystallisation processes, the simple power law correlation between growth rate and supersaturation is not sufficient to correlate the inherent phenomena. The above mechanisms could lead to the determination of more complex growth mechanisms, such as the poisoning of growth rate due to impurities, and then to the development of new growth rate equations for more complex cases. The overall linear rate of crystal growth can be described by equations, two of the most common forms are the semi-empirical power law equations:

$$G = k_g \, \Delta c^g \tag{2-12}$$

$$G = k_g (1 - S_a)^g \tag{2-13}$$

where $G$ is the crystal growth (m/s); $k_g$ is the crystal growth constant; $\Delta c$ is the supersaturation; $S_a$ is the relative supersaturation; and $g$ is the exponent constant for growth.

Equations (2-11)and (2-12) are the independent growth rates and follow McCabe's ΔL law (McCabe 1929). The crystal growth can also be size dependent when the growth of a crystal is a function of its size. A growth rate dispersion is another phenomenon that violates McCabe's ΔL law and occurs because of different crystals experiencing different environments in the precipitator, or because of inherent structural differences of the crystals. Two growth-rate dispersion mechanisms have been proposed. First, the random fluctuation growth dispersion for constant conditions where the growth rate of individual crystals vary with time (Randolph et al. 1977). Second, the intrinsic growth dispersion for constant conditions where each crystal grows at a constant rate which is different to the other crystals (Randolph et al. 1988). The growth dispersion model should be included in the model in order to correctly predict the CSD. The growth dispersion model has subsequently been widely applied for a sucrose batch crystalliser and a lactose continuous crystalliser (B. M. Liang 1987; Liang et al. 1991; Mydlarz et al. 1992) .

## 2.2.5 Reaction kinetics

The chemical reaction can normally be described by the following simplified model:

$$aA + bB \rightarrow cC \downarrow + dD,$$

Where A and B are the reactants, and C is the chemical product which is normally precipitated out as solid crystals. The chemical reaction is normally described by the following reaction kinetics:

$$r_A = k\, C_A^m\, C_B^n \tag{2-14}$$

where: $\frac{-r_A}{a} = \frac{-r_B}{b} = \frac{r_C}{c} = \frac{r_D}{d}$

The rate constant, $k$ may be dependent on temperature and can be expressed in the form of the Arrhenius equation:

$$k = k_0\, exp(-E_a/RT) \tag{2-15}$$

Exponents $m$ and $n$ are the partial reaction orders; $k$ is the reaction rate constant; and $E_a$ is the activation energy of the reaction. The values of $m$, $n$, $k$ are obtained by experiment in an ideal, perfectly-mixed batch, semibatch, or continuous reactor at a given temperature. Different values of $k$ are measured at different temperatures and are necessary to obtain the activation energy of the reaction. From these reaction rate equations, the mass balances of the reactants and product can be obtained, coupled with the crystallisation kinetics used to obtain the required data outputs for the solution-side and solid-side of the balance.

### *2.2.6 Agglomeration and breakage*

Crystals of certain substances agglomerate during their crystallisation processes while others do not. The mechanism of agglomeration is not well understood as it is very difficult to distinguish from the actual crystal growth. Agglomeration can be observed with or without the state of supersaturation. During the reactive crystallisation process, agglomeration occurs due to the presence of a high degree of supersaturation. Agglomeration even occurs in the size range between 10 to 1000 μm. Agglomeration can be described as a three-step process:

- Collision of particles due to fluid motion.
- Adhesion by weak forces such as van der Waals forces.
- Solidification of agglomerate through crystal growth creating chemical bonding.

To obtain agglomerates, three successive steps have to occur: (a) the collision of two crystals; (b) a sufficient residence time for contacting the two particles; and (c) the adherence of the two particles caused by supersaturation. The key parameters that appear to control agglomeration in many systems are:

1. The level of supersaturation
2. The hydrodynamic state (mixing intensity, turbulence)
3. The particle size and habit
4. The population density
5. The nature of the solution (suspension density and viscosity)
6. The presence of impurities, ionic strength, and the cohesion forces within the solvent

The rate of agglomeration of two particles of sizes $L_i$ and $L_j$ is given by:

$$r_{ij} = \beta\left(L_i, L_j, \varepsilon\right) N_i \, N_j \tag{2-16}$$

The agglomeration kernel, $\beta$ primarily depends on the mother particle sizes $L_i$ and $L_j$, and the specific power input $\varepsilon$, from mixing process. When two particles collide and agglomerate, a new particle is born of size $L_k$, and it again continuously agglomerates with others that leads to its disappearance (particle size $L_k$). The total mass of the two particles into the new one of size $L_k$ has to be conserved. Factors that need to be considered when defining the agglomeration kernel are:

- The collision frequency of the two particles which are related to hydrodynamics, ion strength and van der Waals forces.
- The probability for two particles to stay together is very high (close to 1) for small particles.
- The “sticking-together” frequency is related to the crystal growth rate and hence to the supersaturation.

### *2.2.7 Fluid dynamics and mixing*

In practical cases of reactive crystallisation processes, the perfectly-mixed or plug-flow type of crystalliser does not apply. This is because all the state variables, such as concentration, temperature, crystal size distribution, also depend on the space coordinates in the entire volume of crystalliser. Therefore, the model describing a reactive crystalliser becomes more complex if we consider multiphase fluid dynamics. In addition, as discussed above, all mechanisms such as, nucleation, ripening, growth, agglomeration and breakage, are sensitive to mixing characteristics. The operating mode is one of the contributing factors which determines the mixing characteristic of the fluid dynamics of the system. There are generally three types of reactor-crystalliser operating mode as shown in Figure 2-2, namely batch, continuous, or semi-batch system. The semi-batch system can be equipped with the single-feed (jet) or with the dual-feed arrangement. Each mode will present a different mixing effect and hence result in completely different performance. Assume the simplified stoichiometry reaction: $A + B \rightarrow S$ (solid). Both reactants A and B (as subscripts) have initial concentrations of $C'_{A0}$ and $C'_{B0}$ respectively. The volume of reactant is given by $V$, and the flow rate of reactant is $Q$.

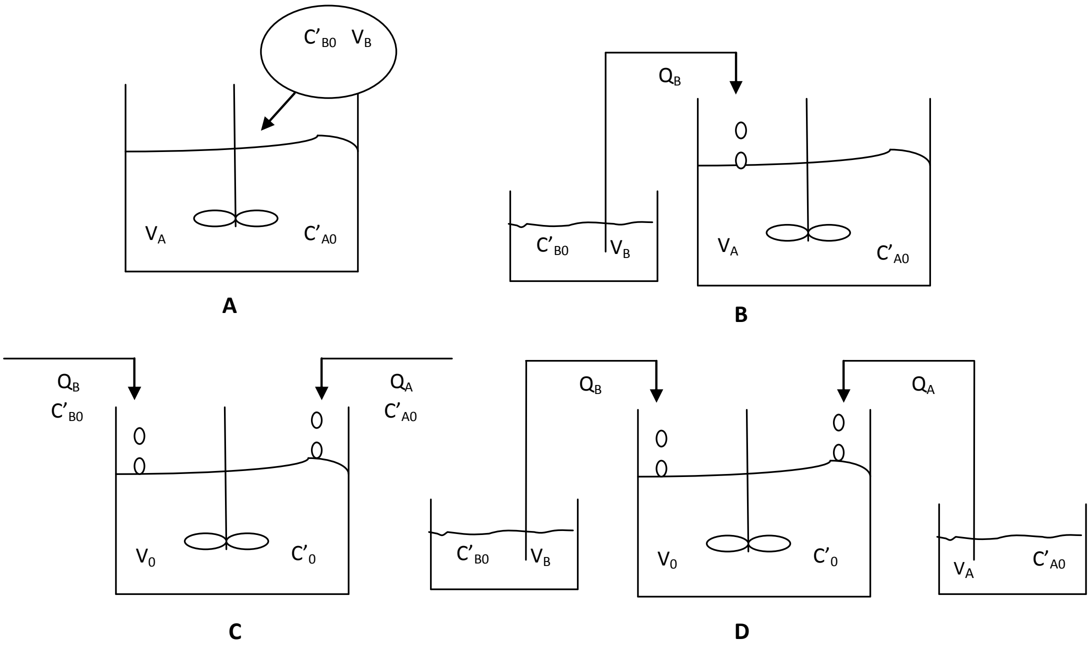

**Figure 2-2. Different types of reactive crystalliser: Batch (A), semi-batch single feed (B), continuous (C), and semi-batch dual feed (D)**

Table 2-2 presents sequential steps in mixing behaviour for an aqueous solution with low viscosity. In reactive crystallisation processes, only the last two steps are controlling the product size distribution and yield.

Macromixing can be defined as the processes determining the uniformity of the local average values of the concentrations of all species present in the vessel. On the other hand, micromixing can be defined as the processes leading to the homogenous condition on the molecular scale between the reactants. From the macromixing point of view in the agitated crystalliser, we can classify three zones, i.e. reactant feed points, in close to the stirrer or circulation pump, and the bulk volume of the vessel itself. Industrial vessels are generally considered to exhibit intermediate conditions between ideally mixed condition and ideal plug-flow type conditions as dead zones or bypasses are present. In order to describe the condition of macromixing, the concept of residence time distribution (RTD) was introduced by Danckwerts (1953). The residence time distribution of the suspension can be studied by examining the RTD of the liquid for the case of small crystals being produced. Consequently, two RTDs need to be determined if big crystals are produced and the assumption for the solids dynamics is not the same as the liquid dynamics. In reactive crystallisation, crystals are usually produced and therefore only a single RTD is needed.

**Table 2-2. Successive Steps of Mixing**

| Process | Size scale | Time scale |
|---|---|---|
| Dispersion by the velocity field (macromixing) | Macro scale | Mixing and circulation times (1-10 s) |
| Size reduction of eddies (mesomixing) | Taylor scale | Taylor time scale (0.1-1 s) |
| Stretching and swirling of eddies (micromixing) | Kolmogorov micro scale | Shear time scale (0.02-0.001 s) |
| Diffusion (micromixing) | Batchelor micro scale | Diffusion time (0.01-0.001 s) |

Primary nucleation is the predominant and the fastest process compared to the other crystallisation mechanisms, therefore we can identify three steps that are competing and controlling at the beginning of reactive crystallisation processes. These are:

- The micromixing, which controls the molecular diffusion.
- The chemical reactions, which produce supersaturation.
- The primary nucleation, which controls the initial crystallisation process.

By also including the micromixing condition, then the supersaturation value is revised and the nucleation efficiency under imperfect mixing conditions can be determined by comparing the real nucleation rate with the theoretical nucleation rate. In the initial period of operation of batch and semi batch crystallisers there are only two important factors to be considered, namely the feed point location and the stirrer speed. As the process continues the primary nucleation is only affected by the feed point location, whereas the stirrer speed influences all the mechanisms. The effects of these significant factors on the physical values such as the number of crystals per unit volume ($N_c$), the average diameter of the crystal ($L$), and the overall reaction rate ($r$) are presented in Table 2-3.

**Table 2-3. Mixing effects on reaction crystallisation**

| | Primary Nucleation | Secondary Nucleation | Growth by Integration | Diffusional Growth | Agglomeration | Overall Effect |
|---|---|---|---|---|---|---|
| Stirring ↑; same feed point | Nc ,L ,r Influenced | Nc ↑,L ↓,r↑ | No influence on Nc ,L ,r | Nc ,L ↑ ,r ↑ | Nc ↓,L ↑,r ↓ | Related to many processes |
| Turbulence zones ↑; same stirring speed | Nc ,L ,r Influenced | No influence on Nc ,L ,r | No influence on Nc ,L ,r | No influence on Nc ,L ,r | No influence on Nc ,L ,r | Primary nucleation only |

Note: $N_C$ = number of crystals per unit volume; L = crystal mean diameter; r = overall crystallisation rate.

By increasing the stirrer speed with the same feed point, then different effects are produced on $N_C$, L, and r. The experimental results obtained for this condition are usually not easy to analyse as it creates opposing effects on the number of particles per unit volume and on the reaction rate. Therefore, to test whether the micro mixing state is achieved, the second set of condition is selected. By changing the feed location with the same stirring speed, allows observation of either the conversion curve or the crystal size distribution. If no variation is observed on the conversion curve or the crystal size distribution, then there is no influence of micro mixing on this state. It should be noted that this conclusion is valid only for the assumptions that primary nucleation is the only process occurring, and it is fast enough to be influenced by micro mixing.

### *2.2.8 Population balance equation*

The concept of the population balance arose as a generalization of the residence time distribution (Rawlings et al. 1992). It was first introduced by Randolph and Larson in 1962 ,and then by Hulburt and Katz in 1964 (Gerstlauer et al. 2002). Hulburt and Katz used crystallisation processes as a case study for the population balance approach. Population balance equation (PBE) can be defined as a mathematical description to characterize particles simultaneously undergoing various mechanisms such as birth, growth, and death within a certain particle phase space. Particle phase space is the coordinate variables of a single particle or group of particles. There are two types of coordinates, internal coordinates refer to the characteristics attached to the particles such as size, temperature, concentration, particle age, shape, purity and several others, whereas external coordinates refer to physical location of the particle itself. A population balance on any system is related to demonstrated changes of the number of entities, which may be solid particles, drops, bubbles, cells or events, whose presence may determine the behaviour of the system under study (Ramkrishna et al. 2002).

The PBE is a hyperbolic partial differential equation, and the form of the PBE is known as an integral-partial differential equation because it has integral forms describing the total size range of particles involved as well as illustrating the dynamic continuous function in time. In addition, there are relationships between the kinetic equations (nucleation, growth), mass transfer, heat and momentum, with population changes for the particular system under study. Therefore, PBE is usually coupled with a set of mass, heat and momentum balances together with the kinetic equations. The general form of a one-dimensional PBE in equation 2-17 is the general form of the original study (Hulburt et al. 1964), and also applied more recently (Randolph et al. 1988; Ramkrishna 2000; Ramkrishna et al. 2002; Hu et al. 2005; Nopens et al. 2005).

$$\frac{\partial n(x,t)}{\partial t}+\frac{\partial[G(x)\,n(x,t)]}{\partial x}=B_{nuc}(x)+B_{agg}(x)-D_{agg}(x)+B_{br}(x)-D_{br}(x) \tag{2-17}$$

where $x$ is the properties of particles such as volume or other spatial coordinate of the particle; t is time; $n(x,t)$ is the number of particles at size $x$ and time $t$; $\dot{G}(x,t)$ is the growth rate of particles; $B_{nuc}$ is the nucleation rate of particle of size $x$ and time $t$. $B_{agg}, D_{agg}$ are the birth and death rates of particles of size $x$ and time $t$ due to the agglomeration process; and $B_{br}, D_{br}$ are the birth and death rates of particles of size $x$ and time $t$ due to the breakage process.

If only agglomeration occurs, then the population balance is such that the $B$ and $D$ terms express the birth and death rates respectively. The population balance is usually modified using the volume, $v$, as the internal coordinate:

$$\frac{\partial n(v,t)}{\partial t}+\frac{\partial[G(v)\,n(v,t)]}{\partial v}=B_{nuc}(v)+B_{agg}(v)-D_{agg}(v)+B_{br}(v)-D_{br}(v) \tag{2-18}$$

$B_{agg}(v)$ and $D_{agg}(v)$ can be written as:

$$B_{agg}(v)=\frac{1}{2}\int_0^v \beta(v-v',\,v')\,n(v-v',t)\,n(v',t)\,dv' \tag{2-19}$$

$$D_{agg}(v)=n(v,t)\int_0^\infty \beta(v,\,v')\,n(v',t)\,dv' \tag{2-20}$$

where $\beta(v,v')$ is the agglomeration kernel. The birth and death rates of particles due to breakage can be written as:

$$B_{br}(v) = \int_{v}^{\infty} \rho(v, v')\, S(v')\, n(v', t) dv' \tag{2-21}$$

$$D_{agg} = S(v)\, n(v, t) \tag{2-22}$$

where $\rho(v, v')$ is the breakage function; and $S(v)$ is the rate of breakage for particles of volume $v$. The population balance is a first-order hyperbolic differential equation for which very few analytical solutions have been obtained, and mainly for some very ideal cases.

### 2.2.9 Summary of the reactive crystallisation process

The challenges in reactive crystallisation processes are due to the complex interactions among the product specifications, the operating conditions, and the nature of the process. For design purpose, the requirements for particular product specifications drive the need to design a suitable crystalliser. However, for improved performance rating, optimization is required to maximise the yield with an increase of product quality. Both purposes can be achieved if the process can be modelled in such a way that takes into account all the controlling factors, and if it can be validated by experimental results. The models are not necessarily very detailed but they should be consistent and able to be verified. The model should be able to quantify the phenomena effectively as required for process design and scale-up purposes, leading to further improvements in product quality and enabling tailoring of product properties to new applications.

The model starts by defining the physical constants such as crystal density, solubility, chemical equilibrium constants, etc., from experimental measurements or from literature data. Batch crystallisation experiments allow determination of the crystallisation kinetics. The semi-batch reactive crystallisation experiments determine the reaction kinetics. The feed point and the stirrer speed are varied in order to test the influence of micromixing. It is known that a complete model is too complex to be tested by a single set of experiments. Once the kinetics and their limitations are established, it is necessary to validate this model by experiments in a semi-batch crystalliser exhibiting perfect mixing behaviour. The population balance, with the related mass and energy balances, can be solved for each ideal zone of the proposed hydrodynamic model. The latest developments in reactive crystallisation equipment are intended to achieve a desirable supersaturation level by controlling the contact between reacting species in a small, well-mixed continuous vessel, and in a highly turbulent or jet mixing crystalliser. Two major issues in reactive crystallisation research are the measurement of kinetic parameters and the simulation of crystalliser performance used to determine the effects of operating conditions on CSD and reaction selectivity. A brief summary of the important early work on reactive crystallisation is provided in Table 2-4, the earliest literature on reactive crystallisation is Nielsen (1964). Today a large amount of information is available in the literature on the experimental and the theoretical aspects of reactive crystallisation, such as; Sohnel and Garside (1992), Myerson (1993), Mersmann (2001), and Mullin (2001), Chen and co-workers (2004), and Tamura and Tsuge (2006).

The next section discusses the research challenges specifically related to obtaining solutions of population balance problems. As outlined above, very few analytical solutions can be obtained if the actual phenomena that occur need to be integrated into the developed model. This situation presents research challenges in order to determine appropriate solutions for industrial problems using a population balance approach.

**Table 2-4. Overview of important published reactive crystallisation research**

| Year | Name | Comment |
|---|---|---|
| **1964** | Nielsen | First book on reactive crystallisation appeared |
| **1984** | Garside and Tavare | Studied the solute transport from bulk solution into crystal lattice |
| **1985** | Matz | Ostwald ripening concept |
| **1988** | Franck et al. | Modelled salicylic precipitation |
| **1990** | Garside | Investigated the effect of feed addition rate and Ostwald ripening |
| **1991** | Wachi and Jones | Analysed a gas-liquid reactive crystallisation system (heterogeneous system) |
| **1994** | Franke and Mersmann | Examined reactive crystallisation from process operation point of view |
| **1999** | Kelkar and Ng | Designed a reactive crystallisation system by incorporating reaction and mass transfer |
| **2001** | Rigopoulos and Jones | Combined models of gas-liquid precipitation and CFD model |

## *2.3 Challenges in Crystallisation Modelling*

In crystallisation modelling as in many chemical engineering fields, in order to study and understand the phenomena, and to design, optimise and control the process typically involves the solutions of systems of partial differential equations (PDEs).

These equations may not allow easy analytical solutions and, therefore, a numerical method may need to be applied. Numerical methods for PDEs are generally classified into two criteria: either discretisation in space and time, or discretisation in space only. The first criteria requires discretising each PDE in space and time resulting in a system of nonlinear equations. The second criteria is also called the method of lines and consists of spatial discretisation, and hence solving the resulting system of ordinary differential equations (ODEs) with an appropriate integrator. When the PDE solution exhibits regular behaviour, essentially any implementation of the "traditional" numerical methods (e.g. finite differences or collocation based) can be successfully applied in the normal resolution. However, singularities and steep profiles often occur in many phenomena, e.g. concentration or temperature fronts in fixed beds, and in particle size distributions for crystallisation processes. In crystallisation processes, the PDE describing the particle size distribution is the population balance equation (PBE).

Substantial research work has been done to develop numerical methods for solving continuous PBE by Hulburt and Katz (1964), Subramanian and Ramkrishna (1971), Middleton and Brock (1976), Singh and Ramakrishna (1977), Gelbard and Seinfeld (1979), Batterham et al. (1981), Sampson and Ramkrishna (1985), Marchal et al. (1988), Hounslow et al. (1988), Hounslow (1990), Kim and Seinfeld (1990), Lister et al. (1995), Kumar and Ramkrishna (1996). All these numerical methods can be grouped into three categories: (a) method of moments; (b) method of weighted residuals; and (c) discretisation methods. The major challenges with these methods are: (i) computation time; (ii) computation capacity (memory needed); (iii) the stability; and (iv) the accuracy of the solutions.

Another numerical method known as the Monte Carlo method is a quite effective method for solving a complex mathematical problem based on probabilistic analogy and solving using a stochastic sampling technique. It was introduced by Spielman and Levenspiel (1965), and subsequently successfully applied by Shah et al (1976), Gupta and Dutta (1991), van Peborgh Gooch and Hounslow (1996), Piotrowski and Piotrowski (2005) to population balance problems.

Kostoglou and Karabelas (1994) compared four previous numerical methods proposed by Batterham et al., Marchal et al., Gelbard et al., as well as Hounslow et al. (1988). In addition, Vanni (2000) gave a comprehensive comparison between the methods of Batterham, Hounslow, Marchal, Litster, Kumar and Ramkriskna, Vanni, and Gelbard. In sections 2.3.1 to 2.3.4, reviews of the major numerical methods are discussed.

### 2.3.1 Method of Moments

The method of moments was first demonstrated for simple systems by Hulbert and Katz (1964) by making moment equations from population balance equations. The method predicts statistical characteristics such as mean, variance, skewness of particle size distribution. However, it is only applicable for estimating the parameters of particulate processes if CSD data is available from experiments. Therefore, this method provides a basic framework for other researchers to apply and solve population balance equations.

### 2.3.2 Weighted residuals

The weighted residual method was introduced by Subramanian and Ramkrishna (1971) and applied to cell populations in a well-stirred culture. This method predicts the mass distribution of cells as statistical formulations. Middleton and Broke (1976) presented a solution to the population balance equations by using cubic spline techniques. The limitations of this method are the computation time and the stability of the method. It takes more time because spline coefficients need to be evaluated at each time step. Singh and Ramkrishna (1977) have applied an orthogonal collocation technique to solve the coagulation population problem. Long computation time and a complex program structure still present problems in this case. Although, the CSD result produced by this method was in continuous form, it was more precise than the discrete experimental data used to determine the kinetics (Kostoglou et al. 1994). Sampson and Ramkrishna (1985) revised the weighted residuals method for solving PBE of Brownian agglomeration for different particle size ranges. Again, the trial functions they used needed to be recalculated when there is a change in system parameters. The solution obtained is unique for a particular case and is then difficult to apply in other applications.

Several researchers proposed finite element methods to solve population balance problems in crystallisation applications (Nicmanis et al. 1998; Mahoney et al. 2002; Rigopoulos et al. 2003), in some studies they combined the Galerkin techniques with the finite element method in order to solve the PBE based on nucleation, growth, aggregation and breakage. Nicmanis and Hounslow only applied the method to a steady-state population balance formulation; however, Rigopoulos and Jones developed the method for solving the dynamic population balance. This method is limited to solving one-dimensional dynamic PBE in a batch or continuous crystalliser. Mahoney and Ramkrishna explored linear basic functions for solving PBE based on nucleation, growth and aggregation and applied the approach to a problem related to particle growth.

### 2.3.3 Discretisation methods

Batterham et al. (1981) proposed a new method for solving PBE problems, referred to as the discretisation method. Although there are some approximations are included in the method such as double calculation for aggregation of particles in the same range, under prediction on total particle number, and failure to yield the correct discrete equations for the total number of any other moments, many authors have stated that this method provides an excellent approach compared to other more recent discretisation methods. This method has become the fundamental approach for development of extended discretisation methods. Hounslow et al. (1988; 1990) developed a discretised PBE model for batch and continuous crystallisation systems which used length as a domain of discretisation, and identified four types of interactions that can change the total population. This method requires less computation time and better predictions for particles in the medium size range. However, this technique is limited to a fixed and coarse geometric grid and the results obtained are not suitable for predictions over long times and/or particles with a large size range (Kostoglou et al. 1994; Vanni 2000).

In comparison with the Kumar and Ramkrishna method (1996; 1997) that used a flexible grid, the fixed pivot technique attempted to improve the solution accuracy by reducing errors associated with discretisation by selecting a proper refinement grid for a certain size range and use of a non-uniform or geometric-type grid. The moving pivot technique (Kumar et al. 1996) subsequently used variations in pivotal size for each interval, adapting to the prevailing non-uniformity of the number density. This method gives more accurate predictions for all particle size ranges, even though it produces slightly over-predicted (for fixed pivot) and under-predicted results (for moving pivot) in a size range that contains steep variations in the number density, when compared to analytical solutions. However, there remains the issue of computational efficiency, which can be further improved in these methods.

### 2.3.4 Monte Carlo method

The Monte Carlo method considers a complex mathematical problem of a particular process or system by substituting a probabilistic analogy, and then obtaining a solution from stochastic sampling experiments. Kostoglou and Karabelas (2002) claim that the Monte Carlo simulation method is the only effective method for simulation of population balance equations, both for one-dimensional or multi-dimensional process models. This method was first applied to chemical engineering applications by Spielman and Levenspiel (1965) for dispersed liquid-liquid systems, followed by Shah et al. (1976) for biological population systems where the simulation of a large number of internal coordinates is desirable. For crystallisation processes, this method has been applied by Gupta and Dutta (1991), van Peborgh Gooch and Hounslow (1996) and recently by Piotrowski and Piotrowski (2005). The computational disadvantage of using this method is the requirement for summation of the number, size, area, volume and mass of all particles within the sample for each time interval (Piotrowski et al. 2005). Moreover, this method is not suitable for model reduction or control systems design.

It can be seen that the major drawbacks from all the available methods described above are: (i) computation time due to the large number of equations; (ii) the stability of the method; (iii) whether these techniques can be included in other process models, or with control systems designs; and (iv) the accuracy of the simulated results obtained from the models. Liu and Cameron (2001, 2003) proposed the wavelet-based method in order to overcome these problems, especially for population balance systems. A review update of research in PBE solution are summarised in Table 2-5.

**Table 2-5. Previous research for the solution to the PBE problem**

| Year | Authors | Method | Result | Limitation |
|---|---|---|---|---|
| 1964 | Hulbert and Katz | Moments | Statistical characteristics, such as mean, variance, skewness of particle size distribution. | Only suitable to estimate parameter of particulate processes if CSD is available from experiment |
| 1971 | Subramanian and Ramkrishna | Weighted Residuals | Solutions were obtained for microbial cell growth in a well-stirred vessel for batch and continuous systems by method of weighted residuals. | Iterative calculation needed to increase solution's accuracy, the results were found to be sufficient. |
| 1976 | Middleton and Broke | Weighted Residuals | Solution to PBE by using cubic splines. | Computationally inefficient because spline coefficients need to be evaluated at each time steep and suffer from numerical stability problem for moving sharp gradients in the distribution. |
| 1977 | Singh and Ramkrishna | Weighted Residuals | Solved coagulation population with orthogonal collocation technique | Time consuming and require specific sub-routines to decompose PBEs.<br>The CSD result is in continuous form and much more precise than the discrete experimental data that is used to determine kinetics. (Kostoglou and Karabelas 1994). |
| 1978 | Gelbard and Seinfeld | Weighted Residuals | Used a finite element method in combination with collocation procedures for coagulation equations. | |
| 1981 | Batterham et al. | Discretisation | Batterham et al. used M-I approach to decrease the number of equations needed to obtain a numerical solution of PBEs for pure agglomeration. | This method conserves mass but under-predicts total particle number.<br>Failed to yield the correct discrete equations for total number or any other moments. |
| 1985 | Sampson and Ramkrishna | Weighted Residuals | Solution to the PBE of Brownian agglomeration in particle size ranges | Need to recalculate the trial functions if there is a change in system parameters.<br>Unique solution for a specific case, but difficult to apply for alternative applications. |
| 1988 | Marchal et al. | The Method of Classes | Applied in crystallisation of adipic acid with no restriction on classes and give well agreement between experimental and model simulation. | Using decomposition technique for transforming the density function on a set of orthogonal functions.<br>The method conserves mass but not number of particles. |

| Year | Authors | Method | Result | Limitation |
|---|---|---|---|---|
| 1988 | Hounslow et al. | Discretisation | Model for batch crystallisation system.<br>Using length domain discretisation.<br>Identified four types of mechanisms that can change the total population in a size range and derived model for each mechanism.<br>Provided a correction factor for previous approach of Batterham et al. (1981) | Limited to a fixed and coarse geometric grid and can result in poor predictions at long times.<br>Inaccuracy with large classes of particle distribution (Kostoglou and Karabelas 1994). |
| 1990 | Hounslow et al. | Discretisation | Model for continuous steady state system.<br>It is analogue with model for batch system in their previous work.<br>Gives excellent agreement with analytical and/or experimental data. | |
| 1990 | Kim and Seinfeld | Moving Sectional | Good results in pure growth of aerosol particles. | Unsuitable for extension to particle agglomeration and nucleation. |
| 1991 | Gupta and Dutta | Monte Carlo | Able to handle multivariate integral or integro-differential problem in multidimensional particle-state space. | The requirement for summation of number, size, area, volume and mass of all particles within the sample for each time interval.<br>Not suitable for model reduction and control system designs. |
| 1995 | Litster et al. | Discretisation (Adjustable) | Extends the work of Hounslow (1988, 1990) with adjustable parameter q, suggested result q = 3 or 4.<br>Good agreement from results in four case studies. | There is a trade-off between accuracy and computational time. |
| 1996a | Kumar and Ramkrishna | Discretisation (Fixed Pivot Technique) | Applicable to binary or multiple breakage, aggregation, simultaneous breakage and aggregation.<br>Attempts to improve the solution accuracy due to errors associated with discretisation by selecting a proper refinement grid for a specific size range and a non-uniform or geometric-type grid. | One exception, consistent over-prediction in a size range that contains steep variations in number density. |
| 1996b | Kumar and Ramkrishna | Discretisation (Moving Pivot Technique) | Improved results than from previous work by the same authors (1996a). They used variations in pivotal size for each interval adapting to the prevailing non-uniformity of the number density. | For given cases, gives lower predicted results when compared to analytical solutions. |

| Year | Authors | Method | Result | Limitation |
|---|---|---|---|---|
| 1996 | Chen et al. | Wavelet | Apply wavelet-Galerkin scheme for solving population balance (binary equal breakage only). | Some errors have been identified and corrections have been made recently by (Tonghua Zhang et al. 2007). |
| 1998 | Nicmanis and Hounslow | Finite element | Applied to aggregation, growth, nucleation and breakage in continuous crystallizer. Use Galerkin techniques with quadratic basis functions. | Only for steady-state conditions. |
| 2001 | Liu and Cameron | Wavelet | Applied to nucleation, growth and agglomeration cases, using wavelet collocation method | Fixed resolution level, high computational time and load. |
| 2002 | Mahoney and Ramkrishna | Finite element | Applicable to aggregation, growth and nucleation. Use Galerkin on finite elements with linear basic functions. | Problems with particle growth due to special treatment of moving discontinuities. |
| 2003 | Rigopoulos and Jones | Finite element | Solution for 1-D dynamic population balance, applicable for continuous and batch crystallizer. For nucleation, growth, agglomeration and breakage. Use Galerkin on FE with linear basic functions. | |
| 2003 | Liu and Cameron | Wavelet | Extends the previous work with an adaptive collocation method | Less computational time with same degree of accuracy |

## *2.4 Challenges in Crystalliser Operation and Control*

Braatz (2002) stated that control of the crystal size distribution (CSD) is critical for efficient downstream operations such as filtration, drying, and product characterisation (e.g. transport and storage properties). He explained that poor control of crystal size can result in unacceptable long filtration or drying times, or in extra processing steps such as re-crystallisation and milling. Christofides et al. (2007) reviewed recent developments and future challenges for particulate processes. The challenges in controlling the crystallisation process are significant. First, the main issues of uncertainty in the model parameters, such as crystallisation kinetics, mixing and reaction kinetics; also un-modelled actuator/sensor dynamics and constraints in the capacity of control actuators. Second, the model solution for CSD needs to cover a wide magnitude, i.e. range of length (0.01 nm to 1000 μm) and time scale (20 μs to 200 min). Required developments in sensor technology to be applied to crystallisation processes also present a challenge to instrument manufacturers. The crystal size distribution must be measured accurately and directly, and in a timely manner in order to perform real-time control.

The requirements of low-dimensional models and solution of a small set of ODEs so that the controllers can be implemented in real-time with acceptable computation time and capacity, is also a major challenge for controlling crystallisation processes. Conventional feedback controllers have been used in both batch and continuous crystallisation processes. Continuous crystallisation processes exhibit highly oscillatory behaviour which can lead to off-specification products, overloading of dewatering equipment, and increased equipment fouling. Sustained oscillations in continuous crystallisers can be effectively controlled by feedback controllers. Non-linear feedback controllers have also been installed in order to improve the control performance of linear feedback controllers (Chiu et al. 1999). There have been relatively few studies, and no experimental implementation, of multivariable controllers for continuous crystallisers(Rawlings et al. 1993). Batch crystallisation processes need to achieve the desired CSD with specific purity and with other input and output constraints by manipulating the crystalliser temperature. A programmed cooling policy gives superior CSD characteristics compared to either natural or linear cooling policies. The optimisation goal is to maximise the mean particle size and minimise the CSD variance in the minimum time. A model predictive control strategy has been implemented on a seeded batch cooling crystalliser (Shi et al. 2006) and a protein crystalliser (Shi et al.

2005) . Other researcher implement their optimal control strategy based on the method of moments, which assumes that the moments of the CSD can be measured or estimated correctly (Hu et al. 2005). The limitations associated with the method of moments apply to the results obtained for the controlled variables.

In reactive crystallisation, feed flow rate can be used as a manipulated variable since the supersaturation depends on the chemical reactions. Despite developments in the control of crystallisation processes, there is still a need for a validated population balance-based model to be implemented in the robust and simple control methods. Most of the crystallisation control research focuses only on controlling an individual unit or series of crystallisers. At present, closed-loop CSD control is not accepted industrial practice; furthermore, there is no study available to date on controlling an integrated crystallisation system. Therefore in this study, the wavelet-based reaction-crystallisation process model would be a valuable development when implemented on a reactive crystallisation processes. The developed model will then be suitable for control purposes, which is straightforward and can be adapted to the real-time control environment. The integration of an advanced control strategy with population balance modelling is the real challenge in this rapidly growing research area for a wide-range of particulate processes.

## 2.5 Direction of this Research Study

The challenges in reactive crystallisation are due to the complex interactions between the product specifications, the operating conditions, and the mechanisms inherent in the process. The mechanism of reactive crystallisation is unique due to the relationships between, and the effects produced by, the chemical reactions, masses transferred, mixing and fluid hydrodynamics. In addition, all of the crystallisation mechanisms such as nucleation, growth, ripening, agglomeration and breakage must be included. Complex integrated models can be developed but they cannot be applied until they are verified by reliable experimental data. The verified models would be of great value for process design and scale-up, as this would lead to improved product quality and enable tailoring of product properties to new applications.

Significant research has been done on developing numerical methods for solving continuous PBE because of the system complexity and a lack of analytical techniques or experimental data required to validate the earlier simple models. All of these numerical methods can be categorized into four types: (a) method of moments; (b) method of weighted residuals; (c) discretisation methods; and (d) statistical based methods. The major challenges associated with these methods are: (i) long computation times required to solve the equations; (ii) computation capacity (memory needed); (iii) the stability of the modal; (iv) the accuracy of the simulated results obtained; and (v) application to design or for operational control. Despite control developments of crystallisation processes, there is still no validated population balance-based model available which can be implemented with robust and simple control methods. Therefore in this research study, the development of the wavelet-based reaction-crystallisation process model has been identified as having significant potential for implementation in reactive crystallisation applications.

Considering all the challenges identified in this chapter with the reactive crystallisation process, this research will focus on and be limited to specific aspects in an attempt to bridge the gap between published theoretical studies and particular industrial applications. Specific research areas to be studied are:

- A single-phase reactive crystallisation was studied in detail in order to obtain the kinetics data; hence, establish a model of the crystalliser system based on verified experimental data.
- The effects of mixing and fluid dynamics on the kinetics of a liquid-liquid reactive crystallisation process were studied experimentally. Feed-point location, agitation rate, gas flow rate were studied as the significant controlling factors.
- A new numerical technique was proposed for generating alternative solutions of the reactive crystallisation models. A wavelet-based method was applied to rectify some limitations of the previous methods, in term of accuracy and stability issues. However, in this study, the methods were currently only applied for uni-dimensional population balance problems.

## *2.6 References*

Anon. (2003). Current world fertilizer trends and outlook to 2007/08. Rome, Food and Agriculture Organi**z**ation of The United Nations**:** 65.

Abbasi, E. and A. Alamdari (2007). Mixing effects on particle size distribution in semi-batch reactive crystallization of maneb. *Journal Of Chemical Engineering of Japan*, 40(8), 636.

B. M. Liang, R. W. H., K. A. Berglund, (1987). Growth rate dispersion in seeded batch sucrose crystallization. *AIChE Journal*, 33(12), 2077-2079.

Batterham, R. J., J. S. Hall and G. Barton (1981). Pelletizing kinetics and simulation of full-scale balling circuits. A136-A151, Nurnberg, W. Germany.

Chen, P.-C., C. C. Chen, M. H. Fun, O. Y. Liao, J. J. Jiang, Y. S. Wang and C. S. Chen (2004). Mixing and crystallization kinetics in gas-liquid reactive crystallization. *Chemical Engineering Technology*, 27(5), 519-528.

Chiang, P. and M. D. Donohue (1988). A kinetic approach to crystallization from ionic solution. I: Crystal growth. *Journal of colloid and interface science*, 122(1), 230-250.

Chiu, T. and P. D. Christofides (1999). Nonlinear control of particulate processes. *AIChE Journal*, 45(6), 1279-1297.

Christofides, P. D., M. Li and L. Madler (2007). Control of particulate processes: Recent results and future challenges. *Powder Technology*, 175(1), 1-7.

David, R. and J. P. Klein (2001). Reaction crystallization. Crystallization technology handbook. A. Mersmann. New York, Marcel Dekker, Inc**:** 513-561.

Davies, C. W. and A. L. Jones (1955). The precipitation of silver chloride from aqueous solution: Kinetics of growth of seed crystals. *Trans. Faraday Soc.*, 51.

Doremus, R. H. (1958). Precipitation kinetics of ionic salts from solution. *J. Phys. Chem*, 62.

Garside, J. (1985). Industrial crystallization from solution. *Chemical Engineering Science*, 40(1), 3-26.

Gelbard, F. and J. H. Seinfeld (1979). Exact solution of the general dynamic equation for aerosol growth by condensation. *Journal of colloid and interface science*, 68(1), 173-183.

Gerstlauer, A., S. Motz, A. Mitrovic and E.-D. Gilles (2002). Development, analysis and validation of population models for continuous and batch crystallizers. *Chemical Engineering Science*, 57(20), 4311-4327.

Gupta, B. S. and T. K. Dutta (1991). Monte carlo simulation of the crystal size distribution in a continuous sucrose crytallizer. *The Chemical Engineering Journal*, 46(2), B35-B41.

Hounslow, M. J. (1990). A discretized population balance for continuous systems at steady-state. *AIChE Journal*, 36, 106-116.

Hounslow, M. J., R. L. Ryall and V. R. Marshall (1988). A discretized population balance for nucleation, growth and aggregation. *AIChE Journal*, 34, 1821-1832.

Hu, Q., S. Rohani and A. Jutan (2005). New numerical method for solving the dynamic population balance equations. *AIChE Journal*, 51(11), 3000-3006.

Hu, Q., S. Rohani, D. X. Wang and A. Jutan (2005). Optimal control of a batch cooling seeded crystallizer. *Powder Technology*, 156(2-3), 170-176.

Hulburt, H. M. and S. Katz (1964). Some problems in particle technology : A statistical mechanical formulation. *Chemical Engineering Science*, 19(8), 555-574.

Jones, A., S. Rigopoulos and R. Zauner (2005). Crystallization and precipitation engineering. *Computers & Chemical Engineering*, 29(6), 1159-1166.

Jones, A. G. (2002). *Crystallization process systems*. Butterworth Heinemann, Oxford.

Kim, Y. P. and J. H. Seinfeld (1990). Simulation of multicomponent aerosol condensation by the moving sectional method. *Journal of colloid and interface science*, 135(1), 185-199.

Kostoglou, M. and A. J. Karabelas (1994). Evaluation of zero order methods for simulating particle coagulation. *Journal of colloid and interface science*, 163(2), 420-431.

Kostoglou, M. and A. J. Karabelas (2002). An assessment of low-order methods for solving the breakage equation. *Powder Technology*, 127(2), 116-127.

Kumar, S. and D. Ramkrishna (1996). On the solution of population balance equations by discretization--i. A fixed pivot technique. *Chemical Engineering Science*, 51(8), 1311-1332.

Kumar, S. and D. Ramkrishna (1996). On the solution of population balance equations by discretization--ii. A moving pivot technique. *Chemical Engineering Science*, 51(8), 1333-1342.

Kumar, S. and D. Ramkrishna (1997). On the solution of population balance equations by discretization--iii. Nucleation, growth and aggregation of particles. *Chemical Engineering Science*, 52(24), 4659-4679.

Liang, B., Y. Shi and R. W. Hartel (1991). Growth rate dispersion effects on lactose crystal size distributions from a continuous cooling crystallizer. *Journal of Food Science*, 56(3), 848-854.

Litster, J. D., D. J. Smit and M. J. Hounslow (1995). Adjustable discretized population balance for growth and aggregation. *AIChE Journal*, 41(3), 591-603.

Mahoney, A. W. and D. Ramkrishna (2002). Efficient solution of population balance equations with discontinuities by finite elements. *Chemical Engineering Science*, 57(7), 1107-1119.

Marchal, P., R. David, J. P. Klein and J. Villermaux (1988). Crystallization and precipitation engineering--i. An efficient method for solving population balance in crystallization with agglomeration. *Chemical Engineering Science*, 43(1), 59-67.

Matz, G. (1985). Ostwald ripenning. A modern concept. *German chemical engineering*, 8(4), 255-265.

McCabe, W. L. (1929). Crystal growth in aqueous solutions. *Industrial & Engineering Chemistry*, 21, 30.

Middleton, P. and J. Brock (1976). Simulation of aerosol kinetics. *Journal of colloid and interface science*, 54(2), 249-264.

Mullin, J. W. (2001). *Crystallization*. Butterworth-Heinemann, Oxford.

Mydlarz, J. and D. Briedis (1992). Growth rate dispersion vs size-dependent growth rate for msmpr crystallizer data. *Computers & Chemical Engineering*, 16(9), 917-922.

Myerson, A. S. and R. Ginde (1993). Crystals, crystals growth, and nucleation. Handbook of industrial crystallization. A. S. Myerson. Newton, Butterworth-Heinemann: 33-63.

Nicmanis, M. and M. J. Hounslow (1998). Finite-element methods for steady-state population balance equations. *AIChE Journal*, 44(10), 2258-2272.

Nopens, I., D. Beheydt and P. A. Vanrolleghem (2005). Comparison and pitfalls of different discretised solution methods for population balance models: A simulation study. *Computers & Chemical Engineering*, 29(2), 367-377.

Piotrowski, K. and J. Piotrowski (2005). Monte carlo modelling of continuous adiabatic msmpr crystallizer. *Chemical Engineering and Processing*, 44(5), 517-528.

Ramkrishna, D. (2000). *Population balance : Theory and applications to particulate systems in engineering*. Academic Press, London.

Ramkrishna, D. and A. W. Mahoney (2002). Population balance modeling. Promise for the future. *Chemical Engineering Science*, 57(4), 595-606.

Randolph, A. D. and M. A. Larson (1988). *Theory of particulate processes : Analysis and techniques of continuous crystallization*. Academic Press, San Diego.

Randolph, A. D. and E. T. White (1977). Modeling size dispersion in the prediction of crystal-size distribution. *Chemical Engineering Science*, 32(9), 1067-1076.

Rawlings, J. B., S. M. Miller and W. R. Witkowski (1993). Model identification and control of solution crystallization processes: A review. *Industrial and Engineering Chemistry Research*, 32(7), 1275-1296.

Rawlings, J. B., W. R. Witkowski and J. W. Eaton (1992). Modelling and control of crystallizers. *Powder Technology*, 69(1), 3-9.

Rigopoulos, S. and A. G. Jones (2003). Finite-element scheme for solution of the dynamic population balance equation. *American Institute of Chemical Engineers. AIChE Journal*, 49(5), 1127.

Sampson, K. J. and D. Ramkrishna (1985). Particle size correlations and the effects of limited mixing on agglomerating particulate systems. *Journal of Colloid and Interface Science*, 104(1), 269-276.

Shah, B. H., J. D. Borwanker and D. Ramkrishna (1976). Monte carlo simulation of microbial population growth. *Mathematical Biosciences*, 31(1-2), 1-23.

Shi, D., N. H. El-Farra, M. Li, P. Mhaskar and P. D. Christofides (2006). Predictive control of particle size distribution in particulate processes. *Chemical Engineering Science*, 61(1), 268-281.

Shi, D., P. Mhaskar, N. H. El-Farra and P. D. Christofides (2005). Predictive control of particle size distribution in protein crystallization. American Control Conference. Portland, OR, USA: 944-948.

Singh, P. N. and D. Ramkrishna (1977). Solution of population balance equations by mwr. *Computers & Chemical Engineering*, 1(1), 23-31.

Spielman, L. A. and O. Levenspiel (1965). A monte carlo treatment for reacting and coalescing dispersed phase systems. *Chemical Engineering Science*, 20(3), 247-254.

Subramanian, G. and D. Ramkrishna (1971). On the solution of statistical models of cell populations. *Mathematical Biosciences*, 10(1-2), 1-23.

Tamura, K. and H. Tsuge (2006). Characteristics of multistage column crystallizer for gas-liquid reactive crystallization of calcium carbonate. *Chemical Engineering Science*, 61(17), 5818-5826.

Tavare, N. S. (1995). *Industrial crystallization: Process simulation analysis and design*. Plenum Press, New York.

Tonghua Zhang, Yu-Chu Tian, Moses O. Tadé and J. Utomo (2007). Comments on 'the computation of wavelet-galerkin approximation on a bounded interval'. *International Journal for Numerical Methods in Engineering*.

van Peborgh Gooch, J. R. and M. J. Hounslow (1996). Monte carlo simulation of size-enlargement mechanisms in crystallization. *AIChE Journal*, 42(7), 1864-1874.

Vanni, M. (2000). Approximate population balance equations for aggregation-breakage processes. *Journal of Colloid and Interface Science*, 221(2), 143-160.

Villadsen, J. (1997). Putting structure into chemical engineering proceedings of an industry/university conference. *Chemical Engineering Science*, 52(17), 2857-2864.

Wibowo, C., W. C. Chang and K. M. Ng (2001). Design of integrated crystallization systems. *AIChE Journal*, 47(11), 2474-2492.

# 3. Modelling of Mono-Ammonium Phosphate Systems

## 3.1 Mono-Ammonium Phosphate (MAP) systems

### Description of the system

Two systems were studied: a batch crystalliser for the cooling crystallisation process, and a semi-batch reactor-crystalliser. The models developed for each system incorporate a population balance equation, and also include the lumped dynamic models for the mass and/or energy balances which describe the process models for each system.

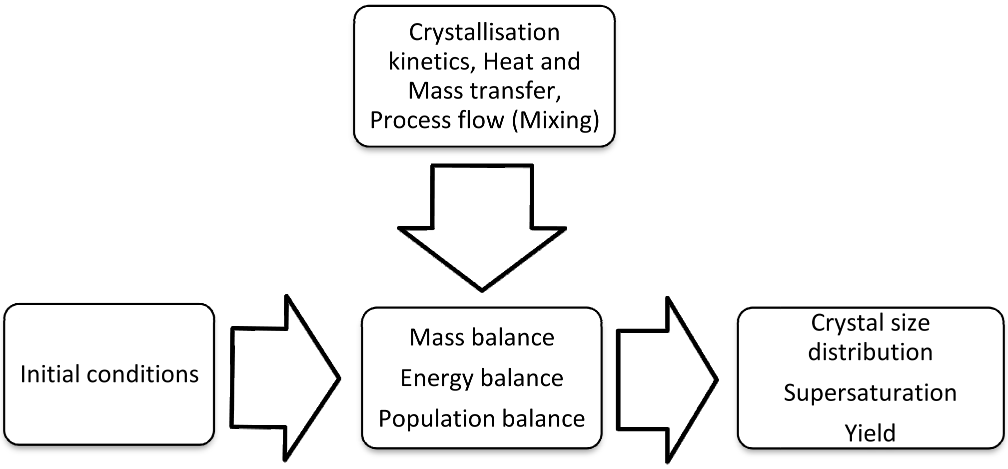

**Figure 3-1. Crystallisation modelling schematic**

In Figure 3-1, it is shown that two inputs are required in order to model the crystallisation process and perform the simulations. Initial conditions, such as design parameters and operational data, combined with the crystallisation kinetics, heat and mass transfer properties, and process flow and mixing data are required in order to begin the modelling computations and determine (for example) the crystal size distribution, supersaturation and yield of crystallisation. In practical case, the process is not so straightforward and experimental kinetics data need to be obtained, then optimisation of the conditions for obtaining supersaturation will be done and followed by revision of some variables in order to obtain realistic simulation data.

## 3.2 Problem definition

**Modelling objective**

This model is to be used as a simulation tool in order to study the performance of both types of crystallisers. The output from the model is expected to be within 10% accuracy.

**Anticipated inputs/disturbances/outputs**

*Inputs/disturbances:* initial concentration of reactants, initial temperature of reactants, cooling water temperature, mixing intensity, liquid hold up. Different initial concentrations and cooling water temperatures can also be used as inputs.

*Outputs:* temperature and concentration of the suspension, crystal yield, size distribution.

## 3.3 Controlling factors

For a non-reactive system, only the crystallisation process takes place. Crystallisation includes several mechanisms such as nucleation, crystal growth, agglomeration and breakage. The kinetics of each of these processes is explained in the next section.

*A. Batch cooling crystalliser:* In the case of the cooling crystalliser, the heat needs to be removed from the system at a specified rate, whereas for an evaporative crystalliser heat is supplied at a set rate. Heat transfer between the cooling jacket and the crystalliser vessel is controlled mainly by convection and conduction. Some heat loss to the surrounding may occur because the system is not well insulated. A typical overall heat-transfer coefficient for this type of application is often quoted in the heat transfer literature to be within the range of 100-1000 W/m$^2$K (Shilling et al. 1999). In addition, the temperature difference between the solution and the crystalliser wall should be lower than that occurring in the corresponding metastable zone width in order to control the nucleation.

*B. Semi-batch reactive crystalliser:* For this system, the chemical reactions between ammonia and phosphoric acid releases heat due to the exothermic reactions. Chemical reactions take place until the system reaches a certain degree of supersaturation, then nucleation, growth and other crystallisation mechanisms occur until chemical equilibrium is achieved.

Mass transfer from solid to liquid determines the rate of diffusion in any process, thus reflecting the effect of mixing on the fluid film around the solid particles. Solid-liquid mass transfer in stirred suspensions are usually determined from differential dissolution experiments, and can be correlated by Frossling-type equations using the Reynolds number (as defined in terms of the agitator speed and the characteristic dimensions) (Dahlstrom et al. 1999). The mass transfer coefficient increases sharply with the agitator speed until the particles become fully suspended in the liquid, after which the rate of increase is reduced considerably.

The transfer of momentum in the crystalliser is controlled mainly by the mixing conditions. The mixing process influences the reaction, crystallisation mechanisms, and the heat transfer process. In order to achieve conditions of complete suspension, the characterisation of the critical impeller speed is necessary. The goal is to reach the speed at which no particle is observed to remain at rest at the base of the vessel for more than one or two seconds.

## 3.4 Property data

***Mono and Di- Ammonium Phosphate Solubility***

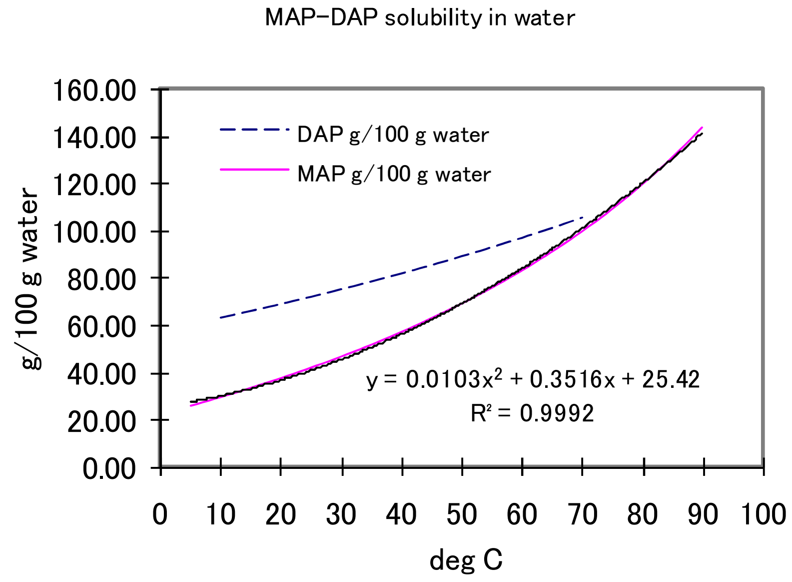

**Figure 3-2. MAP and DAP solubility in water**

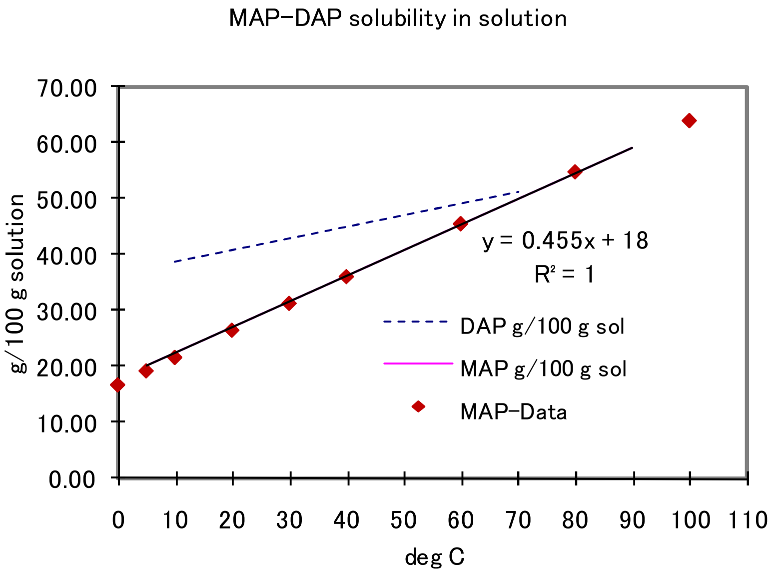

**Figure 3-3. MAP and DAP solubility in its solution (water and MAP/DAP)**

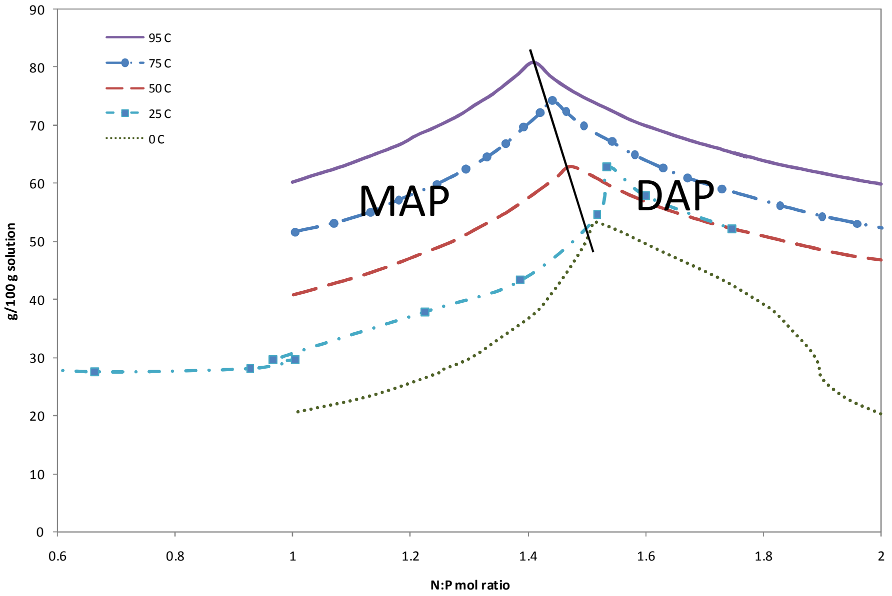

**Figure 3-4. MAP-DAP solubility at various temperature in the solution of phosphoric acid and ammonia**

In Figure 3-2 and Figure 3-3, we can determine the solubility of mono-phosphate and di-phosphate salts as a function of temperature in the water or its solution. For the operating temperature range, we can observe that di-ammonium phosphate (DAP) solubility is 50-100% higher than mono-ammonium phosphate (MAP). The solubility model developed here is based on several sources, such as Buchanan and Winner (1920), Ross et al. (1929), Seidell and Linke (1952), and Stokka (1985). For MAP solubility as shown in Figure 3-3, experimental data validated the solubility model. For the reactive system, different solubility data is shown in Figure 3-4. The solubility of the salts is a function of the temperature as well as the nitrogen to phosphorous (N/P) molar ratio. Between N/P molar ratio of 1.4 – 1.5, the solubilities are at their maximum; the left hand side of the peak is the area where MAP is mainly produced, and the right hand side is the area where DAP is prevalent. If the N/P mole ratio is increased to 3, then the tri-ammonium phosphate (TAP) is easily precipitated because it has a lower solubility than DAP or MAP.

***Density***

The density of the solution is needed for the mass balance, product flow rate, and yield calculations. Density is also needed to convert the concentration based on solution volume to concentration based on mass volume or moles of the solution. However, if the solution density data is not available, then density can be estimated by using the density of the pure solvent and pure solid solute at the particular temperature and by assuming volumes are additive.

$$\frac{1}{\rho_{solution}} = \frac{w_{crystal}}{\rho_{crystal}} + \frac{w_{solvent}}{\rho_{solvent}} \tag{3-1}$$

where $w$ is the mass fraction and ρ is the density.

***Viscosity***

Viscosity data are needed since crystallisation involves stirring and movement of suspensions of particles in fluids. Viscosity is important in crystalliser design and operation. By definition, viscosity is the ratio of the shear stress and the shear rate. Viscosity increases with increasing concentration in solution and decreases with increasing temperature. In crystallisation operations, viscosity of the slurry of solution and crystals is important. The slurry viscosity usually does not obey Newton’s law of viscosity but follows more complex empirical relations obtained from experimental data, this system is termed non-Newtonian. The viscosity can also be significantly affected by the particle size, size distribution, and particle shape. In general, as particles shape changes from spheres to needles, the viscosity moves further from Newtonian behaviour.

***Diffusivity***

Diffusion is the movement of molecules due to their thermal energy under the influence of a concentration gradient. The diffusion coefficient is a rate property of a given solute diffusing under a concentration gradient in a given solvent. Diffusivity is the most fundamental property of any chemical system and it is incorporated into mass transfer correlations. Diffusion coefficients vary with temperature and with solute concentration. This is important as it can determine the degree of agitation required to effect a desirable crystal growth. Diffusion coefficients can be obtained either experimentally or from theory for simple and ideal systems. However, the empirical correlations currently available in the literature are unreliable at higher concentrations. Data on the diffusion coefficients of the solid solutes in liquid solvents are difficult to find and, if available, are usually found at low concentrations (or infinite dilution) and at only one temperature.

The procedure below will give a reasonable estimate of the supersaturated diffusivity, if no data is available at any concentration.

- Estimate the infinite dilution diffusivity using Wilkie-Chang (1955) method:

$$D_{21}^{0} = 7.4 \times 10^{-8} \frac{(\phi M_1)^{1/2} T}{\mu_l V_2^{0.6}} \tag{3-2}$$

- Estimate the supersaturation diffusivity using Hartley-Crank (1949) equation:

$$D = \left( \frac{d \ln a_2}{d \ln \gamma_2} \right) \left( x_1 D_{12}^{0} + x_2 D_1^{*} \right) \frac{\mu_s}{\mu_l} \tag{3-3}$$

where:

$D_{12}^{0}$ = infinite dilution diffusivity

$D_1^{*}$ = self-diffusion coefficient of the solvent

$\mu_s$ = viscosity of the solution

$\mu_l$ = viscosity of the solvent

$D_{21}^{0}$ = infinite dilution diffusivity of the solute (2) in the solvent (1) [cm$^2$/s]

$M_1$ = molecular weight of the solvent

$T$ = temperature [K]

$V_2$ = molal volume of the solute at its normal boiling point [cm$^3$/g mol]

$\phi$ = association factor (2.6 for water; 1.5 for ethanol; 1 for others)

### *Heat of mixing, solution and crystallisation*

When two liquids are combined and mixed, or a concentrated solution is diluted, or a solute is dissolved in a solution, or a solute is crystallised from the solution, then heat effects will occur and these can be very significant in the energy balance calculations. The heat of crystallisation is normally assumed to be about the same magnitude as the heat of solution, but having the opposite sign. For a special case of reactive crystallisation, when reaction takes place, there is also a contribution due to heat of reaction. Therefore, these thermal changes should be included in the development of the system model.

### *Heat transfer*

Convection and conduction heat transfer modes are included in our model. Conduction occurs through the crystalliser vessel wall and in the cooling jacket wall. The internal convection occurs inside the crystalliser due to mixing, and in the cooling jacket due to fluid flow.

### *Energy balance*

Several assumptions are made for the case of a cooling batch crystalliser:

- constant crystalliser volume
- constant cooling water temperature and flow rate
- negligible heat losses to surroundings
- negligible heat of mixing
- constant physical properties

Additional assumptions for the case of a semi-batch reactive crystalliser are:

- negligible heat of solution and dissolution of MAP
- negligible heat of crystallisation
- constant heat of reaction

The overall dynamic energy balance for such systems is described as follows:

$$-m\,C_p\frac{dT_C}{dt} = UA(T_C - T_j) \tag{3-4}$$

where m is mass hold-up inside the crystalliser; Cp is the heat capacity of the crystalliser contents; Tc is the temperature in the crystalliser; Tj is the jacket temperature; U is the overall heat transfer coefficient; A is the heat transfer area.

### ***Nucleation and Growth***

The nucleation and growth rates are expressed by a simple power law. The nucleation rate constant, $k_b$, is a function of several variables such as temperature, hydrodynamics, impurities, crystal properties, and others. Typical values of nucleation order (b) are between 0.5 to 2.5 for secondary nucleation. In cases where secondary nucleation is dominant, then most values of suspension density order (j) are close to unity which indicates the dominance of the collision between crystals and stirrer or walls rather than between two crystals. The stirrer speed can be included in the nucleation rate equation and the exponent factor values generally lie between 2 to 4 (Tavare 1995).

$$B = k_b M_T^j \Delta c^b \tag{3-5}$$

The growth order (g) is generally between 0 and 2.5 (Tavare 1995). The growth constant $k_g$ depends on temperature, crystal size, hydrodynamics and impurities. The effect of the temperature on the overall growth rate can be expressed by the Arrhenius relation. Sometimes it is more convenient to define the overall linear growth rate instead of the mass deposition:

$$G = \frac{dL}{dt} = k_g \Delta c^g \tag{3-6}$$

Nucleation rate can be efficiently expressed by the growth rate where $i = b/g$ and $K_R = k_b/{k_g}^i$. Nucleation constant is expressed by $k_b$; $M_T$ is suspension density; j and b are the exponent of suspension density and nucleation order respectively; Δc is the degree of supersaturation. Growth constant is expressed by $k_g$, and g is the growth order. Hence:

$$B = K_R M_T^j G^i \tag{3-7}$$

### ***Reaction rate***

The reactions between ammonia and phosphoric acid can produce a series of products such as mono-ammonium phosphate (MAP), di-ammonium phosphate (DAP) and tri-ammonium phosphate (TAP).

$$NH_3 + H_3PO_4 \rightarrow NH_4H_2PO_4 \tag{3-8}$$

$$NH_3 + NH_4H_2PO_4 \rightarrow (NH_4)_2HPO_4 \tag{3-9}$$

$$NH_3 + (NH_4)_2HPO_4 \rightarrow (NH_4)_3PO_4 \tag{3-10}$$

The first chemical reaction between ammonia and phosphoric acid (4-8) is described by the following second order reaction kinetics as:

$$A + B \rightarrow C$$

$$r = k_r C_A^m C_B^n \tag{3-11}$$

For a semi-batch system, ammonia (A) solution is fed into the crystalliser containing phosphoric acid (B). Since A is continuously introduced with a constant concentration, the kinetics can be written as:

$$r = k_r^1 C_B^n \tag{3-12}$$

where $k_r^1 = k_r C_A^m$

and $k_r = k_0 \exp\left(-\frac{E_A}{RT}\right)$ follows Arrhenius law

and $E_A$, R, T are the activation energy, the universal gas constant, and temperature, respectively. The exponent constant (n), the kinetics rate constant ($k_0$), and $E_A$ are all obtained from experiments in an ideal, perfectly mixed semi-batch reactor at various temperatures.

***Mass and mole balances***

When seed crystals are used in the system, the total suspension density, surface area, crystal average size, and voidage can be expressed in term of mass of seed ($W_0$) and mass of crystals (W), as given by:

$$M_T = M_{T0}(W/W_0) \tag{3-13}$$

$$A_T = A_{T0}(W/W_0)^{2/3} \tag{3-14}$$

$$L = L_0(W/W_0)^{1/3} \tag{3-15}$$

$$\varepsilon = 1 - (W/(\rho_c V)) \tag{3-16}$$

where $W$ is mass (kg) of crystals in the crystalliser at a given time t by:

$$W = W_0 + (\Delta c_0 - \Delta c)S \tag{3-17}$$

The initial values, $M_{T0}$ and $A_{T0}$, can be evaluated from initial mass and size of seed crystals by using the expressions:

$$A_{T0} = (FW_0)/(\rho_C L_0 S) \tag{3-18}$$

$$M_{T0} = W_0/S \tag{3-19}$$

In a batch crystalliser, the rate of solids deposition per unit mass of solvent on the seed (S-subscript) crystals is:

$$\frac{dW_S}{dt} = \frac{3W_{S0}L_S^3 G}{L_{S0}^3 S} \tag{3-20}$$

For the new nuclei (N-subscript) crystals:

$$\frac{dW_N}{dt} = \rho f_v \frac{d\mu_3}{dt} = \frac{3\rho f_v A_N G}{f_a} \tag{3-21}$$

For this semi-batch operation, the capacity of the crystallizer varies with time:

$$\frac{dm}{dt} = \frac{d(\rho V)}{dt} = F_A + F_B \tag{3-22}$$

Therefore, the mole balance of the reacting species takes the following form of ordinary differential equations:

$$\frac{d(C_A.V)}{dt} = -r\,V + \frac{F_A}{M_{r,A}} \tag{3-23}$$

$$\frac{d(C_B.V)}{dt} = -r\,V + \frac{F_B}{M_{r,B}} \tag{3-24}$$

$$\frac{d(C_C.V)}{dt} = r\,V + \frac{k_v\,\rho_c}{M_{r,C}}\frac{d(\mu_3\,V)}{dt} \tag{3-25}$$

***Supersaturation***

The supersaturation balance can be written as:

$$-\frac{d\Delta c}{dt} = \frac{dW_S}{dt} + \frac{dW_N}{dt} = \frac{3W_{S0}L_S^3G}{L_{S0}^3S} + \frac{3\rho f_v A_N G}{f_a} \tag{3-26}$$

$$-\frac{d\Delta c}{dt} = B_S + A_T G = k_B M_T^j \Delta c^b + k_G A_T \Delta c^g \tag{3-27}$$

***Population balance***

The first assumption regarding our process is that the mechanism of precipitation only includes nucleation and growth. The agglomeration mechanism will be neglected because the subsequent process of granulation will include agglomeration and breakage mechanisms. The time-dependent population balance equation that describes the evolution of the crystal size distribution in a finite and spatially uniform domain, with particle volume as the internal coordinate, and including nucleation and growth, is formulated as (Randolph et al. 1988):

$$\frac{\partial n(v,t)}{\partial t} = \frac{n_{in}(v,t) - n(v,t)}{\tau} - \frac{\partial}{\partial v}[G(v).n(v,t)] + B_0\delta(v - v_0) \tag{3-28}$$

where $n(v,t)$ and $n_{in}(v,t)$ represent the population density in the reactor and in the inlet, respectively. $G(v)$ represents the volumetric growth rate, and $B_0$ represents the nucleation rate. The following initial and boundary conditions apply:

$n(v,0) = n_0(v)$ (initial distribution)

$n(0,t) = 0$ (no crystals of zero size)

In this thesis, population density was defined as the quantity of crystals or particles at a certain size range and at a specific course of time. Population density can be described in terms of mass density or number density. Mass density is a percentage of weight of crystals at a certain size range and time. Number density is a percentage of number of crystals at a certain size range and time. Crystal size distribution can also be illustrated in term of total number of crystals at a certain size and time.

***Moment equations***

The $j$th moment is defined by Hulburt and Katz (1964):

$$\mu_j = \int_0^\infty v^j \ n(v) \, dv \tag{3-29}$$

The first four moments are important because they are related to total number, total length, total area, and total volume of solid per unit volume of suspension (Hounslow et al. 1988):

$$N_T = \mu_0 \tag{3-30}$$

$$L_T = k_l \, \mu_1 \tag{3-31}$$

$$A_T = k_a \, \mu_2 \tag{3-32}$$

$$V_T = k_v \, \mu_3 \tag{3-33}$$

For the case of nucleation and growth only, in a semi-batch reactor, the moment equations may be generated by the ordinary differential equations:

$$\frac{d\mu_j}{dt} = 0^j \, B^0 + j \, G \, \mu_{j-1} \qquad for \, j = 0,1,2,3 \tag{3-34}$$

Therefore:

$$\frac{d\mu_0}{dt} = B \tag{3-35}$$

$$\frac{d\mu_1}{dt} = \mu_0 \, G \tag{3-36}$$

$$\frac{d\mu_2}{dt} = 2 \, \mu_1 \, G \tag{3-37}$$

$$\frac{d\mu_3}{dt} = 3 \, \mu_2 \, G \tag{3-38}$$

## 3.5 Model implementation

### *Discretised Population Balance*

$$\frac{dN_i}{dt} = \left(\frac{dN_i}{dt}\right)_A + \left(\frac{dN_i}{dt}\right)_G + \left(\frac{dN_i}{dt}\right)_B + \left(\frac{dN_i}{dt}\right)_F \tag{3-39}$$

$$\left(\frac{dN_i}{dt}\right)_B = \begin{cases} B^0 & i=1 \\ 0 & i>1 \end{cases} \tag{3-40}$$

Hounslow et al. (1988) developed a size-independent discrete growth relation that satisfy the criterion:

$$\frac{d\mu_j}{dt} = j\ G\ \mu_{j-1} \tag{3-41}$$

They developed two discretised growth models, namely a two-term and a three-term discretised model. The two-term growth model is given as:

$$\left(\frac{dN_i}{dt}\right)_G = \frac{G}{(r-1)L_i}\ (r\ N_{i-1} - N_i) \tag{3-42}$$

where $r = L_{i+1}/L_i = 2^{1/3q}$ is the geometric size discretisation ratio; the terms $L_i$ and $L_{i+1}$ are the lower and upper bounds of the i^th^ size interval, respectively; $q$is the size resolution parameter and is an integer greater than zero. This model predicts the zero moment correctly, but over predicts all the other moments. However, we are generally more interested in the first four moments (i.e. $\mu_j$ and $j = 0,1,2$ and 3).

The three-term growth model has the form:

$$\left(\frac{dN_i}{dt}\right)_G = \begin{cases} \dfrac{2G}{(1+r)L_i}\left(\left(1-\dfrac{r^2}{r^2-1}\right)N_1 - \dfrac{r}{r^2-1}N_2\right) & i=1 \\ \dfrac{2G}{(1+r)L_i}\left(\dfrac{r}{r^2-1}N_{i-1} + N_i - \dfrac{r}{r^2-1}N_{i+1}\right) & i\neq 1 \end{cases} \tag{3-43}$$

Based on previous research by Hounslow et al. (1988) and Hounslow et al. (1990), the three-term growth model gives satisfactory agreement with the analytical solution of the size-dependent and size-independent growth systems. This model may lead to numerical oscillations and they suggested for a seeded system to replace any negative values of $N_i$ with zero; for the non-seeded system, the two-term growth model should be used instead of the three-term model. Similarly for a system that involves nucleation and growth, the three-term model will lead to oscillation in the crystal size distribution.

## 3.6 Case Studies

### 3.6.1. Batch seeded crystalliser

- **Problem definition**

  This model presents the time evolution of crystal number and size and other performance-related variables of a seeded isothermal batch crystalliser. The model is tested for its sensitivity against the growth and nucleation kinetics, initial degree of supersaturation, seed loading, seed size, and solvent capacity. The crystalliser is initially charged with supersaturated solution in order to induce nucleation and growth simultaneously. The kinetics parameters are obtained experimentally and follow the power law empirical equation.

- **Controlling factors**
  - Nucleation and growth of crystals
  - No reactions occurring
  - Seeded crystallisation
- **Data**
  - Volume of crystalliser, $V = 25\ l$
- **Process model**

  ✓ **Assumptions**
  - Isothermal
  - Perfect mixing condition
  - Constant crystal density
  - Constant solubility

  ✓ **Main equations**

$$\frac{\partial n}{\partial t} + G\frac{\partial n}{\partial L} = 0$$

$$\frac{d\mu_0}{dt} = B$$

$$\frac{d\mu_1}{dt} = \mu_0\, G$$

$$\frac{d\mu_2}{dt} = 2\,\mu_1\,G$$

$$\frac{d\mu_3}{dt} = 3\,\mu_2\,G$$

$$-\frac{d\Delta c}{dt} = \frac{dW_S}{dt} + \frac{dW_N}{dt} = \frac{3W_{S0}L_S^3G}{L_{S0}^3S} + \frac{3\rho f_v A_N G}{f_a}$$

✓ **Consecutive equations**

$$B = k_b M_T^j \Delta c^b$$

$$G = \frac{dL}{dt} = k_g \Delta c^g$$

$$B = K_R M_T^j G^i$$

✓ **Variables**

| | |
|---|---|
| t | time [s] |
| $n$ | population density [number/m kg solvent] |
| $b$ | nucleation order [-] |
| $B$ | nucleation rate [number/ kg solvent s] |
| $c$ | concentration of solute [kg solute/kg solvent or kg hydrate/ kg solvent] |
| $\Delta c$ | supersaturation [kg solute/kg solvent or kg hydrate/ kg solvent] |
| $F$ | surface to volume shape factor [-] |
| $g$ | growth order [-] |
| $G$ | overall linear growth rate [m s$^{-1}$] |
| $i$ | relative kinetic order = b/g [-] |
| $j$ | exponent of magma density [-] |
| $k_b$ | nucleation rate coefficient [number/kg s (kg/kg)$^b$ (kg/kg)$^j$] |
| $k_g$ | linear growth rate coefficient [m/s (kg/kg)$^g$] |
| $K_R$ | relative rate coefficient [number/ kg s (m/s)$^i$ (kg/kg)$^j$ ] |
| $L$ | crystal size [m] |
| $\Delta L$ | difference between successive sieve sizes [m] |
| $m$ | exponent of stirrer speed |
| $M_T$ | magma density [kg/ kg solvent] |
| $n^0$ | nuclei population density (at L=0) [number/ m kg solvent] |
| $N$ | stirrer speed [rev/s] |
| $S$ | solvent capacity of the crystalliser [kg] |
| $W$ | seed loading to the crystalliser [kg] |

| | |
|---|---|
| $\Delta W$ | mass of crystals retained on a sieve [kg] |

- ✓ **Initial conditions**

$$n(0, L) = n_0 \, \delta(L - L_0)$$

$$n_0 = \frac{W_{s0}}{\rho \, k_v L_{s0}^3 \, \Delta L \, S}$$

- ✓ **Boundary conditions**

$$n(t, 0) = n^0 = B/G = K_R M_T^j G^{i-1}$$

- ✓ **Parameters (Tavare et al. 1986)**

| | |
|---|---|
| Batch time, $\tau$ $[s]$ | 6000 |
| Solubility, $c^*$ [kg solute/kg solvent] | 0.1243 |
| Initial supersaturation, $\Delta c_0$ [kg solute/kg solvent] | 0.0150 |
| Seed size, $L_{s0}$ [$\mu$m] | 550 |
| Crystal density, $\rho$ [kg/m$^3$] | 2660 |
| Solvent capacity, S [kg $H_2O$] | 25.46 |
| Specific seed loading, $W_{s0}/S$ [kg crystal/kg solvent] | $3.92 \times 10^{-4}$ |
| Volume shape factor, $k_v$ [-] | 0.525 |
| Surface to volume shape factor, $F$ [-] | 7.0 |
| Growth order, $g$ [-] | 1.5 |
| Growth rate constant, $k_g$ [m/s(kg/kg)$^{1.5}$] | $5.0 \times 10^{-5}$ |
| Nucleation order, $b$ [-] | 3.0 |
| Exponent of magma density, $j$ [-] | 1.0 |
| Nucleation rate constant, $k_b$ [number/kg s (kg/kg)$^4$] | $1 \times 10^{11}$ |
| Relative order, $i$ [-] | 2.0 |
| Relative nucleation rate constant, $K_R$ [number/(kg s (kg/kg) (m/s)$^2$] | $4 \times 10^{19}$ |
| Number of grids | 500 |
| Maximum size of continuum for N crystals, [$\mu$m] | 1000 |

- **Results**

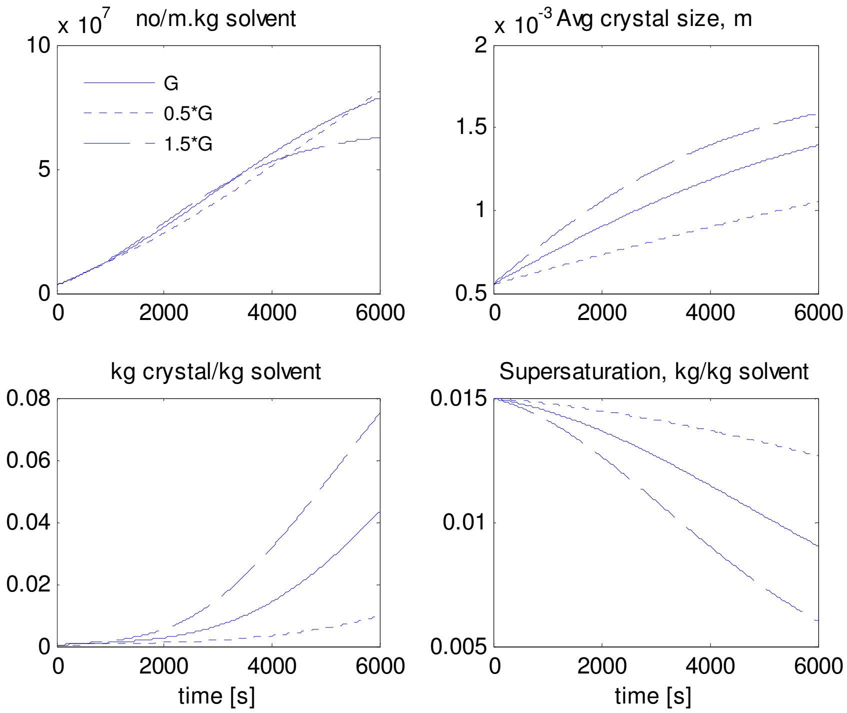

**Figure 3-5. Sensitivity analysis of growth rate ($k_g$ ± 50%) on number of crystals, crystal size, suspension density and supersaturation**

For the base case, the total number of crystals at 6000 seconds is approx. 7 x $10^7$ number of crystals/m kg solvent, of size 1.4 x $10^{-3}$ m. The suspension density increased exponentially to approx. 0.04 kg crystal/kg solvent, and the supersaturation decreased to 0.0009 kg/kg solvent. All the identified process variables are affected by the growth rate within the range ± 50%. The most highly dependent variables are the average crystal size, suspension density, and the degree of supersaturation. The final average crystal size increases by approx. 15% when the growth rate constant was increased by 50%, conversely it decreases by 28% when the growth rate constant decreased by 50%. The reason is that the average size is a linear function of the growth rate, and not the total number of crystals which is directly related to the nucleation rate.

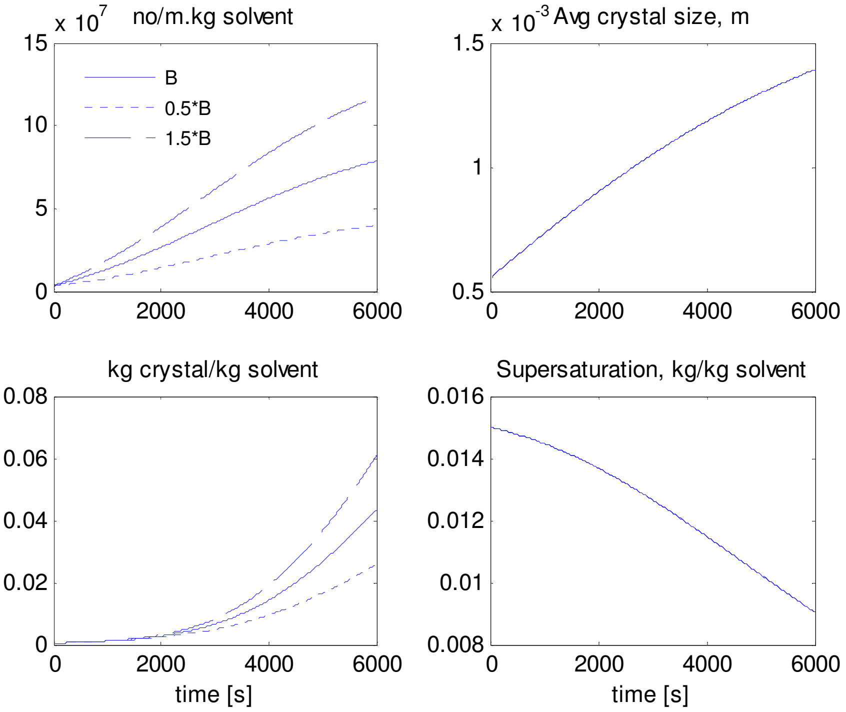

**Figure 3-6. Sensitivity analysis of nucleation rate constant ($k_b$ ± 50%) on number of crystals, crystal size, suspension density and supersaturation**

The average crystal size and degree of supersaturation are not particularly sensitive to the nucleation rate constant, unlike the total number of crystals and the suspension density. A higher nucleation rate produces more crystals and resultant increase in suspension density. A change of ± 50% in the nucleation constant could give ± 65% difference from the base case on the total number of crystals, and ± 42% difference from the base case in the suspension density.

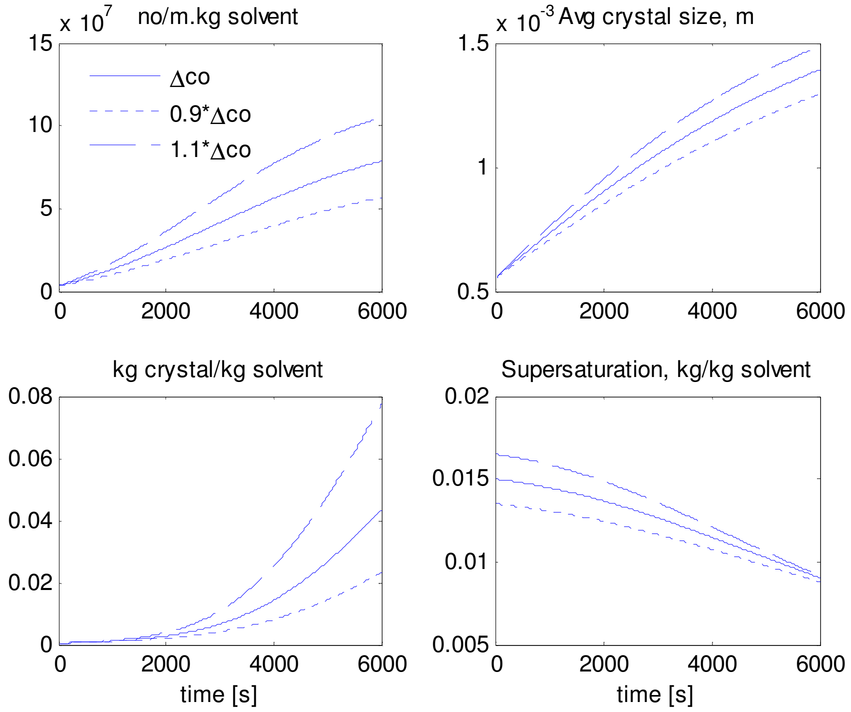

**Figure 3-7. Sensitivity analysis of initial supersaturation (Δco ± 10%) on number of crystals, crystal size, suspension density and supersaturation**

Sensitivity analysis of the initial degree of supersaturation shows that all the selected variables are significantly affected, even when the changes are only ±10%. Initially, it has an effect on nucleation rate, producing a significant change in the number of crystals, and it also affects the growth rate as this is a function of supersaturation. The final suspension density for a higher initial degree of supersaturation is significantly higher than for the base case because it contains more solute. Ultimately the average size is increased by 7% because of the larger growth rate.

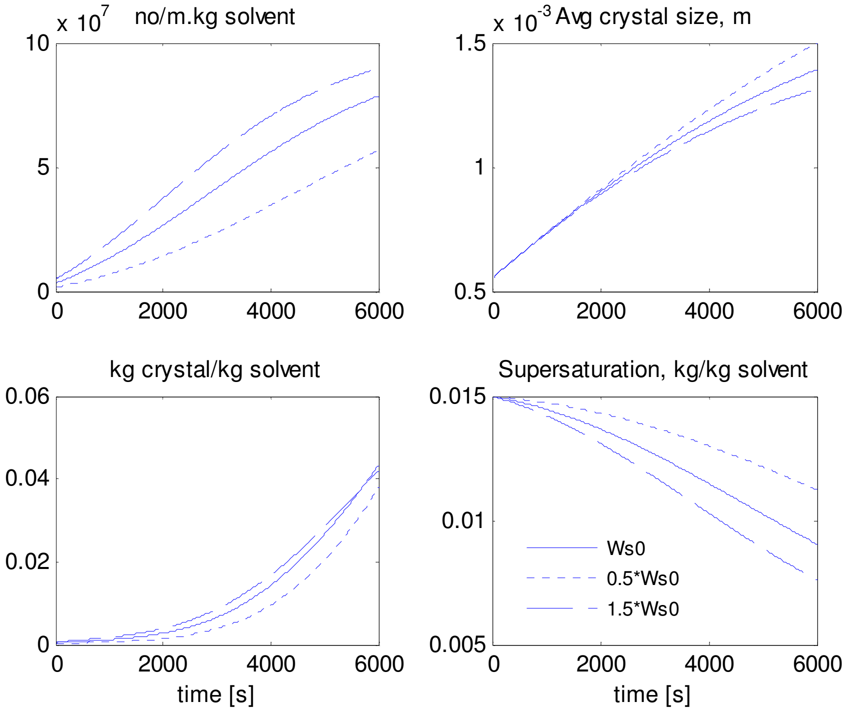

**Figure 3-8. Sensitivity analysis of seed loading (Wso ± 50%) on number of crystals, crystal size, suspension density and supersaturation**

Sensitivity analysis of seed loading in the range of ±50% change from the base case makes a significant difference to the number of crystals and the supersaturation profiles. While average size and suspension density profiles seem to be relatively similar, it can be seen in Figure 3-8 that higher seed loading reduces the effect of nucleation, as the number of nuclei is reduced by 30%. The size of crystals is unchanged around 1300 μm. The suspension density profiles also appear to be unchanged over the range tested, while supersaturation profiles show that a greater desupersaturation rate is obtained with the higher seed loading. This is because more seed crystals are available at higher loading which can consume the same amount of initial supersaturation.

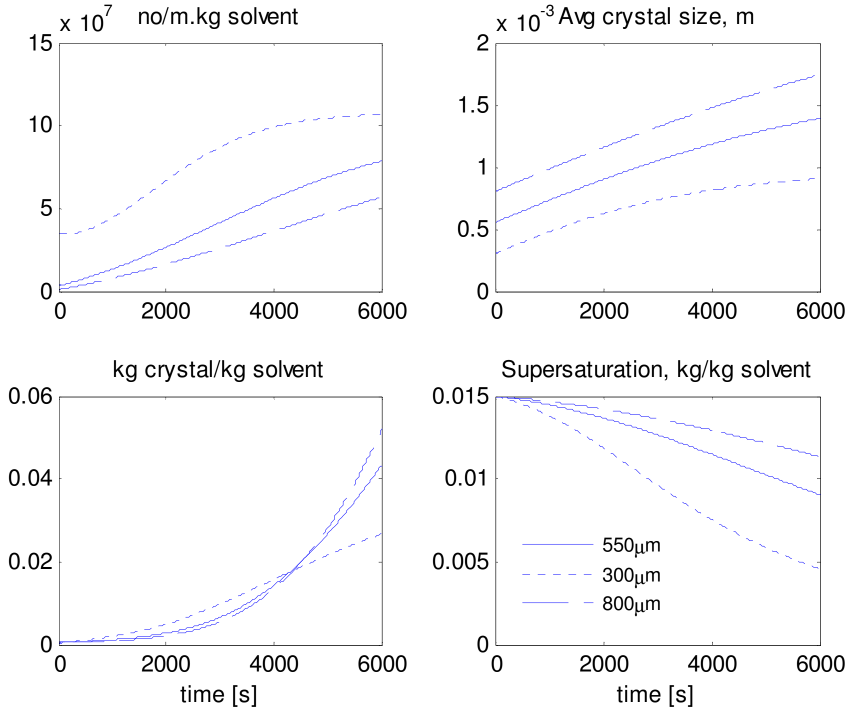

**Figure 3-9. Sensitivity analysis of seed sizes(300, 550 and 800 μm) on number of crystals, crystal size, suspension density and supersaturation**

Sensitivity analysis of the seed size is shown in Figure 3-9 and illustrates that a different number of seed crystals can be produced when the same mass of seeds are used. The smaller seeds mass contains more crystals than the bigger seeds, and so it will have a larger crystal surface area and consequently provide faster desupersaturation. Considering the average size, seed crystals at different sizes exhibit linear growth initially before establishing steady state conditions when no more solute can be used for crystal growth. The suspension density produced from the smallest crystals is 50% less than for the base case.

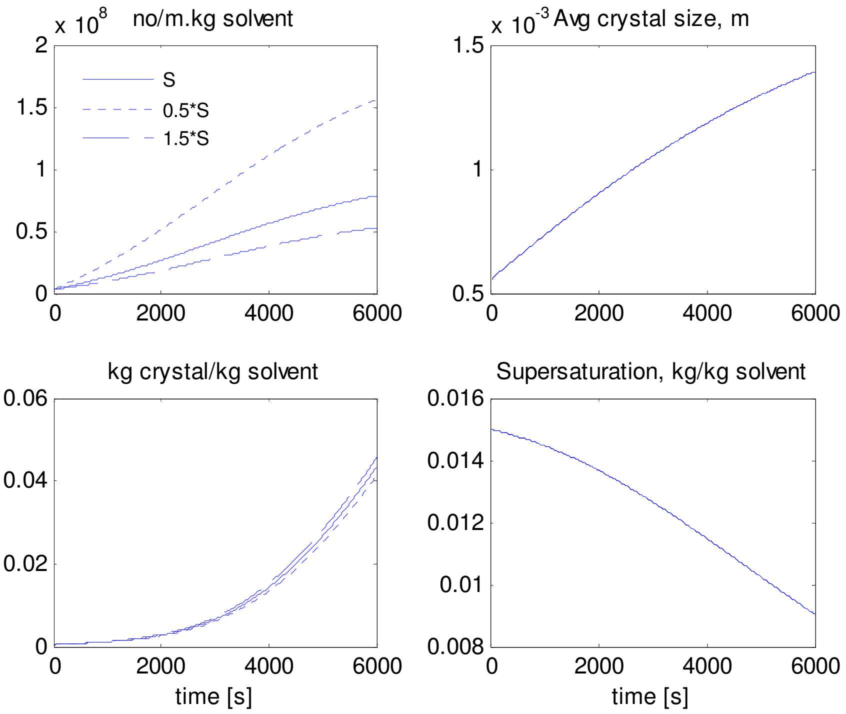

**Figure 3-10. Sensitivity analysis of solvent capacity (S ± 50%) on number of crystals, crystal size, suspension density and supersaturation**

For solvent capacity changes up to ±50%, the results in Figure 3-10 show that only the number of crystals is affected. The other variables such as crystal size, suspension density and supersaturation are not sensitive to changes in the solvent capacity. The reason is that the definition of the number of crystals is calculated on the basis of amount of solvent and hence the less solvent used, the more crystals are produced.

### *3.6.2. Semi-batch reactive crystalliser*

- **Problem definition**

  This reactive crystalliser model predicts the concentration changes of reactants and products over time with chemical reaction, and also calculates crystallisation process data such as number of crystals, average size, and the suspension density. The sensitivity of the model is then determined in relation to the reaction kinetics, nucleation and growth kinetics, reactant flow rate, and the initial concentration of reactant.

- **Controlling factors**
  - Chemical reaction, homogenous with first-order reaction kinetics with respect to each of the reacting components:

    $$\boldsymbol{A} + \boldsymbol{B} \rightarrow \boldsymbol{C}$$

  - Precipitation of the solid product C due to supersaturation follows the conventional power law for nucleation and growth.

- **Data**
  - Vessel capacity 200 kg
  - Crystal density, $\rho$ = 2000 kg/m$^3$
  - Batch time, $\tau\ [s]$ = 10000 seconds

- **Process model**

  ✓ **Assumptions**
  - Isothermal
  - Perfect mixing conditions
  - Constant crystal density
  - Constant solubility

  ✓ **Main equations**

$$\frac{dm}{dt} = \frac{d(\rho V)}{dt} = F_A + F_B$$

$$\frac{d(C_A.V)}{dt} = -r\,V + \frac{F_A}{M_{r,A}}$$

$$\frac{d(C_B.V)}{dt} = -r\,V + \frac{F_B}{M_{r,B}}$$

$$\frac{d(C_C.V)}{dt} = r\,V + \frac{k_v\,\rho_c}{M_{r,C}}\frac{d(\mu_3\,V)}{dt}$$

$$\frac{\partial n}{\partial t} + G\frac{\partial n}{\partial L} = 0$$

$$\frac{d\mu_0}{dt} = B$$

$$\frac{d\mu_1}{dt} = \mu_0\, G$$

$$\frac{d\mu_2}{dt} = 2\,\mu_1\, G$$

$$\frac{d\mu_3}{dt} = 3\,\mu_2\, G$$

$$\frac{dL}{dt} = G$$

✓ **Consecutive equations**

$$r = k_r C_A^m C_B^n$$

$$B = k_b \Delta c^b$$

$$G = \frac{dL}{dt} = k_g \Delta c^g$$

✓ **Variables**

| | |
|---|---|
| t | time [s] |
| $n$ | population density [number of crystals/m kg solvent] |
| $b$ | nucleation order [-] |
| $B$ | nucleation rate [number of crystals/ kg solvent s] |
| $C_C$ | concentration of solute [kmol/kg]] |
| $C_C *$ | saturation concentration of a large crystal with flat surface [kmol/kg] |
| $\Delta c$ | supersaturation [kg solute/kg solvent or kg hydrate/ kg solvent] |
| $F$ | mass flow rate of stream [kg/s] |
| $g$ | growth order [-] |
| $G$ | overall linear growth rate [m $s^{-1}$] |
| $i$ | relative kinetic order = b/g [-] |
| $k$ | reaction rate coefficient [kg/kmol s] |
| $k_b$ | nucleation rate coefficient [number of crystals/kg s $(kg/kg)^b$ $(kg/kg)^j$] |
| $k_g$ | linear growth rate coefficient [m/s $(kg/kg)^g$] |

| | |
|---|---|
| $k_v$ | volume shape factor |
| $k_a$ | surface area shape factor |
| $K_R$ | relative rate coefficient [number of crystals/ kg s $(m/s)^i$ $(kg/kg)^j$ ] |
| $L$ | crystal size [m] |
| $\Delta L$ | difference between successive sieve sizes [m] |
| $M_T$ | magma(suspension) density [kg/ kg solvent] |
| $N$ | total number of crystals [number of crystals/kg] |
| $n^0$ | nuclei population density (at L=0) [number of crystals/ m kg solvent] |
| $r$ | reaction rate [kmol/s kg] |
| $m$ | solvent capacity of the crystalliser [kg] |
| $Mc$ | molecular weight of crystal [kg/kmol] |

- ✓ **Initial conditions**

$$m = m_0, \quad C_A = C_{A0}, \quad C_B = C_{B0}, \quad C_C = C_{C0}$$

$\mu_j = 0$, where $j = 0,1,2,3$

$$n(0, L) = 0$$

$$L = 0$$

- ✓ **Boundary conditions**

$$n(t, 0) = n^0 = B/G = K_R M_T^j G^{i-1}$$

- ✓ **Parameters (Tavare et al. 1990)**

| | |
|---|---|
| M$c$ [kg/kmol] | 100 |
| $C_C{}^*$ [kmol/kg solvent] | $10^{-4}$ |
| $C_{A0}$, [kmol/kg solvent] | $10^{-3}$ |
| $F_A = F_B$ [kg/min] | 1 |
| $k_v$ [-] | 0.52 |
| $k_a$ [-] | 3.68 |
| k [kg/kmol s] | 1 |
| $g$[-] | 1.5 |
| $k_g$[m/s$(mol/kg)^{1.5}$] | $7.9 \times 10^{-8}$ |
| $b$ [-] | 4.5 |
| $k_b$ [number of crystals/kg s $(kg/kg)^4$] | $3.1 \times 10^{10}$ |
| $i$ [-] | 3.0 |
| $K_R$ [number of crystals/(kg s (kg/kg) $(m/s)^2$] | $6.4 \times 10^{31}$ |

- **Results**

The simulation results for the batch mode of operation are presented in Figure 3-11. The profiles of moles of A, moles of C, total number of crystals, and total mass of crystals are shown a function of time. As shown, the moles of reactant A decreases over time from 0.2 kmol to 0.1 kmol, while C increases to approx. 0.057 kmol at 4500 seconds and then gradually decreases to 0.025 kmol. Initially only chemical reaction occurs, this continues until product C has sufficient saturation to initiate the crystallisation processes. The crystallisation processes consist of nucleation and crystal growth. From Figure 3-11, it can be seen that initially no nuclei are produced and after a certain time then there is an exponential rate of crystal production, followed by subsequent crystal growth to approx. 7.5 kg of crystal mass at the end of the batch cycle.

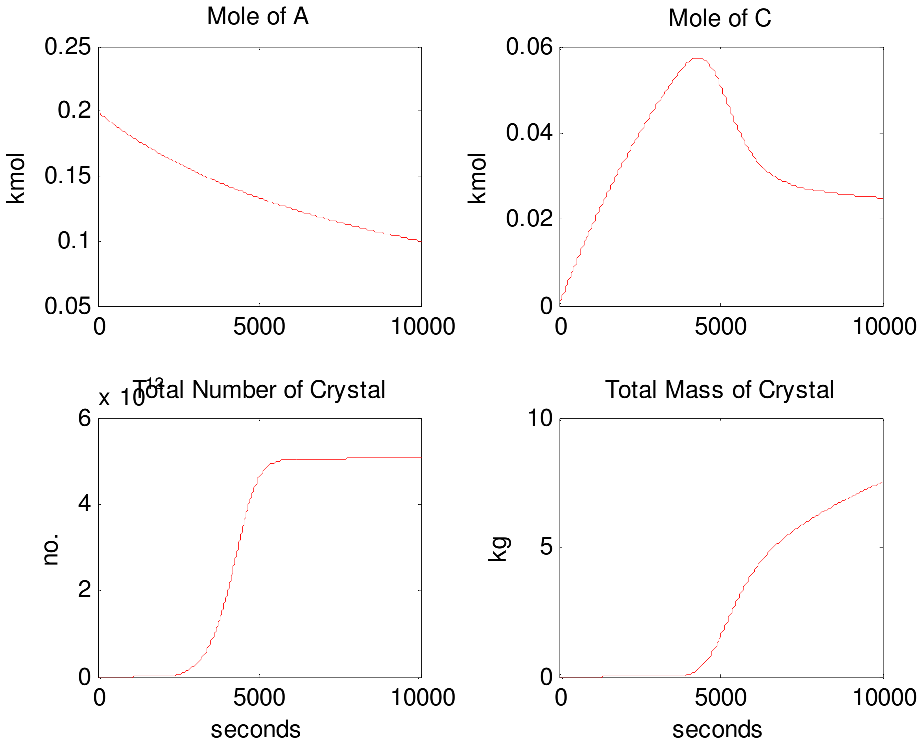

**Figure 3-11. Simulation results for 10000 seconds in batch operation mode (k=1 kg/kmol s]**

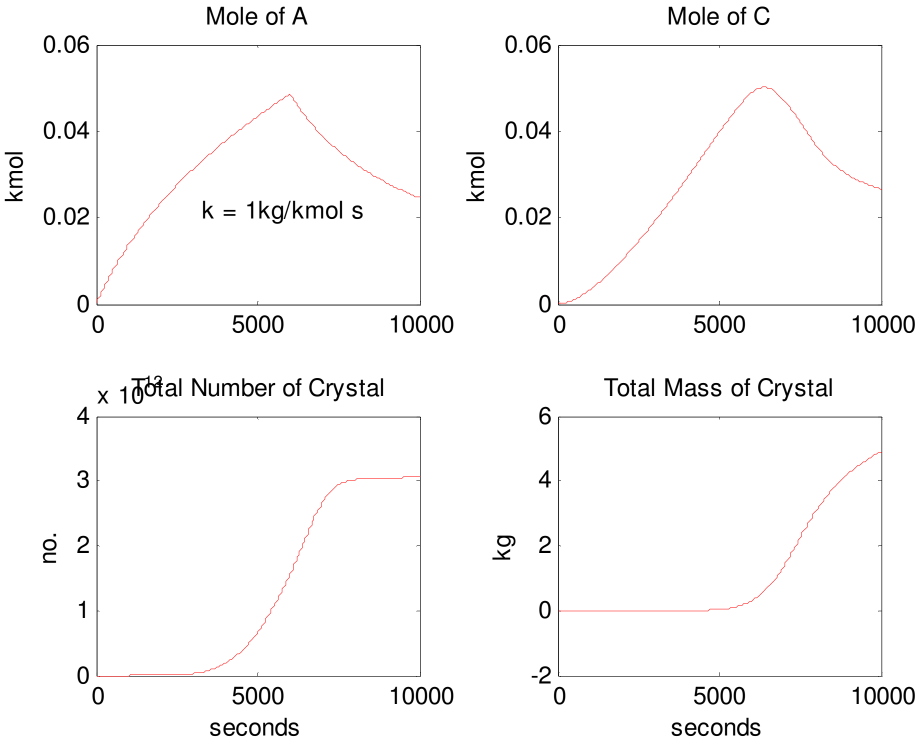

**Figure 3-12. Simulation results of semi-batch reactive crystalliser for 10000 seconds (k=1 kg/kmol s]**

Now compare the results of semi-batch to batch operation, where a dual-feed constant-flow system of A and B is introduced into an empty reactor until the final crystalliser capacity of 200 kg is achieved. The profiles of reactant A (kmol) in the batch and semi-batch system are different since the semi-batch reactor is initially empty. The moles of A increases during the feed time, and the reaction takes place as seen from the profile of moles of C in Figure 3-12. The rate of production of C is slightly lower in the semi-batch mode. The combine flow rate of 2 kg/min will require 6000 seconds to reach the set capacity of 200 kg. From the mole C profile in Figure 3-12, it can be seen that approx. 1000 seconds after the feed stops, then the moles of C start to decrease due to the crystallisation occurring. The C-solute already has sufficient supersaturation to drive the nucleation process, followed by crystal growth of C. The total number of crystals produced in this mode is significantly less than in the batch mode due to a lower degree of supersaturation, and hence a lower yield of crystals due to the smaller growth rate.

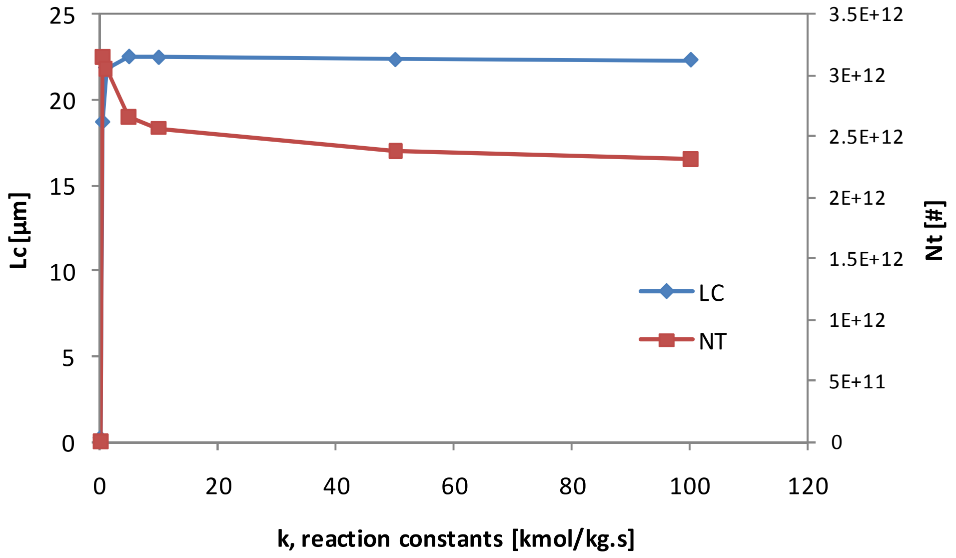

**Figure 3-13. Sensitivity analysis of reaction rate coefficient (k) on average size (Lc) and number of crystals (Nt)**

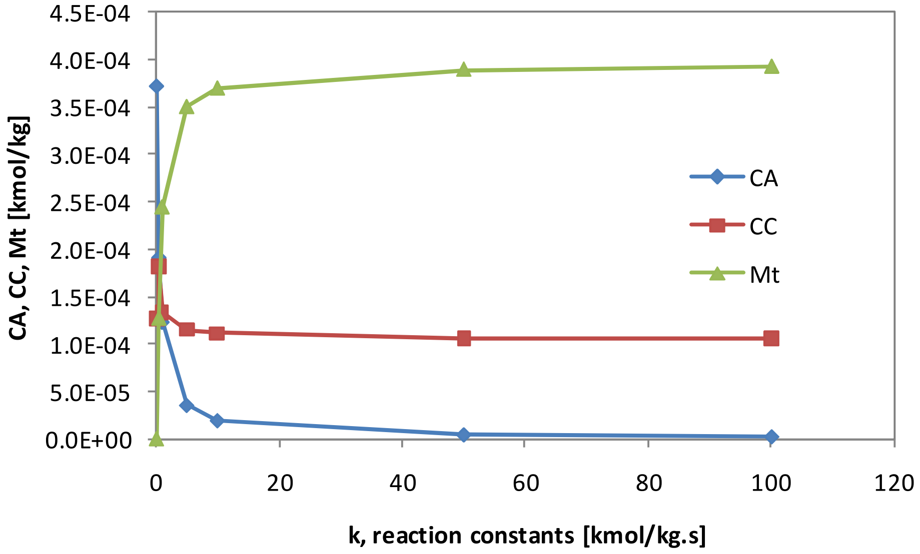

**Figure 3-14. Sensitivity analysis of reaction rate coefficient (k) on $C_A$ $C_C$ and suspension density ($M_T$)**

The main difference with reactive crystallisation compared to non-reactive crystallisation processes is that at least one chemical reaction occurs. The reaction kinetics may have great impact on crystallisation mechanisms which occur during, and after, the reaction takes place. Therefore, sensitivity analyses on the reaction rate coefficient (k) are performed for its effects on the solute-side (reactants and products concentrations and yield) and on the solid-side results such as average size and total number of crystals. When the reaction rate constant (k) is reduced from 1.0 to 0.1, the reaction rate is too slow for the generation of solute C. Therefore, almost no crystals are formed, or they are created and only grow to a very small size. As shown in Figure 3-13, the k value greater than 1.0 will have no significant effect on the average size, and only lowers the number of crystals by 26% from the maximum total number of crystals at $k = 1$k = 1. In Figure 3-14, the effects of reaction rate constant on the solute-side can only be seen up to $k = 10$k = 10; above that value then the effects are not significant.

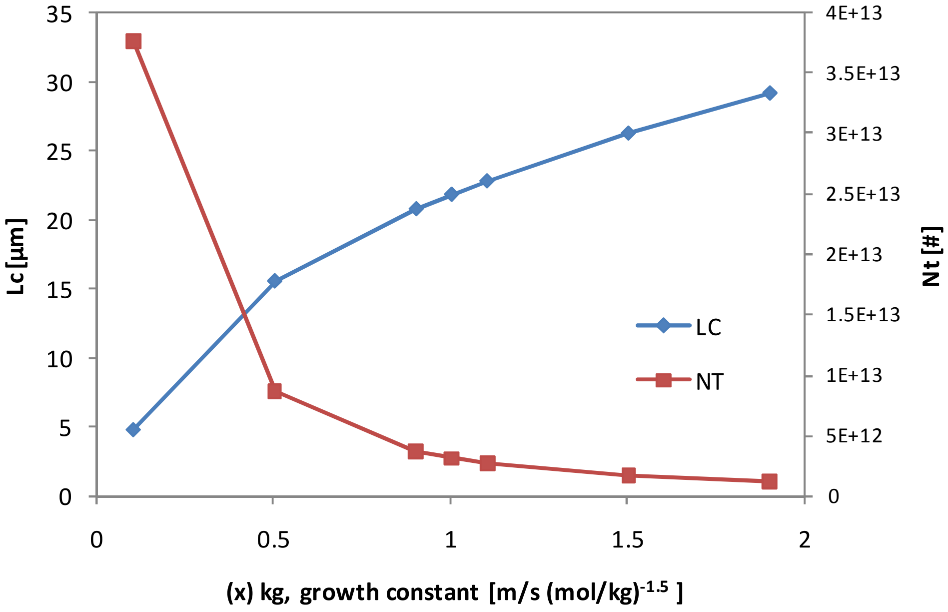

**Figure 3-15. Sensitivity analysis of growth rate constant ($k_g$) on average size (Lc) and number of crystals (Nt)**

The effects of growth rate constant ($k_g$) on the average size and number of crystals were studied and the results are shown in Figure 3-15. The growth rate constant will not have any impact on the consumption of reactant because it is only affected by the chemical reaction; therefore, the effects on its solute-side and solid-side are not reported here. The sensitivity range for $k_g$ is 10% to 190% from its original value, as expected the results show that average size increases as the value of $k_g$ increases. The reason is simply because the $k_g$ value, which is the crystal growth, directly affects the average crystal size. Alternatively, the number of crystals decreases when $k_g$ is increased. The explanation is that the rate of nucleation decreases as the growth rate dominates, thus the birth rate of the crystals declines.

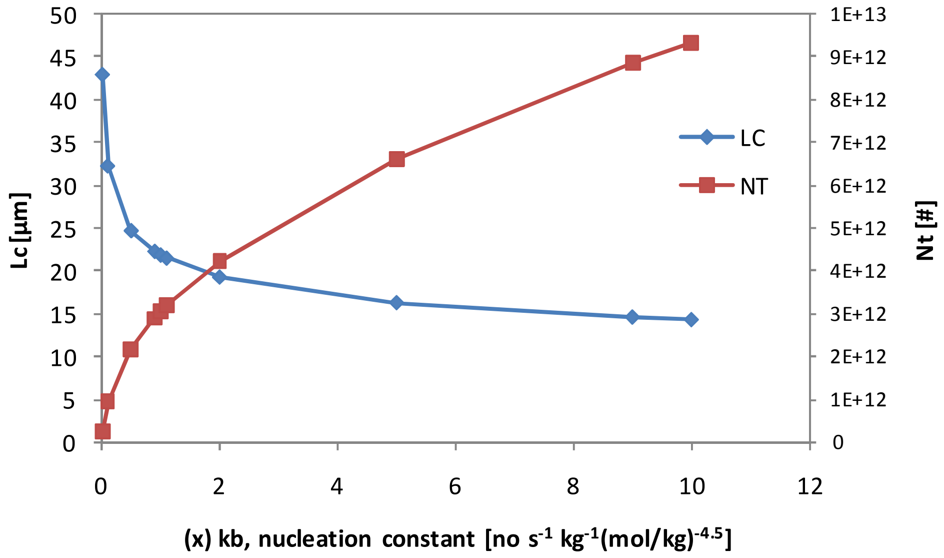

**Figure 3-16. Sensitivity analysis of nucleation rate constant ($k_b$) on average size (Lc) and number of crystals (Nt)**

Figure 3-16 illustrates a different scenario. The sensitivity range for this analysis is 10% to 1000% from the original value. The total number of crystals increased, and the average size decreased, when the nucleation rate constant increased. This is because the solution supersaturation has more effect on the creation of crystals than on their subsequent growth. The nucleation rate becomes the controlling rate in the crystallisation steps. The growth rate is insufficient for cultivating the large number of created nuclei.

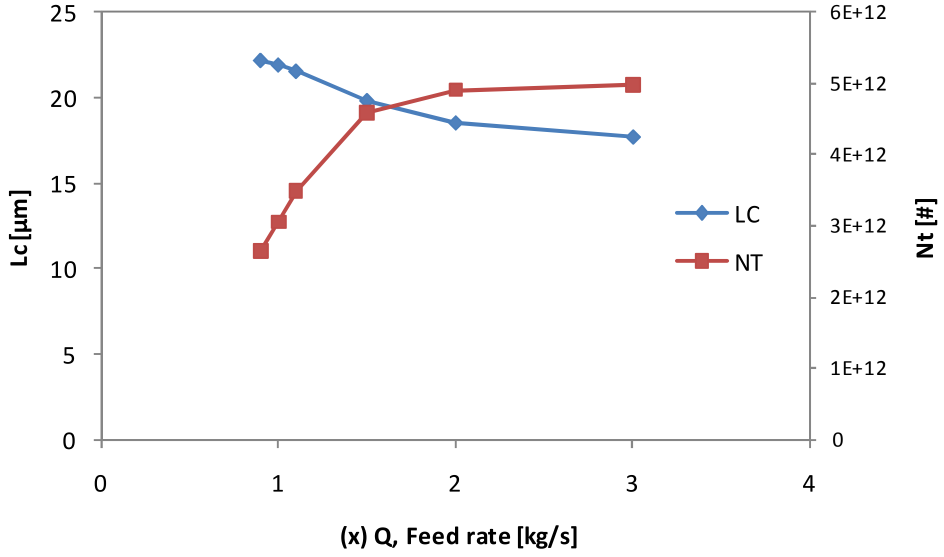

**Figure 3-17. Sensitivity analysis of feed flow rate (Q) on average size (Lc) and number of crystals (Nt)**

The sensitivity of feed flow rate (F) on average size and number of crystals was conducted over the range 100-300% from the basis value. Reaction increases with feed rate and more solute is produced and higher a higher degree of supersaturation is achieved. Therefore, the result show an increased number of crystals and smaller average size of crystal product.

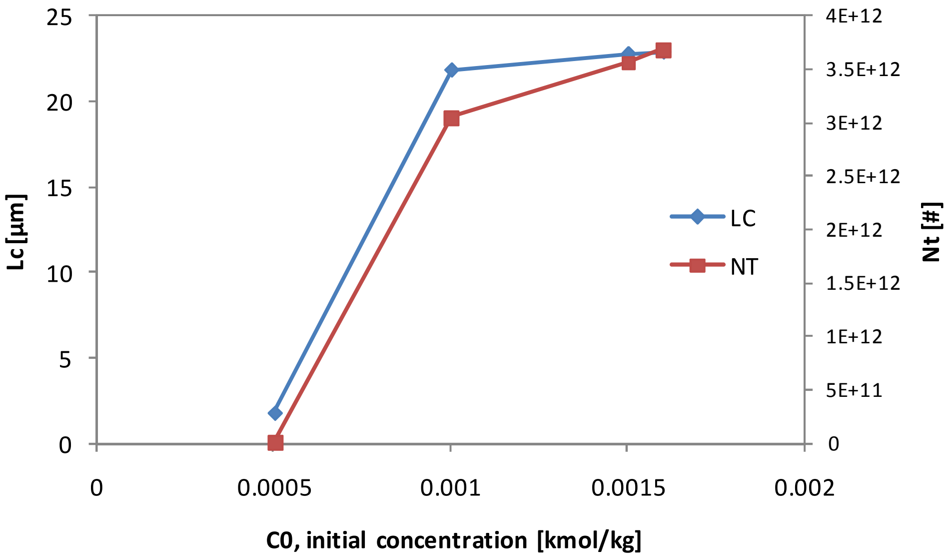

**Figure 3-18. Sensitivity analysis of initial concentration of reactants ($C_0$) on average size (Lc) and number of crystals (Nt)**

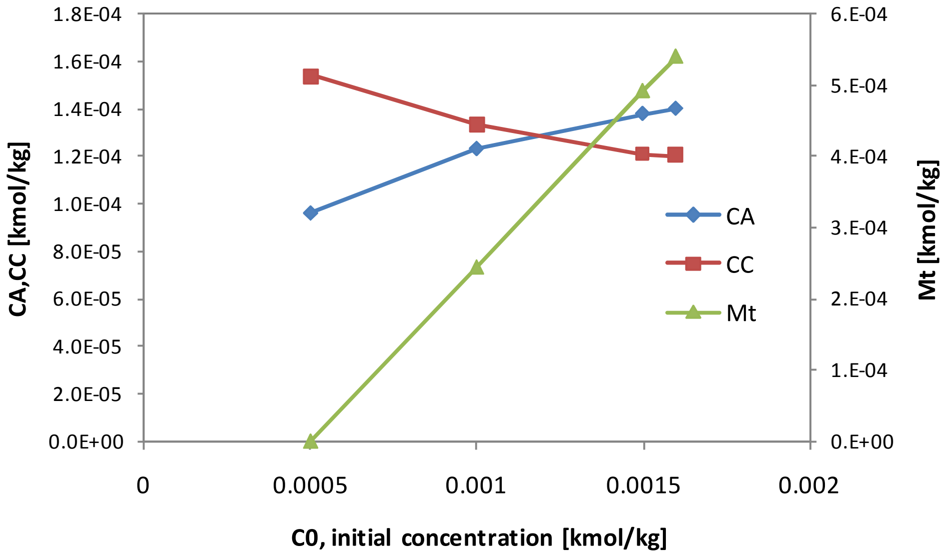

**Figure 3-19. Sensitivity analysis of initial concentration of reactants ($C_0$) on $C_A$ $C_C$ and suspension density ($M_T$)**

The sensitivity analysis of the initial concentration of reactants was conducted over the range of ±50% from the initial base concentration as shown in Figure 3-19. It appears that the profiles of the final product concentration are almost linearly related to the initial concentration as a sensitivity variable. The higher the initial concentration, then the higher the concentration of unused reactant and less product was produced. The problem with a lower initial concentration is that this results in a very low suspension density. This may mean that the degree of supersaturation does not reach the value required to produce crystals out of solution. It can also be seen from the total number of crystals in Figure 3-18.

## *3.7 Summary*

A systematic modelling approach has been developed and discussed for crystallisation and also a combination of reactive crystallisation processes. The similarities and major distinctions between the two processes are illustrated in two specific case studies. Key process variables which will affect the crystallisation products have been identified by sensitivity analysis and will be used for experimentation setup and model validation.

## *3.8 References*

Buchanan, G. H. and G. B. Winner (1920). The solubility of mono-and diammonium phosphate. *Industrial & Engineering Chemistry*, 12(5), 448-451.

Dahlstrom, D. A., R. C. Bennet, R. C. Emmett, P. Harriot, T. Laros, W. Leung, C. McCleary, S. A. Miller, B. Morey, J. Y. Oldshue, G. Priday, C. E. Silverblatt, J. S. Slottee, J. C. Smith and D. B. Todd (1999). Liquid-solid operations and equipment. Perry's chemical engineers' handbook. R. H. Perry, D. W. Green and J. O. Maloney. New York, McGraw-Hill**:** 18-23.

Hounslow, M. J. (1990). A discretized population balance for continuous systems at steady-state. *AIChE Journal*, 36, 106-116.

Hounslow, M. J., R. L. Ryall and V. R. Marshall (1988). A discretized population balance for nucleation, growth and aggregation. *AIChE Journal*, 34, 1821-1832.

Hulburt, H. M. and S. Katz (1964). Some problems in particle technology : A statistical mechanical formulation. *Chemical Engineering Science*, 19(8), 555-574.

Randolph, A. D. and M. A. Larson (1988). *Theory of particulate processes : Analysis and techniques of continuous crystallization*. Acadmic Press, San Diego.

Ross, W. H., A. R. Merz and K. D. Jacob (1929). Preparation and properties of the ammonium phosphates. *Industrial & Engineering Chemistry*, 21(3), 286-289.

Seidell, A. and W. F. Linke (1952). *Solubilities of inorganic and organic compounds*. Van Nostrand, New York.

Shilling, R. L., K. J. Bell, P. M. Bernhagen, T. M. Flynn, V. M. Goldschimdt, P. S. Hrnjak, F. C. Standiford and K. D. Timmerhaus (1999). Thermal design of heat transfer equipment. Perry's chemical engineers' handbook. R. H. Perry, D. W. Green and J. O. Maloney. New York, McGraw-Hill**:** 11-25.

Stokka, P. (1985). Three component phase diagram for map, dap and water. Internal Report. Porsgrunn, Norsk Hydro.

Tavare, N. S. (1995). *Industrial crystallization: Process simulation analysis and design*. Plenum Press, New York.

Tavare, N. S. and J. Garside (1986). Simultaneous estimation of crystal nucleation and growth kinetics from batch experiments. *Chemical Engineering Research and Design*, 64(a), 109-118.

Tavare, N. S. and J. Garside (1990). Simulation of reactive precipitation in a semi-batch crystallizer. *Chemical Engineering Research and Design*, 68(a), 115-122.

# 4. *Wavelet-based Methods as Alternative Solutions for Crystallisation Process*

## 4.1 *Wavelet Applications*

The applicability of the wavelet transform technique is evident from the large number of science and engineering situations in which it has been applied. This technique has been applied in signal and image processing, image or data compression, de-noising, turbulence study, astronomy, acoustics, speech recognition, human vision, numerical analysis and computation. For numerical computations, the wavelet technique is used to solve the partial differential equations.

In chemical engineering modelling related to design, optimisation, and for control purposes, typically requires the solution of partial differential equations (PDEs). These equations may not have analytical solutions and therefore wavelet-based numerical methods can be applied.

Many applications utilise partial differential equations in their mathematical model and face challenges related to the accuracy of the solution, the efficiency (time), and the increased complexity of the problem. Therefore, it is a significant challenge to develop and implement new numerical techniques. Wavelets offer significant advantages, such as:

- ✓ Wavelet can track the moving steep profile.
- ✓ Wavelet can compress the matrices so the computation is lighter and faster.
- ✓ Wavelet can treat non-linear and integral terms.
- ✓ Wavelet can decompose the functions in order to speed up calculation.
- ✓ Wavelet has capability to present functions at different levels of resolution.

- ✓ Wavelet can easily treat the PDEs boundary conditions.

Daubechies (1992) predicted, in her famous textbook “Ten lectures on wavelets”, that a wavelet-based software package to solve partial differential equations would become commercially available. The prediction has not yet been realised and the only software available is for the Wavelet Toolbox in MATLAB®, but it cannot be used for solution of any partial differential equation. This presents a challenge to the author of this research to contribute significantly in this area, especially for chemical engineering applications.

## 4.2 *Wavelet Methods in Numerical Analysis*

After the success with the wavelet method in different applications, wavelets provide an alternative approach in numerical analysis, in particular to solve PDEs problems. PDEs solutions often contain nonlinear behaviour such as formation of shock and turbulence, and this type of solution can be closely represented and systematically approached using wavelets. Depending upon the methodology selected, wavelet techniques used to solve partial differential equations can be classified into several categories, e.g. method based on scaling functions expansions, method based on wavelet expansion, finite differences wavelet method, and several other methods as briefly described below and illustrated in Figure 4-1.

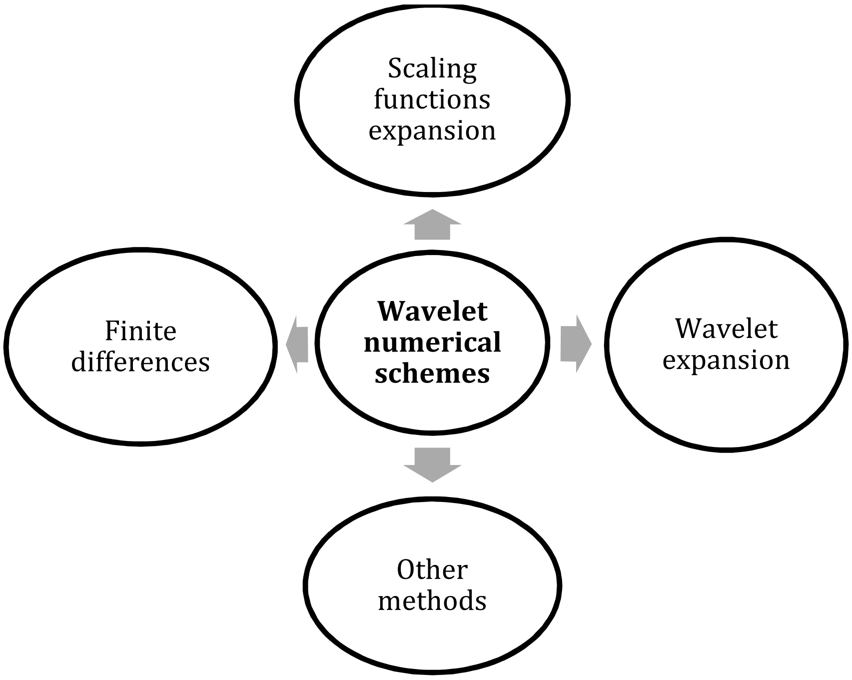

**Figure 4-1. Classification of wavelet-based numerical methods**

1. **Methods based on scaling function expansions**

   Scaling function is expanded at a specified level of J, and is solved using a Galerkin approach. These methods are not adaptive since they do not exploit wavelet compression properties.

2. **Method based on wavelet expansions**

   Wavelet function is expanded and wavelet compression characteristic is applied to the solution, differential operator, or both of them.

   Methods 1 and 2 are known as projection methods.

3. **Wavelets and finite differences**

   Wavelets are used to derive adaptive finite difference methods instead of expanding the solution. The wavelet transform is used to determine where the finite difference grid must be refined or made coarse in order to obtain an optimal solution.

4. **Other methods**

   There several approaches that use wavelets in ways that do not conform to any of the above methods, e.g. operator wavelets, anti-derivatives of wavelets, the method of travelling wavelets, and wavelets preconditioning.

There is a significant number of publications describing the development of wavelet theory (Daubechies 1988; Qian et al. 1993; Bertoluzza et al. 1994; Bertoluzza et al. 1996; Vasilyev et al. 1996; Hsiao 1997), and the wavelet method is now one of the accepted applied numerical methods used to solve an integral-partial differential population balance equation. Wavelet transforms provide information about a function with respect to scale and location, in contrast to Fourier transforms which provide information based on the frequency only. The first attempt to implement the wavelet method in a chemical engineering computational application was reported by Chen et al. (1996) who developed, and applied, the Wavelet-Galerkin (WG) method for breakage mechanisms in population balance equations for a continuous crystalliser system. The WG methods are compactly supported in the physical space, and orthogonal under translation and dilatation. The expansion coefficients in WG methods are not in the physical space. Partial differential equations are generally specified as the equations in the physical space and, therefore, there is no strong reason to use WG methods in these circumstances when other methods can easily be implemented directly in the physical space. Treatment of the boundary condition is another weakness with WG methods as only periodic boundary condition problems can be accurately solved by WG methods. However, even the very simple, non-periodic boundary condition cannot be easily solved with WG methods. A second problem in using WG methods is the evaluation of nonlinear terms. The WG methods cannot represent the nonlinear term such as exponential functions.

Jameson (1998) developed finite-difference wavelet-based methods called Wavelet Optimised Finite Difference (WOFD) for computing partial differential equations. In the first WOFD method, wavelets are only used in grid refinement. The WOFD method comprises two elements: the grid generation mechanism; and the differentiation mechanism. First, the wavelet analysis is carried out to find the local variation of the solution, and arrange the sparse grid in the low variation regions and place the finer grid in the high variation regions. Second, the finite difference scheme is used to evaluate the function on the generated grid. Later developments were the wavelet optimised finite difference version 2 (WOFD2) and the wavelet optimised finite difference-adaptive high order (WOFD-AHO) as extensions of the original WOFD (Jameson et al. 2000). In these two later methods, wavelet analysis was further extended for use in construction of grid generation as well as order selection for the difference operator used in the grid. A practical case study in combustion modelling was performed using this WOFD method, and it was found that the result was consistent with the theory.

Liu and Cameron (2001) developed and applied Wavelet Orthogonal Collocation (WOC) methods for a chromatographic (Liu et al. 2001) and population balance (Liu et al. 2001) application. They developed wavelet interpolation functions based on the standard WOC and adaptive WOC (Liu et al. 2003) in order to solve population balance problems. The main improvements with WOC methods compared to WG methods are the ability to treat nonlinear terms confidently, and ability to treat both fixed and periodic boundary condition problems. They used the collocation scheme directly in the physical space, so that no extra computation is required. However, a straightforward WOC method will not have the same rate of convergence for the differentiation operator as the WG method, this is due to the super-convergence which occurs with a Galerkin approach. The main advantages of using this method are: efficiency in computation time and structure; effectiveness in overcoming the numerical diffusion and stability problems; and easy evaluation of integral and derivative terms appearing in the equations. Those three methods can be compared based on their basis of calculation, boundary condition treatment, non-linearity handling, adaptive characteristic and computation capacity. The summary of comparison is described in Table 4-1.

**Table 4-1. Comparative components of three wavelet-based methods**

[WG: Wavelet Galerkin, WOFD: Wavelet Optimised Finite Difference and WOC: Wavelet Orthogonal Collocation]

| *Comparative components* | ***WG*** | ***WOFD*** | ***WOC*** |
|---|---|---|---|
| *Basis calculation* | Wavelet | **Physical** | **Physical** |
| *Boundary condition treatment* | Difficult | **Easy** | Moderate |
| *Hnadling non-linearity* | Difficult | **Moderate** | **Moderate** |
| *Adaptive scheme* | No | **Yes** | **Yes** |
| *Computation capacity* | Fixed | Fixed | **Reduced** |

## 4.3 *Wavelet Definitions and Transformation*

Wavelet concepts originate from the Fourier transform. Fourier transform is a mathematical procedure to decompose a function into its compositional frequencies. Fourier transforms a time domain signal into Fourier coefficients in a frequency domain. It is very difficult to determine the specific time of the signal if only the frequencies are known. However, wavelets can transform the signal into both time and frequency domains. The concept of Fourier transform is well know and generally accepted by engineers. Fourier coefficients have a physical meaning, while wavelet coefficients do not and hence, it is harder for most engineers to use wavelet transform. Fourier transform is suited to very regular periodic signals, while wavelets are suited to highly non-stationary signals with sudden peaks or discontinuities.

The wavelet transform represents general functions in terms of simple, fixed building blocks at different scales or resolutions and specified positions. This characteristic allows investigation of both the large-scale and the small-scale features of a function simultaneously. Therefore, the wavelet allows us to see both “the forest and the trees”. These building blocks, which are actually a family of wavelets, are generated from a single fixed function, called the “mother wavelet”, by translation and dilatation (scaling) operations.

The conventional basis of trigonometric functions in Fourier transforms have infinite support, while wavelets have compact support. Therefore wavelets are able to approximate a function not by cancellation, but by locations. The multi-resolution properties in wavelets are able to represent the integral, non-linear, and differential terms, which are being solved numerically (Motard et al. 1994).

The term wavelet is used to describe a spatially localised function. 'Localised' means that the wavelet has compact support in a certain interval, and outside that interval the wavelet will vanish exponentially. In this research, we will only consider the wavelet defined by Daubechies which are supported on $[0, D-1]$, where $D$ is the number of wavelet coefficients. The basic scaling function, $\phi$, and the mother wavelet, $\psi$, are expressed by a two-scale relation using a set of $D$ coefficients as follow: where $\phi(0) = \phi(D-1) = 0$

$$\phi(x) = \sum_{k=0}^{D-1} a_k \phi(2x-k) \tag{4-1}$$

$$\psi(x) = \sum_{k=2-D}^{1} (-1)^k a_{1-k} \phi(2x-k) \tag{4-2}$$

The support for the scaling function is in the interval $[0, D-1]$, and for the mother wavelet in the interval $[1-D/2, D/2]$. The coefficients $a_k$ appearing in the scaling function are called the wavelet filter coefficients, where $k = 0,1, \dots, D-1$. The translations and dilatations of level $J$ for $\phi(x)$ and $\psi(x)$ are defined as:

$$\phi_{J,k}(x) = 2^{J/2} \phi(2^J x - k) \tag{4-3}$$

$$\psi_{J,k}(x) = 2^{J/2} \psi(2^J x - k) \tag{4-4}$$

The simplest form of Daubechies wavelet, when $D = 2$, is a Haar wavelet. The fundamental supports of the Haar wavelet scaling function and mother wavelet on the compact support $[0,1]$ and $[0,1]$ respectively, are shown in Figure 4-2.

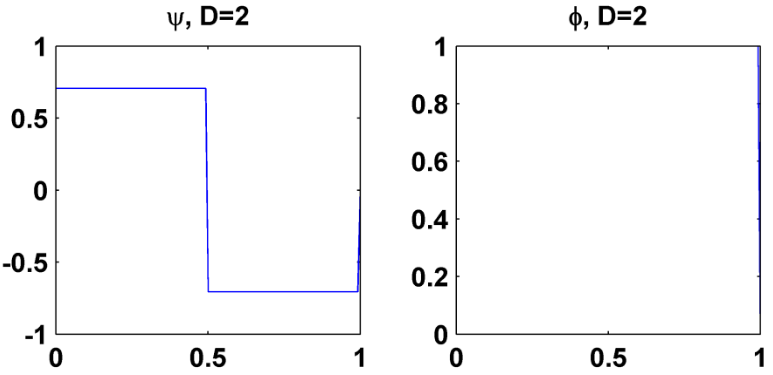

**Figure 4-2. Wavelet (left) and scaling functions (right) of Haar wavelet (D=2).**

The scaling function and the mother wavelet for Daubechies wavelet when $D = 4, 6, 8, 10$ on their compact support is illustrated in Figure 4-3 and Figure 4-4.

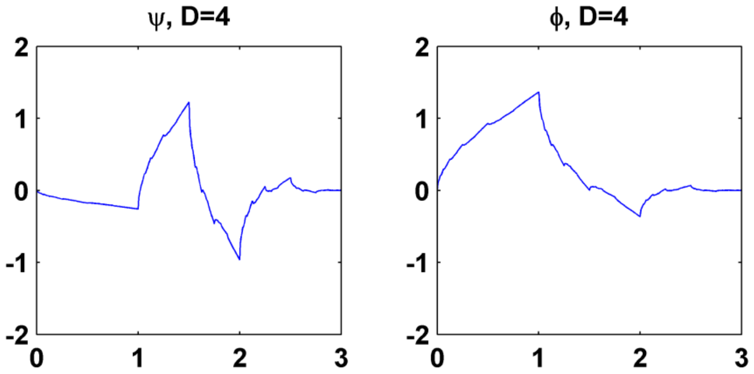

**Figure 4-3. Wavelet (left) and scaling functions (right) for Daubechies wavelet (D = 4)**

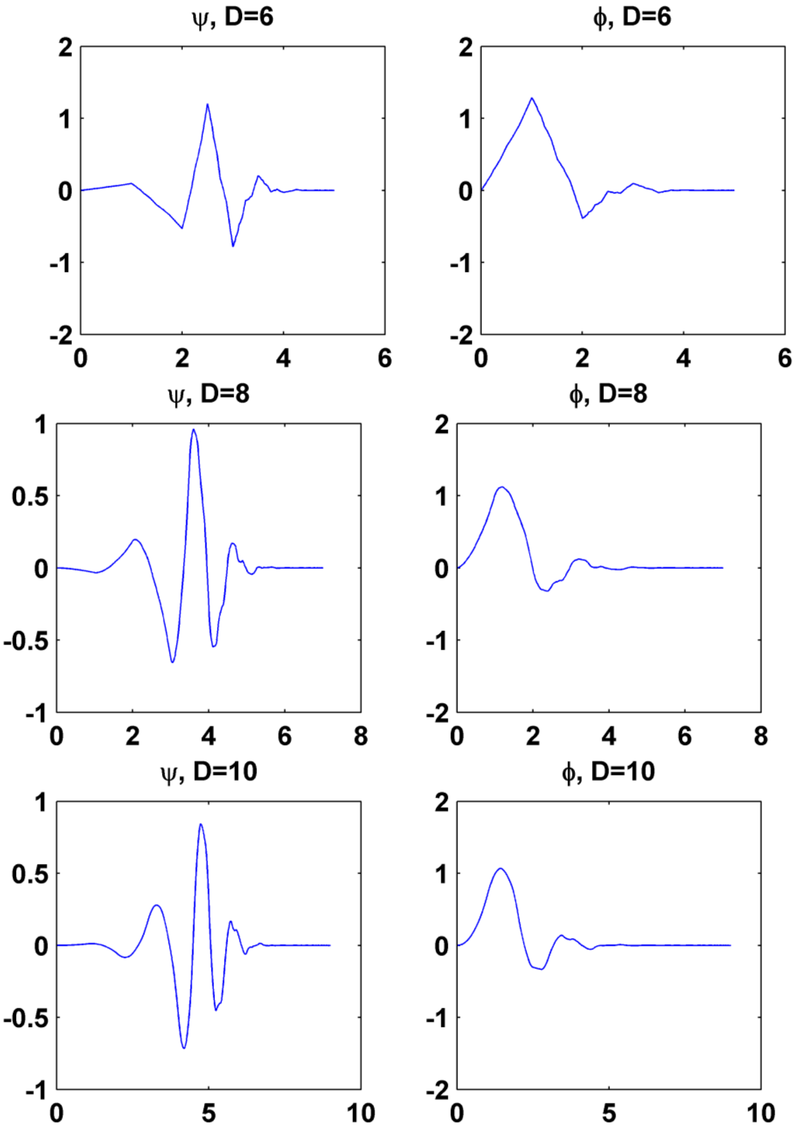

**Figure 4-4. Wavelet (left) and scaling functions (right) for Daubechies wavelet (D = 6, 8, and 10)**

The Daubechies wavelet filter coefficients uniquely satisfy the following conditions:

$$\sum_{k=0}^{D-1} a_k = 2 \tag{4-5}$$

$$\sum_{k=0}^{D-1} a_k a_{k-m} = \delta_{0,m} \tag{4-6}$$

$$\sum_{k=2-D}^{1}(-1)^k a_{1-k}a_{k-2m} = 0 \qquad \text{for integer } m \tag{4-7}$$

$$\sum_{k=0}^{D-1}(-1)^k k^m a_k = 0, \quad m = 0,1,\ldots,\frac{D}{2}-1 \tag{4-8}$$

where $\delta_{0,m}$ is the Kronecker delta function. Similarly, the constructed scaling function $\phi(x)$ and wavelet function $\psi(x)$ have the following properties:

$$\int_{-\infty}^{\infty}\phi(x)dx = 1 \tag{4-9}$$

$$\int_{-\infty}^{\infty}\phi(x-j)\phi(x-m)dx = \delta_{j,m} \tag{4-10}$$

$$\int_{-\infty}^{\infty}\phi(x-j)\psi(x-m)dx = 0 \qquad \text{for integer } m \tag{4-11}$$

$$\int_{-\infty}^{\infty}x^k\psi(x)\,dx = 0, \quad k = 0,1,\ldots D/2-1 \tag{4-12}$$

Since there are no explicit expressions available for computing the values of the scaling function $\phi(x)$ and the mother wavelet $\psi(x)$ at any point of $x$. The function values of $\phi(x)$ and $\psi(x)$ at the dyadic points $k/2^j$ for integer $j$ and $k$ can be computed from the two-scale relations of equations (4-1) and (4-2) provided those $\phi(1),\phi(2),\ldots,\phi(L-1)$ values have been obtained.

The scaling function $\phi(x)$ has the following property:

$$\sum_{l=-\infty}^{\infty}l^n\phi(x-l) = \sum_{j=0}^{n}(-1)^j\binom{n}{j}M_j^{\phi}x^{n-j}\ , n = 0,1,\ldots,D/2-1 \tag{4-13}$$

where $M_j^{\phi}$ is the $j^{th}$ moment of the $\phi(x)$, which is defined by the following equation:

$$M_j^{\phi} = \int_{-\infty}^{\infty}x^j\,\phi(x)dx \tag{4-14}$$

with the initial condition $M_0^{\phi} = 1$. If we define the $n^{th}$ derivative of the scaling function $\phi(x)$ by $\phi^{(n)}(x)$, then we have:

$$\phi^{(n)}(x) = \frac{d^n\phi(x)}{dx^n} = \frac{d}{dx}\phi^{(n-1)}\ , \phi^{(0)} = \phi(x) \tag{4-15}$$

The compact support of $\phi^{(n)}(x)$ is the same as the compact support of $\phi(x)$. By substituting (4-13) and (4-14) gives:

$$\phi^{(n)}(x) = 2^n \sum_{k=0}^{L-1} a_k \phi^{(n)}(2x-k)\,,\ n = 0,1,\ldots,D/2-1 \tag{4-16}$$

## 4.4 *Wavelet-Galerkin (WG) Methods*

Chen et al. (1996) developed an algorithm to compute the connection coefficients for the wavelet Galerkin approximation, however, Zhang et al. (2007) discovered some fundamental errors in the work for which no correction has been published in the open literature. In order to complete the wavelet-Galerkin algorithms used to solve a partial differential problem, the relations given below are required. Details and applications of WG algorithms and its revisions can be found in the papers of Chen and Zhang (Chen et al. 1996; Chen et al. 1996; Zhang et al. 2007; Zhang et al. 2008).

- Evaluation of multiple integrals of $\phi(x)$:

$$\begin{aligned}\theta_n(x) &= \int_0^{y1}\int_0^{yn}\ldots\int_0^{y2}\phi(y_1)\,dy_1\ldots dy_{n-1}\,dy_n \\ &= \int \theta_{n-1}(y)\,dy\end{aligned} \tag{4-17}$$

- Computation the connection coefficients of wavelets over a bounded interval:
  - ✓ Evaluation of the integral product of $y^m$ and $\phi(y-k)$:

$$M_k^m(x) = \int_0^x y^m \phi(y-k)\,dy \tag{4-18}$$

  - ✓ Evaluation of the integral product of $\phi(x)$ and its derivative:

$$\Gamma_k^n(x) = \int \phi^{(n)}(y-k)\phi(y)\,dy \tag{4-19}$$

  - ✓ Evaluation of non-constant coefficients:

$$\Lambda_k^{m,n} = \int_0^x y^m \phi^{(n)}(y-k)\phi(y)\,dy \tag{4-20}$$

  - ✓ Evaluation of an integral-differential equation with non-constant coefficients:

$$\Upsilon_k^{m,n} = \int_0^x y^m \theta_n(y-k)\phi(y)\,dy \tag{4-21}$$

- ✓ Evaluation of non-linear differential equations:

$$\Omega_{j,k}^{m,n} = \int_0^x \phi(y)\phi^{(m)}(y-j)\phi^{(n)}(y-k)dy \tag{4-22}$$

## 4.5 *Wavelet Orthogonal Collocation (WOC) Method*

The WOC method was developed by Bertoluzza and Naldi (1996) and uses trial functions generated by autocorrelation of the usual compactly supported Daubechies scaling functions. The autocorrelation function $\theta$ verifies in simple form the equality $\theta(n) = \delta_{0n}$, and these generate a multi-resolution analysis. The function $\theta$ is called the autocorrelation function of $\phi$ and it verifies some properties which will be required in the following analysis. Due to the ortho-normality property of the set $\{\phi(x-k)\}$, the function $\theta$ verifies what is termed the interpolation property:

$$\theta(0) = \int \phi(x)\phi(x)dx = 1 \tag{4-23}$$

$$\theta(n) = \int \phi(x)\phi(x-n)dx = 0, \quad n \neq 0 \tag{4-24}$$

The derivatives of the function $\theta$ may be computed by differentiating the convolution product. In particular for $l$, $s$ integers, $0 \leq l \leq s$, for integer values of $x$ the function is:

$$\theta^{(s)}(k) = (-1)^{s-l} \int \left(\phi^{(l)}(x)\phi^{(s-l)}(x-k)\right) dx \tag{4-25}$$

The approximate solution of our problem will be a function of $u_j$ which will be written in terms of its value in the dyadic points $x_n$. The unknowns of our problem are the values of the approximate solution $u_j$ at the dyadic points $x_n = n2^{-j}$:

$$u_j = \sum_n u_j(x_n)\theta\left(2^j x - n\right) \tag{4-26}$$

The boundary condition will be imposed by simply setting $u_j(0) = a$ and $u_j(1) = b$. Since these operators are already in the physical space, then no extra computation is required for the passage between wavelet coefficients and physical space. By using the collocation scheme, no extra computation is required for the passage between wavelet coefficients and the physical space due to nonlinear operators.

Bertoluza and Naldi (1996) demonstrated that the wavelet method works well when applied to problems with Neumann type boundary condition, but when applied to the solution of a Dirichlet boundary problem it appears to generate instability. Therefore, suitable general boundary treatment is needed for most wavelet algorithms.

This method is based on the use of modified interpolating functions which are constructed in order to achieve an interpolating operator on the interval of the same accuracy as the one on the line. Consider a function $f(\cdot)$ on $[0,1]$, instead of the value of $f(\cdot)$ at $x_k, k=-L+1,\dots,-1$ and $k=2^j+1,\dots,2^j+L-1$, we may use values which are extrapolated from the values in those dyadic interval points to the interval $[0,1]$. More precisely we define $P_1$ and $P_2$ to be polynomials of degree $2M-1$ that interpolate $u(\cdot)$ at $x_0, x_1, \dots, x_{2M-1}$ and at $x_{2^j-2M+1}, x_{2^j-2M+3}, \dots, x_{2^j}$ respectively as follows:

$$P_1(x_k) = f(x_k), \quad k = 0,\dots,2M-1 \tag{4-27}$$

$$P_2(x_k) = f(x_k), \quad k = 2^j - 2M + 1,\dots,2^j \tag{4-28}$$

Thus:

$$P_1(x_n) = \sum_k a_{nk}\, f(x_k), \quad n = -L+1,\dots,-1, \quad k = 0,\dots,2M-1 \tag{4-29}$$

$$P_2(x_n) = \sum_k b_{nk}\, f(x_k), \quad n = 2^j+1,\dots,2^j, \quad k = 2^j - 2M + 1,\dots,2^j \tag{4-30}$$

With:

$$a_{nk} = l_k^1(x_n), \qquad b_{nk} = l_k^2(x_n), \tag{4-31}$$

where $l_k^1$ and $l_k^2$ are the Langrange polynomials related to the two $(2M-1)$- tuples of interpolation points $\{x_0,\dots,x_{2M-1}\}$ and $\{x_{2^j-2M+1},\dots,x_{2^j}\}$ given by:

$$l_k^1(x) = \prod_{\substack{i=0\\ i\neq k}}^{2M-1} \frac{x-x_i}{x_k-x_i}, \qquad l_k^2(x) = \prod_{\substack{i=2^j-2M+1\\ i\neq k}}^{2^j} \frac{x-x_i}{x_k-x_i} \tag{4-32}$$

From the definition:

$$I_j f = \sum_{n=-L+1}^{-1} P_1(x_n)\theta_{jn} + \sum_{k=0}^{2^j} f(x_k)\theta_{jk} + \sum_{n=2^J+1}^{2^j+L-1} P_2(x_n)\theta_{jn} \tag{4-33}$$

and combining (4-29), (4-30) , and (4-33) , we have:

$$I_j f = \sum_{k=0}^{2M-1} f(x_k)\left(\theta_{jk} + \sum_{n=-L+1}^{-1} a_{nk}\,\theta_{jn}\right) + \sum_{k=2M}^{2^j-2M} f(x_k)\theta_{jk} + \sum_{k=2^j-2M+1}^{2^j} f(x_k)\left(\theta_{jk} + \sum_{n=2^j+1}^{2^j+L-1} b_{nk}\,\theta_{jn}\right) \tag{4-34}$$

Thus defining modified interpolating functions by:

$$\theta_{jk}^{l} = \theta_{jk} + \sum_{n=-L+1}^{-1} a_{nk}\,\theta_{jn} \quad \text{and} \quad \theta_{jk}^{r} = \theta_{jk} + \sum_{n=2^j+1}^{2^j+L-1} b_{nk}\,\theta_{jn} \tag{4-35}$$

Hence:

$$I_j f = \sum_{k=0}^{2M-1} f(x_k)\,\theta_{jk}^{l}(x) + \sum_{k=2M}^{2^j-2M} f(x_k)\theta_{jk} + \sum_{k=2^j-2M-1}^{2^j} f(x_k)\,\theta_{jk}^{r}(x) \tag{4-36}$$

It should be noted that the function of $\theta_{jk}^{l}$ and $\theta_{jk}^{r}$ still verify the interpolation property $\theta_{jk}^{l}(x_n) = \delta_{nk}$ and $\theta_{jk}^{r}(x_n) = \delta_{nk}$ for $n,k = 0,\ldots 2^j$. Furthermore, the operator $I_j$ is well defined for functions in $H^s(0,1)$, $s > 1/2$ and it satisfies the error estimation if $f \in H^{2M-1}(0,1)$, then:

$$\left\| f - I_j f \right\|_{s,(0,1)} \le 2^{-j(2M-1-s)} \| f \|_{2M-1,(0,1)} \tag{4-37}$$

The approximate solution of $u_j$ can now be developed using the $2^j + 1$ basis functions. The final function obtained from the WOC method is shown as:

$$I_j f = \sum_{k=0}^{L} f_j(x_k)\theta_{jk}^{l} + \sum_{k=L+1}^{2^J-L-1} f_j(x_k)\theta_{jk} + \sum_{k=2^j-L}^{2^j} f_j(x_k)\theta_{jk}^{r} \tag{4-38}$$

## 4.6 *Wavelet Finite Difference (WFD) Methods*

In this section, it will be shown that Daubechies-based wavelet methods when considered in the physical space are equivalent to explicit finite difference methods with grid refinement. In Daubechies wavelet method, the “refinement” is accomplished by adding wavelet basis functions in regions where structure exists corresponding to the scale of the wavelet used for analysis. In a finite difference method, the “refinement” is accomplished by adding grid points in regions chosen by a grid refinement mechanism. It can be argued that since wavelet methods correspond to central finite difference operators when the grid is uniform, and because wavelet methods contain a natural and effortless mechanism for "grid refinement", then it is possible to use the wavelets to refine a grid for finite difference operators. Furthermore, there is then no difficulty with nonlinear terms requiring constant transformation between the physical space and the coefficient space since all calculations are done in the physical space.

### *Wavelet decomposition matrix*

The wavelet decomposition matrix is the matrix embodiment of the dilatation equation defining the scaling function and the accompanying equation defining the wavelet. The following two recursion relations for the coefficients $s_k^j$ and $d_k^j$ can be found from:

$$s_k^j = \sum_{n=1}^{n=2M} h_n \, s_{n+2k-2}^{j-1} \tag{4-39}$$

$$d_k^j = \sum_{n=1}^{n=2M} g_n \, s_{n+2k-2}^{j-1} \tag{4-40}$$

Note that the decomposition matrix embodied by these two equations, assuming periodicity, by $P_{N\times N}^{j,j+1}$ where the matrix subscripts denote the size of the matrix, and the superscripts indicate that $P$ is decomposing from scaling function coefficients at scale $j$ to scaling function and wavelet coefficients at scale $j+1$. Therefore the function $P$ maps $\vec{s}_j$ onto $\vec{s}_{j+1}$ and $\vec{d}_{j+1}$ by:

$$P_{N\times N}^{j,j+1}: \left[\vec{s}_j\right] \rightarrow \begin{bmatrix} \vec{s}_{j+1} \\ \vec{d}_{j+1} \end{bmatrix} \tag{4-41}$$

Suppose the wavelet being used is the four coefficient $D_4$ wavelet, and it is required to project from 8 scaling function coefficients at scale $j$ to 4 scaling function coefficients at scale $j+1$ and 4 wavelet coefficients at scale $j+1$. Then the decomposition matrix is:

$$p_{8x8}^{j,j+1} = \begin{bmatrix} h_1 & h_2 & h_3 & h_4 & 0 & 0 & 0 & 0 \\ 0 & 0 & h_1 & h_2 & h_3 & h_4 & 0 & 0 \\ 0 & 0 & 0 & 0 & h_1 & h_2 & h_3 & h_4 \\ h_3 & h_4 & 0 & 0 & 0 & 0 & h_1 & h_2 \\ g_1 & g_2 & g_3 & g_4 & 0 & 0 & 0 & 0 \\ 0 & 0 & g_1 & g_2 & g_3 & g_4 & 0 & 0 \\ 0 & 0 & 0 & 0 & g_1 & g_2 & g_3 & g_4 \\ g_3 & g_4 & 0 & 0 & 0 & 0 & g_1 & g_2 \end{bmatrix}$$

Let the four matrices $A_{N\times N}^{j}$ , $B_{N\times N}^{j}$ , $C_{N\times N}^{j}$ , and $R_{N\times N}^{j}$ contain the derivative projection coefficients:

$$A^j : \overrightarrow{d_J} \rightarrow \overrightarrow{\acute{d}_J} ,$$

$$B^j : \overrightarrow{s_J} \rightarrow \overrightarrow{\acute{d}_J} ,$$

$$C^j : \overrightarrow{d_J} \rightarrow \overrightarrow{\acute{s}_J} ,$$

$$R^j : \overrightarrow{s_J} \rightarrow \overrightarrow{\acute{s}_J} ,$$

where $\overrightarrow{\acute{d}_J}$ and $\overrightarrow{\acute{s}_J}$ are the coefficients of the expansion of the derivative of a function which is initially defined by the expansion coefficients $\overrightarrow{d_J}$ and $\overrightarrow{s_J}$ . The form of matrices A, B, C is not important here. The important point is that the form of matrix R is always a finite difference operator. For the $D_4$ wavelet, then $R$ corresponds to the optimal central 4th-order finite difference operator, but it is not optimal in the sense of using the minimum number of coefficients to obtain a specified accuracy. For the $D_4$ wavelet, an explicit 8 × 8 example of matrix $R$ is:

$$R_{8x8} = \begin{bmatrix} 0 & \frac{2}{3} & -\frac{1}{12} & 0 & 0 & 0 & \frac{1}{12} & -\frac{2}{3} \\ -\frac{2}{3} & 0 & \frac{2}{3} & -\frac{1}{12} & 0 & 0 & 0 & \frac{1}{12} \\ \frac{1}{12} & -\frac{2}{3} & 0 & \frac{2}{3} & -\frac{1}{12} & 0 & 0 & 0 \\ 0 & \frac{1}{12} & -\frac{2}{3} & 0 & \frac{2}{3} & -\frac{1}{12} & 0 & 0 \\ 0 & 0 & \frac{1}{12} & -\frac{2}{3} & 0 & \frac{2}{3} & -\frac{1}{12} & 0 \\ 0 & 0 & 0 & \frac{1}{12} & -\frac{2}{3} & 0 & \frac{2}{3} & -\frac{1}{12} \\ -\frac{1}{12} & 0 & 0 & 0 & \frac{1}{12} & -\frac{2}{3} & 0 & \frac{2}{3} \\ \frac{2}{3} & -\frac{1}{12} & 0 & 0 & 0 & \frac{1}{12} & -\frac{2}{3} & 0 \end{bmatrix}$$

This new method applies finite difference on a grid which is defined by the magnitude of wavelet coefficients at various scales. Wavelets can detect oscillations in a function at any location and scale. Given a function $f(x)$ into a set of wavelet coefficients which depend on two parameters, one for location and one for scale, say $d_k^j$, where $k$ is the location parameter and $j$ is the scale parameter. If a wavelet coefficient is large:

$$|d_k^j| > T,$$

Or the energy is significant:

$$\left(d_k^j\right)^2 > T,$$

where $T$ is a coefficient threshold chosen by the user, then a grid point (or two) will be added at location $k$ and at a grid density corresponding to the scale $j$. Therefore, WFD defines a grid which will completely resolve a function across the entire domain without over solving it where it is relatively smooth, or composed only of large scale structure. For the specific case of $D_4$, then wavelet decomposition provides the optimal grid for 4th-order finite differencing.

The grid definition should be made by a Daubechies wavelet which corresponds in terms of super convergence accuracy to the accuracy of the finite difference operator. The differentiation matrix for the Daubechies wavelet $D_{2M}$, where $M$ is the number of vanishing moments, displays differentiation accuracy of order $2M$ under the assumptions of periodicity and a uniform grid. The wavelet subspace can only represent exactly the first $M$ polynomials as determined by the number of vanishing moments. This order of accuracy $2M$ should equal the order of accuracy of the finite difference operator for optimal grid selection.

### *Wavelet Finite Difference algorithms*

In this study, a wavelet method combined with finite difference approximation was developed. This method combines the finite difference approximation techniques with the resolution and refinement techniques borrowed from the Daubechies wavelet characteristics. The WFD algorithm for solving a partial differential equation is decribed below and illustrated in Figure 4-5:

1. Define the range of wavelet resolution, for example J=6-9.
2. Determine the uniform grid for the lowest level of resolution, $x = [0{:}\ 1/2^J : 1]$.
3. Calculate the wavelet decomposition matrix and the derivative matrices.
4. Determine the solution, $y^J$ , initially for the lowest level of resolution.
5. Add new grids ($x_{new} = 1/2^J,\ 3/2^J, \dots, 2^{J-1}/2^J$) for an increased resolution, $J_{new} = J_{old} + 1$.
6. Evaluate the numerical solution for the added grid points for an increase in resolution, $y^{J+1}$
7. Interpolate the solution, $f$ for the added grid points based on $x$, $x_{new}$, and $y^J$, otherwise use available analytical solutions.
8. Determine for each point added, the residual, $R = |f - y^{J+1}|$; if $R < \epsilon$ (threshold) then the point is removed, otherwise it is retained.
9. Define new grid points which are based on non-uniform grid and then select the corresponding matrices can be selected.
10. Repeat steps 4 to 9 above until the maximum defined resolution is achieved and the final adapted solution and grids are obtained.

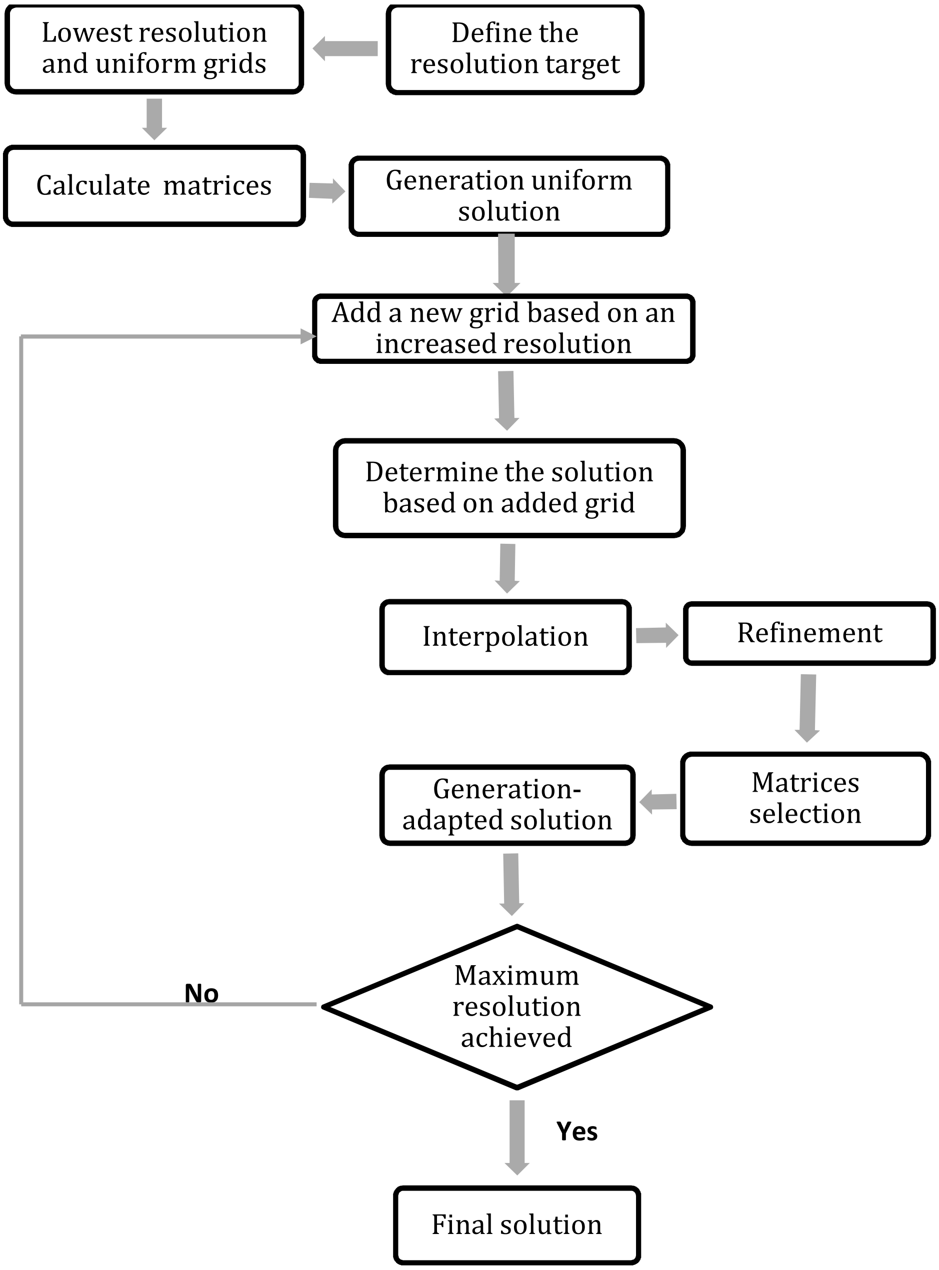

**Figure 4-5. Algorithms for wavelet finite difference (WFD) method.**

## 4.7 *Numerical Computational Experiments*

In this work, three case studies of population balances with sharp transition phenomena in their particle size distribution in a batch crystallizer were tested in order to apply the wavelet-based method as an alternative solution. Some straightforward case studies were considered because their analytical solutions were available for comparison.

The work from a previous study (Utomo et al. 2006) has been extended by comparing with finite difference based methods, such as upwind finite difference (U-FD), biased upwind finite difference (BU-FD), and method of weighted residuals, such as orthogonal collocation with finite element method (OCFE). Different types of population balances are illustrated in the three case studies discussed in the paper. They show a high non-linearity, a steep-front profile, and stiff characteristic. The solutions are benchmarked with respect to their size (spatial grid points used), accuracy (mean and average error), and the computation time (t-CPU).

The upwind finite difference and biased upwind finite difference schemes were applied to effectively handle the instability, and to avoid the spurious oscillation as generated by a centred FD scheme. The five-point (fourth-order accuracy) upwind, and biased upwind on uniform grids, were implemented as described by Wouwer et al. 2005. Orthogonal collocation technique was developed and applied in various cases of boundary value problems. The trial functions are chosen as sets of orthogonal polynomials and the collocation points are the roots of these polynomials, hence the solution can be calculated from the collocation points. The use of orthogonal polynomials is intended to reduce the error as the polynomial order increases (Gupta 1995; Hangos et al. 2001). OCFE is the combination method of dividing the regions into a number of elements, and by applying orthogonal collocation techniques for each element it can improve the solution where the profile is very steep. In the region where there is a sharp transition, then a number of small elements can be applied while the remainder utilize a larger size of elements. Therefore, selection of the correct elements size is essential.

### 4.7.1 *Case I: Population balance with nucleation and size-independent growth*

The population balance for the nucleation mechanism and size independent growth is described by the partial differential equation:

$$\frac{\partial n(x,t)}{\partial t} + G\frac{\partial n(x,t)}{\partial x} = B_0 \tag{4-42}$$

$$G = 1; B_0 = \exp(-x) \tag{4-43}$$

where $n$ is the number of particles (population density); $x$ is the particle size; $G$ is the growth rate; and $B_0$ is the nucleation rate.

With the initial and boundary conditions:

$$n(t,0) = 0; \quad n(0,x) = 0 \tag{4-44}$$

The analytical solution for this case is:

$$\begin{aligned} n(t,x) &= 1 - \exp(-x) & x - t < 0 \\ n(t,x) &= \exp(-x)\left[\exp(-t) - 1\right] & x - t > 0 \end{aligned} \tag{4-45}$$

The dimensionless particle size $L$ is defined as:

$$L = x/x,\max = [0:1]$$

$$\text{where : } \quad x = [x,\min : x,\max] = [0:2]$$

This first case describes a simple population balance system which presents sharp front size distribution profiles. The PBE has nucleation as a function of size and a constant growth rate, and the analytical solution was available from Chang et al. 1984. Four numerical schemes were applied in this case, their performances were tested in order to see the suitability, accuracy and stability of tested methods when handling the non-linearity and the sharp profile characteristic. The orthogonal collocation with finite elements (OCFE) scheme with 2 elements, which comprises 31 grid points, was applied. The other two methods were based on a finite difference scheme. The upwind finite difference (U-FD) of 2 points, and the biased upwind finite difference (BU-FD) of 5 points, were employed. Both of these were discretised in space to generate 129 grid points. Finally, wavelet orthogonal collocation (WOC) was used, and the performance was benchmarked against the analytical solution.

The average error (AE) was defined as: the square root of the sum of squares error divided by the number of grid points. It was calculated on an individual time basis, and the AE then does not depend on the number of equations (grid points). The AE value can illustrate the total absolute error of the grids for a particular time. A small value of AE may also illustrate a stable solution. While AE is the error overview, the maximum error (ME) could show a local error or an overshoot from the reference value. The ME was defined as: the maximum value of the square root of the sum of squares error at a particular time. The summary of numerical simulation performance for case I is presented in Table 4-2.

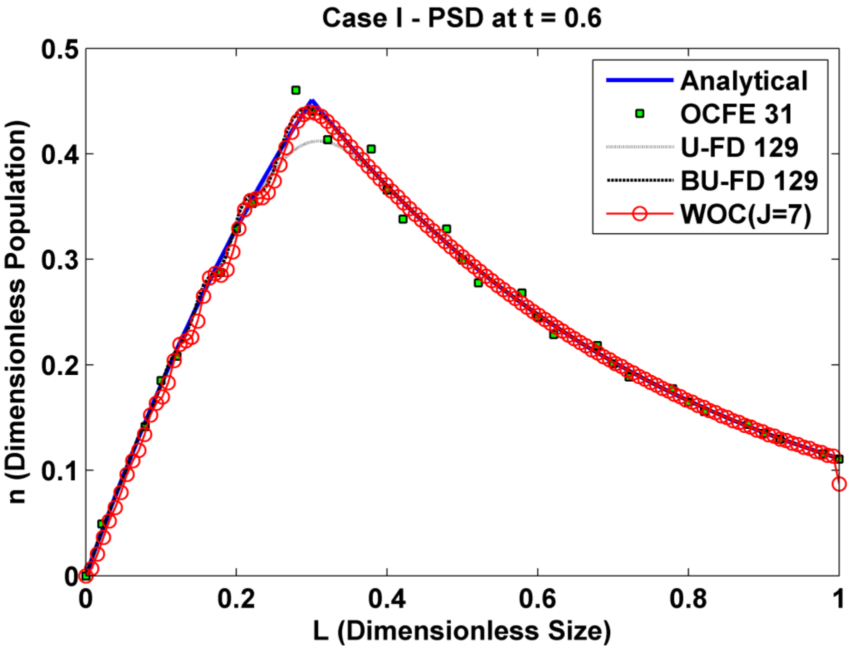

**Figure 4-6. Particle size distribution, case I at 0.6 seconds, simulated by four methods and compared to analytical solution.**

Figure 4-6 shows a comparative particle size distribution (PSD) at 0.6 seconds. The particle distribution was initially zero and nucleation begins to generate nuclei, the born nuclei grow at a constant rate of 1.0. The OCFE 31 profile produced a slightly overestimated particle density compared to the analytical solution, whereas all the other numerical schemes (including WOC) with the same resolution gave comparable results. The simplest two points upwind scheme gave an underpredicted population at the peak point, while the simulation results from biased upwind and wavelet are equivalent in term of minimising the error at the peak point. Considering the AE, then BU-FD was the most accurate, followed by WOC, then U-FD was the least accurate. When the wavelet level (J) was increased from 7 to 9, the ME values were about the same; but 62% increased accuracy was achieved and, at the same time, the computation time (t-CPU) was 440% higher.

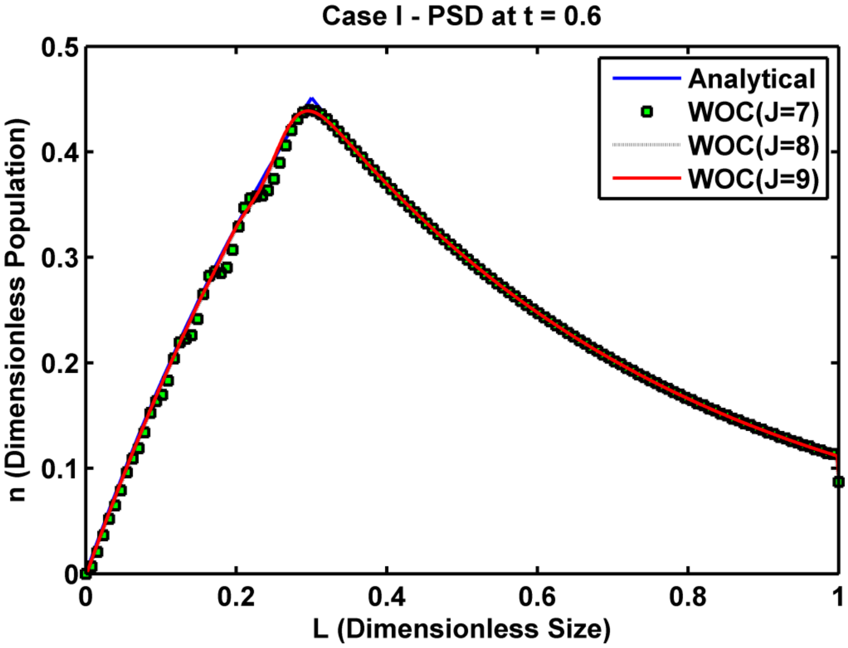

**Figure 4-7. Particle size distribution, case I at 0.6 seconds, simulated by WOC (M=1; J=7, 8, 9) and compared with analytical solution.**

Figure 4-7 shows the WOC solutions of particle size distribution at 0.6 seconds when applying various wavelet resolutions at constant M. The results show that at J=7, there was a small instability observed in the profile compared to the analytical solution. However, this problem can be rectified by increasing the wavelet resolution as shown at J=8 and 9, and the instability became negligible.

**Table 4-2. Numerical performance results for case I: N: grid points; AE: average error; ME: maximum error; t-CPU: computation time.**

| Case I @ 0.6 s | N | AE | ME | t-CPU (s) |
|---|---|---|---|---|
| **OCFE (2)** | 31 | 0.4383 | 0.7861 | < 1 |
| **U-FD (2)** | 129 | 0.0082 | 0.0391 | < 1 |
| **BU-FD (5)** | 129 | 0.0031 | 0.0120 | < 1 |
| **WOC (J=7)** | 129 | 0.0064 | 0.0243 | < 1 |
| **WOC (J=8)** | 257 | 0.0033 | 0.0242 | 1.4 |
| **WOC (J=9)** | 513 | 0.0024 | 0.0239 | 4.4 |

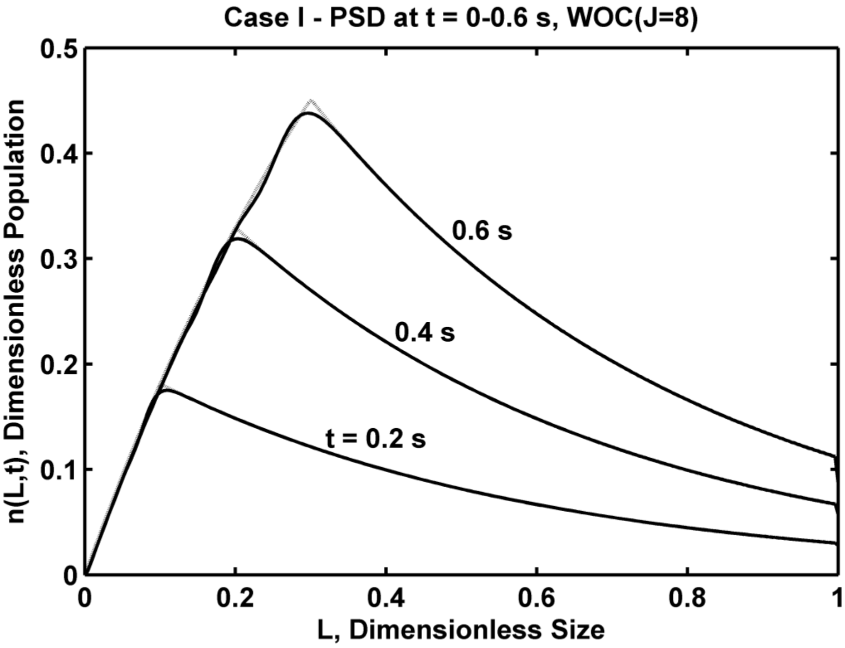

**Figure 4-8. Particle size distribution of WOC (J=8) at 0.2, 0.4 and 0.6 second, the black line: WOC solution and grey line: analytical solution.**

For these simulation results, all the computation times were short (less than 5 seconds) because all the methods have the same matrix-type structure. Matrix to matrix calculation was superior to the loop calculation (using *for* loop) in terms of its computation time and its adaptability to more complex cases. Figure 4-8 shows the solutions produced by WOC (J=8) at various times of t = 0.2, 0.4 and 0.6 seconds. It can now be concluded that OCFE methods can be used with reasonable levels of accuracy, whereas the WOC method can be employed as an alternative equivalent solution for handling the case of a sharp fronts profile caused by a non-linear nucleation function. Case II that follows addresses whether these methods are able to track a very sharp profile.

### 4.7.2 Case II: Population balance with size-independent growth only and initially seeded

The one dimensional population balance for size dependent growth mechanism is described by the partial differential equation:

$$\frac{\partial n(x,t)}{\partial t}+G\frac{\partial n(x,t)}{\partial x}=0 \tag{4-46}$$

$$G=1 \tag{4-47}$$

With initial and boundary conditions:

$$n(t,0)=0; \quad n(0,x)=\exp(-100(x-1)^2\times 1/6.6) \tag{4-48}$$

The analytical solution for this case is:

$$n(t,x)=\exp(-100(x-G.t-1)^2\times 1/6.6) \tag{4-49}$$

The dimensionless particle size *L* is defined as:

$$L=x/x,\max=[0:1]$$

where: $x=[x,\min:x,\max]=[0:5]$

In a seeded batch crystalliser, where the nucleation can be minimised, particle size distribution will be controlled only by the initial condition of seeding and the crystal growth. In this case, the crystal growth was again assumed constant, and the seed condition was artificially made to represent a very sharp front of particle size distribution. The previous study by Utomo et al. (2006) reported that the OCFE method cannot be applied because unstable solutions were obtained, and the upwind finite difference scheme gave delayed solutions. Therefore, only the WOC method as an equivalent method was tested in this case. The effect of wavelet resolution (J) and vanishing moments (M) were observed in order to study their performance.

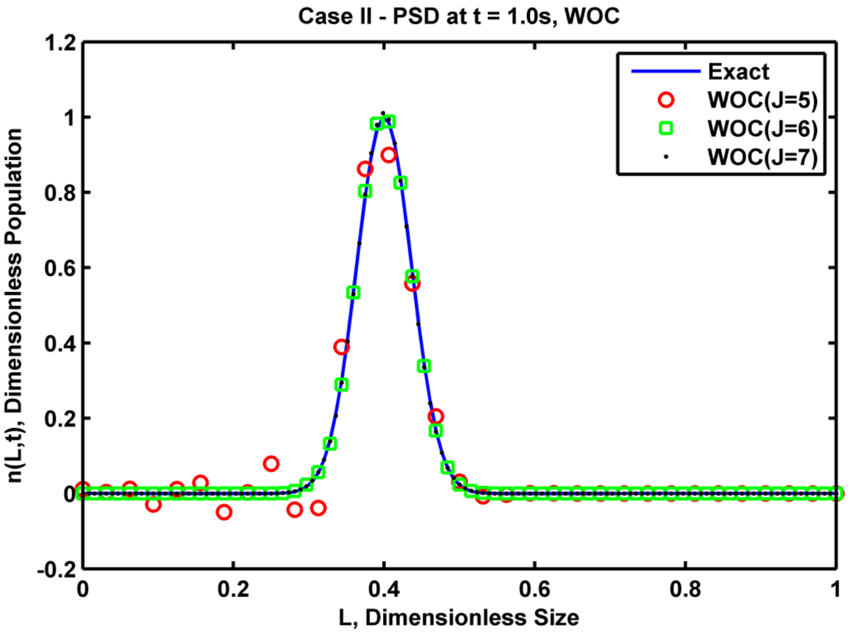

**Figure 4-9. Particle size distribution of WOC at t = 1s, using various J =5, 6, 7.**

Figure 4-9 shows the WOC solutions with wavelet resolutions of J=5, 6, and 7, and compared to the exact analytical solution. It can be seen that, except for J=5, the WOC produced a good validation result with high accuracy. However the WOC for J=5, not only gave a high ME but also oscillation and a negative value problem. The final solution of J=5 was stable, but early oscillation recorded the highest average error in the solution. The same problem was considered by Muhr et al. (1996), and can be easily rectified by decreasing the spacing or utilising adaptive gridding. The full PSD profiles up to 1.0 second simulation time are presented in Figure 4-10 ,and it is clear that the numerical diffusion and oscillation, which are common in the period of time integration of a sharp function, did not occur in this case. Error analysis at t = 1 second (Figure 4-11) shows that in the peak region, a greater degree of error was observed. The numerical diffusion can be observed from this result, but the error did not build up throughout the entire simulation time.

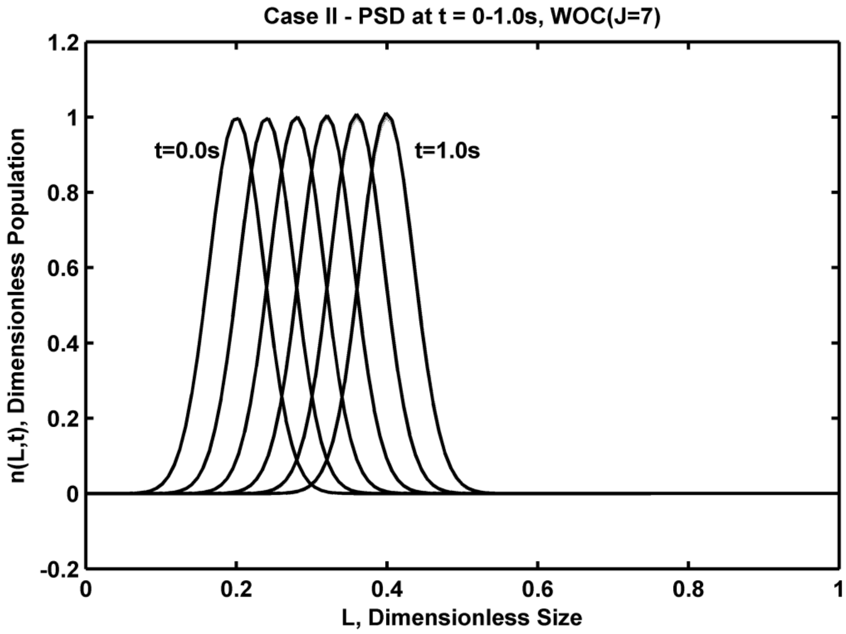

**Figure 4-10. Particle size distribution profiles at various time from 0s to 1.0s (0.2s increment) when using WOC (J=7 and M=1).**

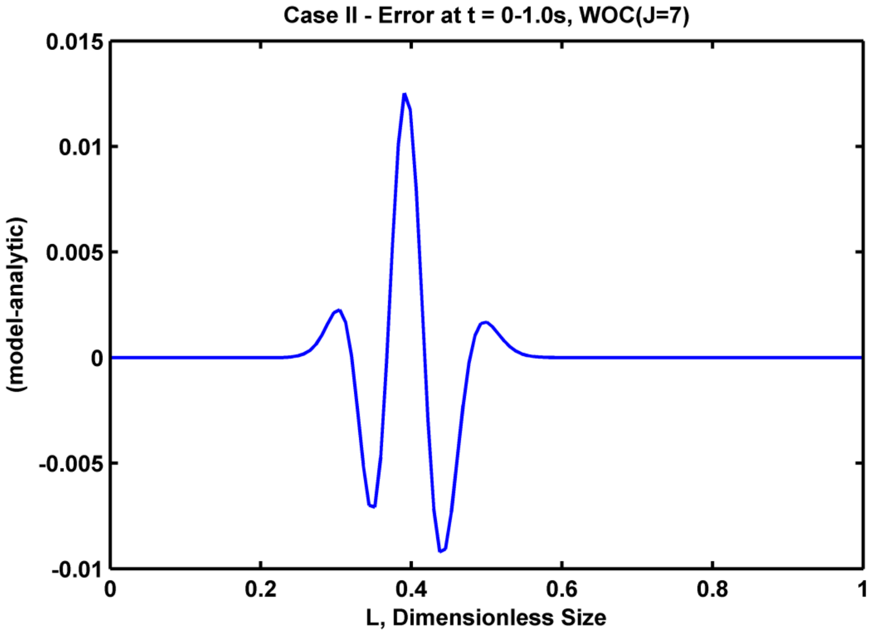

**Figure 4-11. Error at t = 1.0s when using WOC (J=7 and M=1) for case II.**

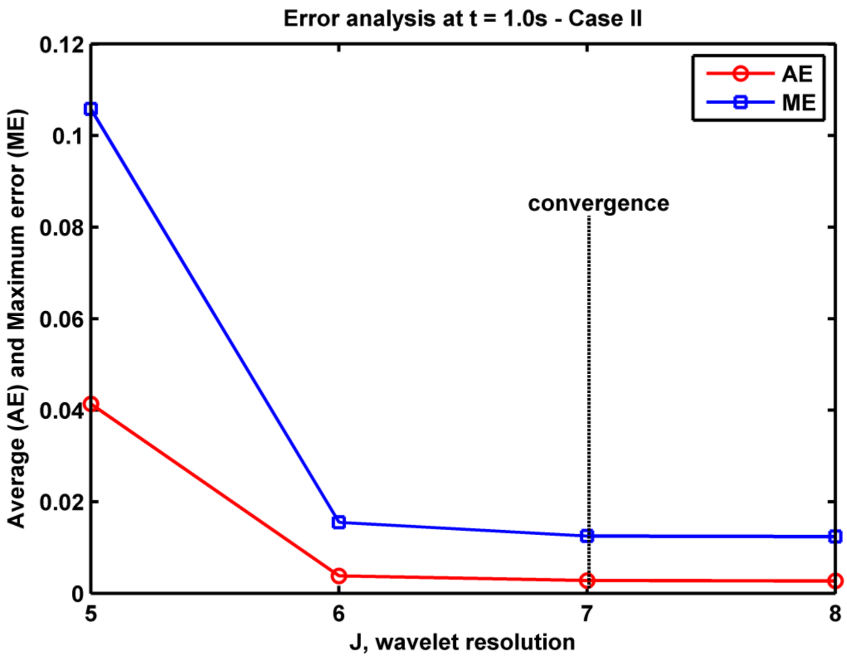

Figure 4-12. The error analysis at t = 1s for various J, where AE is average error and ME is maximum error.

Table 4-3. Numerical performance results for case II: M: vanishing moments; N: grid points; AE: average error; ME: maximum error; t-CPU: computation time.

| Case II @ 1.0 s | M | N | AE | ME | t-CPU (s) |
|---|---|---|---|---|---|
| WOC (J=5) | 0 | 33 | 0.0369 | 0.0933 | < 1.0 |
| | 1 | | 0.0368 | 0.0933 | |
| | 2 | | 0.0406 | 0.0931 | |
| | 3 | | 0.0414 | 0.1058 | |
| WOC (J=6) | 0-3 | 65 | 0.0038 | 0.0155 | < 1.0 |
| WOC (J=7) | 0-3 | 129 | 0.0028 | 0.0125 | < 1.0 |
| WOC (J=8) | 0-3 | 257 | 0.0027 | 0.0124 | 1.3 |

The convergence issue is important when developing numerical simulations. The WOC method for the tested resolution gave good convergence at a resolution as low as 6. Both AE and ME could be used for error analysis to show the convergence at a particular time. The numerical performance for case II is presented in Table 4-3. As shown in Figure 4-12, convergence was actually reached as J was increased from 6 to 7, and any further increase in resolution would not give any improvement in the accuracy. The effect of vanishing moments (M) could only be observed in this case when the lowest resolution was applied. M = 0 and 1 were the optimal values that gave the lowest level of error. In summary, the WOC could also have been used as an alternative technique for a very sharp front profile. The selection of resolution is more sensitive to the computational performance than to the sequential choice of vanishing moments. Selection of M becomes sensitive only when the symptom of instability was observed. To demonstrate the WOC capabilities as an alternative method, the case study of more complex population balance in a batch crystalliser case study is presented in the next case study.

### 4.7.3 Case III: Seeded batch crystalliser with nucleation and growth

$$\frac{\partial n(L,t)}{\partial t} + G\frac{\partial n(L,t)}{\partial L} = B \qquad (4\text{-}50)$$

where:

$$B = k_b\, M_T^j\, \Delta c^b \qquad (4\text{-}51)$$

$$G = k_g\, \Delta c^g \qquad (4\text{-}52)$$

With initial and boundary conditions:

$$\begin{aligned} n(0,L) &= n_0\, \delta(L-L_0) \\ n(t,0) &= B/G \end{aligned} \qquad (4\text{-}53)$$

The supersaturation balance can be written as:

$$\frac{d\Delta c}{dt} = \frac{3W_{S0}\, L_S^2\, G}{L_{S0}^3\, S} + \frac{3\rho\, k_v\, A_N\, G}{k_a} \qquad (4\text{-}54)$$

The particle size $L$ is defined as:

$$L = [L, \min : L, \max] = [400 : 1400]\mu m$$

This fourth case considers a seeded batch crystalliser with capacity of 25.5 kg solvent, running at isothermal conditions, for a batch time of 6000 seconds. The nucleation and growth kinetics are described by equations (4-51) and (4-52). The initial condition was the seed condition of average size 500 μm, and the boundary condition is given by equation (4-53). To solve this system, a set of moment equations for the population balance of equation (4-50) can be implemented, coupled with the mass (supersaturation) balance for the solute and solid phase in equation (4-54); hence the dynamics of the crystal size distribution can be computed. All the parameters used in this case were obtained from Section 3.6.1.

Figure 4-13 shows the profile of supersaturation and crystal growth rate during 6000 seconds batch operation, the initial condition of 0.015 kg/kg solvent would give a corresponding crystal growth of $1.68 \times 10^{-10} \times 10^{-10}$m/s. The total number of crystals and the nucleation rate for the complete simulation are shown in Figure 4-14. As nucleation occurred in the process, the total number of crystals increased from about $1 \times 10^6$ up to $7 \times 10^7$ particles/m.kg solvent, while the rate of nucleation reached the optimum at 600 particles/s.kg solvent and then decreased slightly to 490 particles/s. kg solvent after 6000 seconds. The CSD profiles shown in Figure 4-15 describe the evolution of the sharp seed-size distribution to a wider distribution at t = 1450 seconds, and at the final time. When the CSD became wider, the average size density was also sharply decreased from 14% in the seed, to about 8 and 6% after 1450 and 6000 seconds respectively. This behaviour is similar to the population balance which includes a growth rate dispersion model (Randolph et al. 1977). Finally, the WOC method with J = 7 and M = 1 was employed and an acceptable result was obtained as shown in Figure 4-16, although experimental results were not available for comparison.

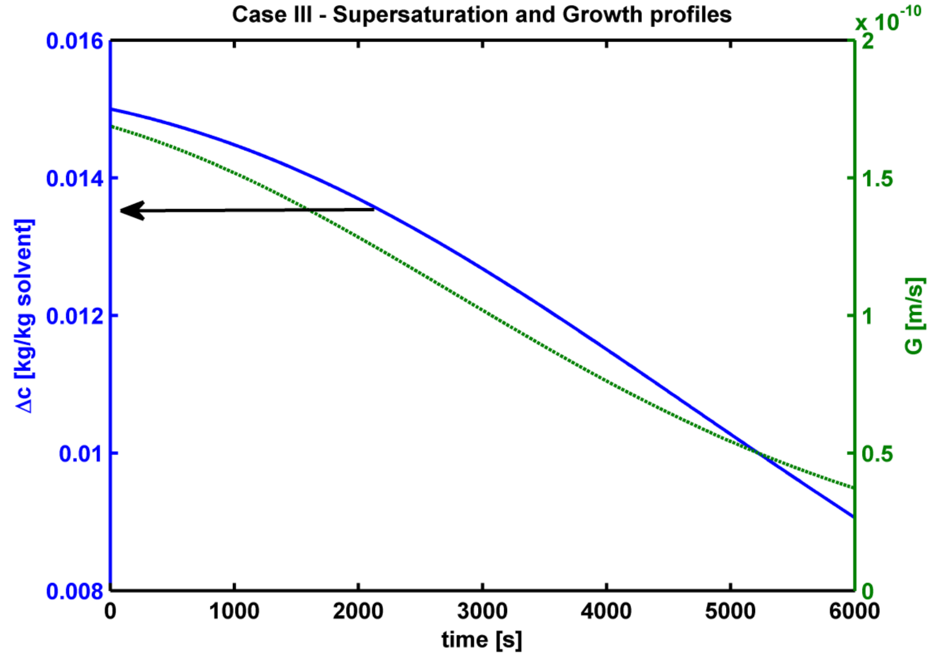

Figure 4-13. Supersaturation (left) and crystal growth rate (right) profiles for up to 6000 seconds.

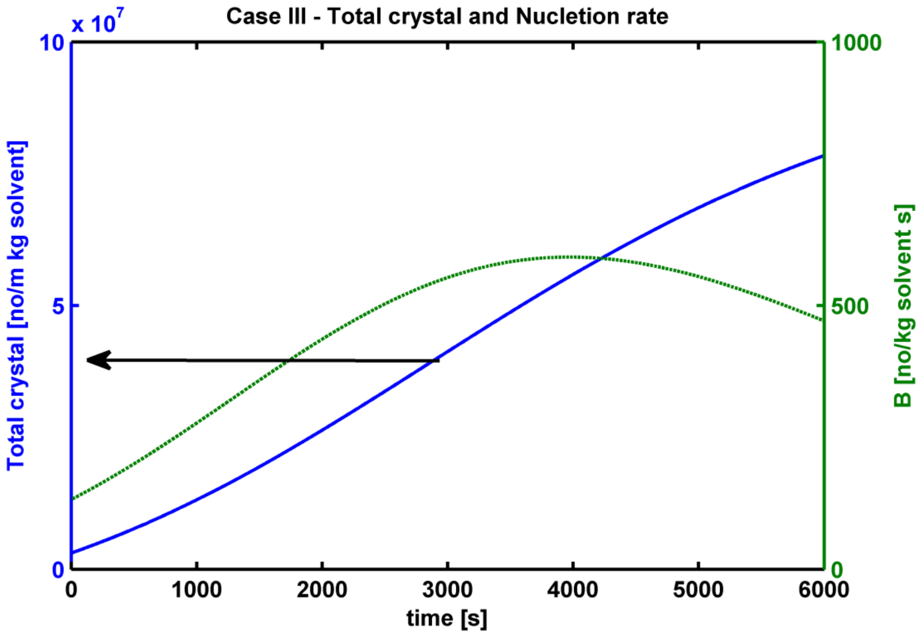

Figure 4-14. Total crystal (left) and nucleation rate (right) profiles for up to 6000 seconds.

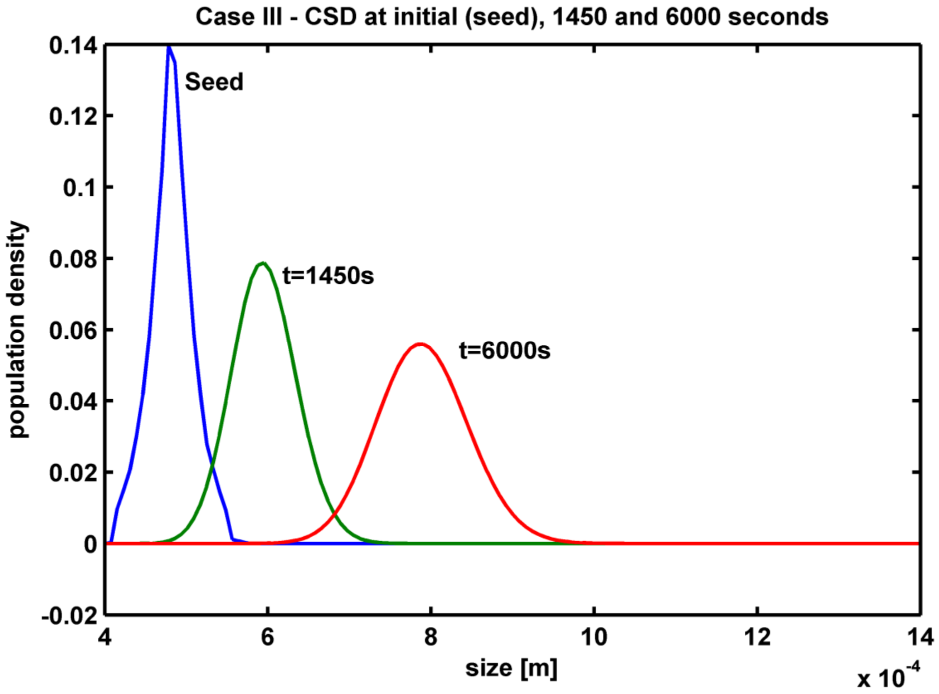

Figure 4-15. Crystal size distribution at seed condition, at t = 1450 and 6000 seconds.

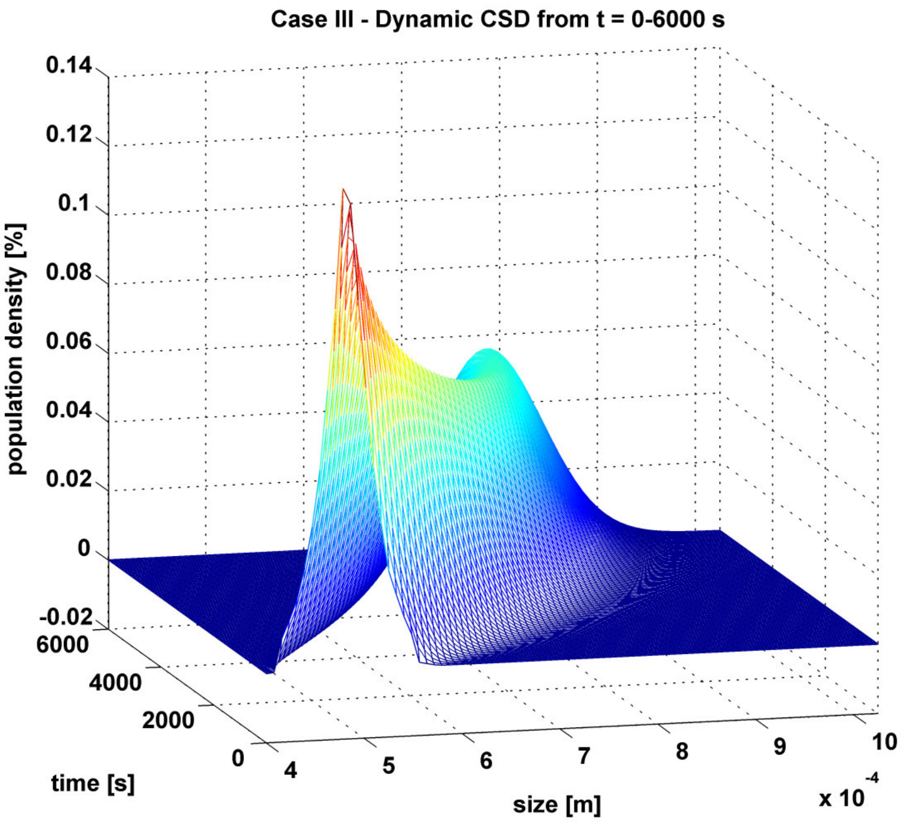

**Figure 4-16. Dynamic crystal size distribution for case III, for 400-1000 µm size and simulation from 0-6000 seconds.**

## 4.8 *Remarks*

1. Depending upon the methodology employed, the wavelet-based methods for solving partial differential equations can be categorized as: methods based on scaling functions expansions, methods based on wavelet expansion, finite differences wavelet method, and other alternative methods.

2. A comparative review of existing wavelet-based methods, such as Wavelet Galerkin (WG), Wavelet Optimised Finite Difference (WOFD), and Wavelet Orthogonal Collocation (WOC), has shown that a further development of a new method based on wavelet and finite difference approximation, referred to as the Wavelet Finite Difference (WFD), provided benefits in boundary condition treatment, calculation basis, and a reduced computation capacity compared with the same adaptive WOC method.

3. Three case studies, which present a very sharp size distribution profile, have demonstrated the potential of wavelet-based numerical schemes as an alternative for providing accurate, fast and robust solutions. This new wavelet numerical technique and wavelet application has much potential in for chemical engineering applications.

## 4.9 *References*

Bertoluzza, S., Y. Maday and J. C. Ravel (1994). A dynamically adaptive wavelet method for solving partial differential equations. *Computer Methods in Applied Mechanics and Engineering*, 116(1-4), 293-299.

Bertoluzza, S. and G. Naldi (1996). A wavelet collocation method for the numerical solution of partial differential equations. *Applied and Computational Harmonic Analysis*, 3(1), 1-9.

Chen, M.-Q., C. Hwang and Y.-P. Shi (1996). The computation of wavelet-galerkin approximation on a bounded interval. *International Journal for Numerical Methods in Engineering*, 39, 2921-2944.

Chen, M.-Q., C. Hwang and Y.-P. Shih (1996). A wavelet-galerkin method for solving population balance equations. *Computers & Chemical Engineering*, 20(2), 131-145.

Daubechies, I. (1988). Orthonormal bases compactly supported wavelets. *Communications Pure and Applied Mathematics*(41), 909-996.

Hsiao, C.-H. (1997). State analysis of linear time delayed systems via haar wavelets. *Mathematics and Computers in Simulation*, 44(5), 457-470.

Jameson, L. (1998). A wavelet-optimized, very high order adaptive grid and order numerical method. *Siam J. Sci. Comput.*, 19(6), 1980-2013.

Jameson, L. and T. Miyama (2000). Wavelet analysis and ocean modeling: A dynamically adaptive numerical method "WOFD-AHO". *Montly Weather Review*, 128, 1536-1548.

Liu, Y. and I. T. Cameron (2001). A new wavelet-based method for the solution of the population balance equation. *Chemical Engineering Science*, 56(18), 5283-5294.

Liu, Y. and I. T. Cameron (2003). A new wavelet-based adaptive method for solving population balance equations. *Powder Technology*, 130(1-3), 181-188.

Liu, Y., I. T. Cameron and S. K. Bhatia (2001). A wavelet-based adaptive technique for adsorption problems involving steep gradients. *Computers & Chemical Engineering*, 25(11-12), 1611-1619.

Motard, R. L. and B. Joseph (1994). *Wavelet applications in chemical engineering*. Kluwer Academic Publisher, London.

Qian, S. and J. Weiss (1993). Wavelets and the numerical solution of partial differential equations. *Journal of Computational Physics*, 106(1), 155-175.

Randolph, A. D. and E. T. White (1977). Modeling size dispersion in the prediction of crystal-size distribution. *Chemical Engineering Science*, 32(9), 1067-1076.

Vasilyev, O. V. and S. Paolucci (1996). A dynamically adaptive multilevel wavelet collocation method for solving partial differential equations in a finite domain. *Journal of Computational Physics*, 125(2), 498-512.

Zhang, T., M. O. Tade, Y. C. Tian, Y. Zhang and J. Utomo (2008). Wavelet approach incorporated with optimization for solving stiff systems. *Journal of Mathematical Chemistry*, 43(4), 1533-1548.

Zhang, T., Y. C. Tian, M. O. Tade and J. Utomo (2007). Comments on ‘the computation of wavelet-galerkin approximation on a bounded interval’. *International Journal for Numerical Methods in Engineering*, 72, 244-251.

# 5. Batch Cooling Crystallisation of Mono-Ammonium Phosphate

## 5.1 Introduction

Batch crystallisers are used extensively in the chemical industry, particularly for the manufacture of fine chemicals. Batch crystallisers are generally used in small-scale operations, especially when working with chemical systems that are difficult to handle due to their highly viscous or toxic properties. They are simple, flexible, require less investment and generally involve less process development. On the other hand, there are several disadvantages such as inconsistency in product quality, a higher labour demand and the need for more space. A continuous crystalliser is usually operated at a constant degree of supersaturation, whereas a batch crystalliser is difficult to operate at constant supersaturation. Batch crystallisers can be operated over a wide range of sizes and should be used for a very slow growing crystal. Operationally, batch crystallisers can be used in different modes such as with seeding, without seeding, forced cooling, and programmed cooling mode.

The basic steps in any crystallisation process are the achievement of supersaturation, formation of crystal nuclei, and their subsequent growth to form crystals of the specified size. All three processes may occur simultaneously in a batch crystallisation process. For process analysis or modelling, the crystallisation process in any configuration may be considered as a competitive process from the solution-side to the solid-side. The required degree of supersaturation is achieved by cooling, or evaporation, or addition of precipitant or diluent, or by chemical reaction, or a combination of these techniques. Supersaturation in batch crystallisation is usually generated by one or more of these four methods, in series or parallel.

In cooling crystallisers, supersaturation occurs due to reduced solubility with temperature. In evaporative crystallisers, the supersaturation is produced by loss of solvent with subsequent reduction of solvent capacity with time. In dilution crystallisers, generation of supersaturation is effected by an added diluent reducing the solute solubility, and the solvent capacity of the system consequently increases with time. In reactive crystallisers, the supersaturation is created as a consequence of the production of a desired component by virtue of a reaction. The solubility and solvent capacity may remain constant and both reaction and crystallisation steps can be treated as occurring in series.

The fundamental phenomena controlling the crystallisation process is the saturation concentration of a substance in a solvent, i.e. solubility. Solubility data are generally obtained experimentally by determining the maximum amount that is soluble at a given temperature. Buchanan and Winner (1920) undertook work on mono-ammonium phosphate (MAP) and di-ammonium phosphate (DAP) solubilities. The range of temperature investigated was 5 – 90°C. Their work provided fundamental studies on MAP and DAP crystallisation for later researchers. Ross et al.(1929) reported properties of ammonium phosphates, including MAP, DAP and tri-ammonium phosphate (TAP). The results of MAP solubility data were also presented, and there was good agreement with the previous work of Buchanan and Winner.

Studies on MAP crystallisation were initiated by Mullin and Amatavivadhana (1967). They studied the growth kinetics of a single crystal of MAP and of potassium dihydrogen phosphate (KDP). They found that MAP requires a significant level of supersaturation before spontaneous nucleation starts. The Arrhenius growth constant and activation energy were successfully predicted. The effect of impurities such as $Cr^{3+}$, $Fe^{3+}$, and $Al^{3+}$ on the growth kinetics and habit of MAP and KDP crystals was studied by Mullin et al. (1970). They found that only z-axis faces grow excessively at a low supersaturation level and a low pH of 3.8. The critical supersaturation found was 0.03 kg MAP/kg water. The habit of MAP is influenced by pH, supersaturation and impurities in the solution. Within the scope of single crystal studies, the growth rate of several faces of MAP crystal was studied in the presence of impurities. It was found that the surface diffusion is rate controlling because $NH_4^+$ and $H_2PO_4^-$ ions diffuse easier in the 010-direction than in the 001-direction. The adsorption of impurities at the step discontinuity of a crystal layer is important for the reduction of layer velocities and thus controls the growth process. Later Garside et al. (1983) investigated studies on growth rate of several small crystals were measured both in the 010- and 001-directions and exhibited different growth rates. The growth rate is controlled by the surface integration process rather than the volume diffusion step, and it follows the Burton-Cabrera-Frank spiral growth theory.

The use of seeds in batch crystallisation processes improves the product quality, mainly the crystal size distribution (CSD) and the purity (Mullin 2001; Kubota et al. 2002; Warstat et al. 2006). However, the known effects are rather qualitative and highly dependent on the operating conditions and the solute thermodynamics. Quantitative information is limited, for example it is not possible to specify the amount of seeds and their sizes that should be introduced in order to obtain a desired size distribution. Therefore, a seeding technique is adopted on the basis of a trial-and-error approach in industry and is not guaranteed to perform optimally. Certain important aspects such as seed loading ratio, seed sizes and supersaturation effects have been studied to obtain more information on the process and to obtain the crystallisation kinetics.

In conclusion, the information derived from such studies does indeed provide valuable guidelines for specific problems but may not be useful for the direct design and operational analysis of industrial crystallisers. Therefore, our studies on suspension crystallisation in a batch mode have been conducted in order to obtain essential information on the kinetics and to provide insight into the process characteristics.

## 5.2 Experimental Details

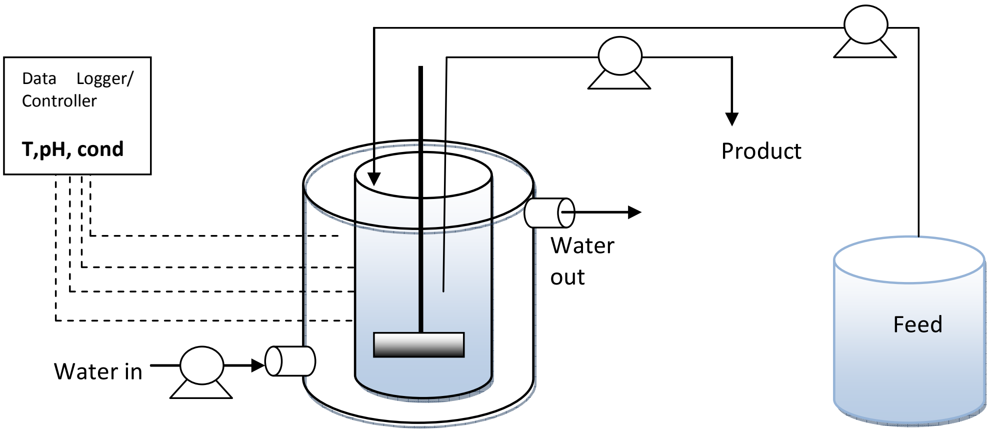

**Figure 5-1. Experimental setup for batch cooling crystallisation**

For batch-suspension cooling crystallisation experiments, two conditions have been investigated. First, the non-seeded system, and the seeded system. The non-seeded batch process experiments were conducted in order to study the effect of cooling rate and initial supersaturation. These experiments were also used to produce the seed crystals for the subsequent experiments. The seeded batch experiments were conducted to study the effects of seed sizes (for two conditions: same number of crystals and same loading ratio), the effects of seed loading, and supersaturation. The crystallisation nucleation kinetics and crystal growth can be deduced from the seeded batch experiments, and can be used to validate the previous experiments on the non-seeded batch processes. The arrangement of cooling batch crystallisation is shown in Figure 5-1.

The experimental procedures used for both processes are similar. First, a saturated mono-ammonium phosphate solution was prepared in accordance with its saturation temperature in the feed tank. A 300 ml glass jacketed vessel with impeller (turbine with inclined blades) was used as the crystalliser. The water temperature in the jacket is set at either 10 or 20°C to ensure isothermal conditions. Supersaturation and temperature were measured online by a conductivity meter and thermocouples. The conductivity calibration model previously developed by Torgesen and Horton (1963) was revised by using a non-linear regression methodology and showed satisfactory agreement with the calibration data. The relationship between conductivity and MAP concentration can be written as follow:

$$\kappa_w = a + (b + c.w)\,T + (d + e.w)\,T^2 + (f + g.w)\,w \tag{5-1}$$

where $\kappa_w$ is the conductivity in ohm$^{-1}$ cm$^{-1}$; T is the temperature in Celcius; w is the solute concentration in g/100 g solution; and $a, b, c, d, e, f$ and $g$ are constants. The derivation of equation (5-1) and sample of calculations are included in Appendix A.

A Pt-conductivity probe which has range from 2.0 – 19.99 S/m was connected to the conductivity meter. Temperature and conductivity output data were transferred and recorded in a data logger. Batch time was equal to one hour. Finally, the product slurry was pumped out, filtered, washed with acetone, and dried. Crystal size distribution (CSD) was determined by applying a sieving method and was able to size from 75 μm up to 1400 μm. In addition, a laser diffraction method was used and can measure crystals from 0.1 μm to 700 μm. The percentage crystal mass data is converted to number of crystals using the following Equation 5-2, where N is number of crystals, $W_p$ is mass of crystal [kg], $\rho_s$ is crystal density [kg/m$^3$] and $L$ is average length [m] of crystal in a certain class:

$$N = \frac{W_p}{k_v \, \rho_s \, L^3} \tag{5-2}$$

The experimental design conditions for the seeded crystallisation experiments are shown in Table 5-1. The methodology and details of experiments are summarised in Appendix A.

**Table 5-1. Experimental condition for seeded crystallisation**

| Set | ΔC-initial [g/100 g solution] | Cs [%] | Ls [µm] |
|---|---|---|---|
| 67 | 4.55 | 5 | 82.5 |
| 68 | 2.21 | 5 | 82.5 |
| 72 | 2.21 | 5 | 165 |
| 73 | 2.21 | 20 | 165 |
| 78 | 2.21 | 30 | 165 |
| 77 | 2.21 | 5 | 137.5 |
| 80 | 2.21 | 18 | 196 |
| 79 | 2.21 | 50 | 275 |

There were four main experiments for the seeded crystallisation system specified in order to study the crystallisation kinetics and determine the effects of several factors such as initial supersaturation, seed loading ratio, and seed size. A total of 8 runs were performed for the seeded experiments which were conducted twice each to ensure the repeatability. In order to ensure isothermal conditions for each run, the maximum initial supersaturation allowed were set up to 4.55 g/100 g solution. The seed loading ratio varied from 5 to 30% and the seed size ranged from 82.5 µm to 275 µm.

## 5.3 *Results and Discussion*

### 5.3.1 *Non-seeded experiments*

The non-seeded cooling batch crystallisation was conducted at various supersaturation and two sets of cooling rate. The condition of experimentation and yield results are presented in Table 5-2.

**Table 5-2. Non-seeded crystallisation conditions and results**

| Set | Cooling rate | ΔT [C] | ΔC [g/100 g sol] | Yield [g/100 g sol] |
|---|---|---|---|---|
| **60a** | High | 5 | 2.28 | 1.97 |
| **61** | | 7.5 | 3.41 | 3.65 |
| **62** | | 10 | 4.55 | 5.21 |
| **64** | | 10 | 4.55 | 5.16 |
| **63** | | 15 | 6.45 | 8.45 |
| **56** | | 20 | 8.3 | 11.13 |
| **55** | Low | 10 | 5.10 | 5.73 |
| **59** | | 15 | 6.83 | 8.50 |
| **57** | | 20 | 8.25 | 11.98 |

Table 5-2 contains data for the theoretical degree of supersaturation that can be produced and the crystal yield based on experimental results. Some of the theoretical supersaturation data are lower values than experimental results. One possible explanation for this behaviour is that the solubility data is in error, or there was some consistency error in the preparation of the supersaturated solution. The theoretical value should be higher than the measured crystal yield because not all solute will be crystallised, and some of solute will be used to compensate the metastable limit in the solubility.

#### *5.3.1.1 Effect of cooling rate*

In a cooling batch crystalliser, the heat transfer rate is important in order to generate supersaturation and is the product of the overall heat transfer coefficient, surface area and temperature difference. Assuming that the heat transfer area is constant, heat transfer is controlled only by the product of the overall heat transfer coefficient and the temperature difference. Therefore, coolant physical properties, flow rate and crystalliser mixing mode are the controlling factors.

There are many types of cooling crystalliser that can be used; there are natural cooling, constant cooling rate, or controlled cooling rate. In Figure 5-2, two cooling rates having effects on concentration and temperature profiles are observed and show that a different cooling speed produced a different nucleation time and different suspension time. Set 64 having a higher cooling rate starts a spontaneous nucleation at 950 seconds, and forms a suspension at 1200 seconds.

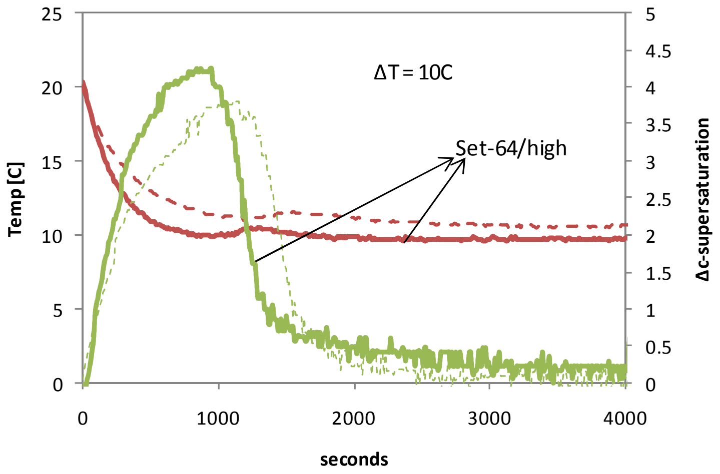

**Figure 5-2. Supersaturation and temperature profiles for two cooling rates (solid line: high cooling rate and dashed line: slow cooling rate)**

The supersaturation profiles were calculated by online measurement data of MAP concentration in the solution using a conductivity meter, and the conductivity data were converted to concentration data by using (5-2). Higher cooling speeds produced a higher maximum supersaturation level. The maximum supersaturation is 4.5 and 4.0 g/100 g solution for a high and slow cooling rate, respectively. When the maximum supersaturation was reached, nucleation occurred and full suspension was started.

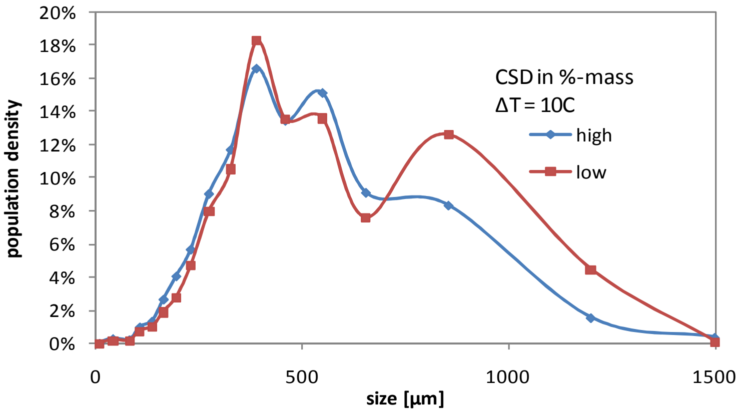

**Figure 5-3. Crystal size distribution (CSD) in mass density for ΔT = 10 °C supersaturation**

The mass density profile in Figure 5-3 shows that a high cooling rate results in a smaller proportion of coarse crystals due to increased nucleation. This was confirmed by the number density profile in Figure 5-4 where high nucleation causes finer particle sizes. The higher cooling rate produces quicker supersaturation; hence it reaches a higher supersaturation level above the metastable limit and then causes a higher nucleation rate at the time of nucleation.

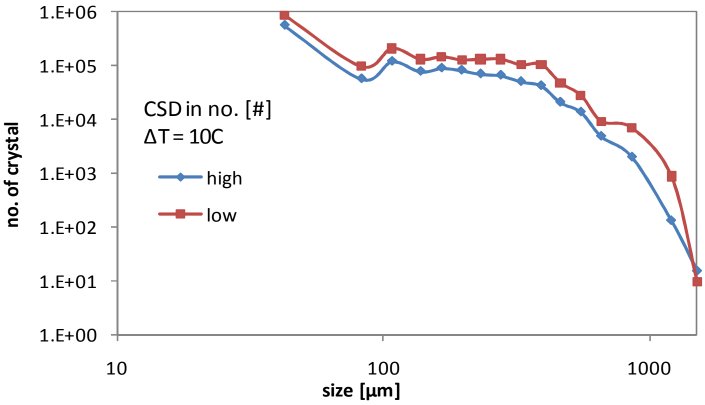

**Figure 5-4. CSD (as number of crystals) for ΔT = 10°C supersaturation**

### *5.3.1.2 Effect of initial supersaturation*

Initial supersaturation is defined as the concentration of MAP in the saturated solution. A higher MAP supersaturation would result in a higher saturation temperature. For the same cooling rate, the system which has a higher initial saturation temperature will have a higher cooling rate due to a higher temperature difference. Initial saturation temperature results in a different cooling profile and, therefore, causes a distinctive desupersaturation profile due to a decrease in solubility.

Figures 5-5 to 5-7 show the concentration, temperature and supersaturation profiles for Runs 61, 62 and 63, 56 and 60a. They had different initial saturation temperatures of 17.5, 20, 25, 30 and 15 °C respectively. The noticeable distinction between these results is the nucleation time and the time for the full suspension to form. The solution with the higher initial saturation only needs a short period of time to start the suspension (600 seconds), while the lowest saturation needs 10 times longer (6000 seconds) to start the suspension. The gradient of the concentration profiles indicates the crystal growth rate. The results with highest gradient produce the highest growth rate (Set 63 and 56) and have 15 °C and 20 °C degrees of supersaturation.

The mass density distribution profiles (see Figure 5-8) indicate that the CSD based on crystal number shows that the higher initial supersaturation produces more crystals, which means higher supersaturation and thus leads to a higher nucleation rate. In Figure 5-9, the 15°C initial supersaturation has more crystals than other profiles, and it shows that the birth of nuclei was predominantly controlled by the higher nucleation rate, which was generated by the higher degree of supersaturation.

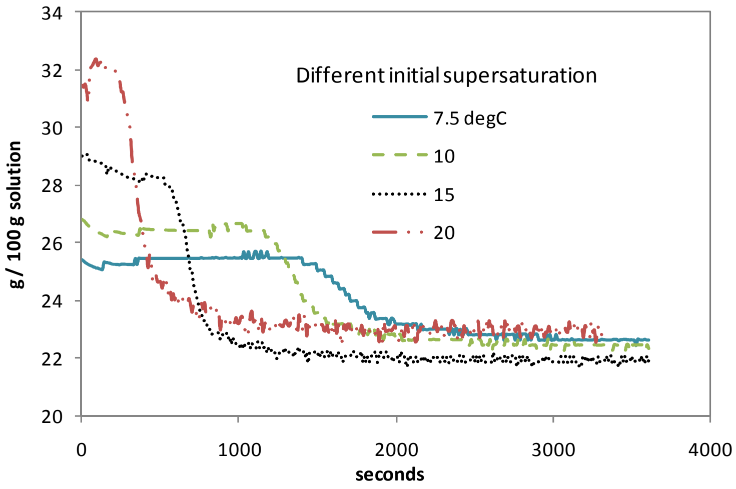

**Figure 5-5. Supersaturation profiles for different initial supersaturation (7.5, 10, 15 and 20°C)**

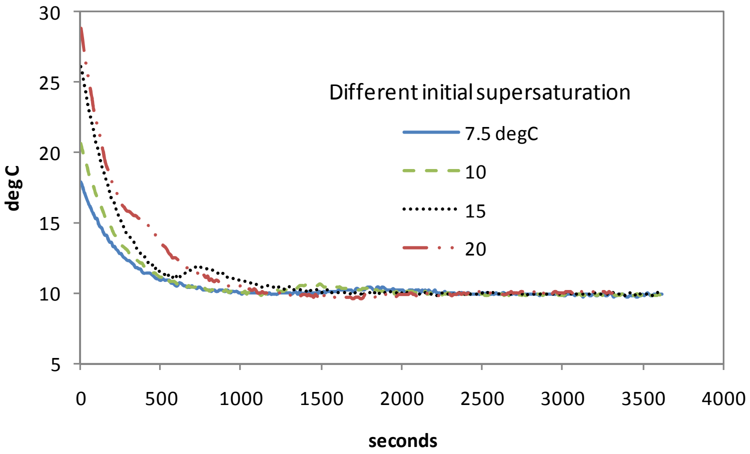

**Figure 5-6. Temperatures of crystalliser for different initial supersaturation (7.5, 10, 15 and 20°C)**

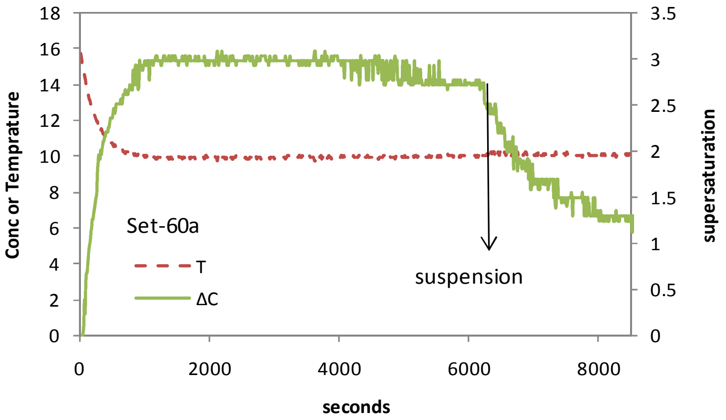

**Figure 5-7. Supersaturation and temperature profiles for Set-60a (5°C initial supersaturation)**

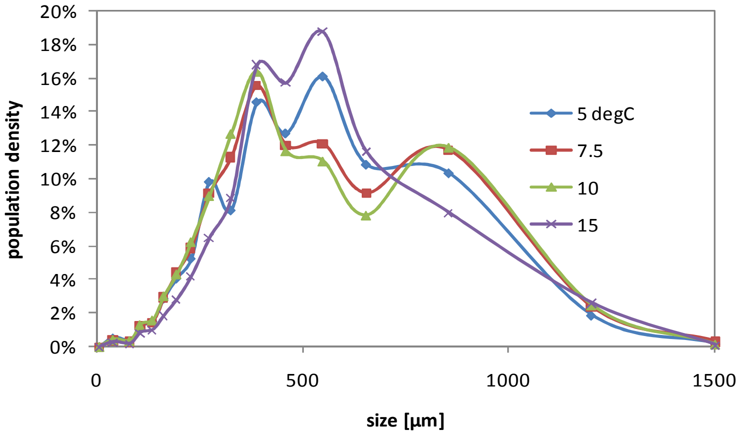

**Figure 5-8. CSD (as mass density) for different initial supersaturation (5, 7.5, 10 and 15°C)**

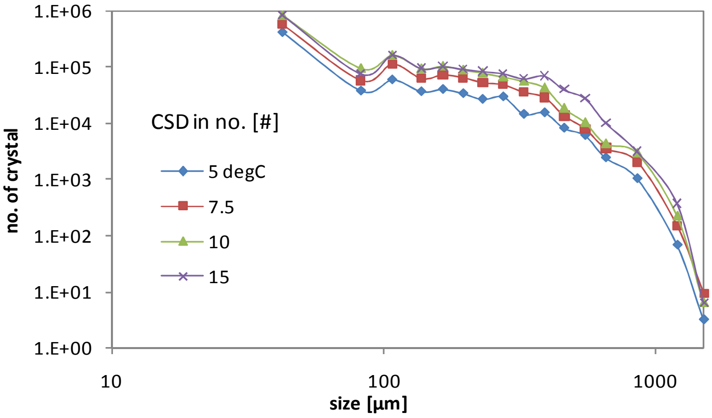

**Figure 5-9. CSD (as number of crystals) for different initial supersaturation (5, 7.5, 10 and 15°C)**

## *5.3.2 Seeded experiments*

### *5.3.2.1 Effect of seed size (same number of crystals)*

In order to study the effect of seed size, the same number of particles but with three different average sizes were introduced into the system. The mass of crystals is proportional to the size because larger seeds need greater mass to constitute the same amount of particles. The total number of seeds calculated was approx. 90,000-100,000 particles. The initial degree of supersaturation used in these experiments was 2.21 g/g solution. The average seed size was determined by the sieving method and then analysed by laser diffraction method to obtain more detailed size distribution information. Analysing the volume density distribution results in Figure 5-10**,** the product profiles are very similar. The average particle size and the width of the distribution for three different seeds are the same. The 137.5 μm seed exhibits the highest growth due to having the lowest initial seed amount. Compared to the highest seed size (275 μm), the product size only increased slightly from 350 μm to 500 μm and resulted in a wider distribution. The absence of the fine crystals in the product density profiles, indicates that nucleation was suppressed.

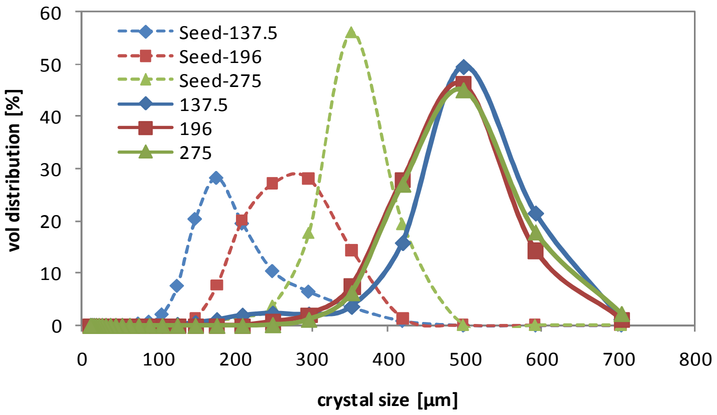

Figure 5-10. CSD (as mass density) for three average seed sizes with same number of crystals (solid line: product, dashed line: seeds)

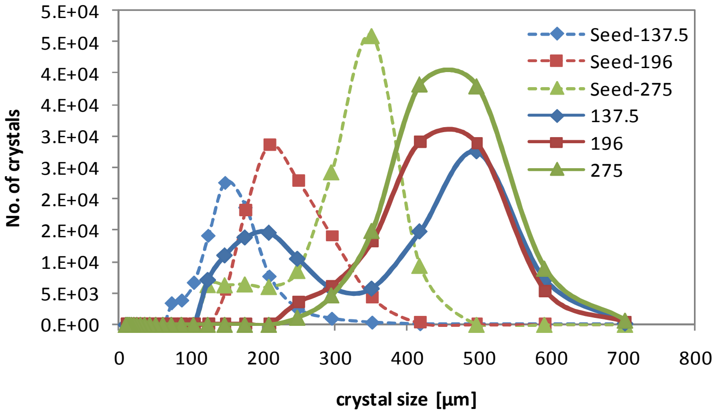

Figure 5-11. CSD (as number of crystals) for three average seed sizes with same number of crystals (solid line: product, dashed line: seeds)

The results in Figure 5-11 reveal some interesting points. First, the small seeds produced a bimodal peak while the larger sizes produced a single peak distribution. For the same batch time, small seeds need more time to attain a larger size, while the large seeds need less time. Second, as the final average size based on number is approximately the same, therefore, small seeds showed more growth. The effect of seed size for the same number of crystals shows that the different average sizes will change the distribution due to the differences in surface area. Larger crystals have more surface area but also higher suspension density which can lead to secondary nucleation. Figure 5-12 shows the images from three sets of experiments. The sizes and shapes shown are similar in appearance except for Set-77 which contains more fine crystals than the others.

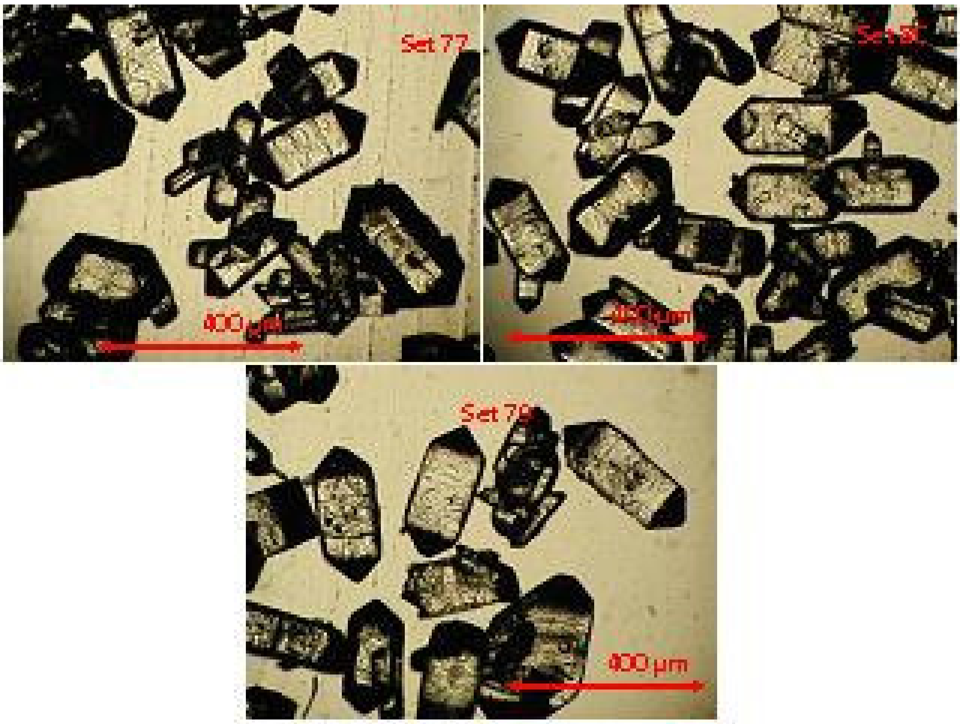

**Figure 5-12. Crystals images for Set 77 (137.5 µm), Set 80 (196 µm), and Set 79 (275 µm)**

#### *5.3.2.2 Effect of seed size (same seed loading)*

The seed loading ratio or seed concentration ($C_s$) is defined as the ratio of the actual mass of seeds loaded to the theoretical yield of crystal mass due to maximum supersaturation (Jagadesh et al. 1999). For the same seed loading ratio, i.e. $C_s$ = 5%, the different seed sizes will result in different average sizes of the final crystal product. The seeds with a single peak distribution grew and formed a dual peak product size distribution. The 137.5 µm and 165 µm seeds grew to sizes of 510 µm and 580 µm (2nd peak) respectively as shown in Figure 5-13. The presence of the dual peak was caused by the crystal to crystal, crystal to wall, and crystal to impeller contacts. The contact nucleation that produced finer crystals becomes more apparent in the number distribution results. The first two peaks at 170 μm and 210 μm combined with the second peaks described previously are indicative of secondary nucleation as shown in Figure 5-13. The coarse growth crystals may break and form finer crystals during the batch processing time where the impeller speed is constant at 300 rpm. Therefore, the effect of impeller speed on the secondary nucleation was constant throughout the process.

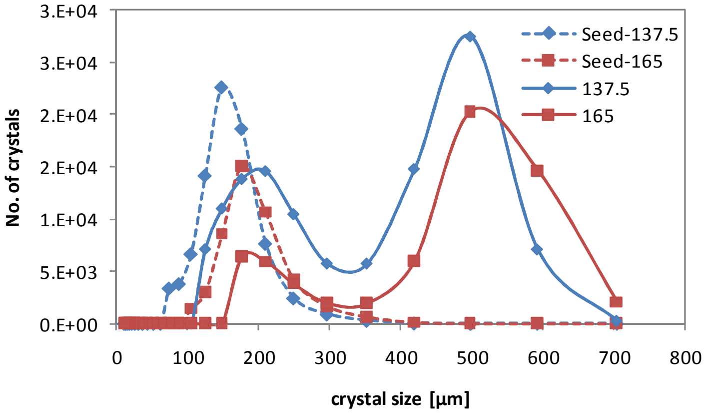

**Figure 5-13. CSD (as number of crystals) for two average seed sizes with same seed loading (solid line: product, dashed line: seeds)**

By analysing the results in Figure 5-13, when the low seed loading ratio was used, the first peak represents grown-nuclei and the second peak is the grown seeds. This trend was not observed in the previous results of Figure 5-11 where larger seeds had a loading seed ratio greater than 5%. A seed loading ratio greater than 5% was sufficient to suppress the impact of nucleation. The seed sizes from set-77 are smaller than for set-72 and this led to the final CSD where set-77 resulted in smaller and finer products for both peaks than from set-72. Visual observations of Figure 5-14 confirm that set-77 contains much finer products than set-72.

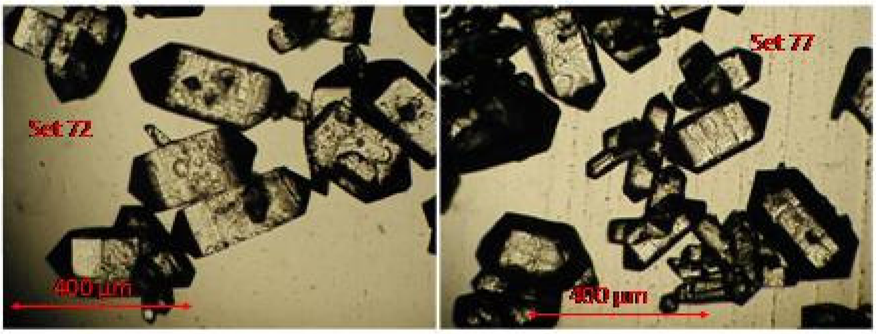

**Figure 5-14. Crystals images for Set 72 (165 μm), and Set 77 (137.5 μm)**

### 5.3.2.3 *Effect of supersaturation*

Mullin et al. (1970) reported the effect of supersaturation for a single crystal of mono-ammonium phosphate already knowing that supersaturation influences the growth rate, crystal habit and quality of crystal. The critical value of supersaturation ($\Delta c_c$) was reported to be 0.03 kg/kg water or 2.91 g/100 g of solution. In our set of experiments, the initial supersaturations used were 4.55 and 2.21 g/100 g solution for set 67 and set 68 respectively (see Table 5-1). The seed loading ratio was 5% but the seed amount for set 67 was higher due to higher supersaturation.

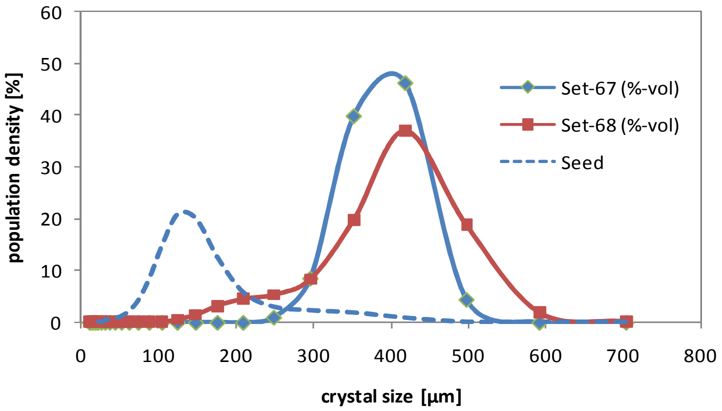

**Figure 5-15. CSD (as mass density) for different initial supersaturation, Set 67 = 4.55 and Set 68 = 2.21 g/100 g sol. (solid line: product, dashed line: seeds)**

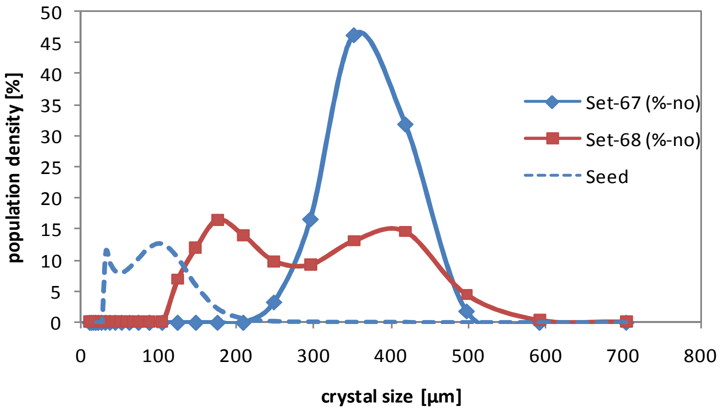

**Figure 5-16. CSD (as number density) for different initial supersaturation, Set 67 = 4.55 and Set 68 = 2.21 g/100 g sol. (solid line: product, dashed line: seeds)**

The CSD profile for the low initial supersaturation (set 68) reflects the grown-seeds because a similar shaped distribution is shown in Figure 5-16. However, set 67 with a high initial supersaturation generated crystals as shown by a completely different profile as the nucleation becomes apparent, and the crystals tend to be a combination between grown-nuclei and grown-seeds. The 5% seed loading ratio was found not to be effective for suppression of nucleation at high initial supersaturation, only at low supersaturation. The growth rate in set-67 was probably very high due to the high supersaturation. The coupled effects of high nucleation and high growth will result a distinctive CSD profile as shown in Figure 5-15 and Figure 5-16.

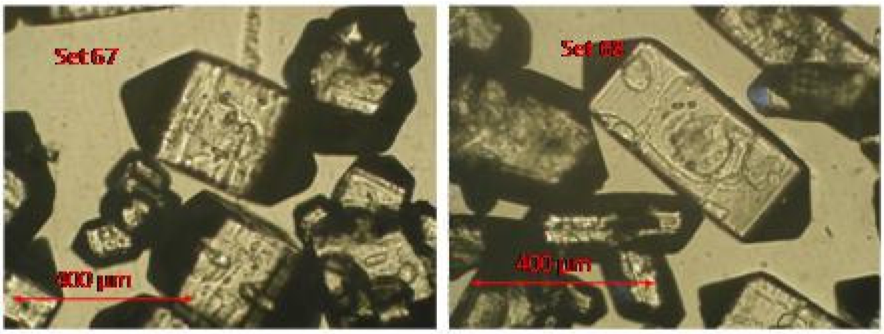

**Figure 5-17. Crystals images for Set 67 (4.55 g/100g sol.), and Set 68 (2.21 g/100 g sol.)**

A different crystal habit can be seen in the crystal images shown in Figure 5-17 and Figure 5-18. As the supersaturation was lowered from 4.55 to 1.36 g/100 g solution, the crystal shape becomes needle-like. An individual face growth on the z-axis becomes significantly greater than on the other axes. Crystals tend to grow only in the z-direction and form a needle shape which is easier to stick together thus forming agglomerates. Our work confirms the critical supersaturation proposed by Mullin (1970) that triggers MAP crystal habit alteration from low to high aspect ratio.

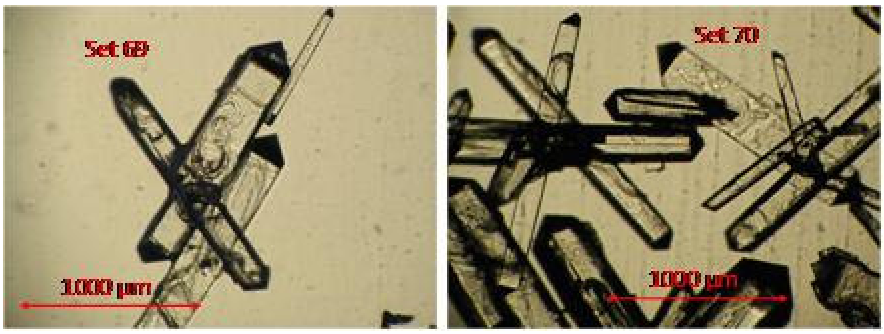

**Figure 5-18. Crystals images for Set 69 and 70 (1.36 g/100 g sol.)**

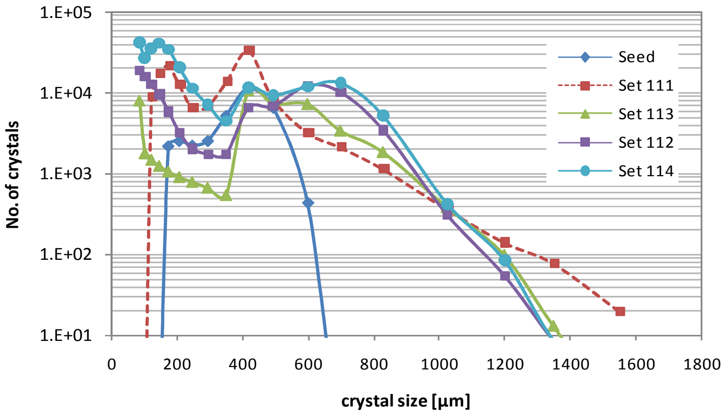

**Figure 5-19. CSD (as number of crystals) for different supersaturations and conditions (Set 111: Non-seeded, ΔT=5; Set 113: seeded, ΔT=3; Set 112: seeded, ΔT=5; Set 114: seeded, ΔT=7°C).**

Additional experiments have been performed to verify the repeatability of the results and to further investigate the effect of the initial supersaturation and the non-seeded condition on the final CSD. Figure 5-19 shows that in a seeded condition supersaturation initiate the birth rate of the crystal nuclei, i.e. the nucleation process. When supersaturation increased, the small crystals of 40 – 400 µm also increased significantly. The rest of the size ranges remained similar as grown seeds (having a largest size of 1300 µm) having grown from seeds of an average size of 400 µm. To compare the seeded and non-seeded condition, two sets of experiments at the same supersaturation (set 111 and set 112) were performed. The non-seeded experiments generated more fine and coarse crystals and, therefore, the width of the distribution was wider than for the seeded condition. These additional experiments validated the effects of supersaturation as proposed from the previous results.

#### *5.3.2.4 Effect of seed loading*

To study the effect of seed loading ratio, seed crystals with average size 137.5 µm were used. The initial supersaturation level was set at 2.21 g/ 100 g solution. Three values of loading ratio were used, namely Cs=5%, 20% and 30%.

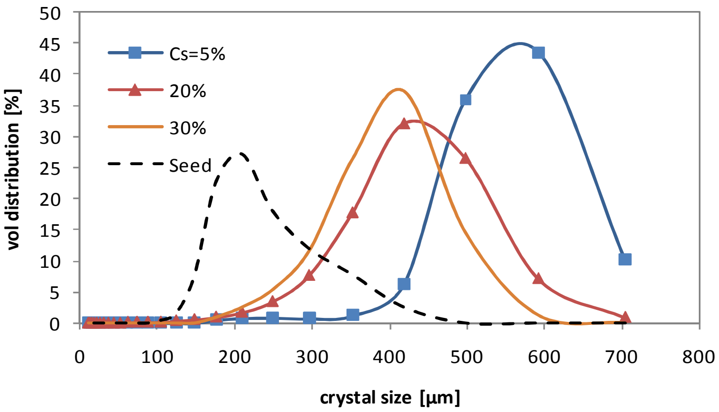

**Figure 5-20. CSD (as mass density) for different seed loadings, Cs=5. 20 and 30% (solid line: product, dashed line: seeds)**

As already discussed, at a low seed loading the nucleation becomes more prevalent while growth was dominant with a high seed loading. These phenomena cannot be seen clearly in the mass density results; however, in the number density figures (see Figure 5-22 and Figure 5-23) we can observe bimodal profiles. The first peak is considered to be a grown-nuclei and the other consists of grown-seeds. In addition for Cs=30%, nucleation was reduced resulting in the uni-nodal profile.

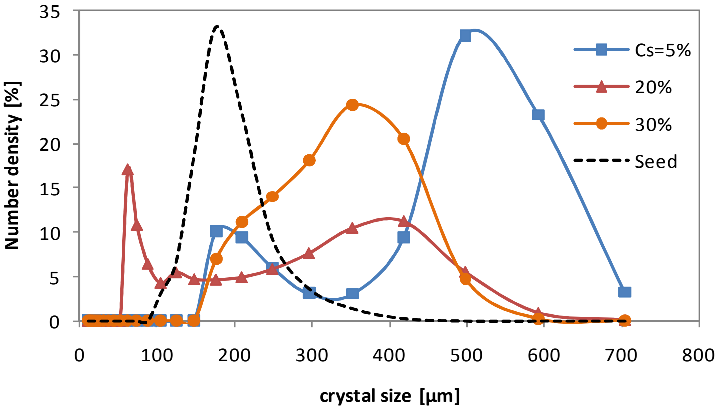

**Figure 5-21. CSD (as number density) for different seed loadings, Cs=5. 20 and 30% (solid line: product, dashed line: seeds)**

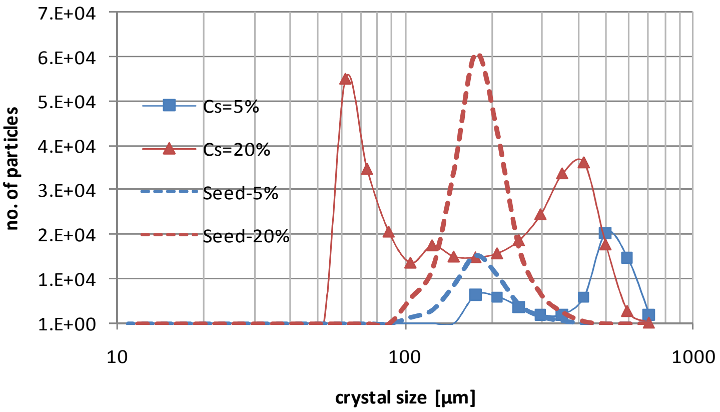

**Figure 5-22. CSD (as number of crystals) for different seed loadings, Cs=5 and 20 (solid line: product, dashed line: seeds)**

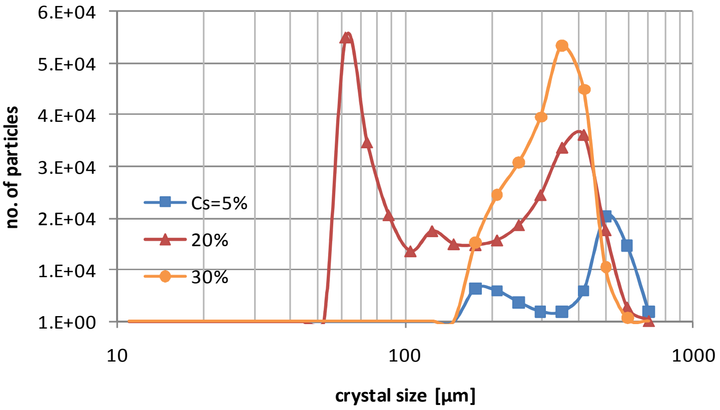

**Figure 5-23. CSD (as number of crystals) for different seed loadings, Cs=5, 20 and 30 (solid line: product, dashed line: seeds)**

In general, we can establish that as the seed loading ratio increases, then the average size of crystal product decreases. Doki et al. (1999) developed a very simple mass balance equation to predict the product size:

$$\frac{L_p}{L_s} = \left(\frac{1 + C_S}{C_S}\right)^{1/3} \tag{5-3}$$

where $L_p$ is the product size; $L_s$ is the seed size; and $C_s$ is the seed loading ratio. Table 5-3 and Figure 5-24 show the calculated product size from the mass balance equation compared with $d_{50\%}$ results obtained from a particle size analyser. Both values are in good agreement, indicating that the proposed equation can be used to determine, the product average size for each seed loading ratio selected.

Table 5-3. Calculated and experimental crystal average sizes for various seed loadings

| Cs | Lp | d-50 |
|---|---|---|
| **5%** | 551.8 | 504.7 |
| **20%** | 363.4 | 383.4 |
| **30%** | 326.1 | 357.1 |

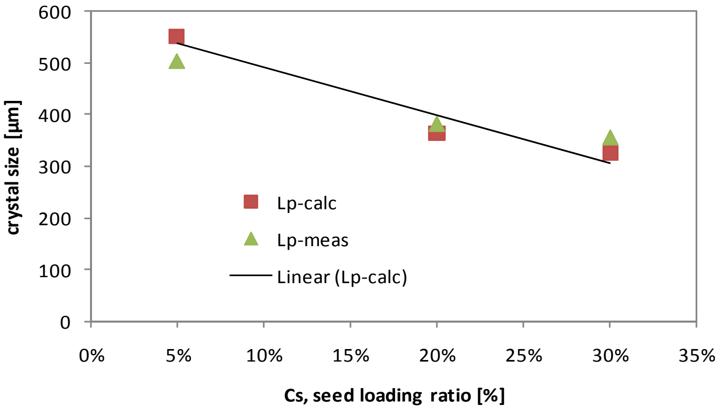

Figure 5-24. Experimental and calculated results of average crystal size for various seed loading ratios

Figure 5-25. Crystals images for Set 72 (Cs = 5%), Set 73 (20%) and 78 (30%)

## 5.4 Remarks

In cooling batch crystallisation, the cooling factor and initial supersaturation have a significant effect on the supersaturation profiles although they do not affect the crystal size distribution (CSD). Higher cooling rate produces higher supersaturation generation rate and, therefore, it attains higher supersaturation level above the metastable limit, and then causes higher nucleation rate at the time of nucleation.

The seed loading ratio has the most significant effect on the CSD profiles, followed by the supersaturation factor and seed size. Bimodal profiles are observed with a low seed loading ratio, indicating that nucleation is present. Good agreement between Kubota's mass balance equation and our experimental results validate the successful seeding technique used with the mono ammonium phosphate system.  Kubota's equation can be used to predict the critical seed loading ratio for the subsequent experiments. Similarly, as in a non-seeded system, the cooling rate, stirring speed and crystal yield do not have significant effects on the CSD product if enough seeds are loaded under well-mixed conditions. Degree of supersaturation influences not only the kinetics but also the crystal shape and habit.

## 5.5 References

Buchanan, G. H. and G. B. Winner (1920). The solubility of mono-and diammonium phosphate. *Industrial & Engineering Chemistry*, 12(5), 448-451.

Doki, N., N. Kubota, A. Sato, M. Yokota, O. Hamada and F. Masumi (1999). Scaleup experiments on seeded batch cooling crystallization of potassium alum. *AIChE Journal*, 45(12), 2527-2533.

Garside, J. and R. I. Ristic (1983). Growth rate dispersion among adp crystals formed by primary nucleation. *Journal of Crystal Growth*, 61(2), 215-220.

Jagadesh, D., N. Kubota, M. Yokota, N. Doki and A. Sato (1999). Seeding effect on batch crystallization of potassium sulfate under natural cooling mode and a simple design method of crystallizer. *Journal Of Chemical Engineering of Japan*, 32, 514-520.

Kubota, N., N. Doki, M. Yokota and D. Jagadesh (2002). Seeding effect on product crystal size in batch crystallization. *Journal Of Chemical Engineering of Japan*, 35(11), 1063-1071.

Mullin, J. W. (2001). *Crystallization*. Butterworth-Heinemann, Oxford.

Mullin, J. W. and A. Amatavivadhana (1967). Growth kinetics of ammoniumand potassium-dihydrogen phosphate crystals. *Journal of Applied Chemistry*, 17, 151-156.

Mullin, J. W., A. Amatavivadhana and M. Chakkraborty (1970). Crystal habit modification studies with ammonium and potassium dihydrogen phosphate. *Journal of Applied Chemistry*, 20, 153-158.

Ross, W. H., A. R. Merz and K. D. Jacob (1929). Preparation and properties of the ammonium phosphates. *Industrial & Engineering Chemistry*, 21(3), 286-289.

Torgesen, J. L. and A. T. Horton (1963). Electrolytic conductance of ammonium dihydrogen phosphate solutions in the saturation region. *The Journal of Physical Chemistry*, 67(2), 376-381.

Warstat, A. and J. Ulrich (2006). Seeding during batch cooling crystallization - an intial approach to heuristic rules. *Chemical Engineering and Technology*, 29(2), 187-190.

# 6. Semi-batch Reactive Crystallisation of Mono-Ammonium Phosphate

## 6.1 Introduction

Ammonium phosphates are produced by reactions (precipitation) between ammonia and phosphoric acid resulting in the formation of the mono, di-basic or tri-basic salts. When the molar ratio of nitrogen from ammonia and phosphorus from phosphoric acid is 1.0, mono-ammonium phosphate ($NH_4H_2PO_4$) is formed, and when the molar ratio is 2.0, then di-ammonium phosphate ($(NH_4)_2HPO4$) is formed. The reaction is exothermic so the mono and di-ammonium phosphate are produced at an elevated, and relatively constant, temperature of 110 $^{o}$C. The equations for the neutralization reaction between ammonia and phosphoric acid are:

$$\mathrm{NH_3 + H_3PO_4 \longrightarrow NH_4H_2PO_4}$$

$$\mathrm{NH_3 + NH_4H_2PO_4 \longrightarrow (NH_4)_2HPO_4}$$

$$\mathrm{NH_3 + (NH_4)_2PO_4 \longrightarrow (NH_4)_3PO_4}$$

The mono-ammonium phosphate (MAP) tends to produce needle-like crystals while the di-ammonium phosphate (DAP) results in more granular forms of crystals. Tri-ammonium phosphate (TAP) is an unstable crystal as it decomposes and releases ammonia at a room temperature and less soluble in water than MAP and DAP. MAP and DAP are used as a major source of phosphorus in fertilizer. Several important characteristics of MAP, DAP and TAP are identified in Table 6-1:

**Table 6-1. Basic properties of three kinds of ammonium phosphates (Ross et al. 1929)**

| | MAP | DAP | TAP |
|---|---|---|---|
| Molar Mass (g/mol) | **115** | **132** | **149** |
| Specific Gravity @ 20°C | **1.803** | **1.619** | **n/a** |
| Melting point (°C) | **190** | **n/a** | **n/a** |
| Solubility@25°C (g/g water) | **40.0** | **69.5** | **17.7** |
| Crystal Form | **Tetragonal** | **Monoclinic** | **Orthorhombic** |

Research in reactive crystallisation has not been as popular as non-reactive crystallisation studies. Most reactive crystallisation research was conducted in liquid-liquid systems, and some in gas-liquid. The applications range from calcium oxalate (Bernard-Michel et al. 1999), benzoic acid (Slund et al. 1992; Ståhl et al. 2001), calcium carbonate (Söhnel et al. 1982; Al Nasser et al. 2008), barium sulphate (Aoun et al. 1999; Uehara-Nagamine et al. 2001), barium carbonate (Chen et al. 2001; Salvatori et al. 2002), potassium dihydrogen phosphate (Barata et al. 1996), and several others. Kotaki and Tsuge (1990) studied reactive crystallisation of calcium carbonate by gas-liquid reactions in a seeded and unseeded batch crystalliser. They concluded that the crystal growth of an unseeded system was controlled by primary nucleation, followed by secondary nucleation.

Tavare and Garside (1990) performed a simulation study on liquid-liquid reactive crystallisation in a semi-batch crystalliser. They examined the effects of reaction kinetics, nucleation kinetics, and a feed addition profile on the product characteristics and compared these with the corresponding results for a batch crystalliser. They found that a reaction engineering approach can be used in the modelling procedure; this simulation approach could provide a starting point for experimental studies, for example in determining the feed addition profile, which a significant factor in controlling the crystal size distribution. The importance of mixing in the reactive crystallisation process was identified in the recent work of Abbasi and Alamdari (2007) who studied the mixing effects on CSD in the semi-batch reactive crystallisation of manganese ethylenebis. For reactive crystallisation, they found that both meso- and micro-mixing are the most influential factors because the reactions take place on a molecular scale. The uniqueness of the nature of reactive crystallisation, and the complexity of the required model, provided a significant challenge in our work to explore the reactive crystallisation of mono-ammonium phosphate in order to understand the underlying mechanisms and interactions on the reactions and crystallisation processes.

Research studies of ammonium phosphates reactive crystallisation are limited by the effects created by impurities. The conventional process of producing ammonium phosphate from phosphoric acid was modified as described by Zhong and co-workers (1999). They modified the ammonium phosphate production process (APPAC process) which needed high quality ores in the process, with a slurry concentration that can utilise middle and low quality ores. A high impurity content that causes scaling and blocking problems in the acid concentrator-heater may be avoided by using the modified process. Campbell and co-workers (2006) in Australia reported the impact of impurities on the ammonium phosphates slurry characteristics, which cause several problems in mixing, flow ability and pumping efficiency. These factors contribute to the unit process/plant efficiency. They found that hydrolysis of metal ions ($Fe^{3+}$ and $Al^{3+}$) initiates solids formation because they act as nucleation sites for crystallisation. In industry, the hydrolysis process leads to some challenges and is less efficient. This is due to a high recycle ratio in the granulation process, the fluidity of the slurry, and uncontrolled product size distribution, which can subsequently reduce the efficiency of the downstream units and produce an off-specification product. Although these are commercial processes which have been well researched, there are still some challenges related to the crystallisation kinetics and solubility which need attention. There is critical need for MAP crystallization models which can be applied to predict, design and optimise the process.

In order to improve our understanding of the process, the following approaches were taken. First, MAP was produced from pure phosphoric acid by a single feed of ammonia solution. N/P molar ratio, initial concentration of phosphoric acid, effect of seeding policy and supersaturation were studied in order to obtain more insights into the reaction and crystallisation mechanisms. Several critical variables, such as pH, temperature, MAP concentration in solution, suspension density, and mean crystal size, were identified. Second, MAP was produced by a dual feed system of phosphoric acid and ammonia solution. A saturated or supersaturated MAP solution was used as a starting solution. The feed flow rate, feeding time, seeding effect, initial supersaturation, mixing effect, and initial concentration effects on product characteristics, were studied experimentally. The same output variables were observed and recorded in order to gain insight into the reaction and crystallisation mechanisms of the MAP system.

## *6.2 Experimental Details*

As shown in Figure 6-1, a closed-jacketed (500 ml) vessel equipped with a dual feed system and a turbine-type agitator was used as a reactor and crystalliser. The reaction was conducted at 10-20°C and 300 rpm. A 28 wt% ammonia solution and a phosphoric acid 40 wt% solution were used as reactants and fed into a saturated MAP solution. A temperature controller, a pH controller, and a conductivity meter were used to manipulate, monitor and record the changes in the process variables during the reaction.

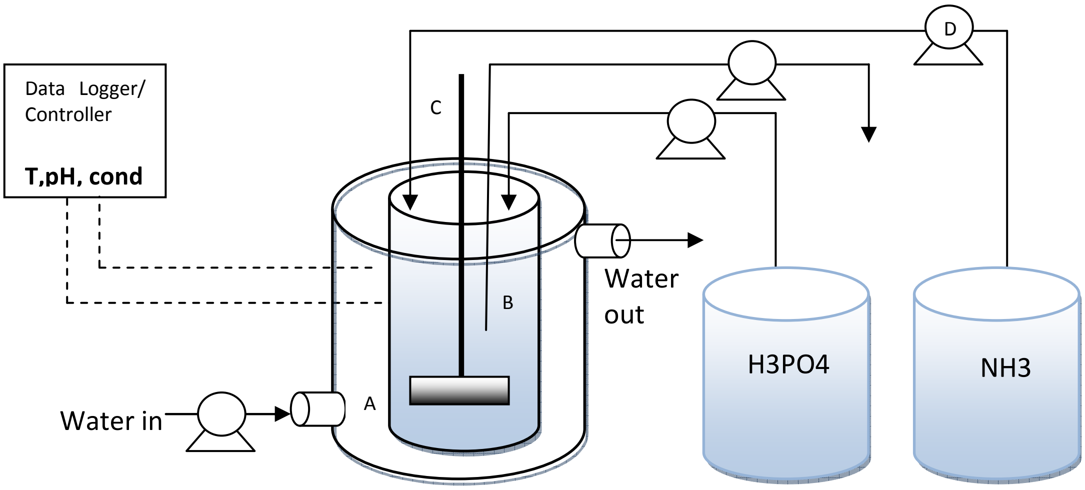

**Figure 6-1. Experimental setup; A: cooling jacket, B: vessel, C: impeller, D: peristaltic pump**

First, a saturated mono-ammonium phosphate solution was prepared based upon its saturation temperature. Once the correct temperature was achieved, the dual feeding system was started. Cooling water temperature was set at either 10°C, 15°C, or 20°C. The conductivity probe had a range from 2.0 – 19.99 S/m. Temperature, pH and conductivity output data were recorded directly by a data logger. For the single-feed system, an $NH_3$ solution was fed into a $H_3PO_4$ solution, with different concentrations for each run, which was already inside the crystalliser. For the seeded system, a known amount of seed was introduced at the same time as the first droplet of reactant(s) was fed into the crystalliser. In the phosphoric acid system, the N/P molar ratio and phosphoric acid concentration were the key variables to be investigated while, in the MAP system, the effects of reaction time, supersaturation and seed amount on the crystal size distribution were determined.

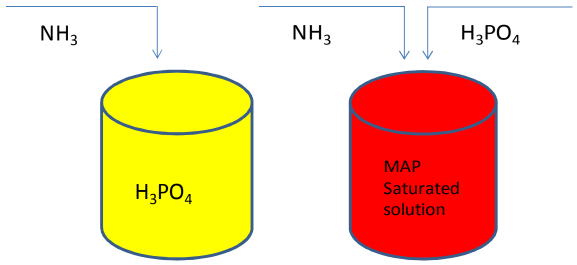

**Figure 6-2 Single-feed and dual-feed systems**

Finally, the slurry was filtered, washed and dried. The crystal size distribution was measured by a laser diffraction apparatus (Microtrac®) and a sieving method. The number of crystal was calculated from the mass of dry crystals. The conductivity data was converted into the concentration of solute MAP in the solution using the technique reported by (Torgesen et al. 1963).

## 6.3 Results and Discussion

### 6.3.1 Single-feed semi-batch reactive crystallisation

**Table 6-2. Summary of experimental results for single-feed systems**

| | | $\Delta c$ | MV | MN | SD | Yield |
|---|---|---|---|---|---|---|
| Set | N/P | [g/g sol] | [µm] | [µm] | [µm] | [g/g sol] |
| 45 | 0.79 | 0.088 | 252.3 | 109.8 | 92.35 | 0.080 |
| 44 | 0.85 | 0.107 | 399.47 | 56.332 | 184.01 | 0.051 |
| 42 | 0.91 | 0.125 | 393.53 | 21.235 | 168.11 | 0.108 |
| 46 | 0.99 | 0.149 | 443.44 | 14.706 | 79.37 | 0.145 |
| 39 | 1.08 | 0.138 | 439.16 | 16.751 | 94.47 | 0.080 |
| 47 | 1.18 | 0.136 | 396.79 | 15.184 | 112.06 | 0.070 |
| 38 | 1.28 | 0.112 | 362.72 | 22.863 | 0.03 | 0.148 |

**Note: N/P = molar ratio of ammonia and phosporic acid; MV = mean size based on volume; MN = mean size based on numbers of crystals; SD = standard deviation of MV.**

As shown in Table 6-2. , the N/P ratio has a significant effect on CSD. Mean size based on volume (MV) increases from 250 to 450 µm as N/P increases (up to N/P=1) and then decreases to 360 µm. An inverse trend appeared in the mean size based on the number (MN), and MN reduced from 110 µm to 15 µm. Smaller crystals are produced when the ratio increased. The N/P molar ratio produces a different degree of supersaturation ($\Delta c$) which governs the crystal size distribution (CSD).

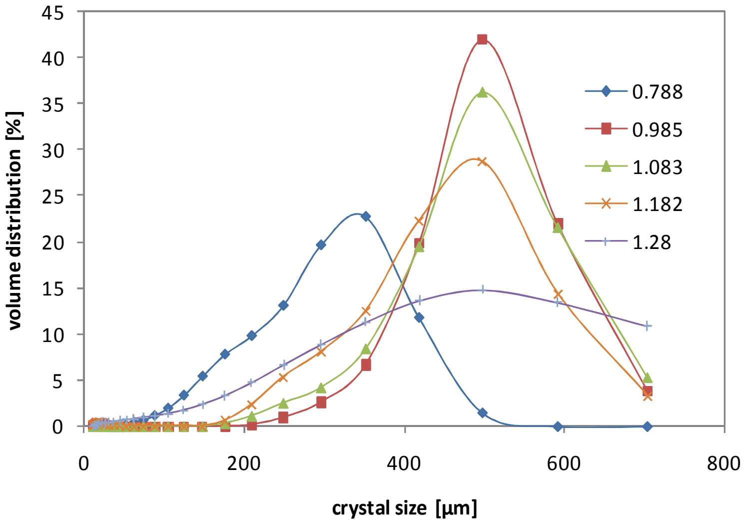

**Figure 6-3. CSD (as mass density) of single-feed system with 40 wt% for various N/P ratios**

From the CSD profiles in Figure 6-3, the low N/P ratio produced finer crystals as the amount of solids formed is small and they do not have time to grow. A high ratio (1.28) gave coarser crystal size. The number density in Figure 6-4 confirms that most of the crystals with N/P = 1.08 were less than 50 µm in size, and the high N/P ratio of 1.28 produced a large number of coarser crystals. From (Campbell et al. 2006), it is known that MAP is least soluble at an N/P ratio of about 1.0 and most soluble at 1.4. It is clear that the CSD results correlate well with the MAP solubility. An N/P closer to 1.0 was experimentally shown to result in the lowest solubility of salt and produced MAP crystals. DAP crystals cannot be formed in the system of 40 wt% phosphoric acid solution and 28 wt% ammonia solution due to its high solubility. However, TAP can easily be produced when the pH exceeded 8.0.

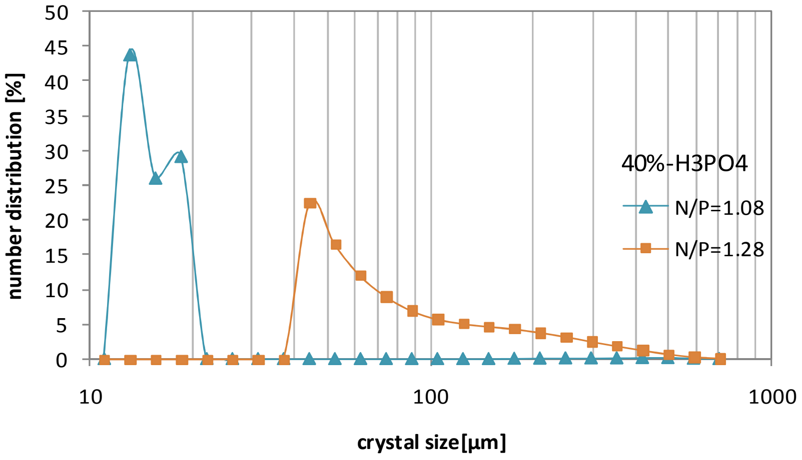

**Figure 6-4. CSD (as number density) for 40 wt% phosphoric acid and with N/P =1.08 and 1.28**

### *6.3.2 Non-seeded reactive crystallisation*

A preliminary study of non-seeded reactive crystallisation was performed by varying the amount of MAP saturated solution used (22.55 g/100 g solution at 10°C), i.e. 100, 200, or 300 g, and feeding it with a dual-feed system. The phosphoric acid and ammonia solution at molar ratio N/P = 1.0 was titrated from a sample obtained from a fixed point below the surface of saturated/supersaturated mono ammonium phosphate. The total combined flow rate of the dual-feed system at high flow rate (high-Q) and low flow rate (low-Q) was 4.45 and 1.96 g/min respectively. Total default feeding time when a high flow rate was used was 5 minutes, and 11 minutes when a low flow rate was applied. Total batch time ranged from 45 to 90 minutes, but usually a 60 minute batch time was employed.

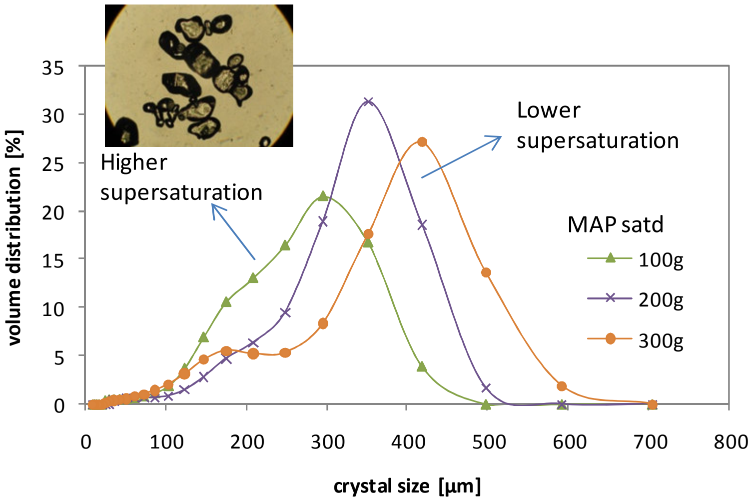

**Figure 6-5. CSD (as mass density) in a non-seeded system for various initial capacities of MAP saturated. (inset: photo of crystals in the 100 g MAP sat. solution)**

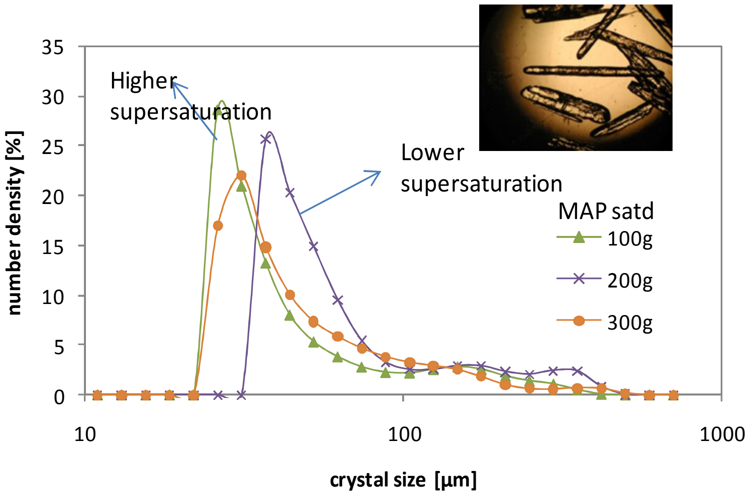

**Figure 6-6. CSD (as number density) in a non-seeded system for various initial capacities of MAP saturated. (inset: photo of crystals in the 300 g MAP sat. solution)**

A CSD analysis for the final product was performed and is shown in Figure 6-5 and Figure 6-6 . When a small amount of MAP saturated solution was used (100 g), a higher supersaturation condition was reached due to a smaller amount of solvent. Consequently when higher supersaturation was created then a smaller crystal size was produced. The mean size of the crystals increased steadily from 300 µm to 450 µm as the capacity of the crystalliser was increased from 100 g to 300 g of MAP saturated solution. The number density results corroborate the volume density results, but at 300 g the profile is lower than 200 g. It is believed that this can happen due to needle-shaped crystals which lead to a high breakage potential in the suspension, or in the sampling and solid form. The crystal shape was round at the high supersaturation conditions and the shape factor of a sphere can be used to predict the number density. However for needle-shaped crystals, the factor deviates from the sphere shape factor, so prediction of the number density is less reliable. The unseeded crystals at low supersaturation have a larger aspect ratio (H/W) compared to seeded crystallisation, which is discussed in the following section.

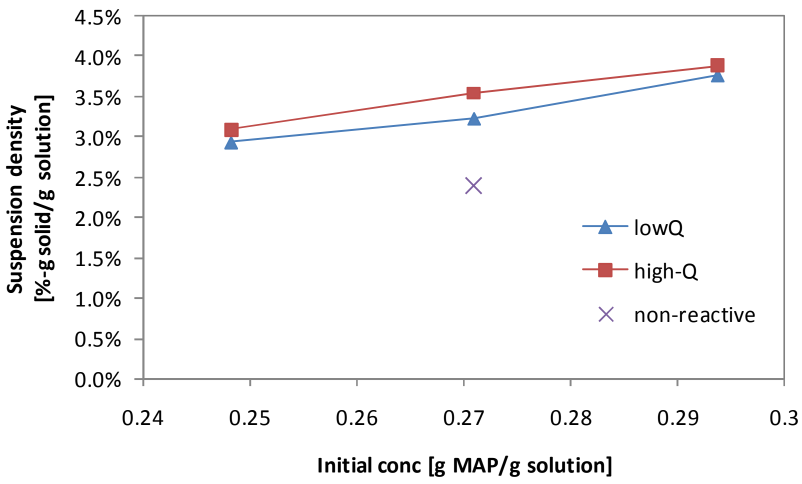

**Figure 6-7. Suspension density of reactive and non-reactive non-seeded system for several initial concentrations**

The results of suspension density presented in Figure 6-7 show that the reaction occurred and produced some MAP solids. This is apparent as the suspension density in the reactive crystalliser is considerably higher than the non-reactive one. The suspension density also increased when higher flow rate and higher initial concentration were used, although the degree of supersaturation was kept constant at 5°C. CSD profiles of the non-seeded reactive crystallisation of MAP for various initial concentrations and two sets of flow rates can be seen in Figure 6-8 and Figure 6-9. A general conclusion can be drawn from the CSD profiles that non-seeded reactive crystallisation has a wider size distribution due to domination of nucleation and growth processes, these occur after the initial stage.

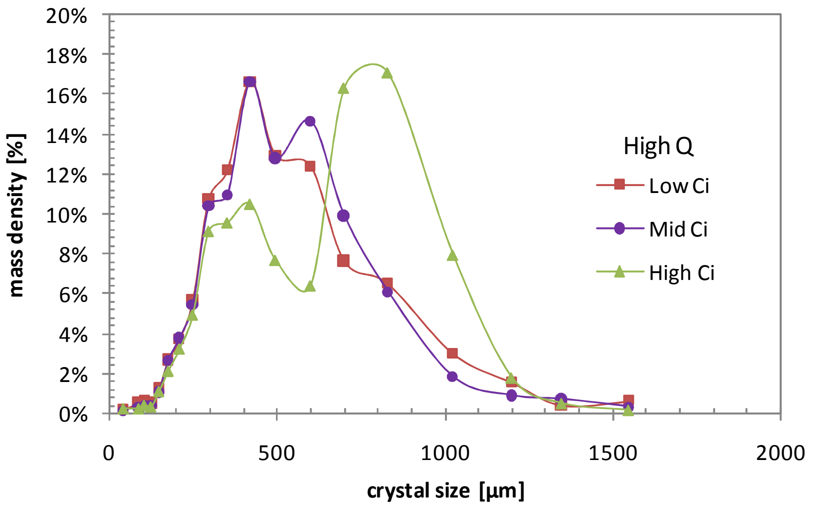

**Figure 6-8. CSD (as mass density) for non-seeded system, high flow rate and various initial concentrations**

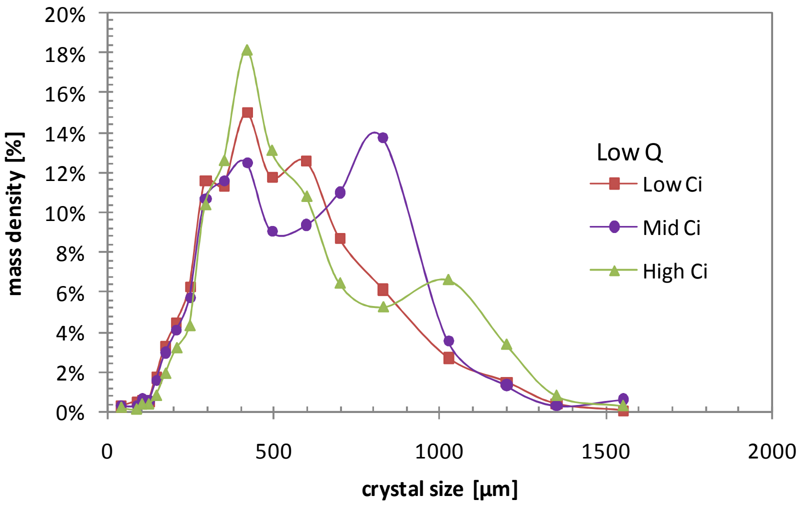

**Figure 6-9. CSD (as mass density) for non-seeded system, low flow rate and at low/middle/high initial concentrations**

In order to confirm that a reaction does occur between ammonia and phosphoric acids, an X-ray diffraction analysis of two powder samples was conducted. One sample was taken from the dual-feed experiment, non-seeded (Set-93) which initially had a supersaturated MAP solution. The tested sample was taken from a single-feed experiment, N/P = 0.79, which had a phosphoric acid solution initially (Set-45). The XRD results are shown in Figure 6-10. The set-45 result indicates that the MAP is a major product component and some traceable impurities from the source of the phosphoric acid may be detected as well. A more obvious result can be seen from Set-93 which has higher intensity as a base case. Further validation with the standard pattern of X-ray diffraction from (Xu et al. 2006) shows a perfect agreement in both cases. The conclusion is that the MAP was produced both in single- and dual-feed systems.

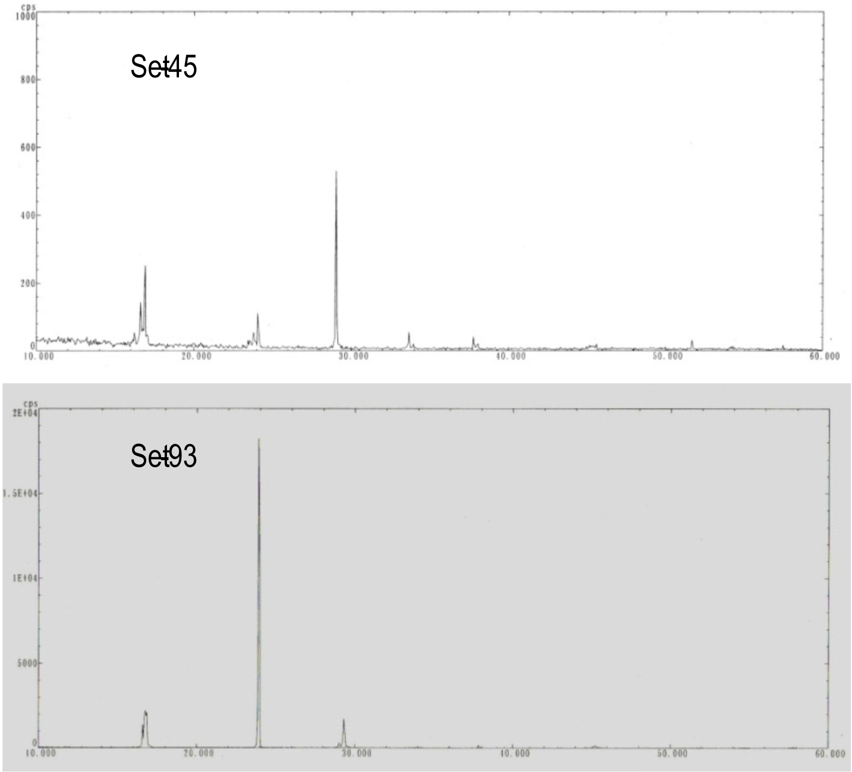

**Figure 6-10. X-ray diffraction results for Set-45 (single feed) and Set 93 (dual feed)**

### *6.3.3 Seeded reactive crystallisation*

In seeded reactive crystallisation, a known seed concentration and seed size were employed after considering an appropriate seeding policy based on the previous study of the non-reactive batch crystallisation case (Chapter 5). A seeded crystallisation behaves differently to a non-seeded one. In a typical seeded crystallisation, the supersaturation level directly decreases during the process. Crystal growth is controlled at all time, while a secondary nucleation may also take place in the form of contact nucleation. In this study, under the same initial supersaturation, the dynamic supersaturation of the non-reactive seeded system decreased more rapidly compared to the reactive seeded system. As in the reactive system, the solute mass balance was positive in the initial stage and became negative when the reaction was stopped.

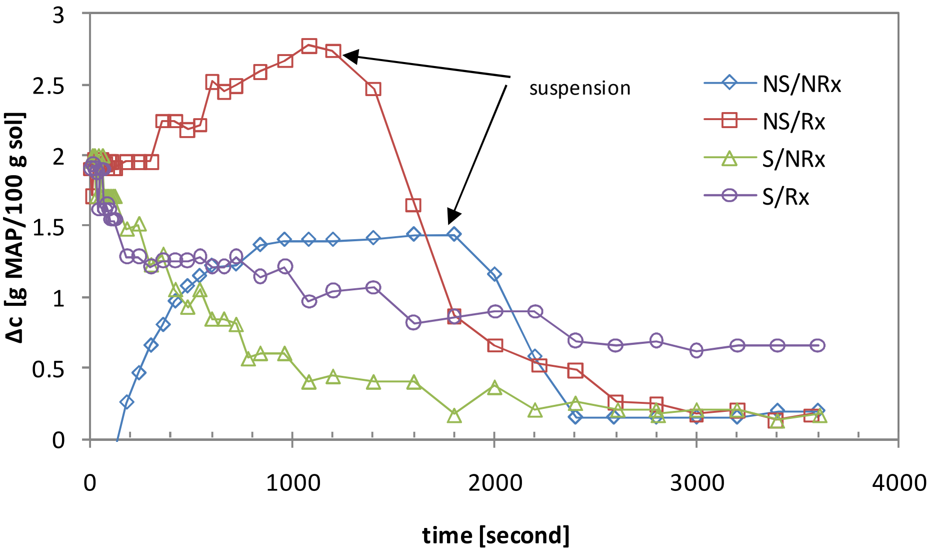

**Figure 6-11. Supersaturation profiles for various systems, NS: non-seeded, S: seeded, Rx: reactive, NRx: non-reactive**

For non-seeded reactive crystallisation, the supersaturation profile increased initially as feeding begins and reaction occurs. During feeding time, the nucleation process took place; however, the supersaturation did not decline. The reason for this is that reaction rate was much higher than the nucleation rate; therefore, the MAP solute was accumulated in the solution. Another possible explanation is that there was a higher dynamic solubility as the temperature increases slightly. Comparison of the supersaturation profiles of non-seeded and non-reactive systems (NS/NRx) in Figure 6-11, it is seen that the induction time for the non-reactive system is much longer than the reactive, because the maximum supersaturation was almost doubled. The nucleation rate is inversely related to induction time. Therefore, a higher nucleation rate for non-seeded reactive than for a non-seed non-reactive system was predicted. It can be seen that in the non-seeded system, primary and secondary nucleation were the rate controlling steps.

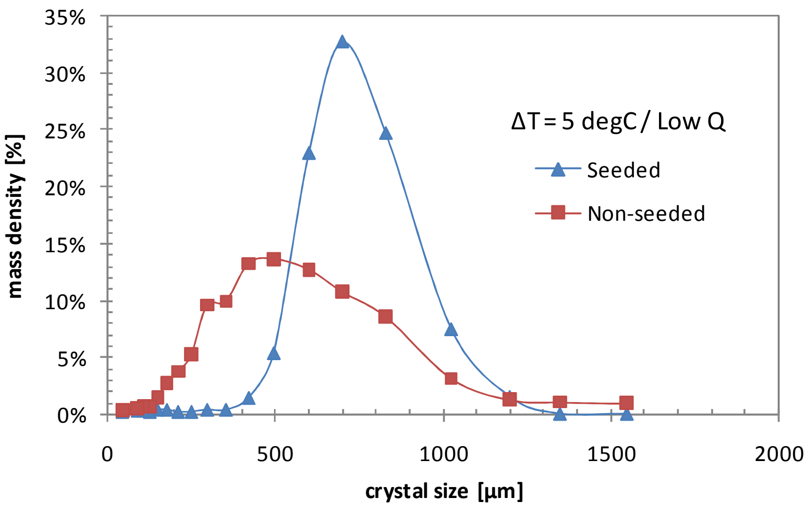

**Figure 6-12. CSD (as mass density) for ΔT=5C, low flow rate both in seeded and non-seeded**

Since a seeding policy reduces the nucleation process (Doki et al. 1999; Kubota et al. 2002), growth will mainly take place in the seed crystals. Seed crystals grow in size while still maintaining the same width of the size distribution as in the seed specification. Figure 6-12 shows the non-seeded results for finer crystals and wider distribution compared to 750 µm mean size and narrow distribution obtained from the seeded system. A small fraction of large crystals (1000-1500 µm) was produced in the non-seeded system, which indicates primary nucleation taking place from the initial stage and a long growth process of those crystals. Subsequently, the secondary nucleation continued and only a short growth period occurred for the majority of the crystals. This is shown by the wide distribution of crystals between 40 µm to 800 µm.

### *6.3.4 Feed flow rate effect*

The flow rate of the dual-feed system was set at two conditions, a high flow rate (high-Q) and low flow rate (low-Q) of 4.45 and 1.96 g/min respectively. It is assumed that the feed rate for both the ammonia solution and phosphoric acid changes the CSD due to a different reaction rate, followed by different supersaturation profiles. A high flow rate triggered a maximum reaction rate due to higher reactant concentration in the system. The temperature profile in Figure 6-13 confirms that the reaction rate did increase and, therefore, created higher local supersaturation and dynamic overall supersaturation levels in the initial stage. By maintaining a molar ratio (N/P) equivalent to 1, then 4.45 g/min total combined flow rate requires 5 minutes to reach 0.1-0.12 S/m increase in conductivity. The low flow rate of 1.96 g/min requires 11 minutes to reach the same state. Some technical problems with the experimental setup determined the choices below the minimum flow rate or higher than maximum flow rate. This was due to the pump capacity and the vessel volume used. However, some significant results were obtained and are presented here.

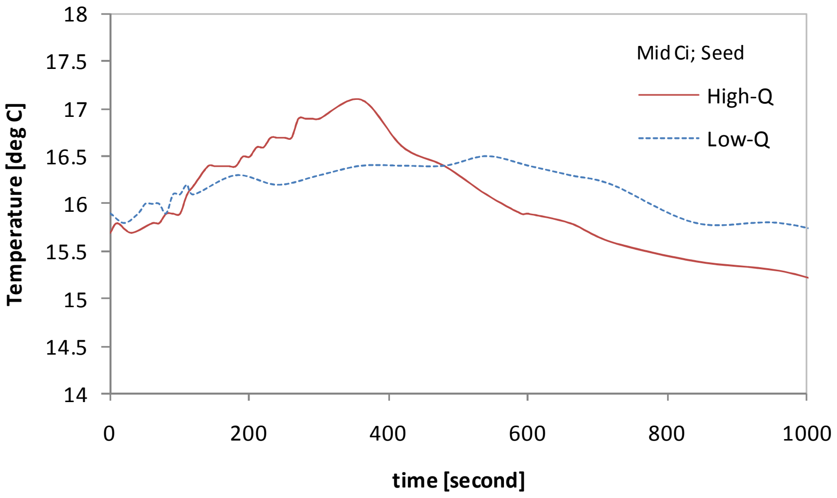

Figure 6-13. Temperature profiles of seeded, medium initial concentration, high/low flow rates

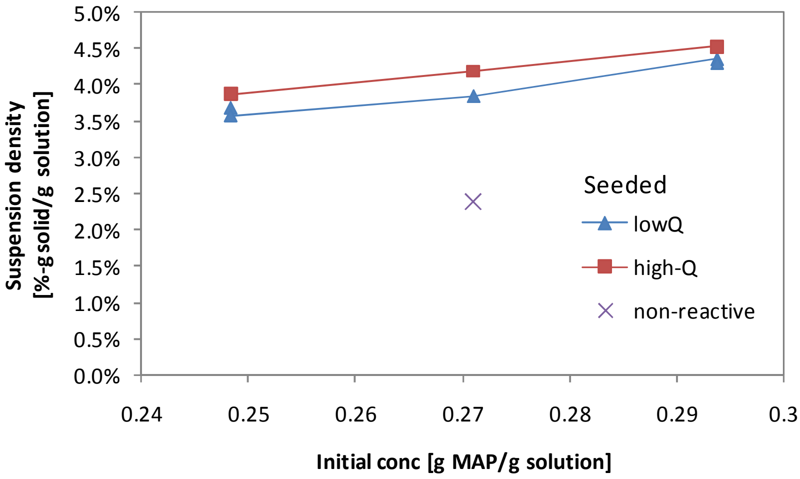

Figure 6-14. Suspension density of seeded system in low and high flow rate for various initial concentrations, (x) : non-reactive

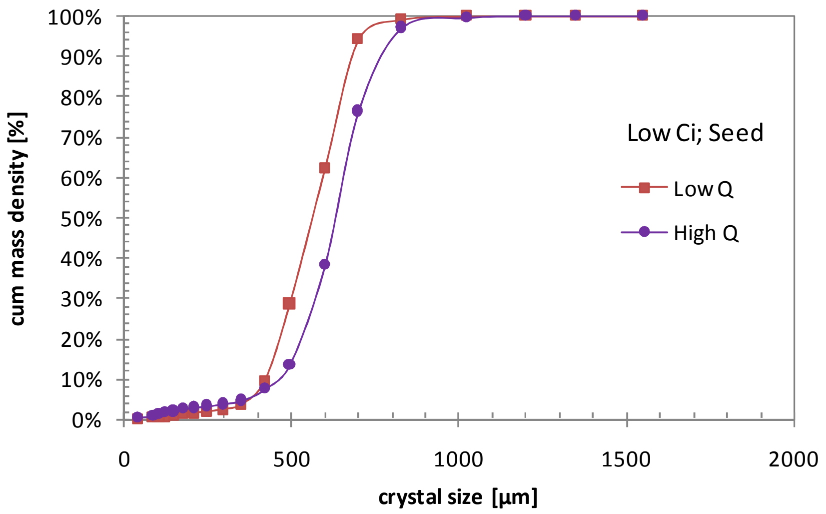

**Figure 6-15. Cumulative CSD (as mass density) for seeded, low initial concentration, both in high/low flow rates**

Considering Figure 6-7 and Figure 6-14, they both show the same trend - the high flow rate has a higher suspension density. In the seeded system, the suspension density range is 4.0-4.5 g/100 g solution for high-Q and 3.5-4.0 g/100 g solution for the low-Q. The higher flow rate also produced finer crystals. This is due to the higher supersaturation level which leads to increased nucleation. The cumulative CSD results presented in Figure 6-15 indicate coarser crystals produced by high-Q. The reason for this is that the batch time (total time reaction plus cooling steps) for high-Q is 400 seconds longer than for the low-Q batch time of 4000 seconds. The effects of flow rate cannot be seen in these results because only final CSD data were available.

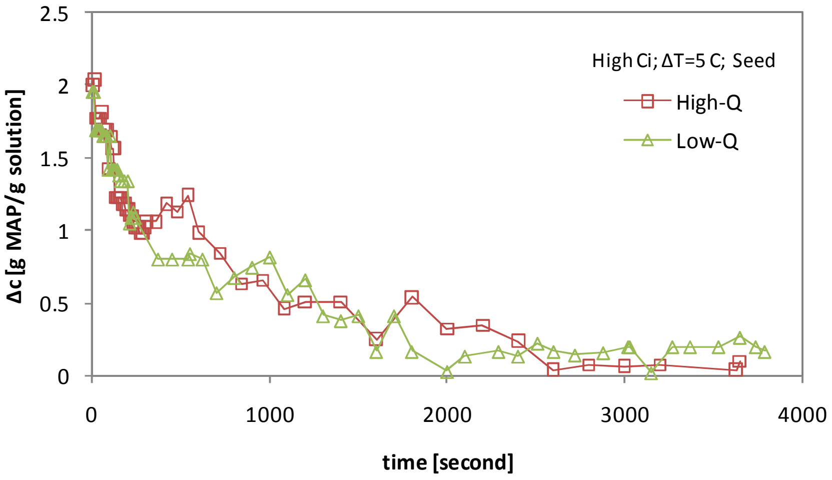

**Figure 6-16. Supersaturation profiles for a high initial concentration, ΔT=5ºC, seeded, both in the high and low flow rates**

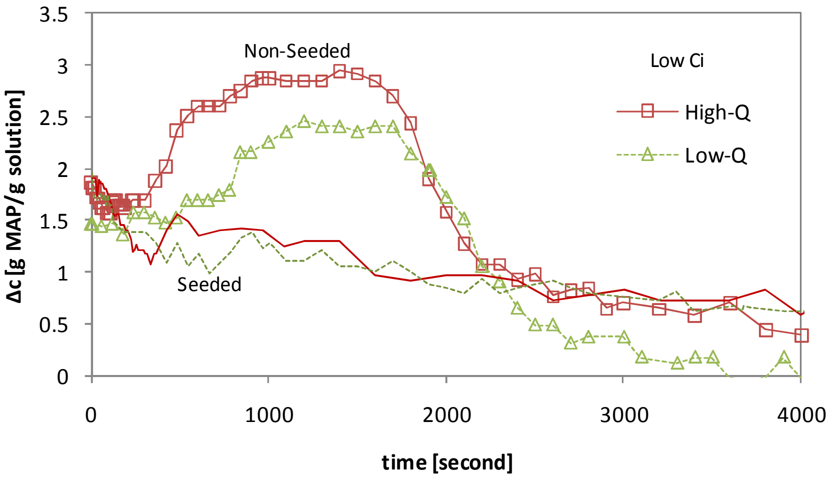

**Figure 6-17. Supersaturation profiles for a low initial concentration, ΔT=5°C, both in the seeded and non-seeded, and in the high/low flow rates**

From Figure 6-16, it appears that the variation in flow rate does not significantly affect the desupersaturation profiles. Both supersaturation values dropped quickly initially even though the high feeding rate was used. The reaction was fast and promoted even more by the high-Q flow. However, the mass transfer rate of solute is as high as the reaction rate. The crystal growth then consumed supersaturation as if the reaction did not occur. The results of the low initial concentration (in Figure 6-17) show the same tendency for the seeded system but indicate different behaviour in the non-seeded system. The peak for the high-Q experiment is higher because the degree and speed of reaction was higher. The decrease of supersaturation profile for the high-Q was also greater than the low-Q which confirms that in a semi-batch system the feeding rate of reactants can be used as a manipulated variable to control the reaction.

### *6.3.5 Effect of initial supersaturation*

Controlling the supersaturation level is the key to successful operation in reactive crystallisation. Generation of supersaturation can be achieved by cooling, evaporation, anti-solvent addition, chemical reaction, or a combination of these methods. In this study, supersaturation was first generated by a chemical reaction between phosphoric acid and ammonia and followed by the cooling method. Because the reaction occurred, a heat of reaction was generated and this heat needs to be transferred to the cooling jacket system in order to keep the crystalliser temperature constant. Supersaturation level was measured on-line by the conductivity method (Torgesen et al. 1963).

Therefore, solute concentration in the solution can be monitored continuously at real time. Crystalliser temperature, cooling water temperature and pH were also automatically monitored.

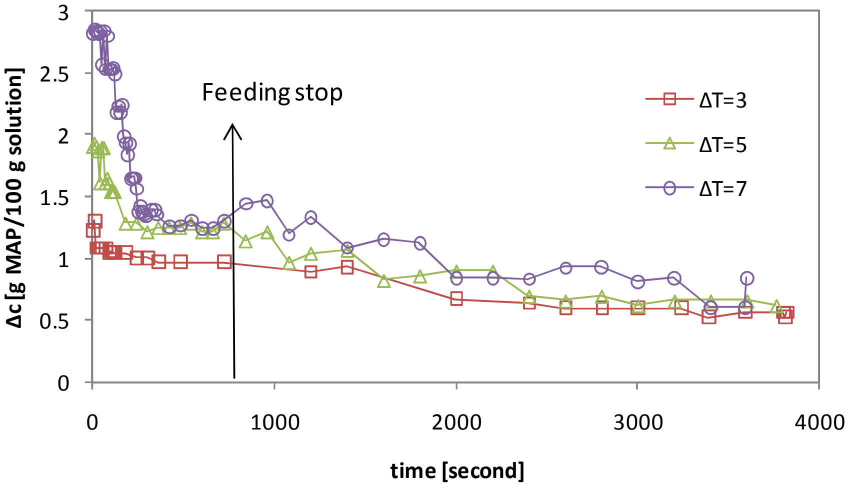

**Figure 6-18. Supersaturation profiles for various initial supersaturations, ΔT=3, 5, and 7°C.**

Crystals begin to form when supersaturation exceeds the metastable limit and a nucleus is present. This mechanism can be found in the non-seeded system and is called homogenous nucleation. In the seeded system, supersaturation is mainly used for seed growth. Secondary nucleation may occur at the same time either by initial breeding, fluid shear phenomenon or contact mechanism between crystals, crystalliser wall, crystals and impeller or crystals. Figure 6-18 shows desupersaturation profiles from three experiments that have different initial supersaturation. As expected, higher supersaturation generated a higher mass deposition rate and, therefore, sharper falls were observed. The high supersaturation (ΔT=5-7°C) profiles consist of two parts; a high slope in the initial process and then a much lower slope occurred until the end of the batch. However, only one gradient was observed with the low supersaturation experiment (ΔT=3°C). At high supersaturation and in the presence of seed crystals, nucleation dominates the process in the initial stage causing a sharp drop in supersaturation profile. The subsequent growth process can be described by the second slope (lower gradient) which is similar to others observed.

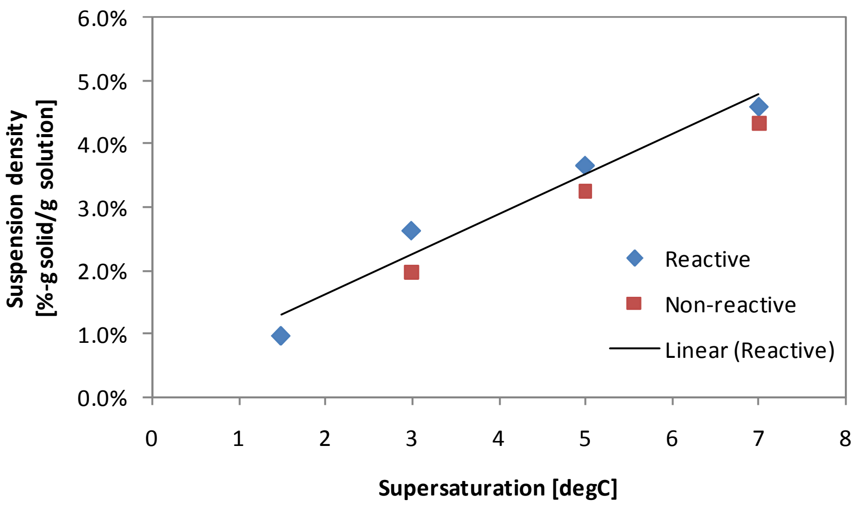

**Figure 6-19. Suspension density of reactive and non reactive systems in various initial supersaturations**

Figure 6-19 shows the suspension density results for the seeded reactive and the seeded non-reactive systems. The suspension density ranges from 1% up to 5% as g solid per g solution. Secondary nucleation may occur due to hydrodynamic conditions and the physical state of the suspension. In a high suspension density that may have a significant fraction of coarse particles, secondary nucleation is easily triggered even though it is operating in a moderate state of mixing (300 rpm stirring speed was employed). Contact nucleation and particle brakeage may occur at the highest supersaturation ($\Delta T=7^{o}C$). A fraction of small crystals were produced and can be seen from CSD results in Figure 6-20. This is further emphasised by the number density plot in Figure 6-21, and clearly shows that a significant number of fine crystals were produced in the high supersaturation region. The total crystal number also increases significantly from about 33,000 particles in the seed to approx. 6-700,000 particles for $\Delta C=5^{o}C$ and $\Delta C=7^{o}C$ respectively (see Figure 6-22).

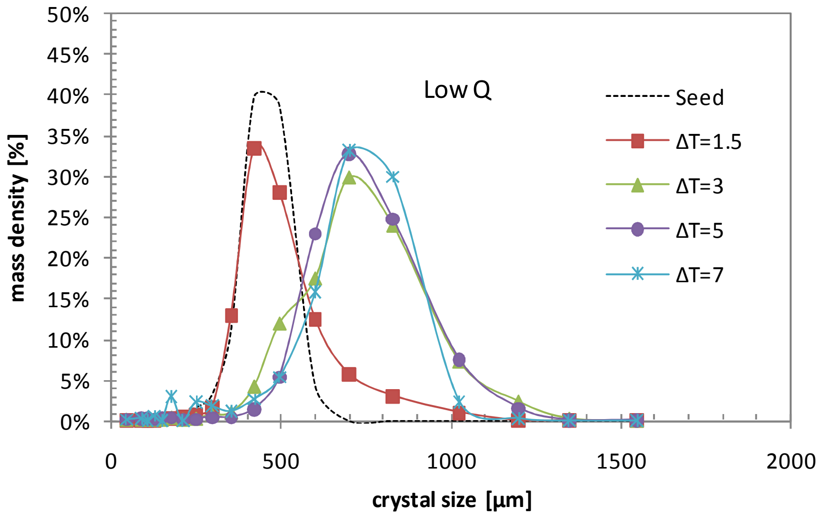

Figure 6-20. CSD (as mass density) for seeded, low flow rate and various supersaturations

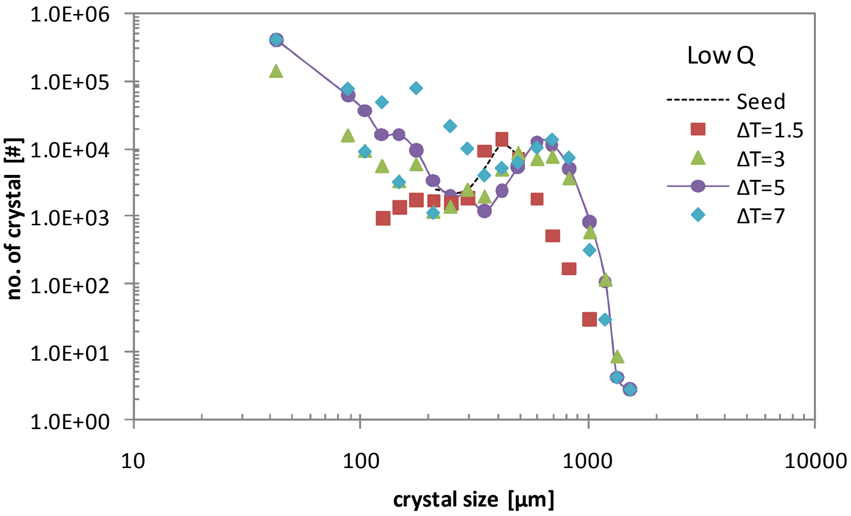

Figure 6-21. CSD (as number of crystals) for seeded, low flow rate and various supersaturations

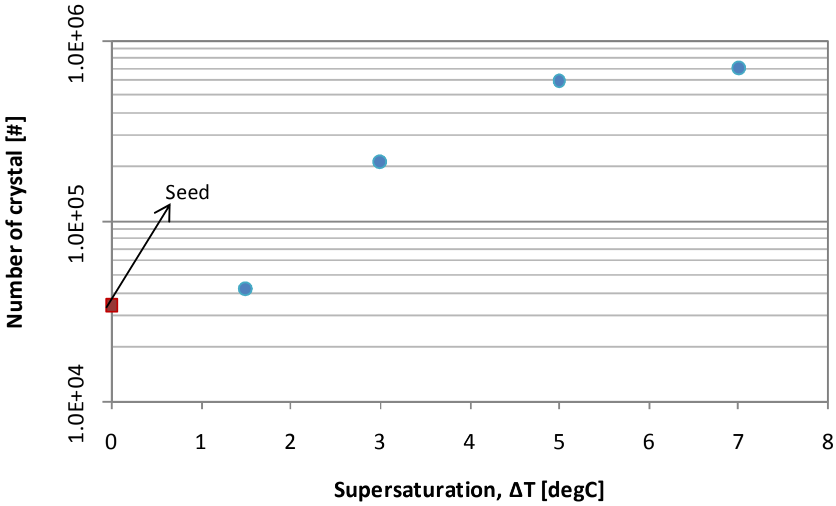

**Figure 6-22. Total number of crystals of seeded system for various supersaturations**

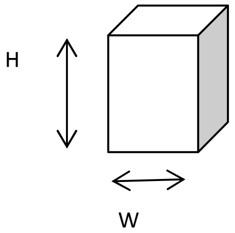

**Figure 6-23. Crystal aspect ratio in height (H) and width (W)**

CSD is an important requirement of crystal products that can be controlled by manipulating the supersaturation level. In the batch or semi-batch crystalliser, a programmed cooling and optimal feed strategy are the most effective ways to obtain desirable crystal size and distribution. In this study, constant cooling and constant feeding rates were utilised and typical CSD results are shown in Figure 6-20. The same total batch time was employed for these experiments, i.e. 3600 seconds. In addition to CSD, the shape of the crystal becomes an important feature for several applications. Knowledge of the crystal shape also helps the correct prediction of CSD measurement and is required for CSD modelling. Typically, a higher supersaturation leads to needle-like crystals being produced. In this study, lower supersaturation leads to the needle shape, which is different from the normal habit of an MAP crystal which has a cubical or tetragonal bipyramid shape. The ratio of height (H) to width (W) from the crystal images enabled more detailed study of the range of effects of supersaturation.

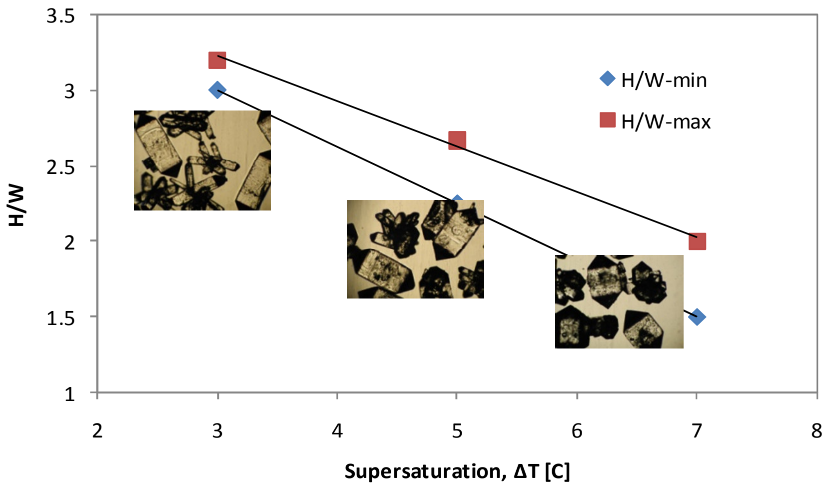

**Figure 6-24. Aspect ratio and crystal images for several initial supersaturations**

### 6.3.6 *Effect of initial concentration*

While maintaining the total supersaturation difference at 5°C, different initial concentrations were employed in order to study the effects on suspension density and size distribution. Hence, the operating temperatures increase in accordance with the initial concentrations. The higher initial concentration means higher temperature. In this study 10°C, 15°C and 20°C were the saturated temperatures for three set of concentrations. Figure 6-25 shows that at a low temperature (initial concentration, Ci), supersaturation decreases at a slower pace compared to a higher temperature. Therefore, suspension density reduced in a lower temperature compared to a higher temperature. This indicates that the actual supersaturation at a lower temperature was smaller than the initial set value. This may be due to the non-linearity of solubility as a function of temperature. However, the final CSD may not affected by the dynamics of the supersaturation. For seeded high-flow rate (Figure 6-26) and the results of non-seeded already presented (Figure 6-8 and Figure 6-9), then the CSDs were not sensitive to the temperature or initial concentration. Therefore, in a narrow temperature range, it can be assumed that nucleation and growth is not affected by temperature as they are typically correlated by the Arrhenius equation.

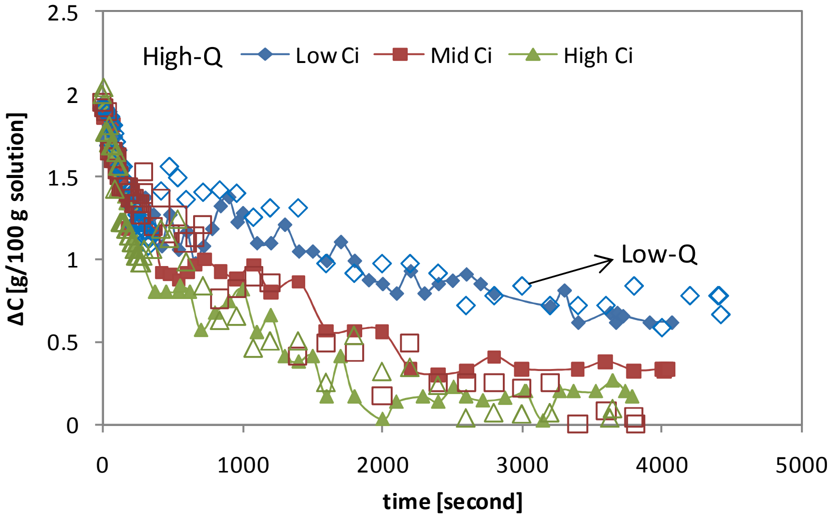

**Figure 6-25. Supersaturation profiles of seeded system, high flow rate and at low/middle/high initial concentrations**

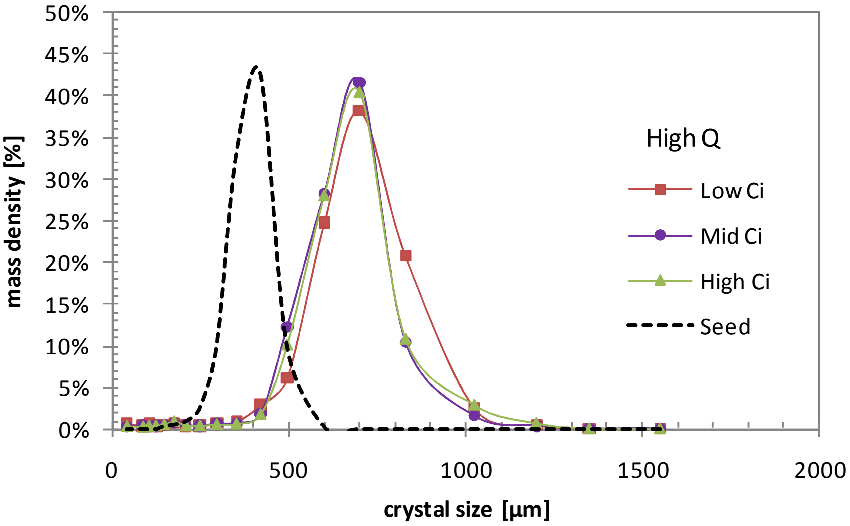

**Figure 6-26. CSD (as mass density) for seeded system, high flow rate and at low/middle/high initial concentrations**

### *6.3.7 Effect of feeding time*

Feeding time is one of the key variables in this study. Feeding allows the system to receive additional mass of reactant which can react, and can generate the supersaturation by producing more solute into the system. Total batch time in the semi-batch reactive crystallisation process consists of a feeding step (in which reaction takes place) and a cooling step (where crystallisation and cooling occur). The base cases used for feeding time (for high flow rate) were 5 minutes and 11 minutes (for low flow rate) operation. Both feeding time conditions are theoretically and experimentally valid as they can produce the same amount of supersaturation. By observing the conductivity profiles of the unseeded system, both conditions result in 0.1-0.12 S/m increase in conductivity.

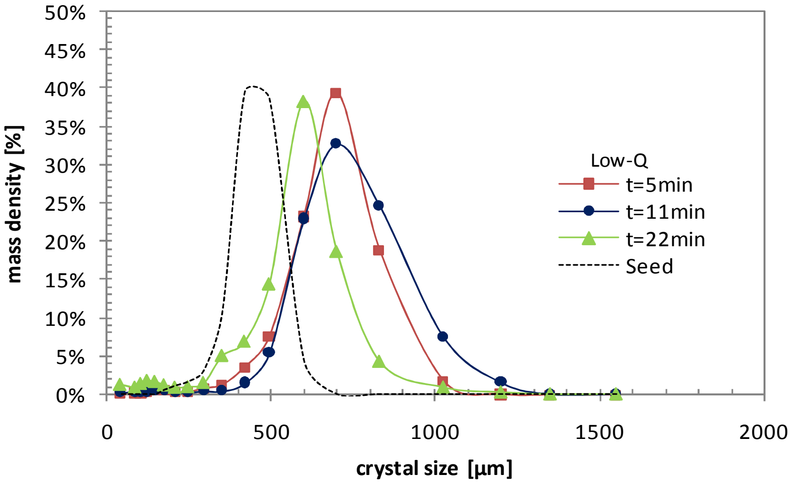

Figure 6-27. CSD (as mass density) for seeded system, low flow rate and several feeding times

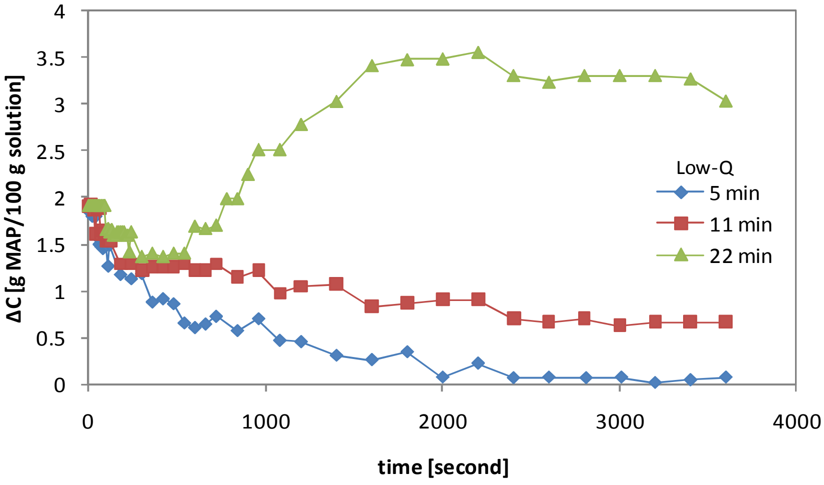

Figure 6-28. Supersaturation profiles for seeded system, low flow rate and several feeding times

The three distinct CSD profiles in Figure 6-27 show that feeding time changes produced different crystal size distributions in the seeded system. A longer feeding time means more MAP solute is produced in the system, this causes higher supersaturation and higher crystal yield. The supersaturation profile for 5 minutes drops quickly because only a small quantity of solute was produced in a short time, and the seed crystals continue to grow by consuming the remaining supersaturation. After 22 minutes, there was a net production of solute due to the limitation of seed crystals ability to consume the supersaturation. A very high supersaturation occurred and triggered further nucleation and growth of new nuclei. Finally, the supersaturation profile falls toward the end of the batch time, and finer crystals were produced.

For a non-seeded operation, supersaturation profiles are shaped like a bell-curve followed by a slight decrease as shown in Figure 6-29. A longer feeding time produced a higher overshoot of supersaturation. The shorter time gave a longer induction period prior to spontaneous nucleation and, finally, a suspension state was reached. As expected, a higher total number of nuclei and smaller nuclei were produced in 10 and 15 minutes feeding compared to the base case. The falling area (L-shape) in the supersaturation profiles consists of two parts. The first quickly dropped due to both nucleation and the growth process; the second drop demonstrates crystal growth only. The first drop profile has a higher rate due to the high surface area of generated nuclei, followed by rapid growth.

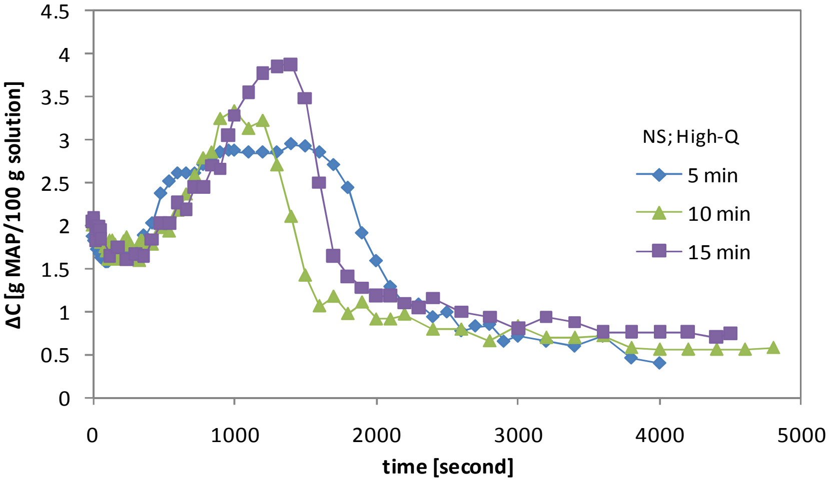

**Figure 6-29. Supersaturation profiles of non-seeded system, high flow rate and several feeding times**

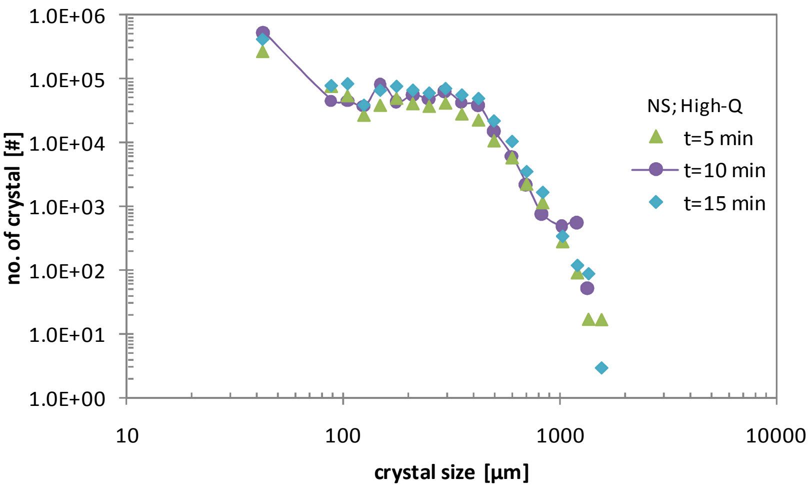

**Figure 6-30. CSD (as number of crystals) for non-seeded system, high flow rate and several feeding times**

### *6.3.8 Mixing effects*

Fluid mixing is an important factor in this study. Since perfect-mixing is assumed, efforts have been made in the experimental setup to ensure a constant well-mixed regime for every run. Vessel geometry and shape, impeller size and placement, coupled with the liquid holdup and stirring speed produced a particular flow pattern in the crystalliser. Macro-scale mixing, which is the overall flow pattern in the crystalliser, affects particles with a size above 1000 µm. The ratio of power input and fluid capacity will only govern the particles below 100 µm in a micro-scale environment. In this study, the stirrer speeds were 200 and 300 rpm, the geometry and the liquid holdup were kept constant. Both these stirrer speeds have been confirmed to avoid the imperfect mixing condition in the seeded reactive crystalliser. Stirrer speed below 200 rpm will not give a perfect mixing condition due to a solid deposition at the bottom of crystalliser; above 300 rpm is too high for this system geometry and capacity.

For high flow rate conditions, the rapid production of solute can only be utilised by a smaller amount of crystal because at low stirring speed the remaining crystals stay un-mixed at the crystalliser bottom. The surface area of active crystals is significantly reduced so that the same amount of supersaturation will only be beneficial and grow active crystals larger than the condition of a well-mixed system at 300 rpm. Alternatively in the low flow rate operation, the solute generation is moderate and, even at 200 rpm, the growth rate of active crystals can compete because a low supersaturation level was maintained. By observing the supersaturation history in Figure 6-33 for a high flow rate and a low stirring speed, the profile deviates in the initial stage due to different degrees of reaction. Once the crystals are large enough, they stay at the bottom and the total active surface area is continuously reduced. It can be concluded that the seeded reactive system studied behaves differently and the micro-mixing is an important factor to consider in a small-scale experiment. For an unseeded reactive system as quoted in the literature (Chen et al. 2004; Abbasi et al. 2007), a decrease in stirring speed may cause a decrease in nucleation rate and/or an increase in growth. As a result, higher suspension densities and mean sizes are expected. However, most previous research work which discussed the mixing in a reactive system have been only for low solubility product.

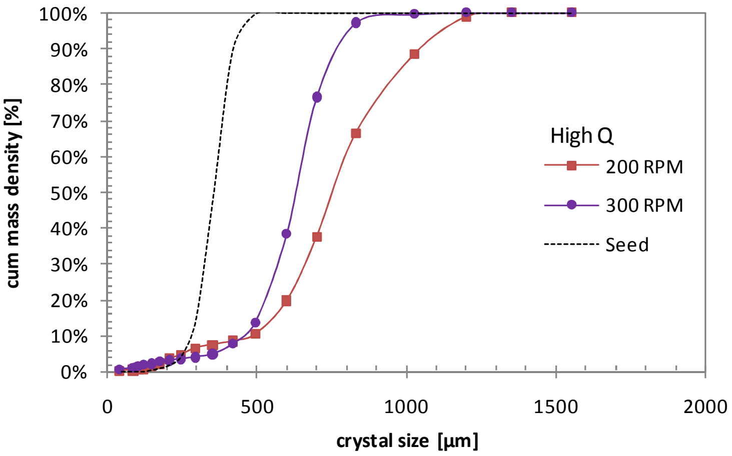

**Figure 6-31. Cumulative CSD (as mass density) for high flow rate at 200 and 300 rpm**

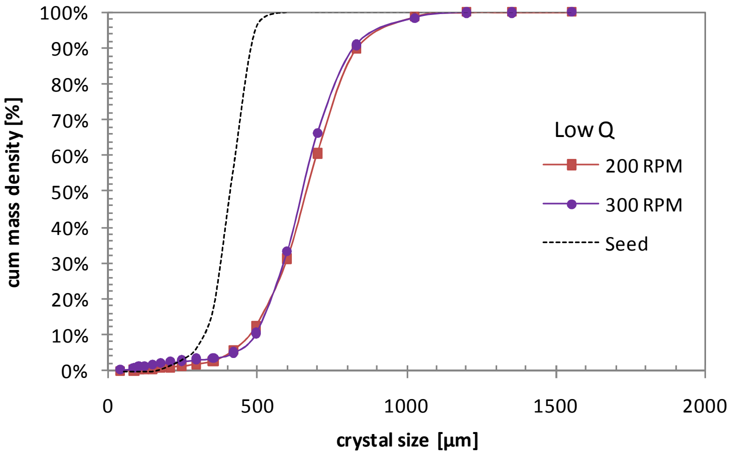

**Figure 6-32. Cumulative CSD (as mass density) for low flow rate at 200 and 300 rpm**

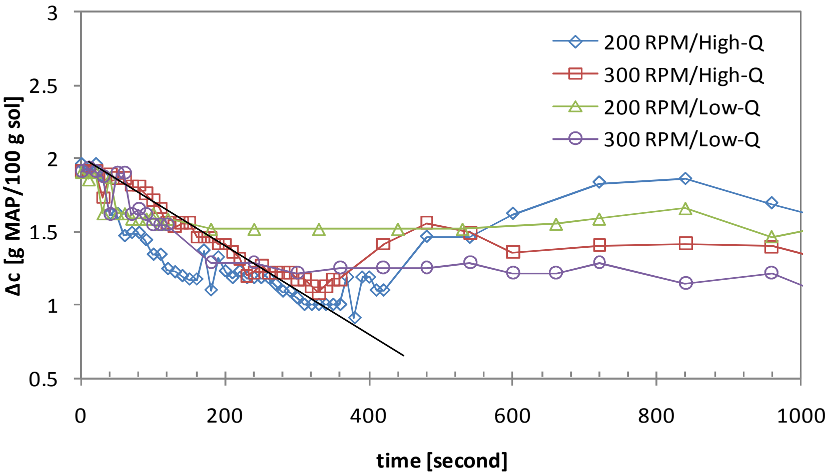

**Figure 6-33. Supersaturation profiles of seeded systems for high/low flow rate at 200 and 300 rpm**

## *6.4 Remarks*

Both single-feed and dual-feed systems can produce mono-ammonium phosphate (MAP) crystals. These have been verified by X-ray diffraction analysis and validated with the standard XRD pattern of MAP. For a single- feed system, the reactants N/P molar ratio controls the degree of reaction and thus governs the CSD of the product. An N/P close to 1.0 is shown by experiment to result in the lowest solubility and produce MAP crystals. DAP crystals cannot be formed in the system due to its high solubility. However, TAP can easily be produced when the pH exceeds 8.0. The mean size of a single-feed system is smaller and its CSD is wider than for the dual-feed system. This indicates that nucleation is more dominant in a single-feed system.

In a non-seeded system, the nucleation process dominates. The supersaturation profiles increase and then stay constant over the induction time before visible nuclei appear. The induction time is significantly long, almost one-third of the total batch time. A seeding strategy is essential in order to minimise the impact of the nucleation process and a wider crystal size distribution can be avoided. Higher flow rate caused finer crystals because of the higher supersaturation level, which leads to further nucleation. The reaction kinetics were affected because higher concentrations of reactants exist with higher flow rates. However because of the fast reaction, at a low flow rate then the accumulation of reactant concentration is negligible during the feeding time. The temperature rose due to higher reaction rates affects the dynamics of the solubility and, hence, the final product size distribution.

In a seeded system, supersaturation is mainly used to determine seed growth. At high supersaturation and with seed crystals, then nucleation dominates the process in the initial stage and can cause a sharp drop in the supersaturation profiles. The subsequent growth process can be described by the second moderate slope, which was similar to other supersaturation profiles. However at low supersaturation, growth dominated over for the whole process. In this study, lower supersaturation also led to needle-shaped crystals which are undesirable and different from the normal structure of MAP crystals, which have a cubical-type or tetragonal bipyramid shape.

Feeding time is one of the important factors in this study. In a seeded system, the longer feeding time denotes more MAP solute produced in the system. This caused higher supersaturation and higher crystal yields. For a non-seeded operation, supersaturation profiles exhibited a bell-curve followed by a slight decreased profile. A longer feeding time produced a higher overshoot of supersaturation. The shorter time gave a longer induction period prior to spontaneous nucleation, and finally a suspension state was reached. For mixing intensity factors, it can be concluded that the seeded-reactive system studied behaves differently and the meso- and micro-mixing are important factors in a small-scale experiment, because the reaction occurred on a molecular scale.

## 6.5 References

Abbasi, E. and A. Alamdari (2007). Mixing effects on particle size distribution in semi-batch reactive crystallization of maneb. *Journal Of Chemical Engineering of Japan*, 40(8), 636.

Al Nasser, W. N., A. Shaikh, C. Morriss, M. J. Hounslow and A. D. Salman (2008). Determining kinetics of calcium carbonate precipitation by inline technique. *Chemical Engineering Science*, 63(5), 1381-1389.

Aoun, M., E. Plasari, R. David and J. Villermaux (1999). A simultaneous determination of nucleation and growth rates from batch spontaneous precipitation. *Chemical Engineering Science*, 54(9), 1161-1180.

Barata, P. A. and M. L. Serrano (1996). Salting-out precipitation of potassium dihydrogen phosphate(kdp). I. Precipitation mechanism. *Journal of Crystal Growth*, 160(3-4), 361-369.

Bernard-Michel, B., M. N. Pons, H. Vivier and S. Rohani (1999). The study of calcium oxalate precipitation using image analysis. *Chemical Engineering Journal*, 75(2), 93-103.

Campbell, G. R., Y. K. Leong, C. C. Berndt and J. L. Liow (2006). Ammonium phosphate slurry rheology and particle properties--the influence of fe(iii) and al(iii) impurities, solid concentration and degree of neutralization. *Chemical Engineering Science*, 61(17), 5856-5866.

Chen, P.-C., C. C. Chen, M. H. Fun, O. Y. Liao, J. J. Jiang, Y. S. Wang and C. S. Chen (2004). Mixing and crystallization kinetics in gas-liquid reactive crystallization. *Chemical Engineering Technology*, 27(5), 519-528.

Chen, P. C., G. Y. Cheng, M. H. Kou, P. Y. Shia and P. O. Chung (2001). Nucleation and morphology of barium carbonate crystals in a semi-batch crystallizer. *Journal of Crystal Growth*, 226(4), 458-472.

Doki, N., N. Kubota, A. Sato, M. Yokota, O. Hamada and F. Masumi (1999). Scaleup experiments on seeded batch cooling crystallization of potassium alum. *AIChE Journal*, 45(12), 2527-2533.

Kotaki, Y. and H. Tsuge (1990). Reactive crystallization of calcium carbonate in a batch crystallizer. *Journal of Crystal Growth*, 99(1-4), 1092-1097.

Kubota, N., N. Doki, M. Yokota and D. Jagadesh (2002). Seeding effect on product crystal size in batch crystallization. *Journal Of Chemical Engineering of Japan*, 35(11), 1063-1071.

Ross, W. H., A. R. Merz and K. D. Jacob (1929). Preparation and properties of the ammonium phosphates. *Industrial & Engineering Chemistry*, 21(3), 286-289.

Salvatori, F., H. Muhr, E. Plasari and J. M. Bossoutrot (2002). Determination of nucleation and crystal growth kinetics of barium carbonate. *Powder Technology*, 128(2-3), 114-123.

Slund, B. L. A. and A. K. C. Rasmuson (1992). Semibatch reaction crystallization of benzoic acid. *AIChE Journal*, 38(3), 328-342.

Söhnel, O. and J. W. Mullin (1982). Precipitation of calcium carbonate. *Journal of Crystal Growth*, 60(2), 239-250.

Ståhl, M., B. L. A. Slund and A. C. Rasmuson (2001). Reaction crystallization kinetics of benzoic acid. *AIChE Journal*, 47(7), 1544-1560.

Tavare, N. S. and J. Garside (1990). Simulation of reactive precipitation in a semi-batch crystallizer. *Chemical Engineering Research and Design*, 68(a), 115-122.

Torgesen, J. L. and A. T. Horton (1963). Electrolytic conductance of ammonium dihydrogen phosphate solutions in the saturation region. *The Journal of Physical Chemistry*, 67(2), 376-381.

Uehara-Nagamine, E. and P. M. Armenante (2001). Semibatch precipitation of barium sulphate. *Trans. IChemE*, 79(A), 979-988.

Xu, D. and D. Xue (2006). Chemical bond analysis of the crystal growth of kdp and adp. *Journal of Crystal Growth*, 286(1), 108-113.

Zhong, B., J. Li, Y. X. Zhang and B. Liang (1999). Principle and technology of ammonium phosphate production from middle-quality phosphate ore by a slurry concentration process. *Industrial & Engineering Chemistry Research*, 38, 4504-4506.

# 7. Kinetics Estimation and Experimental Validation Using a Wavelet-based Model

## 7.1 Introduction

There is a great interest in crystallisation kinetics and many methods to determine nucleation and crystal growth have been developed, see (Tavare 1987; Garside et al. 1990). However, most research has only focused on (non-reactive) crystallisation and the kinetics of reactive crystallisation remains less well understood, and were not discussed in the widely recommended book on precipitation by Sohnel and Garside (1992).

There are two general methods used to determine crystallisation kinetics in batch crystallisers: the method of isolation, and the simultaneous method. The classical approach is to isolate the growth and nucleation processes, and then determine their kinetics separately by direct and/or indirect methods under different hydrodynamic conditions. The isolation method allows calculation of the rates of the elementary processes from separate experimental results. The simultaneous method requires the experimental observation of several output variables during experiment. Kinetics data are then calculated after appropriate mathematical treatment which is intended to separate the contribution of the observed variables on the growth, nucleation, and other mechanisms. This mathematical treatment of data may become complex if all the rates are to be determined accurately.

Two different modes of experiment, i.e. integral and differential modes (Garside et al. 1990), can be used under conditions of negligible mass deposition during nucleation. Integral methods use a wide range of experimental data integrated over a large time interval during crystallisation or reactive crystallisation. However, differential methods use the instantaneous values of process variables and their variations in a very short time interval. Since agglomeration does not take place in many crystallisation or reactive crystallisation processes (Aoun et al. 1999), in this study we only consider nucleation and growth.

In this chapter, crystallisation kinetics and reaction kinetics from data in the previous Chapters 5 and 6 are determined. The crystallisation kinetics for nucleation and crystal growth were estimated from supersaturation data, the growth and nucleation constant as well as the nucleation and growth exponents were calculated by non-linear regression. Four optimised parameters were produced as the minimum value of sum of square error (SSE) between the supersaturation values (data and simulation) was reached. Then the nucleation and growth kinetics were refined by considering the experimental solids mass balance data. Finally, a resultant crystal size distribution (CSD) generated from the estimated kinetics was calculated, and compared with the experimental CSD value.

In the case of reactive crystallisation experiments, the approach of obtaining the crystallisation kinetics was the same as in the (non-reactive) crystallisation experiments explained earlier. The reaction kinetics data was gathered by recording experimental data from a system with seeded crystals and reaction and also from a non-seeded system with reaction. The non-seeded system with reaction exhibits primary nucleation, followed by crystal growth. In this case, the reaction kinetics will be more difficult to predict, but the rate of chemical reaction can be calculated. With the knowledge of rate of reaction from a non-seeded system, then the reaction kinetics of a seeded system can be determined by comparing two systems: the seeded without reaction and seeded with reaction. Finally, the reaction and crystallisation kinetics were also refined by considering the solids mass balance and the CSD data.

## 7.2 Isolation Methods

### Nucleation rate

During the reaction process, new particles are created by nucleation as a result of reactions occurring. The rate of nucleation has a significant effect upon the final characteristics of the solid. However, this step remains the most difficult and the least studied because of the sizes of the fine particles involved. With the development of improved measurement techniques, some researchers have attempted to study this process experimentally (Nielsen 1961; Gunn et al. 1972; Söhnel et al. 1982). The nucleation rate is related to the induction time by the following expression:

$$r_N = \frac{N}{t_{ind}} \tag{7-1}$$

The induction time is measured after the rapid mixing of reactive solutions in T or Y tubes where nuclei are formed. The induction time is of the order of milliseconds, and its measurement currently remains imprecise.

***Crystal growth rate***

Nuclei grow due to the development of individual faces of the crystal. The crystal growth rate can be directly measured experimentally from the overall mass growth rate, which is the total mass flux into the crystal. Garside et al. (1982) have proposed a method based on the initial derivative of the desupersaturation curve obtained from batch experiments performed in integral mode. They used a second-order polynomial to fit the initial part of the desupersaturation-time curve. The growth kinetics, defined by $k_g$ and $g$, can be obtained by using the following equations:

$$\Delta c = a_0 + a_1\, t + a_2\, t^2 \tag{7-2}$$

$$g = \frac{2\, F\, \Delta c_0}{3\, \rho_c\, A_{T0}\, \bar{L}_0} + \frac{\Delta c_0\, \Delta \ddot{c}_0}{\left(\Delta \dot{c}_0\right)^2} = \frac{2\, F\, a_0}{3\, \rho_c\, A_{T0} \bar{L}_0} + \frac{2\, a_0\, a_2}{{a_1}^2} \tag{7-3}$$

$$k_g = -\frac{\Delta \dot{c}_0}{A_{T0}\, \Delta {c_0}^g} = -\frac{a_1}{A_{T0}\, {a_0}^g} \tag{7-4}$$

where $\rho_c$ is the solid density; $A_{T0}$ is the total surface area of seeded crystals; $F$ is the ratio of volume shape factor to the surface shape factor; and $\bar{L}_0$ is the mean size of seeded crystals.

The main advantage of the isolation approach is its simplicity. However, this technique is very sensitive to experimental error because the measurement of the initial part of the desupersaturation curve (where the nucleation is dominant) is usually disturbed by mixing conditions (Villermaux 1986). This technique can be completed quickly and is recommended when a rapid estimation is required. The main weakness is the need for the desupersaturation curve in order to correlate experimental results and to represent the crystal growth rate; information from the solid phase is then ignored. Most of the isolation methods only use one set of data during for the entire process, either the CSD or the solution-phase concentration. Recently Aoun et al. (1999) reported kinetics determination of the reactive crystallisation of barium sulphate based on the simultaneous use of solid-phase and solution-side data.

## 7.3 Simultaneous Methods

The mixed suspension mixed product removal (MSMPR) crystalliser method is classified as a differential method (Randolph et al. 1962), and remains the most common technique used to simultaneously evaluate the nucleation and the crystal growth kinetics. With the simultaneous method, the knowledge of the supersaturation is not sufficient to allow determination of both the rates of nucleation and crystal growth. The particle number concentration is also required in order to obtain the nucleation rate.

The usual method of determining the precipitation kinetics is by fitting of the CSD by empirical functions, and is based on the approximation of population density fraction by either exponential or polynomial functions (Tavare 1987). The approximation by exponential functions gives:

$$\psi(L,t) = c' \exp(-a'L) \exp\left(-b' \frac{\tau}{t}\right) \tag{7-5}$$

Then, the crystal growth and the nucleation rates can be determined by the following relationship:

$$G(t) = \frac{\partial\psi(L,t)/\partial t}{\partial\psi(L,t)/\partial L} = \frac{b'\tau}{a't^2} \tag{7-6}$$

$$r_N(t) = \psi(0,t)\, G(t) = c' \exp\left(-b' \frac{\tau}{t}\right) \tag{7-7}$$

The desupersaturation-time curve can be also be fitted by polynomial functions (Chivate et al. 1975; Palwe et al. 1985). The choice of polynomial order to be used significantly affects the kinetics parameter results, and an order of 4 is often applied. Aoun et al. (1999) described four requirements for an efficient kinetics estimation method: (i) It covers a wide range of operational conditions, such as concentration, and has access to primary nucleation data; whereas the MSMPR method only works for secondary nucleation. (ii) It uses sets of different experimental data in order to enhance the accuracy of the kinetics estimation. (iii) The data should be gathered under the same conditions, such as temperature, hydrodynamics, overall and local supersaturation. (iv) The data should have eliminated any mixing effects.

***Nucleation kinetics***

In a batch reactor, the nucleation kinetics is related to the particle number concentration by:

$$N(t) = \int_0^t r_N\,(t)\,dt \tag{7-8}$$

However, the total particle number concentration can be determined experimentally using the integral equation:

$$N(t) = \int_0^\infty \psi\,(L,t)\,dL \tag{7-9}$$

where $\psi\,(L,t)$ is the number CSD at time $t$ and particle size $L$. After substituting equations 7-8 and 7-9:

$$r_N = \frac{d\left(\int_0^\infty \psi\,(L,t)\,dL\right)}{dt} \tag{7-10}$$

Primary homogenous nucleation occurs spontaneously whereas primary heterogeneous nucleation occurs in the presence of a foreign nucleus, and secondary nucleation occurs in the presence of a solute particle interface. For non-seeded reactive crystallisation, the secondary nucleation can be neglected, especially for small crystals. However, in seeded reactive and seeded non-reactive crystallisations, then the secondary nucleation is important and is coupled with the primary nucleation for reactive systems. The primary and total nucleation rates can be expressed as a function of supersaturation as follows:

$$r_N = k_N\ \Delta c^n \tag{7-11}$$

$$B_s = k_B\,{M_T}^j\,\Delta c^b \tag{7-12}$$

If only primary nucleation is considered in the case of non-seeded reactive crystallisation, then the nucleation rate (7-10) can be written as:

$$r_N\,(t) = k_N\ \Delta c^n = \frac{d\left(\int_0^\infty \psi\,(L,t)\,dL\right)}{dt} \tag{7-13}$$

Integration of (7-13) which makes this equation less sensitive to experimental errors is:

$$N(t) - N(t_0) = \int_{t_0}^{t} k_N \ \Delta c^n \ dt \qquad (7\text{-}14)$$

Calculate $N(t)$ from CSD data by using (7-9), and generate another $N(t)$ value from supersaturation data by using (7-14). The comparison and accurate fitting of those two particle concentration profiles yields the kinetics parameters, $k_N$ and $n$, for determination of the nucleation law. When more than one batch experiment is being carried out, the fitting will be done with several profiles together and an optimisation technique is needed to minimise the error of all sets of data used. The different steps in the calculation are presented in the flow chart in Figure 7-1.

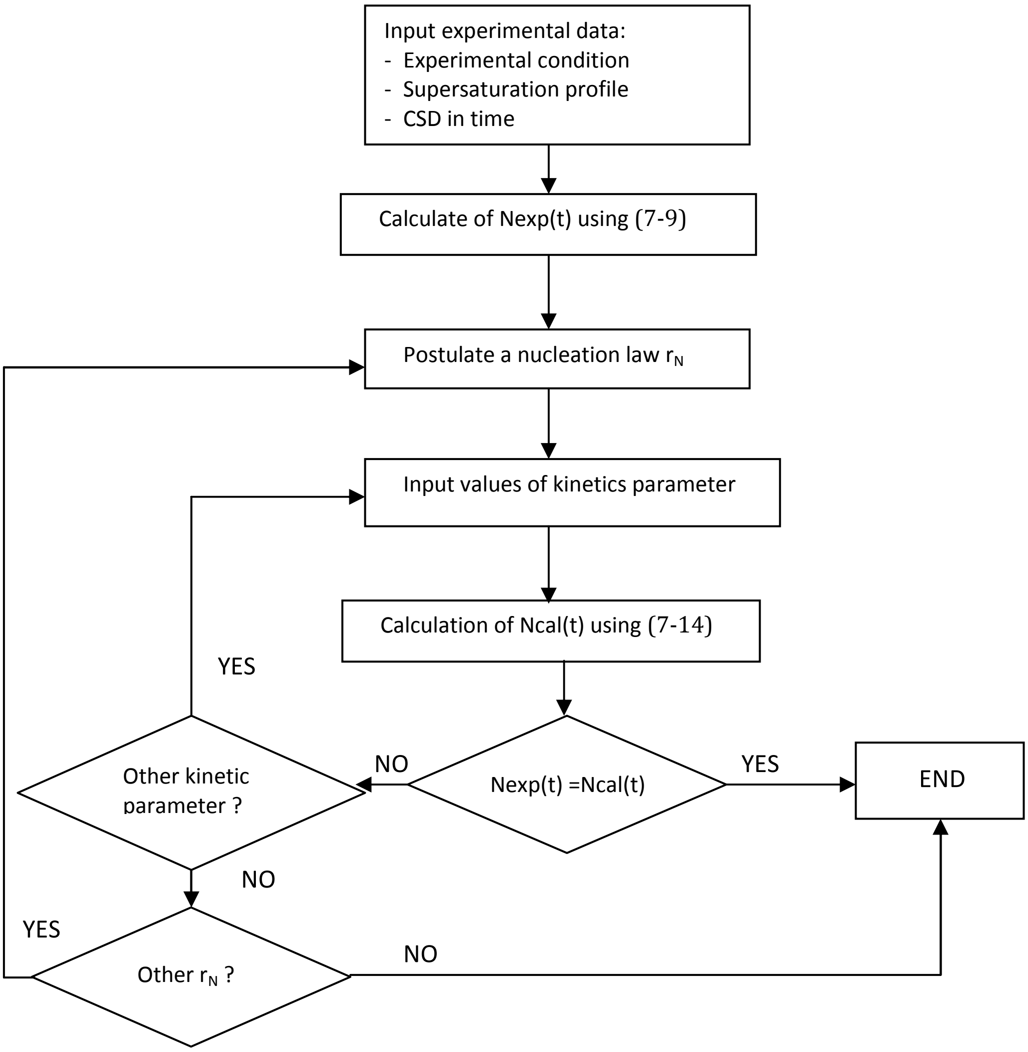

**Figure 7-1. Flow chart of nucleation kinetics determination using simultaneous method**

### *Crystal growth kinetics*

During the crystallisation, the solid concentration or suspension density is given by the following expression:

$$M_T(t) = \rho_C \int_0^t f_v \, L^3 \, \psi(L,t) \, dL \tag{7-15}$$

In the case of reactive crystallisation, the solid concentration (in mol/m$^3$) is given by the following expression:

$$C_s(t) = \frac{\rho_C}{M_s} \int_0^t f_v \, L^3 \, \psi(L,t) \, dL \tag{7-16}$$

By assuming the variation of solid mass occurring during nucleation is negligible for the population balance, the following equation can be obtained:

$$\frac{dC_s(t)}{dt} = \frac{3\,\rho_C}{M_s} \int_0^\infty f_v \, L^2 \, G(L,t) \, \psi(L,t) \, dL \tag{7-17}$$

By integrating (7-17) with respect to time gives:

$$C_s(t) - C_s(t_0) = \frac{3\, f_v \, \rho_C}{M_s} \int_{t_0}^t \int_0^\infty L^2 \, G(L,t) \, \psi(L,t) \, dL \, dt \tag{7-18}$$

The extent of precipitation can be calculated from:

$$X(t) = \frac{C_s(t)}{C_s(t \to \infty)} \tag{7-19}$$

$$X(t) - X(t_0) = \frac{3\, f_v \, \rho_C}{M_s \, C_s(t \to \infty)} \int_{t_0}^t \int_0^\infty L^2 \, G(L,t) \, \psi(L,t) \, dL \, dt \tag{7-20}$$

The classical approach assumes that crystal growth involves transportation of solute in solution followed by a surface reaction or particle integration step; the overall rate then being determined by the relative magnitudes of these two resistances in series. These processes may be represented as:

Bulk diffusion: $G(L,t) = k_d (C - C_i)^d$

Surface integration: $G(L,t) = k_r (C_i - C^*)^r$

By assuming this kinetics occur simultaneously, and no mass accumulation at the interface, the rates of both steps are equal such that:

$$G(L,t) = \frac{f_a\, M_s\, k_d}{3\,\rho_c\, f_v}\,[C(t) - C_i(t)] = k_r\,[C_i(t) - C^*]^r \tag{7-21}$$

The constant $k_d$ is the mass transfer coefficient which is dependent upon the hydrodynamic conditions. The crystal size and the temperature can be calculated by from equation (7-22) (Armenante et al. 1989):

$$\frac{k_d\, L}{D} = 2 + 0.52\, \times \left(\frac{L^{4/3}\, P^{1/3}}{v}\right)^{0.52} \left(\frac{v}{D}\right)^{0.33} \tag{7-22}$$

where $P$ is the power input per unit mass of fluid (m$^2$/s$^3$); $v$ is the kinematic viscosity (m$^2$/s); D is the diffusivity (m$^2$/s); and $L$ is the particle size (m). The overall growth rate is written as:

$$\left[\frac{G(L,t)}{k_r}\right]^{1/r} + \frac{3\,\rho_c\, f_v\, G(L,t)}{f_a\, M_s\, k_d} = C(t) - C^* \tag{7-23}$$

The kinetic order $r$ ranges from 0.83 to about 5 (Garside et al. 1975). The growth kinetics $k_r$ and $r$ can be determined by solving equation (7-17) to yield the calculated profile of the extent of precipitation. Subsequently the experimental profile can be obtained by solving (7-22) and (7-23). The flow chart of growth kinetics determination is similar to the nucleation flow chart in Figure 7-1. The entire calculation process is an iterative procedure and, therefore, the non-linear optimisation technique is employed.

## *7.4 Crystallisation Kinetics Results*

For the solution-side data, we assume that the nucleation and growth are competitive. In a constant-volume isothermal batch crystalliser, a supersaturation balance can be written as:

$$-\frac{d\Delta c}{dt} = B_S + A_T R = k_B\, {M_T}^j\, \Delta c^b + k_G\, A_T\, \Delta c^g \tag{7-24}$$

where $\Delta c$ is the supersaturation (kg/kg solution); $k_B$ is the nucleation constant (kg/[kg s (kg/kg)$^{b+1}$]); $k_G$ is the growth constant (kg/[s m$^2$(kg/kg)$^g$]); $M_T$ is the suspension density (kg solid/kg solution); $A_T$ is crystal surface area (m$^2$ ).

Assuming constant crystal shape factors and negligible breakage and agglomeration, then the magma density $M_T$, crystal surface area $A_T$, average size $\bar{L}$, and solid void in the slurry $\varepsilon$ are defined by:

$$M_T = M_{T0}\,(W/W_0) \tag{7-25}$$

$$A_T = A_{T0}\,(W/W_0)^{2/3} \tag{7-26}$$

$$\bar{L} = \bar{L}_0\,(W/W_0)^{1/3} \tag{7-27}$$

$$\varepsilon = 1 - (W/(\rho_c\, V)) \tag{7-28}$$

where $W$ and $W_0$ are the mass (kg) of crystals and seed respectively, in the crystalliser which has a total solvent of $S$ at any time as given by supersaturation:

$$W = W_0 + (\Delta c_0 - \Delta c)\, S \tag{7-29}$$

The initial values of $M_{T0}$ and $A_{T0}$ can be evaluated from the initial mass $W_0$ and size of seed crystals $L_0$ by using the expressions:

$$A_{T0} = (F\, W_0)/(\rho_c\, \bar{L}_0\, S) \tag{7-30}$$

$$M_{T0} = W_0/S \tag{7-31}$$

Tavare and Garside (1986) suggested the possibility of eliminating the crystallisation kinetics both from solution-side data and/or the solid-side data. A non-linear regression parameter estimation method is used to determine four or five kinetic parameters by fitting the desupersaturation curve for a seeded isothermal batch crystalliser. The supersaturation balance is a non-linear first-order differential equation, and its solution represents the variation of supersaturation within the crystalliser with respect to time. This variation can be determined from experimental measurements, as a function of time and the kinetic parameters. Determination of parameters by matching the solution of the non-linear model directly to experimental data, resulted in a non-linear parameter estimation problem. This may be treated as an optimization problem in parameter space in which the dependent variable ($\Delta c$) and independent variable ($t$) have fixed values and the kinetic parameters are variables.

Table 7-1 presents the results of nucleation and growth rate kinetics for MAP in a seeded cooling batch crystalliser, these parameters were estimated by using a non-linear regression method. The nucleation and growth rate kinetics were first both estimated from the desupersaturation profiles. The average value of the nucleation rate constant ($k_B$) is 1.002 $\pm$ 0.071, while the average value of the growth constant ($k_G$) is 0.089 $\pm$ 0.040. The order of b, which indicates the overall nucleation process, is 2.238 $\pm$ 0.041. The typical value of b when secondary nucleation is dominant lies between 0.5 – 2.5, with higher values (up to 10) when primary nucleation is dominant (Tavare 1995). The order of g, which describes the growth process, is 1.43 $\pm$ 0.064. These results are consistent for the kinetics parameters described above as the 95% confidence level was used in all statistical analysis. These parameters were then converted and refined with the CSD data in the simulataneous method.

**Table 7-1. First estimated nucleation and growth kinetics for seeded batch crystallisation**

| **Set** | $k_B$ kg/[kg s (kg/kg)$^{b+1}$] | **b** | $k_G$ kg/[m$^2$s (kg/kg)$^g$] | **g** |
|---|---|---|---|---|
| **67** | 0.962 | 2.141 | 0.086 | 1.287 |
| **68** | 0.989 | 2.251 | 0.069 | 1.492 |
| **72** | 0.973 | 2.263 | 0.074 | 1.452 |
| **73** | 0.984 | 2.225 | 0.076 | 1.419 |
| **78** | 0.973 | 2.264 | 0.074 | 1.439 |
| **77** | 0.987 | 2.256 | 0.070 | 1.487 |
| **80** | 0.972 | 2.254 | 0.075 | 1.434 |
| **79** | 1.176 | 2.250 | 0.186 | 1.430 |

Figure 7-2 presents the desupersaturation profiles for different intial supersaturation values (different saturation temperatures). A supersaturated solution of 0.015 kg/kg solution was prepared and cooled to 10°C saturation temperature, and another solution of 0.034 kg/kg solution was prepared and then also cooled to 10°C. Figure (7-2) shows that the higher supersaturation profile falls rapidly and reached an equilibrium state before 15 minutes, while the lower supersaturation profile dropped slowly and required 75 minutes to achieve zero supersaturation level. Since the seed amount is proportional to the theoretical crystal yield, the seed amount for high supersaturation is double that of the lower value. The combined effects of higher driving force (initial supersaturation) and the seed amount result in very distinctive desupersaturation profiles. In addition, from the CSD result, higher supersaturation will result in a smaller average size with narrow distribution, when compared to using a lower supersaturation.

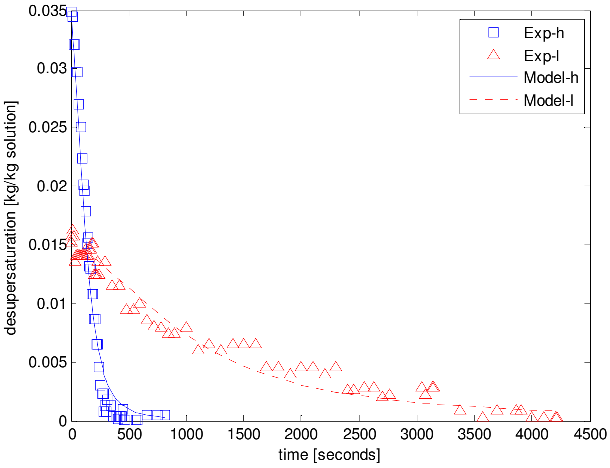

**Figure 7-2. Desupersaturation profiles of a high (0.034 kg/kg solution) and low (0.015 kg/kg solution) initial supersaturation condition**

Sensitivity analysis of the kinetics models was performed in order to determine the effect of the seed size. Three values of average seed size, 40 μm, 82.5 μm and 120 μm, were used in Models 1, 2 and 3, respectively (see Figure 7-3). The sum of squares errors of the 120 μm seed was shown to be minimised, although the difference between the three average sizes was not significant. However, considering this result for the subsequent kinetics estimation, a small error in average seed size input will not cause a significant difference in the kinetics parameters. The fitted models for the desupersaturation profiles for various seed sizes and seed loading ratio are shown in Figure 7-4, 7-5 and 7-6.

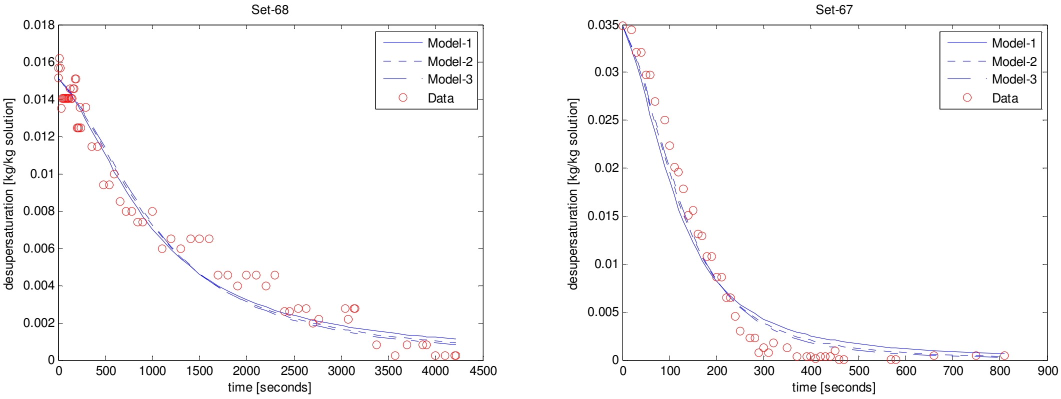

**Figure 7-3. Desupersaturation profiles for Set-68 and Set-67 with different initial seed sizes**

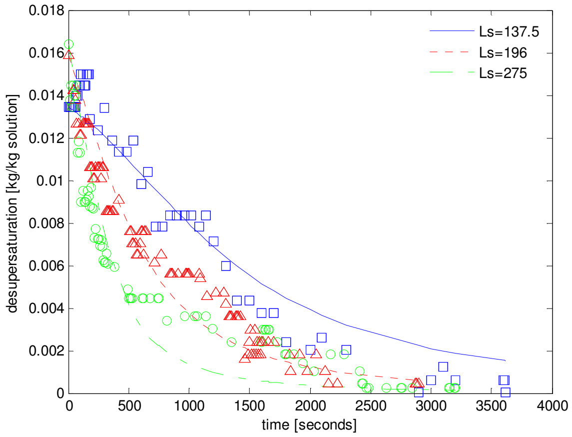

**Figure 7-4. Desupersaturation profiles and fitted models for various seed sizes with same initial number of crystals**

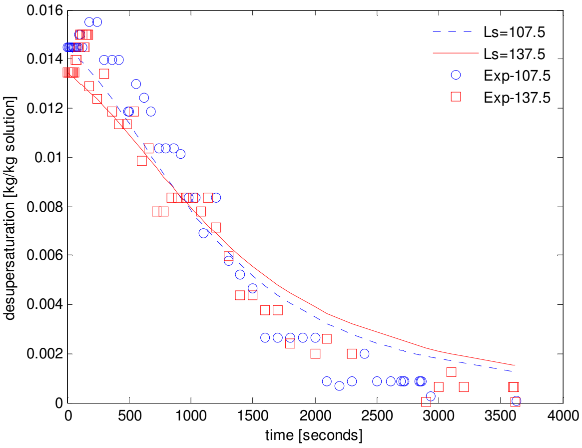

**Figure 7-5. Desupersaturation profiles and fitted models for various seed sizes with same Cs=5%**

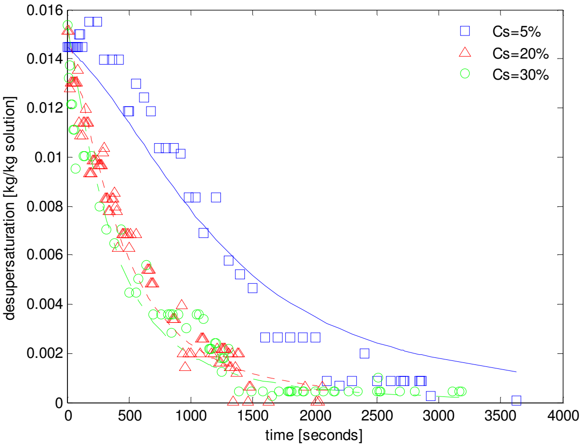

**Figure 7-6. Desupersaturation profiles and fitted models for different Cs using 137.5 µm seed**

## 7.5 *Validation of MAP Non-reactive Crystallisation*

For validation purpose, only two cases are discussed. The first case is the condition of different initial supersaturation for seeded batch crystallisation experiments, i.e. sets 67 and 68. The refined kinetics estimation by simultaneous method in Table 7-2 shows that the nucleation constants were similar and the growth constant for set-67 was about 3 times higher. The nucleation and growth exponents were taken as an average value at 2.20 and 1.40, respectively. For the solution-side, the supersaturation of set-67 dropped quickly to zero in just 1000 seconds, while set-68 required more than 4000 seconds to reach zero supersaturation level. The growth constant value validated the supersaturation, hence the suspension density profiles are in good agreement. The average growth rate for sets 67 and 68 were $2.289 \times 10^{-7}$ m/s and $4.654 \times 10^{-8}$ m/s respectively.

The values of the nucleation constant were similar, but the average nucleation rates were different, i.e. set-67 and set-68 gave nucleation rates of 429 and 61 as number of particles/s. kg solution, respectively. Set-67 exhibited a high nucleation because it was operated at an initial supersaturation twice that of set-68. With the same initial suspension density, set-67 quickly achieved 3.714 g/100 g solution, while set-68 only achieved 1.6077 g/100 g solution. The supersaturation and suspension density profiles of set-67 and set-68 are compared in Figure 7-7.

**Table 7-2. Refined estimation of nucleation and growth kinetics constants for seeded batch crystallisation**

| **Set** | $\boldsymbol{k_b}$ no/[kg s (kg/kg)$^{b+1}$] | $\boldsymbol{k_g}$ m/[s(kg/kg)$^{g}$] |
|---|---|---|
| 67 | 6.832E+08 | 9.357E-05 |
| 68 | 6.562E+08 | 3.089E-05 |
| 72 | 1.274E+08 | 3.971E-05 |
| 73 | 1.272E+08 | 4.770E-05 |
| 78 | 1.310E+08 | 4.171E-05 |
| 77 | 1.477E+08 | 3.672E-05 |
| 80 | 1.038E+08 | 5.036E-05 |
| 79 | 2.563E+07 | 5.408E-05 |

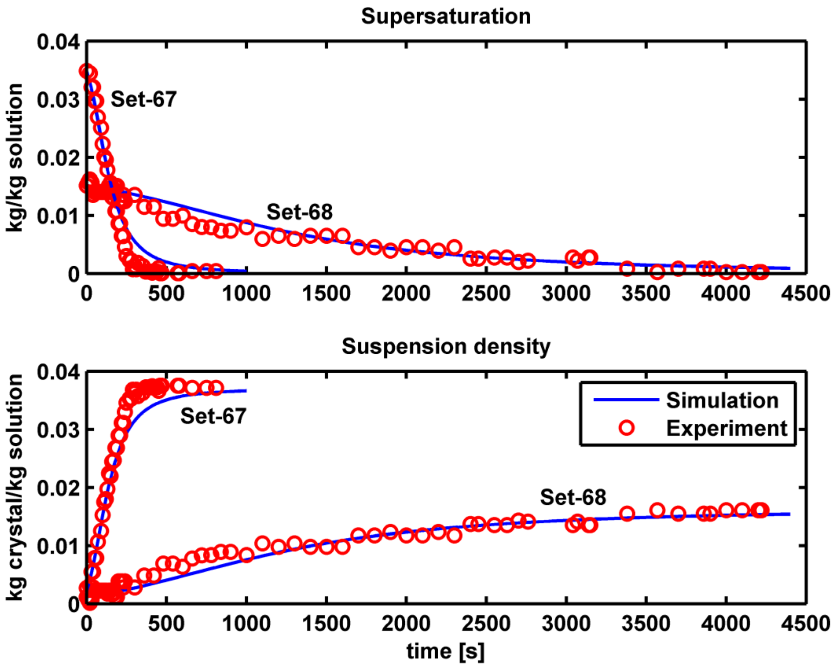

**Figure 7-7. Validation of supersaturation and suspension density for set-67 and set-68; circle dot: experiment data; solid line: simulation result**

**Table 7-3. Absolute error validation of total number of particles**

| **Set** | **$N_T$ (Simulation)**<br>no/[kg solution] | **$N_T$ (Experiment)**<br>no/[kg solution] | **Abs. Error**<br>**%** |
|---|---|---|---|
| 67 | 2.956E+06 | 1.163E+06 | 154.14 |
| 68 | 1.562E+06 | 2.064E+06 | 24.34 |
| 72 | 1.938E+05 | 2.107E+05 | 8.04 |
| 73 | 6.422E+05 | 1.070E+06 | 40.00 |
| 78 | 9.416E+05 | 7.324E+05 | 28.56 |
| 77 | 3.038E+05 | 3.944E+05 | 22.98 |
| 80 | 3.529E+05 | 2.866E+05 | 23.15 |
| 79 | 3.882E+05 | 3.546E+05 | 9.47 |

By considering the experimental solid mass balance data, the validation of total number of particles and mean particle size were conducted and the results presented in Table 7-3 and . Total number of particles for set-67 and set-68 had a significant effect on absolute error. The absolute error of set-67 was very high due to unpredicted experimental error in handling fine solids produced during mass and particle size analysis. However, the prediction of crystal size remains in a good agreement with the mean size obtained from particle size analyser. The seed crystals have a mean size of 120 µm, and are fed in proportion to the initial supersaturation, grow linearly to a mean size of 350 µm.

**Table 7-4. Absolute error validation of mean particle size**

| Set | L-avg (Simulation) m | L-avg (Experiment) M | Abs.Error % |
|---|---|---|---|
| 67 | 3.79E-04 | 3.510E-04 | 7.97 |
| 68 | 3.55E-04 | 3.500E-04 | 1.37 |
| 72 | 4.78E-04 | 5.240E-04 | 8.82 |
| 73 | 3.29E-04 | 3.763E-04 | 12.49 |
| 78 | 3.02E-04 | 3.517E-04 | 14.06 |
| 77 | 4.59E-04 | 4.399E-04 | 4.28 |
| 80 | 4.68E-04 | 4.338E-04 | 7.97 |
| 79 | 4.71E-04 | 4.453E-04 | 5.71 |

The profiles of simulated total number of particles and mean particle size for set-67 and set-68 are shown in Figure 7-8. The effects observed were mainly due to the dynamic nucleation and growth rate, these were simulated and are illustrated in Figure 7-9. Set-67 had a higher initial supersaturation and gave significantly higher nucleation and growth rates at the initial stage, and was quickly followed by rapid decrease up to the final batch time.

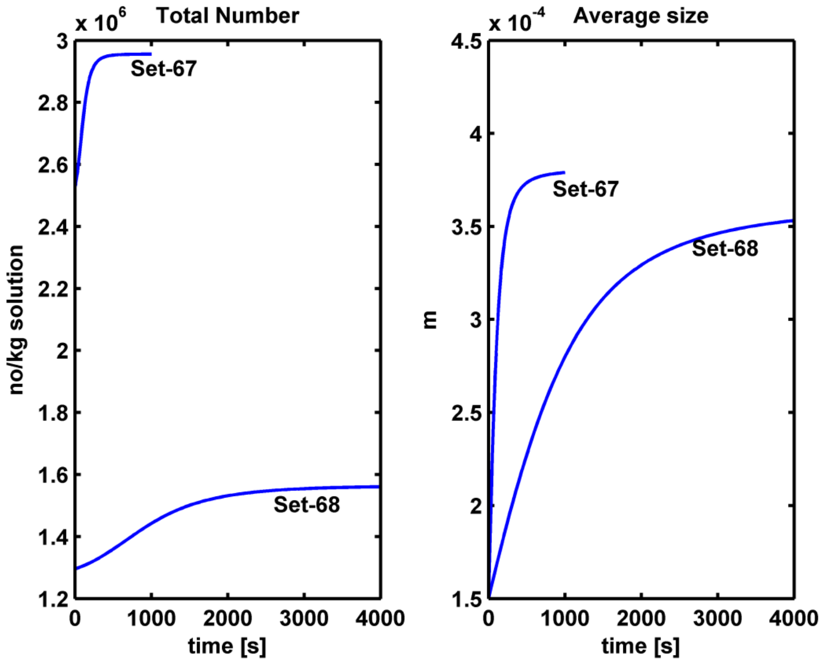

Figure 7-8. Simulation results of total number particles and mean size for set-67 and 68

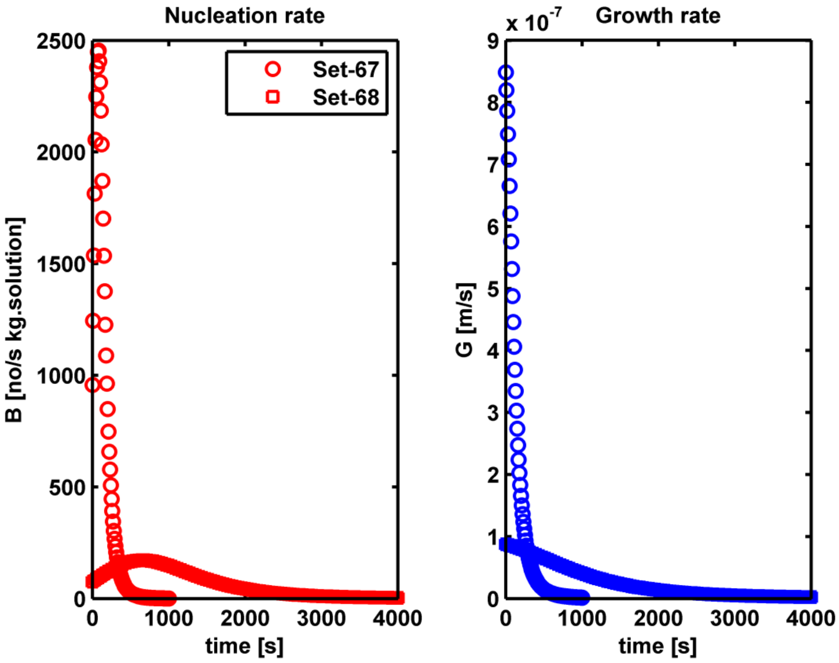

Figure 7-9. Simulated nucleation and growth rate for set-67 and 68

The wavelet-based numerical method introduced in Chapter 4 was applied. The wavelet resolution level constant at J=7 was selected because the CSD was not too sharp. The wavelet solution generated final CSDs for set-67 and set-68 as shown in Figure 7-10. The simulated CSD (as number of particles) for set-67 was over-predicted due to unpredicted experimental error explained previously.  However, the simulated CSD for set-68 was only over-predicted for fine sizes, while for the other size ranges, the simulation results were under-predicted. Therefore, the widths of both CSDs are equal, and it can be concluded that a wavelet-based model successfully validated the MAP crystallisation experiments.

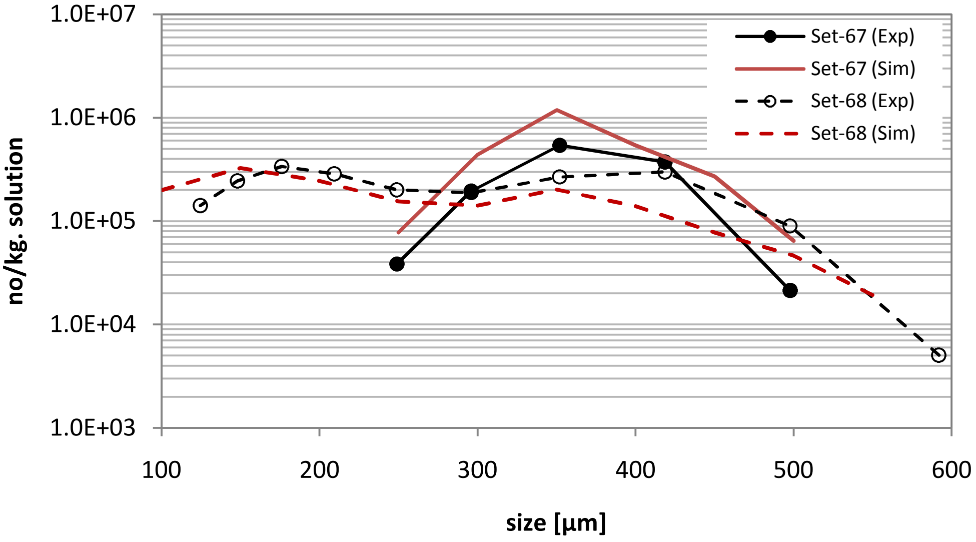

**Figure 7-10. Validation of CSD (as number of particles/kg. solution) for Set-67 and Set-68; (Exp): Experiment result; (Sim): Simulation result.**

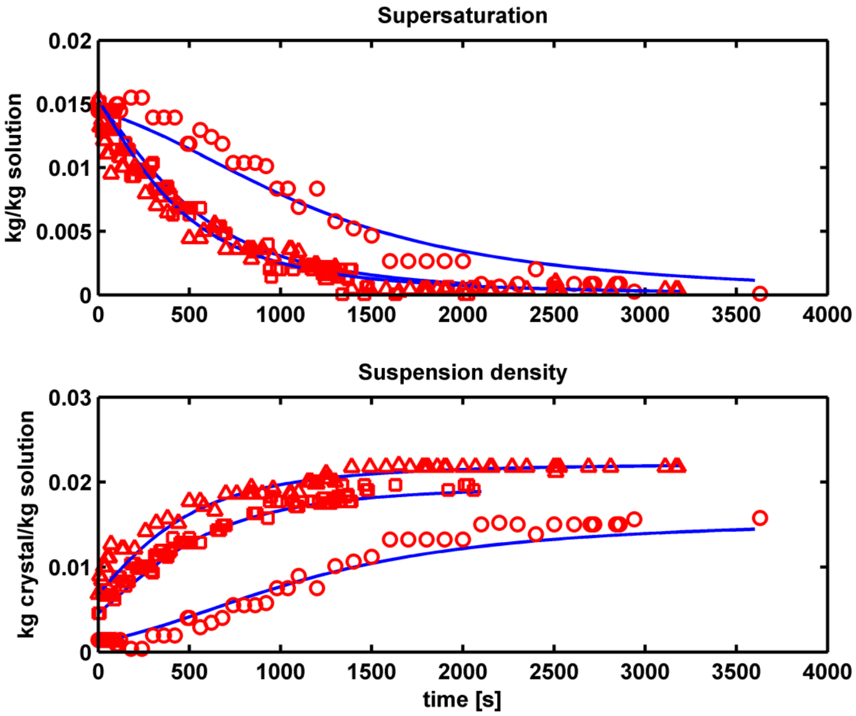

Figure 7-11. Validation of supersaturation and suspension density for set-72, 73 and set-78; solid line: simulation result; circle: set-72; square: set-73; triangle: set-78

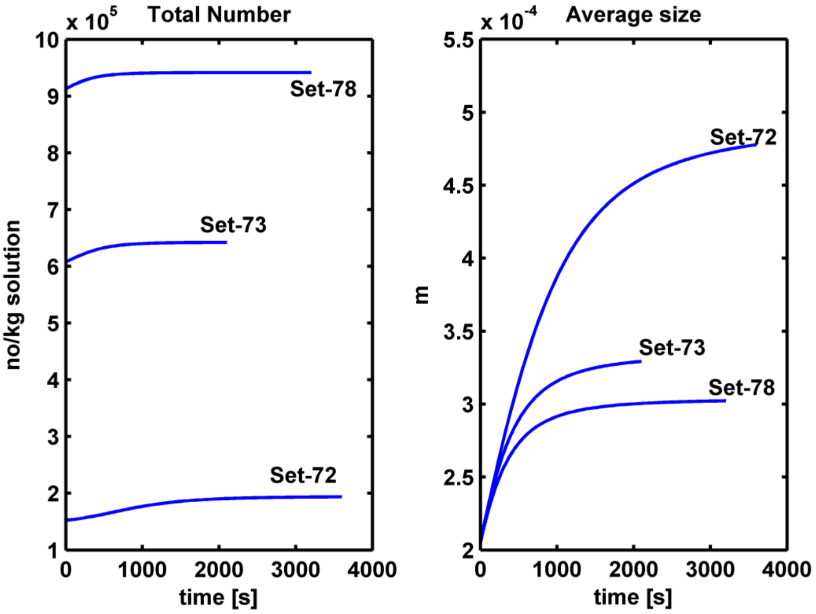

Figure 7-12. Simulation results of total number particles and mean size for set-72, 73 and 78

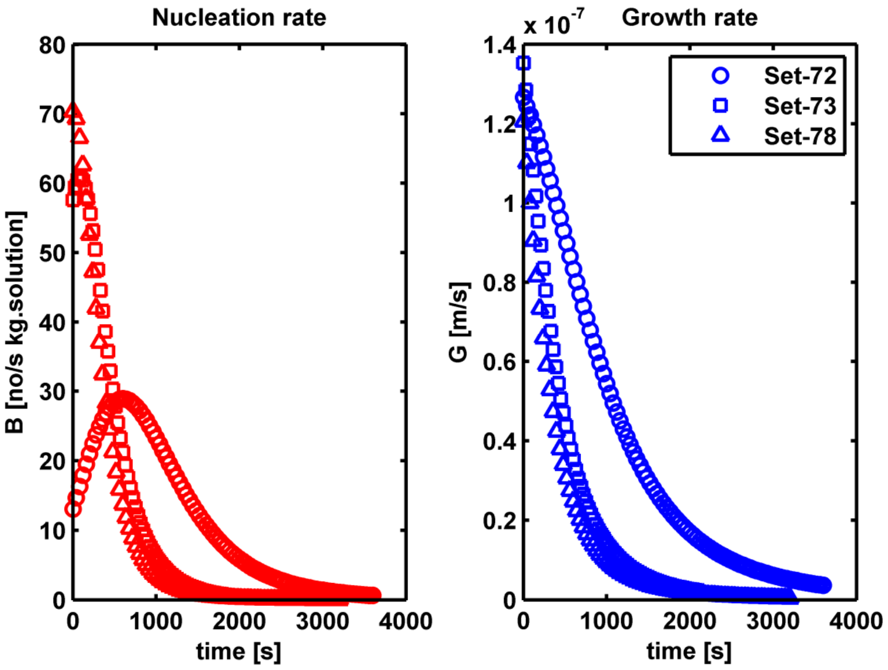

**Figure 7-13. Simulated nucleation and growth rate for set-72, 73 and 78**

The second case where three sets have different seed concentrations or seed loading ratios, i.e. 5, 20, 30% for sets 72, 73, and 78, respectively. From the refined kinetics estimation in Table 7-2, the nucleation constants were similar and approximately $1.2 - 1.3 \times 10^{+8}$ no./s. kg solution $[\mathrm{kg/kg}]^{b+1}$ and the growth constants range were from $3.9 \times 10^{-5}$ to $4.8 \times 10^{-5}$ m/s. $[\mathrm{kg/kg}]^{g}$ . The nucleation and growth exponents were assumed constant at 2.20 and 1.40 respectively. In the solution-side, the supersaturation of set-72 declined more slowly than in sets 73 and 78 (see Figure 7-11). This was because the level of seed concentration used in set-72 was 4 to 6 times lower than in the other two sets. If more seed is used in the system, then less nucleation occurs but also less growth rate was produced. If insufficient seed was used, then moderate growth occurred but excessive level of nucleation will produce a significant amount of off-specification product. Hence, the model can predict correctly the results obtained from the solution-side data.

The validation of the solids mass balance results showed that the simulated total number of particles and the mean crystal size have an improved margin of error. The highest absolute error for total number was 40% for set-73. Set-73 also had 12% of mean size error in comparison to 14% (highest) error observed in set-78. The average nucleation rate of set-73 (as calculated) was 16.33 no./s. kg solution which was the highest among the three sets and may explain the highest absolute error for total number in set-73. The error prediction of mean size remained moderate, and comparable to values obtained from the kinetics estimations procedure. The mean sizes of the three sets were reduced as the average growth rate decreased. The effect of seed concentration was significant only in relation to the growth rate, and was not definitive for the nucleation rate in Table 7-5.

**Table 7-5. Effect of seed concentration of average nucleation and growth rate**

| **Set** | ***Cs* [%]** | $\overline{B}$ no/[kg.solution s] | $\overline{G}$ [m/s] |
|---|---|---|---|
| 72 | 5 | 11.391 | 7.521E-08 |
| 73 | 20 | 16.330 | 6.019E-08 |
| 78 | 30 | 9.215 | 3.050E-08 |

## 7.6 Reaction Kinetics Estimation

In a semi-batch reactive crystalliser, where the reaction between one ammonium ion and one dihydrogen phosphate ion occurred, mono-ammonium phosphate (MAP) was produced. The increasing concentration of MAP in solution will eventually generate crystallisation, with or without additional component being inserted into the system.

The mass balance on the solution-side assumes that the reaction, nucleation and growth occur simultaneously. This occurs in a constant-volume isothermal batch crystalliser where a supersaturation balance can be written as:

$$\frac{d\Delta c}{dt} = +r_C - B_S - A_T R \tag{7-32}$$

The chemical reaction is usually described by the following simplified model:

$$aA + bB \rightarrow cC \downarrow + dD,$$

where A and B are the reactants, and C is the chemical product which is normally precipitated out as solid crystals. The chemical reaction can be described by the following reaction kinetics:

$$r_A = k\, C_A^m\, C_B^n \tag{7-33}$$

where: $\frac{-r_A}{a} = \frac{-r_B}{b} = \frac{r_C}{c} = \frac{r_D}{d}$

The reaction rate cannot be expressed as given by (7-33) as both the reactant concentrations cannot be measured, instead only the MAP solute concentration data is available. The supersaturation value can be used to represent the reaction rate following the power law relation. The proposed form of $r_C$ and rate of supersaturation are given by:

$$r_C = k_r\,(\Delta c_0 - \Delta c)^n \tag{7-34}$$

$$\frac{d\Delta c}{dt} = +r_C - B_S - A_T R = k_r\,(\Delta c_0 - \Delta c)^n - \,k_b\,{M_T}^j\,\Delta c^b + k_g\,\Delta c^g \tag{7-35}$$

where $r_C$ is the reaction rate (kg solute/s. kg.solution); $\Delta c$ is the supersaturation (kg/kg solution); $\Delta c_0$ is the initial supersaturation; $k_b$ is the nucleation constant (number/[kg s (kg/kg)$^{b+1}$]); $k_g$ is the growth constant (m/[s(kg/kg)$^g$]); $M_T$ is the suspension density (kg solid/kg solution); $A_T$ is crystal surface area (m$^2$ ).

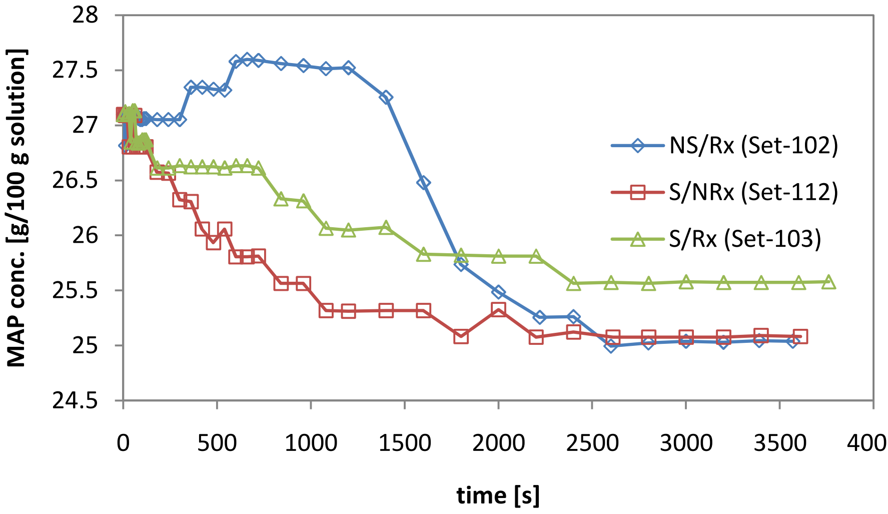

**Figure 7-14. Supersaturation profiles for various systems, NS: non-seeded, S: seeded, Rx: reactive, NRx: non-reactive**

The supersaturation profiles of three experimental sets representing various states such as non-seeded and reactive (NS/Rx), seeded and reactive (S/Rx), and seeded-non reactive (S/NRx) are compared in Figure 7-14. For non-seeded reactive crystallisation, the supersaturation profile increased initially as feeding begins and reaction occurs and the nucleation rate is inversely related to induction time. Therefore, a higher nucleation rate was predicted for non-seeded reactive system than for non-seeded non-reactive system. Figure 7-14 shows that in the non-seeded system, both primary and secondary nucleation were the rate controlling steps. From the NS/Rx system, an estimation of the reaction kinetics can be obtained. The reaction rate versus time for NS/Rx system is presented in Figure 7-15.

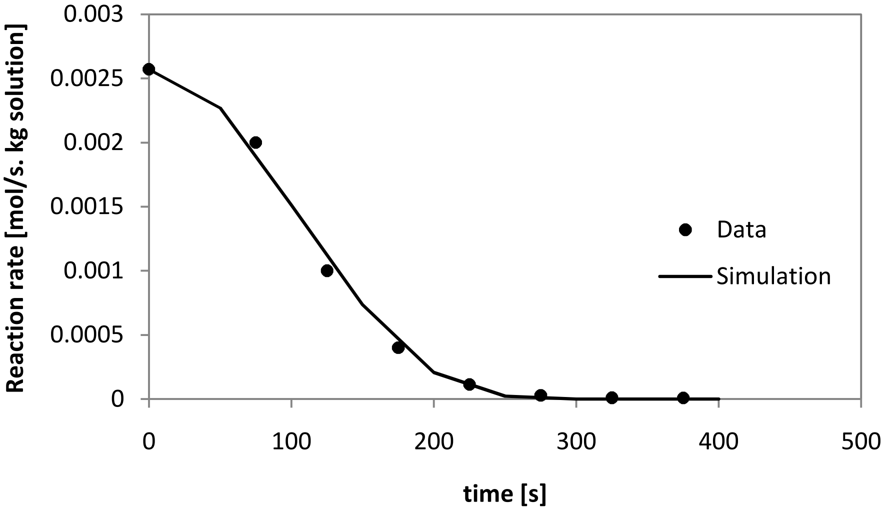

**Figure 7-15. Reaction rate of MAP versus time in seconds for Set-102, circle dot: experiment data, solid line: simulation results**

As previously introduced in section 7.1, the comparison of the reaction kinetics for the S/NRx system (where kinetics can be predetermined by previous method) and the S/Rx system can be obtained. The combined kinetics data then needs to be refined by taking into account the solids data. The mean of the crystallisation and the reaction kinetics for more than 16 sets of experiments are provided in Table 7-6.

**Table 7-6. Summary of reaction and crystallisation kinetics for seeded-reactive (S/Rx) and seeded-non reactive (S/NRx).**

| Parameters | S/Rx | S/NRx | Units |
|---|---|---|---|
| $k_r$ | 0.0001-0.0019 | - | kg/[s. kg solution] |
| $k_b$ | 6.4615E+08 | 3.114E+08 | no/[kg s (kg/kg)$^{b+1}$] |
| $k_g$ | 3.616E-05 | 5.279E-05 | m/[s(kg/kg)$^{g}$] |
| $r$ | 1.0 | - | |
| $b$ | 2.6 | 2.2 | |
| $g$ | 1.8 | 1.4 | |

## 7.7 Validation of MAP Reactive Crystallisation

Initially the supersaturation and suspension density were simulated in order to validate the experimental data. The profiles of supersaturation and suspension density for Set-103 and Set-112 are presented in . By utilising the estimated kinetics, the simulated supersaturation and suspension density for S/Rx continued to exhibit a higher error than S/NRx values. The discrepancy occurred at the initial stage when feeding was in operation and there was an excess of supersaturation generated by the reaction. The profiles of supersaturation still decreased but at a slower rate when compared to the system without reaction. After the feeding was stopped, the reaction rate decreased rapidly and only two governing mechanisms controlled the entire process. At the same batch time, the reactive system still had a higher degree of supersaturation indicating that the growth and nucleation rates were still very high.

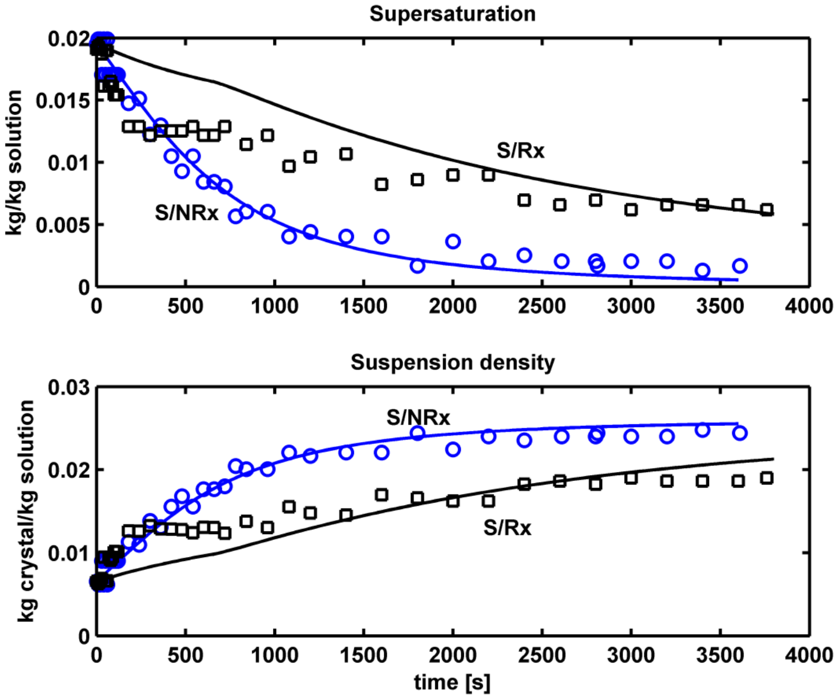

**Figure 7-16. Validation of supersaturation and suspension density for set-103 (S/Rx) and set-112 (S/NRx) solid line: simulation result; circle: set-112; square: set-103.**

The total number of particles and mean particle size were simulated and the results presented in Figure 7-17. The reactive system (Set-103) generated more particles, but they were finer than those in the non-reactive system. The nucleation rate for the reactive system is suppressed by the effect of seeding, and a predictable higher nucleation rate can be obtained if seed crystals are not utilised in the system. The mean size generated from the reactive system was smaller but it still had a significant amount of supersaturation, hence the same mean particle size may be achieved for a longer batch time.

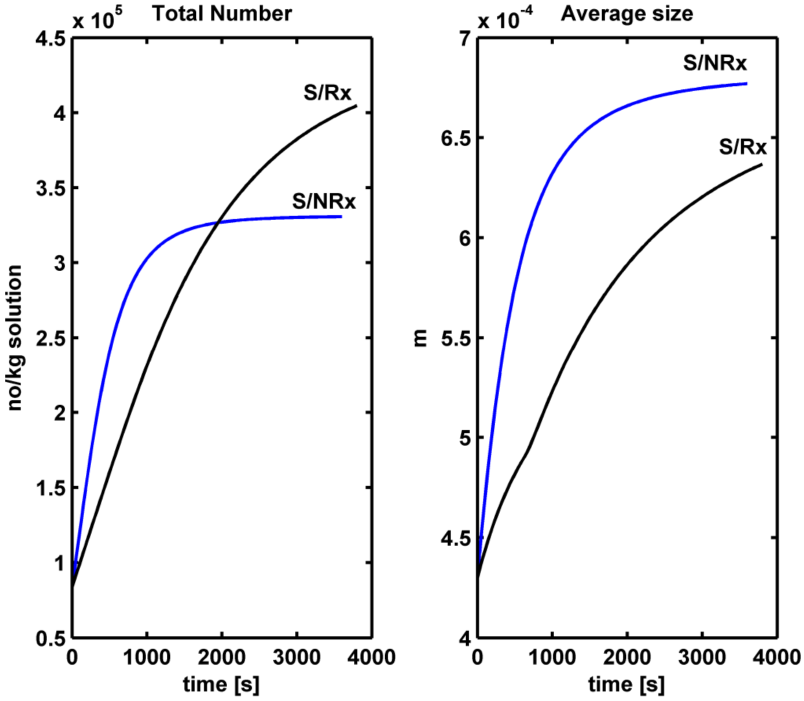

**Figure 7-17. Simulation results of total number particles and mean size for set-103 (S/Rx), and Set-112 (S/NRx)**

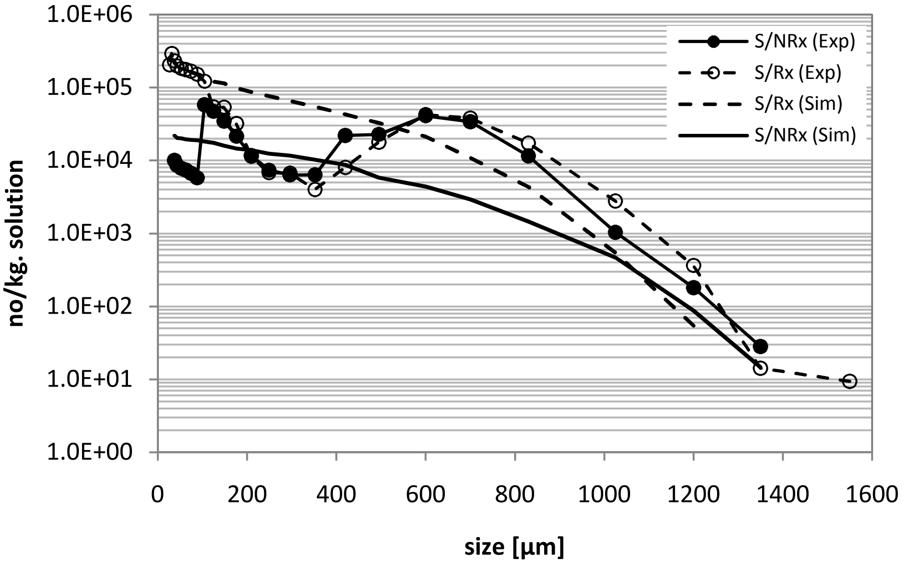

**Figure 7-18. Validation of CSD (as number of particles/kg. solution) for Set-103 (S/Rx) and Set-112 (S/NRx); (Exp): Experiment result; (Sim): Simulation result; S: seeded; Rx: Reactive; NRx: Non-reactive**

Finally, the validation of CSD is considered very important in order to validate the estimated kinetics used, and to test the wavelet-based numerical method used in this study. The population balance solution for a reactive system exhibited a higher number of particles except in the coarse size region. The solution of the wavelet-model (using J=7 of wavelet resolution) was sufficient to validate the results for both reactive and non-reactive systems. Some observable errors were found in the finer size range. The analysis of the solids handling data may be the reason for this discrepancy. The simulated number of crystal for a non-reactive system was also smaller in almost all size ranges. This is understandable because the reaction generated a higher supersaturation and this leads to higher nucleation.

To complete the analysis, the simulated CSD was generated for another three experiments which had different total feeding times. Sets 105, 103 and 110 experienced 5, 11 and 22 minutes of feeding time respectively. The CSD results were as expected with the longer feeding time showing a higher CSD produced, and vice versa. This was due to enhanced reaction which thus initiated a greater degree of supersaturation leading to more nucleation. The validation of the CSD data showed, once again, that it is almost impossible to accurately predict the CSD in a fine size range, and there were observable errors for all runs. Nevertheless, the wavelet-based solutions could provide an excellent prediction of CSD for many reactive systems

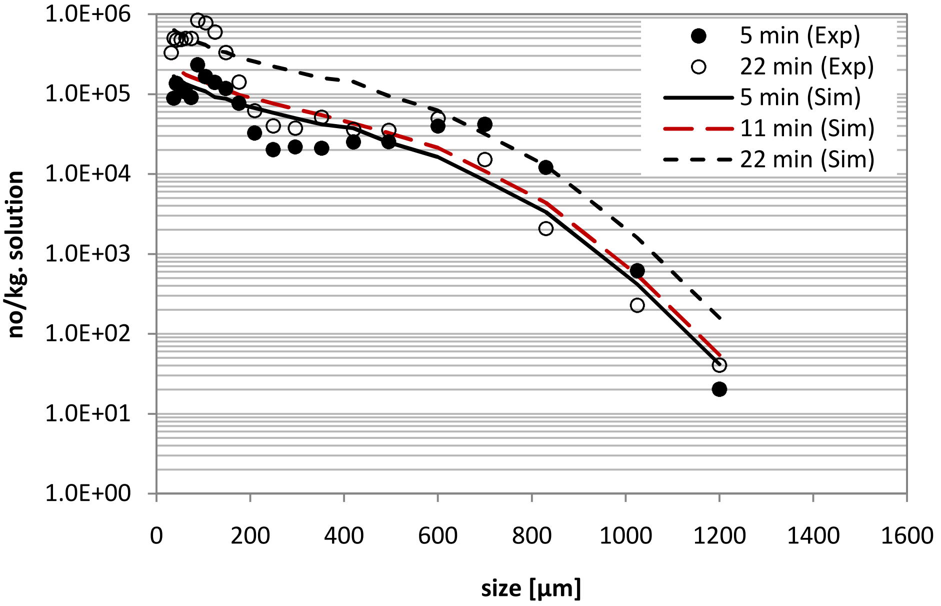

**.Figure 7-19. Validation of CSD (as number of particles/kg. solution) for Set-105 (5 minutes), Set-103 (11 minutes) and Set-110 (22 minutes); (Exp): Experiment result; (Sim): Simulation result.**

## *7.8 References*

Aoun, M., E. Plasari, R. David and J. Villermaux (1999). A simultaneous determination of nucleation and growth rates from batch spontaneous precipitation. *Chemical Engineering Science*, 54(9), 1161-1180.

Armenante, P. M. and D. J. Kirwan (1989). Mass transfer to microparticles in agitated systems. *Chemical Engineering Science*, 44, 2781-2796.

Chivate, M. R. and N. S. Tavare (1975). Growth rate measurements in dtb crystallizer. *Chemical Engineering Science*, 30, 354—355.

Garside, J., L. G. Gibilaro and N. S. Tavare (1982). Evaluation of crystal growth kinetics from a desupersaturation curve using initial derivatives. *Chemical Engineering Science*, 37(11), 1625-8.

Garside, J., R. Janssen-Van Rosmalen and P. Bennema (1975). Verification of crystal growth rate equations. *Journal of Crystal Growth*, 29(3), 353-366.

Garside, J., A. Mersmann and J. Nyvlt (1990). *Measurement of crystal growth rates*. European Federation of Chemical Engineering - Working Party on Crystallization, Germany.

Gunn, D. J. and M. S. Murthy (1972). Kinetics and mechanisms of precipitation. *Chemical Engineering Science*, 27, 1293-1313.

Nielsen, A. E. (1961). Homogenous nucleation in barium sulphate precipitation. *Acta Chemica Scandinavica*, 15, 441-442.

Palwe, B. J., M. R. Chivate and N. M. Tavare (1985). Growth kinetics of ammonium nitrate crystals in a draft tube agitated batch crystallizer. *Industrial and Engineering Chemistry Process Design and Development*, 24, 914-921.

Randolph, A. D. and M. A. Larson (1962). Transient and steady state size distributions in continuous mixed suspension crystallizers. *AIChE Journal*, 8(5), 639-645.

Söhnel, O. and J. Garside (1992). *Precipitation*. Butterworth-Heinemann, London.

Söhnel, O. and J. W. Mullin (1982). Precipitation of calcium carbonate. *Journal of Crystal Growth*, 60(2), 239-250.

Tavare, N. S. (1987). Batch crystallizers: A review. *Chemical Engineering Communications*, 61(1), 259-318.

Tavare, N. S. and J. Garside (1986). Simultaneous estimation of crystal nucleation and growth kinetics from batch experiments. *Chemical Engineering Research and Design*, 64(a), 109-118.

Villermaux, J. (1986). Mixing phenomena in stirred reactors. Encyclopedia of fluid mechanics. Houston, Gulf Publishing Company: 707-771.

# 8. Thesis Conclusions, Practical Implications and Recommendations for Future Research

## 8.1 Thesis Conclusions

1. The overall mechanism governing reactive crystallisation is unique due to the relationships between, and the effects produced by, the chemical reactions, the masses transferred, mixing effects and fluid hydrodynamics. The crystallisation models that we have verified will be of great value in the process design and scale-up of crystallisation processes, as this will lead to improved product quality and also enable the tailoring of product properties to the requirements of new applications.
2. This study presents a review and analysis of the significant published research related to the development of numerical techniques for solving the population balance equations. The major challenges associated with the existing numerical techniques are: (i) long computation times are required to solve the equations; (ii) computation capacity (memory needed); (iii) the stability of the model; (iv) the accuracy of the simulated results obtained; and (v) how to apply the methods and results to process design and for implementing operational control.
3. A systematic modelling approach has been developed and evaluated for use with traditional crystallisation processes, and also extended to several alternative reactive crystallisation processes. The similarities and major differences between the non-reactive and reactive processes are presented for two specific case studies. Key process variables which affect the crystallisation

products have been identified by sensitivity analysis, for both the experimental setup and the model validation requirements.

4. In non-seeded cooling batch crystallisation, both the cooling effect and the initial degree of supersaturation have significant influence on the supersaturation profiles although they do not affect the crystal size distribution (CSD). In seeded cooling crystallisation, the seed loading ratio has the most significant effect on the CSD profiles, followed by the supersaturation factor and the seed size. Similarly, as also observed in a non-seeded system, the cooling rate, stirring speed and crystal yield do not significantly affect the CSD product if enough seeds are loaded under well-mixed conditions. In addition, the degree of supersaturation influences not only the kinetics but also the crystal shape and habit.
5. Experiments performed on the reactive crystallisation of mono-ammonium phosphate (MAP) showed that both single-feed and dual-feed arrangements can produce MAP crystals. These crystals have been verified by X-ray diffraction analysis and validated against the standard XRD pattern of MAP. For a seeded reactive system, supersaturation is mainly used to promote seed growth. A lower level of supersaturation also leads to needle-shaped crystals, which are undesirable and different from the normal structure of MAP crystals. The longer feeding time required indicates that more MAP solute is produced in the system, and this leads to higher supersaturation and higher crystal yields.
6. Two wavelet-based numerical methods, i.e. Wavelet Orthogonal Collocation (WOC) and Wavelet Finite Difference (WFD), have been tested and benchmarked using the established techniques such as finite-difference based, orthogonal collocation and orthogonal collocation with finite element method in three population balance cases. The results have demonstrated the potential of wavelet-based numerical techniques as an alternative approach which can produce accurate, fast and robust solutions. This new wavelet numerical technique and wavelet application approach has great potential for application to other chemical engineering processes.
7. A simultaneous method has been applied in the procedure for the estimation of crystallisation kinetics. The nucleation constant was found to be in the range $1.0 - 6.9 \times 10^{8}$ [no/kg s (kg/kg)$^{b+1}$ ] and the growth constant measured was in the range $3.0 - 9.4 \times 10^{-5}$ [m/s (kg/kg)$^{g}$] with the nucleation and growth exponents determined as 2.2 and 1.4 respectively.

8. Reaction kinetics was estimated simultaneously with crystallisation kinetics by using the semi-batch reactive experimental data. The crystallisation kinetics measured was found to be within the ranges of the non-reactive kinetics results (in section 8.1.7 above). The average nucleation and growth constants were $6.46 \times 10^8$ [no/kg s $(kg/kg)^{b+1}$ ] and $3.62 \times 10^{-5}$ [m/s $(kg/kg)^g$], while the nucleation and growth exponents of 2.6 and 1.8 respectively exhibited slight differences from the values given in section 8.1.7. The first order kinetics was found to provide a suitable representation of the reaction rate with respect to the difference in degree of supersaturation. The reaction constant measured was within the range $1.0 \times 10^{-4}$ to $19 \times 10^{-4}$ [kg/s. kg solution] depending upon the initial degree of supersaturation and the condition of the reactants.
9. The wavelet-based model that we have implemented demonstrated superior adaptability and capability when used to validate the solution-side and solid-side experimental data for reactive and non-reactive MAP crystallisation, within an acceptable degree of error.

## *8.2 Practical Implications*

1. The research preformed and presented in this thesis provides a basic framework of wavelet-based numerical techniques that can be adapted, not only for crystallisation modelling or within the field of chemical engineering in general but also, for any process modelling application that involves systems of partial and/or ordinary differential equations.
2. This work presents a significant body of information concerning various aspects of mono-ammonium phosphate crystallisation, starting with the model development, experimental setup, kinetics estimation, and finally for the validation of the models.
3. The crystallisation and reactive kinetics that have been obtained can be used for crystalliser design, crystalliser performance testing, or as a tool in modelling and simulating data for the mono-ammonium phosphate process requiring only a limited amount of supplementary research to be performed.

## *8.3 Recommendations for Future Research*

1. The codes used for the wavelet-based techniques and models were written in the MATLAB® environment. The application of enhanced programming skills, within and beyond MATLAB, would enable this research to be applied more easily and in a wider range of processes.
2. Some recommendations arising from the MAP experimental work have been reported in June 2008 (see in Appendix C) as part of a continuing collaboration between Curtin University of Technology and University of Hyogo, Japan. An additional study was proposed and is currently under study to investigate MAP anti-solvent crystallisation and the impurity effects in order to significantly improve our understanding of the MAP crystallisation mechanism and its kinetics. The June 2008 report also proposed investigating improvements in the solid analysis, and implementing on-line CSD measurement.

## *8.4 Thesis Reference Declaration*

All references included in this thesis have been alphabetically listed at the end of every chapter or appendix.

**Every reasonable effort has been made to acknowledge the owners of copyright material. I would be pleased to hear from any copyright owner who has been omitted or incorrectly acknowledged.**

# A. Experimental setup and sample of calculations

### A.1.1 Experimental setup for reactive system

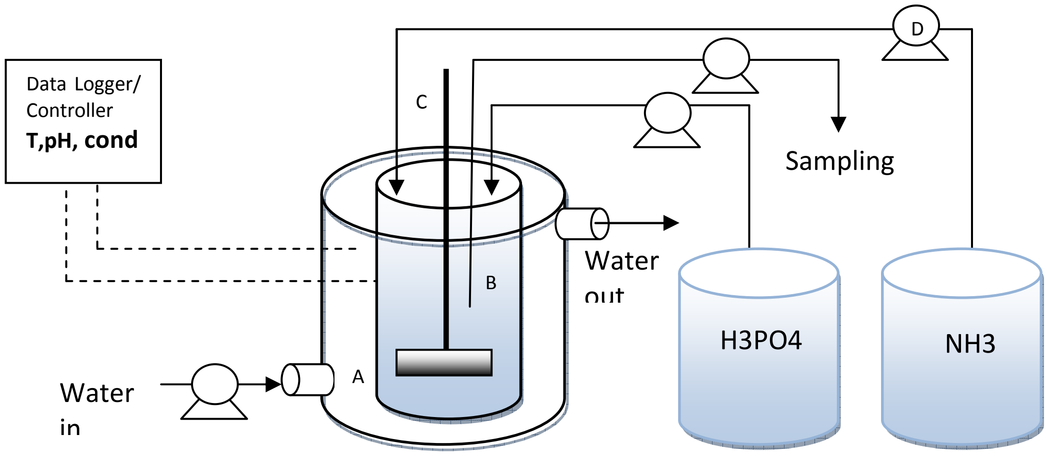

**Figure A-1. The arrangement for reactive crystallization experimentation; A : cooling jacket, B : crystalliser vessel, C : impeller, D : peristaltic pump.**

### A.1.2 Experimental setup for non-reactive system

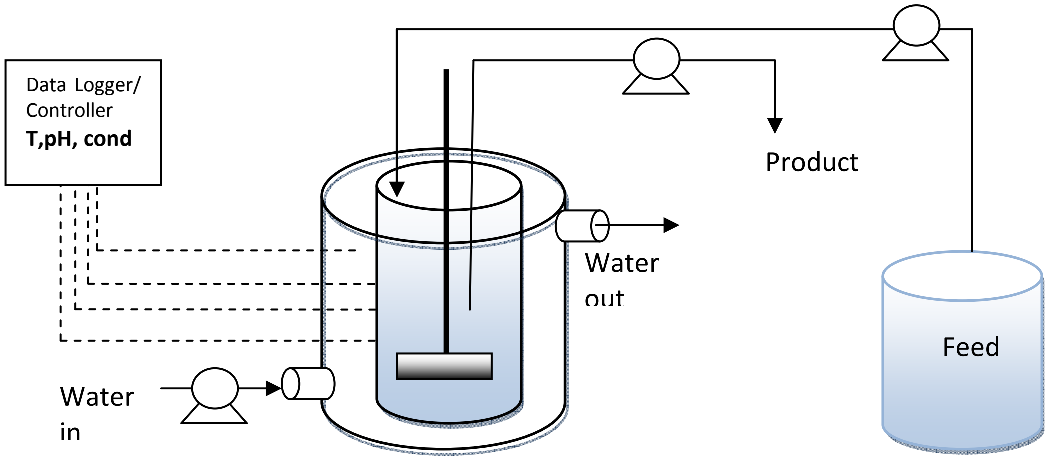

**Figure A-2. The arrangement for cooling batch crystallisation experimentation**

## A.2 Methodology

### *Batch cooling crystallisation experiment (seeded/non-seeded)*

A batch cooling crystallisation can be conducted with and without seed crystals. The natural cooling operation is controlled by flowing a fixed temperature of cooling water into a jacket's vessel. The mixing is maintained constant at certain level which ensures the well-mixed suspension condition inside the vessel and thus enhance the heat transfer rate. The level of supersaturation can be adjusted initially by modifying the concentration and / or by changing the initial temperature. At a certain level of supersaturation, the seeded crystals is charged into the system, and the time is referred as 0 second. The MAP concentration and temperature are monitored by on-line system. Once the batch is finished, the sampling is started to determine the solid-side information by weighing the crystals produced, and determining the crystal size distribution.

The steps of batch cooling experiment are given below:

1. Preparation of saturated or supersaturated solution
2. Cooling is started to reach set point, mixing is started as well
3. If using seed crystals, seed is charged into system at certain supersaturation condition
4. Timing is started
5. Nucleation and crystal growth stage
6. At certain batch time, sampling is started
7. Solution discharge
8. Solid analysis

If an unseeded condition is used, step no. 3 is not applicable. If an isothermal condition is aimed, the preparation of saturated and the cooling rate in step 1 and 2 is modified.

### *Experiment using phosphoric acid as starting solution*

A reactive experiment is conducted by charging a phosphoric acid into a vessel initially as a starting solution and an ammonia solution is fed into in a semi-batch mode for a certain time. The ratio of ammonia used and the phosphoric acid in the solution can be analysed by acid-base titrating method to determine the extent of reaction. At N/P ratio equals to 1, most of mono-ammonium phosphate (MAP) will be produced at the low pH condition. Furthermore di-ammonium phosphate (DAP) will be produced at N/P ratio equals to 2.0 and at a pH 7-8. Once the feeding is stopped, the sampling can be started and finally, the solution is discharged for a total solid analysis, such as suspension density by gravimetric method and crystal size distribution analysis by using sieving and particle size analyser. The solid sampling includes several steps such as, filtration, washing with acetone and drying.

The experimental steps of a reactive system by using phosphoric acid as starting solution are:

1. Preparation of starting solution
2. Preparation of reactants
3. Single feeding start
4. Reaction time
5. Nucleation stage
6. Crystal growth stage
7. Feeding stop
8. Cooling and sampling

### *Experiment using MAP saturated as starting solution*

1. Preparation of starting solution
2. Preparation of reactants
3. Dual feeding start
4. Reaction time
5. Nucleation stage
6. Crystal growth stage
7. Feeding stop
8. Cooling and sampling

### *Experiment using MAP saturated with seed*

1. Preparation of starting solution
2. Preparation of reactants
3. Preparation of seed
4. Dual feeding start
5. Reaction time
6. Crystal growth stage
7. Feeding stop
8. Cooling and sampling

## A.3 Materials

| No. | Materials (form), concentration | Company |
|---|---|---|
| 1. | Ammonium dihydrogen phosphate (solid), 98 wt% | Kishida Kagaku Co. Ltd. |
| 2. | Diammonium hydrogen phosphate (solid), 98.5 wt% | Kanto Chemical Co. Inc. |
| 3. | Phosphoric acid solution, 85 wt% | Kanto Chemical Co. Inc. |
| 4. | Ammonium solution, 28 wt% | Kanto Chemical Co. Inc |
| 5. | Acetone solution, 99 wt% | Kishida Kagaku, Co. Ltd. |
| 6. | Ethanol solution, 99.5 wt% | Kanto Chemical Co. Inc. |
| 7. | Hydrochloric acid solution, 1 M | Kanto Chemical Co. Inc. |
| 8. | Sodium hydroxide solution, 1 M | Kanto Chemical Co. Inc. |

Impurities detail for main reactants as specified are as follow:

1. Ammonium dihydrogen phosphate, 98%, Chameleon Reagen, Kishida Kagaku, Co. Ltd.
   Impurity:

| | |
|---|---|
| - Cl | 0.005% |
| - $SO_4$ | 0.02% |
| - Heavy metal (as Pb) | 0.003% |
| - Fe | 0.003% |
| - As | 3 ppm |
| - Alkali | 0.4% |

1. Diammonium hydrogen phosphate, 98.5%, Kanto Chemical Co. Inc.
   Impurity:

| | |
|---|---|
| - Cl | max 0.005% |
| - $SO_4$ | max 0.01% |
| - H.m (as Pb) | max 0.002% |
| - Na | max 0.1% |
| - K | max 0.05% |
| - As | max 3 ppm |
| - Fe | 0.002% |

2. Phosphoric acid, 85%, Cisca Reagent, Kanto Chemical Co. Inc.
   Impurity:

| | |
|---|---|
| - Cl | max 2 ppm |
| - Nitrate | to pass test |
| - $SO_4$ | max 0.002% |
| - Na | max 0.01% |
| - K | max 0.005% |
| - Cu | max 5 ppm |
| - Zn | max 5 ppm |
| - Cd | max 5 ppm |
| - Pb | max 5 ppm |
| - As | max 0.5 ppm |
| - Mn | max 5 ppm |
| - Fe | max5 ppm |

| | |
|---|---|
| - Ni | max 5 ppm |
| - Permanganate (as O) | max 8 ppm |

3. Ammonia solution, 28-30%-wt, Cisca Reagent, Kanto Chemical Co. Inc.
   Composition:

| | |
|---|---|
| - Residue on evaporation | max 0.002% |
| - $CO_3$ | max 0.002% |
| - Cl | max 0.3 ppm |
| - $PO_4$ | max 0.5 ppm |
| - Silicate (as $SiO_2$) | max 0.001% |
| - $SO_4$ | max 2 ppm |
| - S | max 2 ppm |
| - Na | max 1 ppm |
| - K | max 1 ppm |
| - Cu | max 0.1 ppm |
| - Mg | max 1 ppm |
| - Ca | max 1 ppm |
| - Zn | max 0.1 ppm |
| - Pb | max 0.1 ppm |
| - Fe | max 0.2 ppm |
| - Ni | max 0.1 ppm |
| - Permanganate (as O) | max 8 ppm |

## *A.4 Equipments*

| No. | Equipment Name, Model | Specifications / Quantity | Company |
|---|---|---|---|
| 1. | Microscope | Optiphot | Nikon |
| 2. | Conductivity meter, DS-52 | Cell constant 100 $m^{-1}$<br>Range: 2.00 – 19.99 S/m | Horiba |
| 3. | Multi-channel data logger, GL-200 | 10 channels | Graphtec Co. |
| 4. | pH probe, CE-108C | | Nissin Co. |
| 5. | pH controller, NPH-660NDE | | Nissin Co. |
| 6. | pH tube pump, NRP-75 | | Nissin Co. |
| 7. | Temperature probe, NT-20 | | Nissin Co. |
| 8. | Particle size analyser, FRA | Range: 0.1 – 700 μm | Microtrac |
| 9. | Tube pump | Tornado type | As One |
| 10. | Roller pump, RP-100 | | Eyela |
| 11. | Tube pump – 25N | | Taiyo |
| 12. | Tube pump, L/S 7518-10 | | Masterflex |
| 13. | Thermocouple | Quantity : 3 | Nissin Co. |
| 14. | Water cooler | Quantity : 1 | Nissin Co. |
| 15. | Water-bath with temperature controller | Quantity : 2 | Manufactured |
| 16. | Impeller | Turbine with inclined blades | Manufactured |
| 17. | Vessel | Volume: 4000 ml, 2000 ml<br>700 ml and 500 ml | Manufactured |
| 18. | Sieving plates | Range : 75-1400 μm; Diameter : 150 mm | Japan standard |
| 19. | Vessel lid | 3 channels and 5 channel | Manufactured |
| 20. | X-diffraction analyser | | |

## A.5 Analysis methods

1. N/P molar ratio determination: The ammonia to phosphoric acid molar ratio is determined by titration with 1 M standard solution of hydrochloric acid and sodium hydroxide. A slurry sample was mixed with 90 vol% of distilled water. NaOH was added to bring up the pH to 8.0 and then followed by HCl to lower the pH to 4.0. The amount of HCl and NaOH added was used to calculate the molar ratio (MR) such as (Campbell et al. 2006):

$$MR = 2 - \left(\frac{vol.NaOH}{vol.HCL}\right)$$

2. Conductivity measurement: The electrolytic conductance of an aqueous solution of an ionic substance depends on temperature and on the nature and concentration of the solute. Mono-ammonium phosphate solute concentration in the system can be measured with high precision at known temperatures. The work of (Torgesen et al. 1963) gave a solid background on the relation between conductivity as a function of MAP concentration and temperature. The model was found to be not very accurate due to the difference of electrolytic cell used. The model was corrected by a non-linear optimisation and then successfully implemented in this study.

$$\kappa_w = a + (b + cw)T + (d + ew)T^2 + (f + gw)w$$

| Parameter | (Torgesen et al. 1963) | This study | Units |
|---|---|---|---|
| $a$ | $-1.081 \times 10^{-2}$ | $-2.439 \times 10^{-2}$ | $\text{ohm}^{-1}\ \text{cm}^{-1}$ |
| $b$ | $3.435 \times 10^{-4}$ | $6.397 \times 10^{-3}$ | $\text{ohm}^{-1}\ \text{cm}^{-1}\ \text{deg}^{-1}$ |
| $c$ | $4.940 \times 10^{-5}$ | $2.367 \times 10^{-4}$ | $\text{ohm}^{-1}\ \text{cm}^{-1}\ (\text{wt}\%)^{-1}$ |
| $d$ | $1.334 \times 10^{-5}$ | $2.101 \times 10^{-4}$ | $\text{ohm}^{-1}\ \text{cm}^{-1}\ \text{deg}^{-2}$ |
| $e$ | $-2.081 \times 10^{-7}$ | $7.607 \times 10^{-6}$ | $\text{ohm}^{-1}\ \text{cm}^{-1}\ \text{deg}^{-2}(\text{wt}\%)^{-1}$ |
| $f$ | $4.038 \times 10^{-3}$ | $5.673 \times 10^{-3}$ | $\text{ohm}^{-1}\ \text{cm}^{-1}\ (\text{wt}\%)^{-1}$ |
| $g$ | $-6.636 \times 10^{-5}$ | $-4.404 \times 10^{-5}$ | $\text{ohm}^{-1}\ \text{cm}^{-1}\ (\text{wt}\%)^{-1}$ |

Where : $\kappa_w$ is electrolytic conductance (S/cm) or (1/ohm cm), $T$ is temperature in $^{o}$C and $w$ is the mass percentage of solute (wt %).

The above equations can be solved as a second order polynomial in $w$. The value of $w$ then can be selected from one of the two solutions as appropriate.

3. Crystal yield measurement: Dried solid crysts were weighted from the slurry sample taken or in the total volume of crystalliser. The need of moderate temperature drying was important to remove additional solvent in the washing step.

4. Crystal size distribution measurement: A laser diffraction method was used to measure a fine size range crystal with maximum size of 700 µm and minimum is 0.1 µm. The coarser crystal were sized by sieving tray with the range of 1400 – 75 µm.
5. X-ray diffraction analysis: X-Ray powder Diffraction analysis is a powerful method by which X-Rays of a known wavelength are passed through a sample to be identified in order to identify the crystal structure. The wave nature of the X-Rays means that they are diffracted by the lattice of the crystal to give a unique pattern of peaks of 'reflections' at differing angles and of different intensity, just as light can be diffracted by a grating of suitably spaced lines. The diffracted beams from atoms in successive planes cancel unless they are in phase, and the condition for this is given by the Bragg relationship.

   $$n\,l = 2\,d\,\sin\,(q)$$

   where: $n$ is the number of diffraction line, $l$ is the wavelength of the X-Rays, $d$ is the distance between different plane of atoms in the crystal lattice, and $q$ is the angle of diffraction.

   The X-Ray detector moves around the sample and measures the intensity of these peaks and the position of these peaks [diffraction angle 2q ]. The highest peak is defined as the 100% * peak and the intensity of all the other peaks are measured as a percentage of the 100% peak. The standard XRD for MAP was taken from (Xu et al. 2006).

## *Sample of on-line conductivity and temperature data from logger*

| | | |
|---|---|---|
| Vendor | GRAPHTEC Corporation | |
| Model | GL200 | |
| Version | Ver1.80 | |
| Sampling interval | 10s | |
| Total data points | 662 | |
| Start time | 14/04/2008 | 16:11:19 |
| End time | 14/04/2008 | 18:01:32 |
| Trigger time | 14/04/2008 | 16:11:20 |

AMP settings

| CH | Signal name | Input | Range | Filter |
|---|---|---|---|---|
| CH1 | CH 1 | DC | 5V | Off |
| CH2 | CH 2 | DC | 1V | Off |
| CH3 | CH 3 | DC | 1V | Off |
| CH4 | CH 4 | DC | 50V | Off |
| CH5 | CH 5 | DC | 50V | Off |
| CH6 | CH 6 | DC | 50V | Off |
| CH7 | CH 7 | DC | 50V | Off |
| CH8 | CH 8 | DC | 50V | Off |
| CH9 | CH 9 | TEMP | TC_K | Off |
| CH10 | CH10 | TEMP | TC_K | Off |
| Pulse | OFF | H | 500000 | 0 |
| Logic | Off | | | |
| Alarm | | | | |

Data

| Number | Data&Time | CH1 | CH2 | CH3 | CH9 | CH10 |
|---|---|---|---|---|---|---|
| NO. | Time | V | V | V | degC | degC |
| 1 | 14/04/2008 16:11 | 0 | 0.7319 | 0.1165 | 9.8 | 11 |
| 2 | 14/04/2008 16:11 | 0 | 0.7319 | 0.1154 | 9.9 | 10.9 |
| 3 | 14/04/2008 16:11 | -0.001 | 0.7319 | 0.1155 | 9.8 | 10.9 |
| 4 | 14/04/2008 16:11 | -0.001 | 0.732 | 0.1155 | 9.8 | 10.9 |
| 5 | 14/04/2008 16:12 | 0 | 0.732 | 0.1145 | 9.9 | 10.8 |
| 6 | 14/04/2008 16:12 | 0 | 0.732 | 0.1145 | 9.9 | 10.9 |
| 7 | 14/04/2008 16:12 | 0 | 0.732 | 0.1145 | 9.8 | 10.9 |
| 8 | 14/04/2008 16:12 | -0.001 | 0.7319 | 0.1135 | 9.7 | 10.9 |
| 9 | 14/04/2008 16:12 | -0.001 | 0.7319 | 0.1134 | 9.9 | 10.8 |
| 10 | 14/04/2008 16:12 | 0 | 0.7319 | 0.1134 | 9.9 | 10.7 |
| 11 | 14/04/2008 16:13 | 0 | 0.7319 | 0.1124 | 9.9 | 10.7 |
| 12 | 14/04/2008 16:13 | 0 | 0.7319 | 0.1124 | 9.9 | 10.7 |
| 13 | 14/04/2008 16:13 | 0 | 0.7319 | 0.1124 | 9.9 | 10.7 |
| 14 | 14/04/2008 16:13 | 0 | 0.7319 | 0.1124 | 9.8 | 10.5 |
| 15 | 14/04/2008 16:13 | 0 | 0.7319 | 0.1124 | 9.8 | 10.5 |
| 16 | 14/04/2008 16:13 | 0 | 0.7319 | 0.1114 | 9.8 | 10.5 |
| 17 | 14/04/2008 16:14 | 0 | 0.7319 | 0.1114 | 9.8 | 10.5 |

|  |  |  |  |  |  |  |
|---|---|---|---|---|---|---|
| 18 | 14/04/2008 16:14 | 0.001 | 0.7319 | 0.1114 | 9.8 | 10.5 |
| 19 | 14/04/2008 16:14 | 0.001 | 0.7319 | 0.1114 | 9.7 | 10.5 |
| 20 | 14/04/2008 16:14 | 0 | 0.7319 | 0.1114 | 9.8 | 10.4 |
| … |  |  |  |  |  |  |
| 640 | 14/04/2008 17:57 | 0 | 0.7239 | 0.1055 | 9.7 | 9.9 |
| 641 | 14/04/2008 17:58 | 0 | 0.7239 | 0.1055 | 9.7 | 9.9 |
| 642 | 14/04/2008 17:58 | -0.001 | 0.7239 | 0.1055 | 9.7 | 9.9 |
| 643 | 14/04/2008 17:58 | -0.001 | 0.7239 | 0.1055 | 9.6 | 9.9 |
| 644 | 14/04/2008 17:58 | -0.001 | 0.7239 | 0.1055 | 9.7 | 9.9 |
| 645 | 14/04/2008 17:58 | -0.001 | 0.7239 | 0.1055 | 9.7 | 9.9 |
| 646 | 14/04/2008 17:58 | -0.001 | 0.7239 | 0.1055 | 9.7 | 9.9 |
| 647 | 14/04/2008 17:59 | -0.001 | 0.7239 | 0.1055 | 9.7 | 9.9 |
| 648 | 14/04/2008 17:59 | -0.001 | 0.7229 | 0.1055 | 9.7 | 9.9 |
| 649 | 14/04/2008 17:59 | -0.001 | 0.7239 | 0.1055 | 9.7 | 9.9 |
| 650 | 14/04/2008 17:59 | -0.001 | 0.7239 | 0.1055 | 9.8 | 9.9 |
| 651 | 14/04/2008 17:59 | 0 | 0.7239 | 0.1055 | 9.9 | 9.9 |
| 652 | 14/04/2008 17:59 | 0 | 0.7239 | 0.1055 | 9.8 | 9.9 |
| 653 | 14/04/2008 18:00 | 0 | 0.7239 | 0.1055 | 9.7 | 9.9 |
| 654 | 14/04/2008 18:00 | -0.001 | 0.724 | 0.1055 | 9.7 | 9.9 |
| 655 | 14/04/2008 18:00 | -0.001 | 0.7239 | 0.1055 | 9.6 | 10 |
| 656 | 14/04/2008 18:00 | 0 | 0.7249 | 0.1055 | 9.6 | 10 |
| 657 | 14/04/2008 18:00 | 0 | 0.7249 | 0.1055 | 9.7 | 9.9 |
| 658 | 14/04/2008 18:00 | 0 | 0.7239 | 0.1055 | 9.8 | 9.9 |
| 659 | 14/04/2008 18:01 | 0 | 0.7247 | 0.1055 | 9.8 | 9.9 |
| 660 | 14/04/2008 18:01 | 0 | 0.7249 | 0.1055 | 9.8 | 9.9 |
| 661 | 14/04/2008 18:01 | 0 | 0.7249 | 0.1055 | 9.7 | 9.9 |
| 662 | 14/04/2008 18:01 | -0.001 | 0.7249 | 0.1055 | 9.7 | 9.9 |

## ***Sample of MAP concentration calculation from conductivity data***

| Data Set 65 | a | b | c | d | e | f | g |
|---|---|---|---|---|---|---|---|
| | -0.0244 | 0.0064 | -0.0002 | -0.000210165 | 7.6E-06 | 0.00567 | -4E-05 |

| V-cond | S/m | S/cm | V-T | T | C1 | C2 | C3 | x1 | x2 | time |
|---|---|---|---|---|---|---|---|---|---|---|
| 0.7319 | 9.15742 | 0.09157 | 0.2247 | 11 | -4.40402E-05 | 0.00399 | 0.07103 | 24.3475 | 66.2441 | 0 |
| 0.7319 | 9.15742 | 0.09157 | 0.2187 | 10.9 | -4.40402E-05 | 0.004 | 0.07121 | 24.3522 | 66.3985 | 10 |
| 0.7319 | 9.15742 | 0.09157 | 0.2127 | 10.9 | -4.40402E-05 | 0.004 | 0.07121 | 24.3522 | 66.3985 | 20 |
| 0.732 | 9.16144 | 0.09161 | 0.2077 | 10.9 | -4.40402E-05 | 0.004 | 0.07125 | 24.3739 | 66.3768 | 30 |
| 0.732 | 9.16144 | 0.09161 | 0.2036 | 10.8 | -4.40402E-05 | 0.004 | 0.07143 | 24.3788 | 66.5346 | 40 |
| 0.732 | 9.16144 | 0.09161 | 0.1987 | 10.9 | -4.40402E-05 | 0.004 | 0.07125 | 24.3739 | 66.3768 | 50 |
| 0.732 | 9.16144 | 0.09161 | 0.1946 | 10.9 | -4.40402E-05 | 0.004 | 0.07125 | 24.3739 | 66.3768 | 60 |
| 0.7319 | 9.15742 | 0.09157 | 0.1896 | 10.9 | -4.40402E-05 | 0.004 | 0.07121 | 24.3522 | 66.3985 | 70 |
| 0.7319 | 9.15742 | 0.09157 | 0.1856 | 10.8 | -4.40402E-05 | 0.004 | 0.07139 | 24.3572 | 66.5562 | 80 |
| 0.7319 | 9.15742 | 0.09157 | 0.1826 | 10.7 | -4.40402E-05 | 0.00401 | 0.07158 | 24.3624 | 66.7171 | 90 |
| 0.7319 | 9.15742 | 0.09157 | 0.1786 | 10.7 | -4.40402E-05 | 0.00401 | 0.07158 | 24.3624 | 66.7171 | 100 |
| 0.7319 | 9.15742 | 0.09157 | 0.1747 | 10.7 | -4.40402E-05 | 0.00401 | 0.07158 | 24.3624 | 66.7171 | 110 |
| 0.7319 | 9.15742 | 0.09157 | 0.1716 | 10.7 | -4.40402E-05 | 0.00401 | 0.07158 | 24.3624 | 66.7171 | 120 |
| 0.7319 | 9.15742 | 0.09157 | 0.1686 | 10.5 | -4.40402E-05 | 0.00403 | 0.07197 | 24.3734 | 67.0486 | 130 |
| 0.7319 | 9.15742 | 0.09157 | 0.1656 | 10.5 | -4.40402E-05 | 0.00403 | 0.07197 | 24.3734 | 67.0486 | 140 |
| 0.7319 | 9.15742 | 0.09157 | 0.1627 | 10.5 | -4.40402E-05 | 0.00403 | 0.07197 | 24.3734 | 67.0486 | 150 |
| 0.7319 | 9.15742 | 0.09157 | 0.1597 | 10.5 | -4.40402E-05 | 0.00403 | 0.07197 | 24.3734 | 67.0486 | 160 |
| 0.7319 | 9.15742 | 0.09157 | 0.1576 | 10.5 | -4.40402E-05 | 0.00403 | 0.07197 | 24.3734 | 67.0486 | 170 |
| 0.7319 | 9.15742 | 0.09157 | 0.1547 | 10.5 | -4.40402E-05 | 0.00403 | 0.07197 | 24.3734 | 67.0486 | 180 |
| 0.7319 | 9.15742 | 0.09157 | 0.1527 | 10.4 | -4.40402E-05 | 0.00403 | 0.07217 | 24.3792 | 67.2192 | 190 |
| 0.7319 | 9.15742 | 0.09157 | 0.1506 | 10.4 | -4.40402E-05 | 0.00403 | 0.07217 | 24.3792 | 67.2192 | 200 |
| … | | | | | | | | | | |
| 0.7239 | 8.83606 | 0.08836 | 0.1046 | 9.9 | -4.40402E-05 | 0.00408 | 0.07002 | 22.8015 | 69.731 | 6490 |
| 0.7239 | 8.83606 | 0.08836 | 0.1046 | 9.9 | -4.40402E-05 | 0.00408 | 0.07002 | 22.8015 | 69.731 | 6500 |
| 0.7239 | 8.83606 | 0.08836 | 0.1046 | 9.9 | -4.40402E-05 | 0.00408 | 0.07002 | 22.8015 | 69.731 | 6510 |
| 0.7239 | 8.83606 | 0.08836 | 0.1046 | 9.9 | -4.40402E-05 | 0.00408 | 0.07002 | 22.8015 | 69.731 | 6520 |
| 0.724 | 8.84008 | 0.0884 | 0.1046 | 9.9 | -4.40402E-05 | 0.00408 | 0.07006 | 22.8209 | 69.7115 | 6530 |
| 0.7239 | 8.83606 | 0.08836 | 0.1046 | 10 | -4.40402E-05 | 0.00407 | 0.0698 | 22.7884 | 69.5503 | 6540 |
| 0.7249 | 8.87623 | 0.08876 | 0.1046 | 10 | -4.40402E-05 | 0.00407 | 0.0702 | 22.9843 | 69.3544 | 6550 |
| 0.7249 | 8.87623 | 0.08876 | 0.1046 | 9.9 | -4.40402E-05 | 0.00408 | 0.07042 | 22.9966 | 69.5358 | 6560 |

## *Sample of supersaturation calculation from concentration and solubility data*

| Set-65 | | | | | |
|---|---|---|---|---|---|
| time | g/100 g sol | T-c10 | c*(T) | σ | Δc |
| 0 | 24.34751 | 11 | 23.005 | 0.058357 | 1.342508 |
| 0 | 24.35223 | 10.9 | 22.9595 | 0.06066 | 1.392726 |
| 10 | 24.35223 | 10.9 | 22.9595 | 0.06066 | 1.392726 |
| 20 | 24.37393 | 10.9 | 22.9595 | 0.061605 | 1.41443 |
| 30 | 24.3788 | 10.8 | 22.914 | 0.063926 | 1.464802 |
| 40 | 24.37393 | 10.9 | 22.9595 | 0.061605 | 1.41443 |
| 50 | 24.37393 | 10.9 | 22.9595 | 0.061605 | 1.41443 |
| 60 | 24.35223 | 10.9 | 22.9595 | 0.06066 | 1.392726 |
| 70 | 24.35718 | 10.8 | 22.914 | 0.062982 | 1.443177 |
| 80 | 24.36236 | 10.7 | 22.8685 | 0.065324 | 1.493857 |
| 90 | 24.36236 | 10.7 | 22.8685 | 0.065324 | 1.493857 |
| 100 | 24.36236 | 10.7 | 22.8685 | 0.065324 | 1.493857 |
| 110 | 24.36236 | 10.7 | 22.8685 | 0.065324 | 1.493857 |
| 120 | 24.37339 | 10.5 | 22.7775 | 0.070064 | 1.595889 |
| 130 | 24.37339 | 10.5 | 22.7775 | 0.070064 | 1.595889 |
| 140 | 24.37339 | 10.5 | 22.7775 | 0.070064 | 1.595889 |
| 150 | 24.37339 | 10.5 | 22.7775 | 0.070064 | 1.595889 |
| 160 | 24.37339 | 10.5 | 22.7775 | 0.070064 | 1.595889 |
| 170 | 24.37339 | 10.5 | 22.7775 | 0.070064 | 1.595889 |
| 180 | 24.37923 | 10.4 | 22.732 | 0.072463 | 1.647234 |
| 190 | 24.37923 | 10.4 | 22.732 | 0.072463 | 1.647234 |
| 200 | 24.37923 | 10.4 | 22.732 | 0.072463 | 1.647234 |
| … | | | | | |
| 6400 | 22.80147 | 9.9 | 22.5045 | 0.013196 | 0.296966 |
| 6410 | 22.80147 | 9.9 | 22.5045 | 0.013196 | 0.296966 |
| 6420 | 22.80147 | 9.9 | 22.5045 | 0.013196 | 0.296966 |
| 6430 | 22.80147 | 9.9 | 22.5045 | 0.013196 | 0.296966 |
| 6440 | 22.80147 | 9.9 | 22.5045 | 0.013196 | 0.296966 |
| 6450 | 22.80147 | 9.9 | 22.5045 | 0.013196 | 0.296966 |
| 6460 | 22.6079 | 9.9 | 22.5045 | 0.004595 | 0.103405 |
| 6470 | 22.80147 | 9.9 | 22.5045 | 0.013196 | 0.296966 |
| 6480 | 22.80147 | 9.9 | 22.5045 | 0.013196 | 0.296966 |
| 6490 | 22.80147 | 9.9 | 22.5045 | 0.013196 | 0.296966 |
| 6500 | 22.80147 | 9.9 | 22.5045 | 0.013196 | 0.296966 |
| 6510 | 22.80147 | 9.9 | 22.5045 | 0.013196 | 0.296966 |
| 6520 | 22.82091 | 9.9 | 22.5045 | 0.01406 | 0.31641 |
| 6530 | 22.78839 | 10 | 22.55 | 0.010572 | 0.238394 |
| 6540 | 22.98427 | 10 | 22.55 | 0.019258 | 0.434271 |
| 6550 | 22.99664 | 9.9 | 22.5045 | 0.021868 | 0.492138 |
| 6560 | 22.80147 | 9.9 | 22.5045 | 0.013196 | 0.296966 |

## *Sample of particle size analysis results*

Microtrac Version

| No. | Sample No | Details | Sample Name | MV (µm) | MN((µm) | MA(µm) | CS | SD (µm) |
|---|---|---|---|---|---|---|---|---|
| 1 | 510 | 1 of 2 | Seed355 | 397.01 | 264.41 | 370.7 | 0.0162 | 52.527 |
| 2 | 511 | 2 of 2 | Seed355 | 391.78 | 12.498 | 328.6 | 0.0183 | 50.015 |
| 3 | 512 | Avg. of 2 | Seed355 | 394.39 | 14.874 | 348.38 | 0.0172 | 51.327 |
| 4 | 513 | 1 of 2 | Seed355 | 401.05 | 14.956 | 327.71 | 0.0183 | 61.231 |
| 5 | 514 | 2 of 2 | Seed355 | 398.9 | 12.027 | 315.72 | 0.019 | 59.576 |
| 6 | 515 | Avg. of 2 | Seed355 | 399.97 | 13.148 | 321.64 | 0.0187 | 60.425 |
| 7 | 516 | 1 of 2 | Set90low | 310.27 | 231.77 | 288.71 | 0.0208 | 73.701 |
| 8 | 517 | 2 of 2 | Set90low | 302.18 | 224.32 | 281.31 | 0.0213 | 70.603 |
| 9 | 518 | Avg. of 2 | Set90low | 306.21 | 227.88 | 284.96 | 0.0211 | 72.115 |
| 10 | 519 | 1 of 2 | Set102low | 301.17 | 183.76 | 269.1 | 0.0223 | 86.026 |
| 11 | 520 | 2 of 2 | Set102low | 297.77 | 169.27 | 264.52 | 0.0227 | 83.207 |
| 12 | 521 | Avg. of 2 | Set102low | 299.47 | 176.17 | 266.8 | 0.0225 | 84.654 |
| 13 | 522 | 1 of 2 | Set102low | 231.8 | 67.328 | 157.56 | 0.0381 | 135.82 |
| 14 | 523 | 2 of 2 | Set102low | 235.06 | 58.049 | 156.21 | 0.0384 | 138.63 |
| 15 | 524 | Avg. of 2 | Set102low | 233.43 | 62.267 | 156.89 | 0.0382 | 137.26 |
| 16 | 525 | 1 of 2 | Set103low | 270.06 | 66.588 | 161.43 | 0.0372 | 197.98 |
| 17 | 526 | 2 of 2 | Set103low | 227.49 | 57.562 | 149.38 | 0.0402 | 141.22 |
| 18 | 527 | Avg. of 2 | Set103low | 248.78 | 61.493 | 155.18 | 0.0387 | 177.5 |
| 19 | 528 | 1 of 2 | Set104low | 279.94 | 91.758 | 209.54 | 0.0286 | 132.88 |
| 20 | 529 | 2 of 2 | Set104low | 273.9 | 80.745 | 202.37 | 0.0296 | 129.97 |
| 21 | 530 | Avg. of 2 | Set104low | 276.91 | 85.735 | 205.9 | 0.0291 | 131.14 |
| 22 | 531 | 1 of 2 | Set105low | 289.52 | 79.427 | 206.66 | 0.029 | 147.32 |
| 23 | 532 | 2 of 2 | Set105low | 278.67 | 88.937 | 204.46 | 0.0293 | 135.64 |
| 24 | 533 | Avg. of 2 | Set105low | 284.07 | 83.982 | 205.56 | 0.0292 | 140.35 |
| 25 | 534 | 1 of 2 | Set106low | 342.33 | 108.3 | 262.05 | 0.0229 | 146.21 |
| 26 | 535 | 2 of 2 | Set106low | 336.02 | 94.046 | 253 | 0.0237 | 144.26 |
| 27 | 536 | Avg. of 2 | Set106low | 339.17 | 100.41 | 257.47 | 0.0233 | 145.32 |
| 28 | 537 | 1 of 2 | Set106low | 331.38 | 62.192 | 230.97 | 0.026 | 157.15 |
| 29 | 538 | 2 of 2 | Set106low | 323.86 | 51.045 | 218.28 | 0.0275 | 157.66 |
| 30 | 539 | Avg. of 2 | Set106low | 327.62 | 55.66 | 224.47 | 0.0267 | 157.5 |
| 31 | 540 | 1 of 2 | Set108low | 239.06 | 119.27 | 197.87 | 0.0303 | 100.37 |
| 32 | 541 | 2 of 2 | Set108low | 230.58 | 116.74 | 192.19 | 0.0312 | 94.674 |
| 33 | 542 | Avg. of 2 | Set108low | 234.8 | 117.96 | 194.99 | 0.0308 | 96.913 |
| 34 | 543 | 1 of 2 | Set109low | 358.87 | 265.33 | 334.85 | 0.0179 | 77.155 |
| 35 | 544 | 2 of 2 | Set109low | 345.55 | 258.84 | 323.77 | 0.0185 | 69.015 |
| 36 | 545 | Avg. of 2 | Set109low | 352.19 | 261.95 | 329.21 | 0.0182 | 73.192 |
| 37 | 546 | 1 of 2 | Set110low | 219.6 | 76.667 | 151.48 | 0.0396 | 133.45 |
| 38 | 547 | 2 of 2 | Set110low | 213.17 | 69.061 | 145.7 | 0.0412 | 129.37 |
| 39 | 548 | Avg. of 2 | Set110low | 216.38 | 72.557 | 148.54 | 0.0404 | 131.75 |
| 40 | 549 | 1 of 2 | Set111low | 332.74 | 227.35 | 304.82 | 0.0197 | 76.907 |

# *Sample of sieving results and number of particles calculation*

| Set-111 | Aperture | Lavg | m-empt | m-fill | cum-mass | mass | cum | %-cum | %-m | number |
|---|---|---|---|---|---|---|---|---|---|---|
| 1 | 1400+ | 1550 | 56.9 | 56.97 | 0.07 | 0.07 | 7.249784 | 1.00 | 0.01 | 20 |
| 2 | 1400-1180 | 1350 | 124.14 | 124.39 | 0.25 | 0.18 | 7.179784 | 0.99 | 0.02 | 77 |
| 3 | 1180-1000 | 1200 | 178.45 | 178.93 | 0.48 | 0.23 | 6.999784 | 0.97 | 0.03 | 141 |
| 4 | 1000-850 | 1025 | 242.62 | 243.47 | 0.85 | 0.37 | 6.769784 | 0.93 | 0.05 | 364 |
| 5 | 850-710 | 830 | 294.46 | 295.93 | 1.47 | 0.62 | 6.399784 | 0.88 | 0.09 | 1148 |
| 6 | 710-600 | 700 | 345.91 | 348.07 | 2.16 | 0.69 | 5.779784 | 0.80 | 0.10 | 2130 |
| 7 | 600-500 | 600 | 393.81 | 396.63 | 2.82 | 0.66 | 5.089784 | 0.70 | 0.09 | 3235 |
| 8 | 500-425 | 495 | 441.74 | 445.53 | 3.79 | 0.97 | 4.429784 | 0.61 | 0.13 | 8468 |
| 9 | 425-355 | 420 | 488.11 | 493.03 | 4.92 | 1.31 | 3.459784 | 0.48 | 0.18 | 18651 |
| 10 | 355-300 | 418.6 | 45.32 | 45.49 | 0.17 | 1.03 | 2.154784 | 0.30 | 0.14 | 14880 |
| 11 | 300-250 | 352 | 89.86 | 90.28 | 0.42 | 0.57 | 1.123992 | 0.16 | 0.08 | 13740 |
| 12 | 250-212 | 296 | 132.84 | 133.58 | 0.74 | 0.17 | 0.558035 | 0.08 | 0.02 | 6954 |
| 13 | 212-180 | 248.9 | 176.99 | 178.15 | 1.16 | 0.10 | 0.387712 | 0.05 | 0.01 | 6608 |
| 14 | 180-150 | 209.3 | 218.45 | 220.02 | 1.57 | 0.11 | 0.291483 | 0.04 | 0.02 | 12727 |
| 15 | 150-125 | 176 | 261.68 | 263.5 | 1.82 | 0.11 | 0.181274 | 0.03 | 0.02 | 21722 |
| 16 | 125-106 | 148 | 318.12 | 320.03 | 1.91 | 0.05 | 0.069434 | 0.01 | 0.01 | 17428 |
| 17 | 106-90 | 124.5 | 359.13 | 361.12 | 1.99 | 0.02 | 0.016077 | 0.00 | 0.00 | 8821 |
| 18 | 90-75 | 104.7 | 399.48 | 401.52 | 2.04 | 0.00 | 0 | 0.00 | 0.00 | 0 |
| 19 | end-2 | 88 | 437.91 | 439.98 | 2.07 | 0.00 | 0 | 0.00 | 0.00 | 0 |

| Set-112 | Aperture | Lavg | m-empt | m-fill | cum-mass | mass | cum | %-cum | %-m | number |
|---|---|---|---|---|---|---|---|---|---|---|
| 1 | 1400+ | 1550 | 56.9 | 56.9 | 0 | 0 | 9.748533 | 1.00 | 0.00 | 0 |
| 2 | 1400-1180 | 1350 | 124.14 | 124.16 | 0.02 | 0.02 | 9.748533 | 1.00 | 0.00 | 9 |
| 3 | 1180-1000 | 1200 | 178.45 | 178.56 | 0.11 | 0.09 | 9.728533 | 1.00 | 0.01 | 55 |
| 4 | 1000-850 | 1025 | 242.62 | 243.05 | 0.43 | 0.32 | 9.638533 | 0.99 | 0.03 | 315 |
| 5 | 850-710 | 830 | 294.46 | 296.79 | 2.33 | 1.9 | 9.318533 | 0.96 | 0.19 | 3518 |
| 6 | 710-600 | 700 | 345.91 | 351.58 | 5.67 | 3.34 | 7.418533 | 0.76 | 0.34 | 10311 |
| 7 | 600-500 | 600 | 393.81 | 402.02 | 8.21 | 2.54 | 4.078533 | 0.42 | 0.26 | 12451 |
| 8 | 500-425 | 495 | 441.74 | 450.74 | 9 | 0.79 | 1.538533 | 0.16 | 0.08 | 6897 |
| 9 | 425-355 | 420 | 488.11 | 497.41 | 9.3 | 0.46 | 0.748533 | 0.08 | 0.05 | 6574 |
| 10 | 355-300 | 418.6 | 89.86 | 90.28 | 0.42 | 0.07 | 0.288533 | 0.03 | 0.01 | 1770 |
| 11 | 300-250 | 352 | 132.84 | 133.58 | 0.74 | 0.04 | 0.215636 | 0.02 | 0.00 | 1765 |
| 12 | 250-212 | 296 | 176.99 | 178.15 | 1.16 | 0.03 | 0.172396 | 0.02 | 0.00 | 2056 |
| 13 | 212-180 | 248.9 | 218.45 | 220.02 | 1.57 | 0.03 | 0.142457 | 0.01 | 0.00 | 3262 |
| 14 | 180-150 | 209.3 | 261.68 | 263.5 | 1.82 | 0.03 | 0.11421 | 0.01 | 0.00 | 5979 |
| 15 | 150-125 | 176 | 318.12 | 320.03 | 1.91 | 0.03 | 0.083425 | 0.01 | 0.00 | 9656 |
| 16 | 125-106 | 148 | 359.13 | 361.12 | 1.99 | 0.02 | 0.053862 | 0.01 | 0.00 | 13152 |
| 17 | 106-90 | 124.5 | 399.48 | 401.52 | 2.04 | 0.02 | 0.029892 | 0.00 | 0.00 | 16173 |
| 18 | 90-75 | 104.7 | 437.91 | 439.98 | 2.07 | 0.01 | 0.012361 | 0.00 | 0.00 | 19206 |
| 19 | end-2 | 88 | 56.9 | 56.9 | 0 | 0 | 9.748533 | 1.00 | 0.00 | 0 |

## *Sample of particle size analyser result and number of particles calculation*

Set-112

| L-avg | Vol | Number | %-no | no |
|---|---|---|---|---|
| 704 | 0.54 | 1635.011 | 3.6718E-05 | 0.705205 |
| 592 | 2.71 | 13799.05 | 0.00030989 | 5.951739 |
| 497.8 | 10.83 | 92748.9 | 0.00208289 | 40.004 |
| 418.6 | 19.95 | 287336.1 | 0.0064528 | 123.9324 |
| 352 | 15.51 | 375689.3 | 0.00843697 | 162.0405 |
| 296 | 9.2 | 374763.8 | 0.00841619 | 161.6413 |
| 248.9 | 6.37 | 436425.1 | 0.00980094 | 188.2368 |
| 209.3 | 6.01 | 692487.2 | 0.0155514 | 298.6802 |
| 176 | 6.55 | 1269253 | 0.02850402 | 547.4481 |
| 148 | 6.29 | 2049795 | 0.04603289 | 884.1077 |
| 124.5 | 5.1 | 2791946 | 0.06269962 | 1204.209 |
| 104.7 | 3.73 | 3433316 | 0.07710305 | 1480.841 |
| 88 | 2.63 | 4077113 | 0.09156099 | 1758.52 |
| 74 | 1.81 | 4718765 | 0.10597079 | 2035.275 |
| 62.23 | 1.19 | 5216660 | 0.11715217 | 2250.025 |
| 52.33 | 0.75 | 5529095 | 0.12416861 | 2384.782 |
| 44 | 0.49 | 6076913 | 0.13647114 | 2621.065 |
| 37 | 0.34 | 7091183 | 0.15924893 | 3058.535 |
| 31.11 | 0 | 0 | 0 | 0 |
| 26.16 | 0 | 0 | 0 | 0 |
| 22 | 0 | 0 | 0 | 0 |
| 18.5 | 0 | 0 | 0 | 0 |
| 15.56 | 0 | 0 | 0 | 0 |
| 13.08 | 0 | 0 | 0 | 0 |
| 11 | 0 | 0 | 0 | 0 |
| TOTAL |  | 44528924 |  |  |

## Sample of combined results from sieving and particle size analyser (as number of particles)

| | Number of particles | | | |
|---|---|---|---|---|
| L-avg | Set112 | Set103 | Set105 | Set110 |
| 1550 | 0 | 2.84338579 | 0 | 0 |
| 1350 | 8.60715399 | 4.303577 | 0 | 0 |
| 1200 | 55.1479857 | 110.295971 | 6.12755396 | 12.255108 |
| 1025 | 314.636618 | 845.58591 | 186.815492 | 68.82676 |
| 830 | 3518.44046 | 5240.62448 | 3666.58533 | 629.61566 |
| 700 | 10311.2884 | 11576.2536 | 12735.25 | 4599.6314 |
| 600 | 12457.1414 | 12892.3735 | 12076.7478 | 15076.408 |
| 495 | 6936.72056 | 5412.61299 | 7684.02847 | 10713.503 |
| 420 | 6698.1011 | 2429.58408 | 7655.03466 | 10965.944 |
| 352 | 1931.79303 | 1213.87201 | 6380.65443 | 15580.014 |
| 296 | 1927.03446 | 2041.38892 | 6620.05347 | 11354.728 |
| 248.9 | 2244.09651 | 2060.04851 | 6122.41573 | 12104.96 |
| 209.3 | 3560.76714 | 3464.53101 | 9875.97652 | 18794.528 |
| 176 | 6526.49611 | 9710.97607 | 23393.5408 | 42901.243 |
| 148 | 10540.0407 | 16331.1114 | 35728.1877 | 100484.32 |
| 124.5 | 14356.1805 | 16460.5402 | 42676.5995 | 180786.02 |
| 104.7 | 17654.0996 | 36902.0786 | 50212.5854 | 235570.81 |
| 88 | 1758.52045 | 46107.5127 | 70894.4764 | 255256.42 |
| 74 | 2035.27504 | 50656.8831 | 27553.7783 | 150860.91 |
| 62.23 | 2250.02452 | 53506.1496 | 32332.0952 | 151422.65 |
| 52.33 | 2384.78236 | 55333.1542 | 36435.3269 | 145699.92 |
| 42.5 | 2621.06471 | 60026.7618 | 41491.2162 | 143530.39 |
| 37 | 3058.53487 | 70224.7043 | 26959.0924 | 152253.47 |
| 31.11 | 0 | 88604.6107 | 0 | 99955.909 |
| 26.16 | 0 | 62091.4632 | 0 | 0 |
| 22 | 0 | 0 | 0 | 0 |
| 18.5 | 0 | 0 | 0 | 0 |
| 15.56 | 0 | 0 | 0 | 0 |
| 13.08 | 0 | 0 | 0 | 0 |
| 11 | 0 | 0 | 0 | 0 |

## *Selected photos of experimental setup and crystals product*

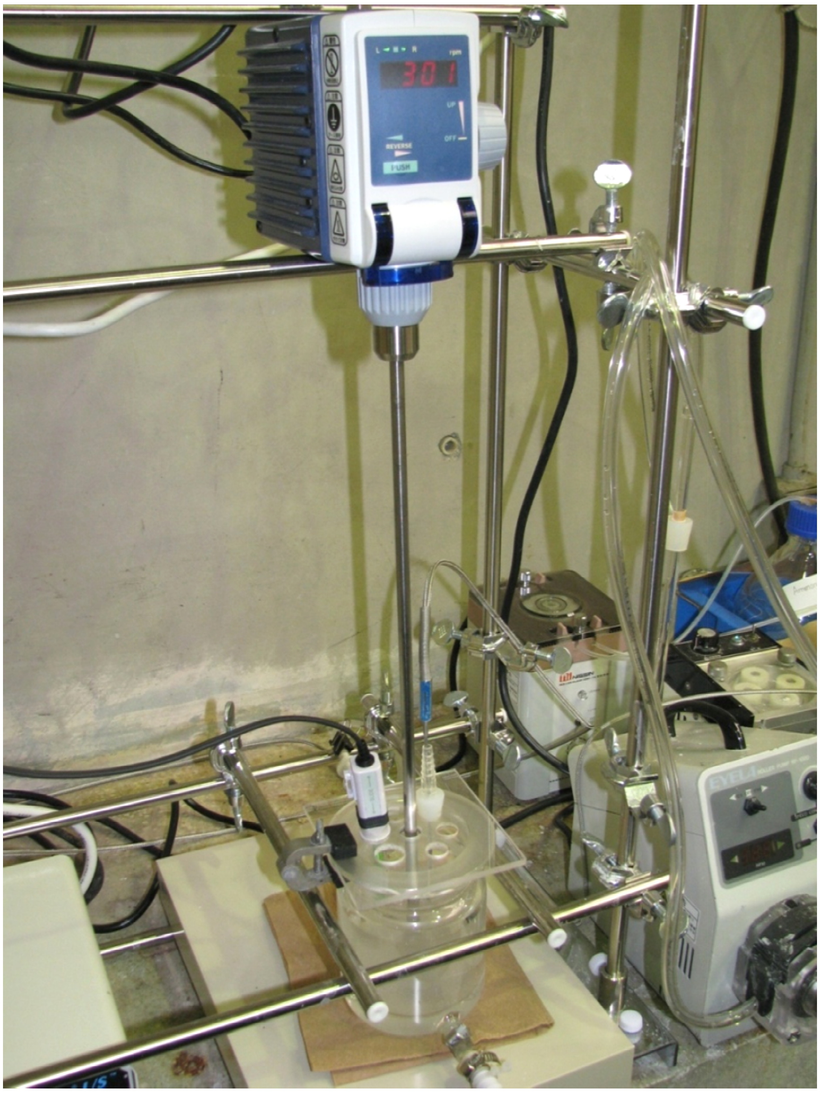

**Figure A-3. Batch cooling crystallizer arrangement**

Figure A-4. Data logger

Figure A-5. Sieving trays

Figure A-6. Crystals product

Figure A-7. Microscope

## *References*

Campbell, G. R., Y. K. Leong, C. C. Berndt and J. L. Liow (2006). Ammonium phosphate slurry rheology and particle properties--the influence of fe(iii) and al(iii) impurities, solid concentration and degree of neutralization. *Chemical Engineering Science*, 61(17), 5856-5866.

Torgesen, J. L. and A. T. Horton (1963). Electrolytic conductance of ammonium dihydrogen phosphate solutions in the saturation region. *The Journal of Physical Chemistry*, 67(2), 376-381.

Xu, D. and D. Xue (2006). Chemical bond analysis of the crystal growth of kdp and adp. *Journal of Crystal Growth*, 286(1), 108-113.

# B. Matlab codes

## 1. Main codes for simulation in Chapter 4

```
% pbe01_adaptive_main.m

%... Adaptive grid solution to PBE equation - Case I(using ode15s)

     close all
     clear all
     clc
%...
%... start a stopwatch timer
     tic
%...
%... set global variables
     global G;
     global z0 zL z nz D1;
%...
%... spatial grid
     z0=0.0;
     zL=1.0;
     J=8;
     nz=2^J+1;
     dz=(zL-z0)/(nz-1);
     z=[z0:dz:zL]';
%...
%... model parameter
     G=1;
%...
%... initial conditions
     for i=1:nz,
       x(i,1) = pbe_exact02(z(i),0);
       %x(i) = 0;
     end;
%...
% %... parameters of the adaptive grid
%      npdes=1;
%      nzmax=nz;
%      alpha=1;
%      beta=100;
%      tolz=0.05;
%      bound=1.1;
%      imesh=0;
%      ilim=0;
%...
% %... refine the initial grid
% %...
%
[z_new,nz_new,ier,tolz_new]=agereg(z,x,npdes,nzmax,alpha,beta,tolz,bound,ime
sh,ilim);
%...
%... interpolate the dependent variables
%...
%      x_new=spline(z,x,z_new);
%      x=x_new';
%      z=z_new';
%      nz=nz_new;
%      tolz=tolz_new;
%...
%... differentiation matrix (convective term)
     %v=x;
     %D1=five_point_biased_upwind_D1(z,v);
```

```
     D1=five_point_biased_upwind_uni_D1(z0,zL,nz,1);
     %[D0,D1,D2]=Basis1(J,6,2);
%...
%... call to ODE solver
%...
     t0=0;
     tf=0.6;
     Dt=0.2;
     tspan=[t0 t0+Dt];
     nout=(tf-t0)/Dt+1;
     tout=t0;
     yout=x;
     zout=z;
     nzout=nz;
%...
%... initial situation
% %...
%      figure(1)
%      subplot(2,1,1)
%      plot(z,x,'k');
%      ylabel('n(L,t)');
%      axis([0 1 0 1]);
%      title('PSD Case I, t = 0-1.0s, Adaptive FD, N=138')
%      hold on
%      subplot(2,1,2)
%      plot(z,t0*ones(nz,1),'.k')
%      xlabel('L, Dimensionless Size')
%      ylabel('t, time (s)');
%      axis([0 1 0 1]);
     hold on
%      figure(2)
%      plot(t0,nz,'*k')
%      xlabel('t');
%      ylabel('nz');
%      title('Number of grid points')
%      hold on
%...
     options = odeset('RelTol',1e-3,'AbsTol',1e-6);
%...
     for iout=2:nout
%...
       [t,y] = ode15s('pbe_pde02',tspan,x);
%...
       tk=t(length(t));
       tspan=[tk tk+Dt];
       x=y(length(t),:);
%...
% %... refine the grid
% %...
%
[z_new,nz_new,ier,tolz_new]=agereg(z,x,npdes,nzmax,alpha,beta,tolz,bound,ime
sh,ilim);
%        pause(0.1)
%...
% %... interpolate the dependent variables
% %...
%           x_new=spline(z,x,z_new);
%           x=x_new';
%           yout=[yout ; x];
% %...
%           z=z_new';
%           nz=nz_new;
%           tolz=tolz_new;
%           zout=[zout ; z];
%           nzout=[nzout ; nz];
%           tout=[tout ; tk];
%...
          figure(1)
```

```
%           subplot(2,1,1)
          plot(z,x,'k');
%...
         for i=1:nz
             yexact(i) = pbe_exact02(z(i),tk);
         end
         plot(z,yexact(1:length(z)),':k')
%...
%           subplot(2,1,2)
%           plot(z,tk*ones(nz_new,1),'.k')
%           figure(2)
%           plot(z,x-yexact(1:length(z))','k');
%...
%... compute new differentiation matrices
%...
%      D1=five_point_biased_upwind_D1(z,v);
%     D2=five_point_centered_D2(z);
%...
     end
%...
%... read the stopwatch timer
     tcpu=toc;
```

```
% pbe02_modif_main.m
%... Adaptive grid solution to PBE equation - Case II(using ode15s)
%... initial condition was modified
     close all
     clear all
%...
%... start a stopwatch timer
     tic
%...
%... set global variables
     global G;
     global z0 zL z D1;
%...
%... spatial grid
     z0=0.0;
     zL=1.0;
     J=8;
     nz=2^J+1;
     dz=(zL-z0)/(nz-1);
     z=[z0:dz:zL]';
%...
%... model parameter
     G=1;
%...
%... initial conditions
     for i=1:nz,
       x(i,1) = pbe_exact01(z(i),0);
     end;
%...
%... parameters of the adaptive grid
     npdes=1;
     nzmax=1001;
     alpha=1;
     beta=100;
     tolz=0.05;
     bound=1.1;
     imesh=0;
     ilim=0;
%...
%... refine the initial grid
%...

[z_new,nz_new,ier,tolz_new]=agereg(z,x,npdes,nzmax,alpha,beta,tolz,bound,ime
sh,ilim);
%...
```

```
%... interpolate the dependent variables
%...
     x_new=spline(z,x,z_new);
     x=x_new';
     z=z_new';
     nz=nz_new;
     tolz=tolz_new;
%...
%% differentiation matrix (convective term)
      v=x;
      D1=five_point_biased_upwind_D1(z,v);
%     [D0, D1, D2]=Basis2(J,z);
%...
%... call to ODE solver
%...
     t0=0;
     tf=1;
     Dt=0.2;
     tspan=[t0 t0+Dt];
     nout=(tf-t0)/Dt+1;
     tout=t0;
     yout=x;
     zout=z;
     nzout=nz;
%...
%... initial situation
%...
     figure(1)
     subplot(2,1,1)
     plot(z,x,'k');
     ylabel('n(L,t)');
     axis([0 1 0 1.4]);

     hold on
     subplot(2,1,2)
     plot(z,t0*ones(nz,1),'.k')
     xlabel('L, Dimensionless size');
     ylabel('t');
     axis([0 1 0 1]);
     hold on
%      figure(2)
%      plot(t0,nz,'*k')
%      xlabel('t');
%      ylabel('nz');
%      title('Number of grid points')
%      hold on
%...
     options = odeset('RelTol',1e-3,'AbsTol',1e-3);
%%%%%%%%%%%%%%%%%%%%%%%%%%%%%%%%%%%%%%%%%%%%%%%%%%%%%%%%%%%%...
%%%%%%%%%%%%%%%%%%%%%%%%%%%%%%%%%%%%%%%%%%%%%%%%%%%%%%%%%%%%...
     for iout=2:nout
%...
%
       [t,y] = ode15s('pbe_pde01',tspan,x);
%...
       tk=t(length(t));
       tspan=[tk tk+Dt];
       x=y(length(t),:);
%...
%... refine the grid
%...

[z_new,nz_new,ier,tolz_new]=agereg(z,x,npdes,nzmax,alpha,beta,tolz,bound,ime
sh,ilim);
   pause(0.1)
%...
%... interpolate the dependent variables
%...
```

```
          x_new=spline(z,x,z_new);
          x=x_new';
          yout=[yout ; x];
%...
          z=z_new';
          nz=nz_new;
          tolz=tolz_new;
          zout=[zout ; z];
          nzout=[nzout ; nz];
          tout=[tout ; tk];
%...
          figure(1)
          subplot(2,1,1)
          plot(z,x,'k');
%...
%          z0=0.0;
%          zL=1.0;
%          J=J;
%          nza=2^J+1;
%          dz=(zL-z0)/(nza-1);
%          za=[z0:dz:zL]';
%          for i=1:nz
%              yexact(i) = pbe_exact01(z(i),tk);
%          end
%          plot(z,yexact(1:length(z)),':k')
%...
          subplot(2,1,2)
          plot(z,tk*ones(nz_new,1),'.k')
          %figure(2)
          %plot(tk,nz_new,'*k');
%...
%... compute new differentiation matrices
%%
     D1=five_point_biased_upwind_D1(z,v);
%     [D0, D1, D2]=Basis2(J,z);
%     D2=five_point_centered_D2(z);
%%
%...
     str1=num2str(J);
     str2=num2str(nz);
     subplot(2,1,1)
%     title(['Case II - PSD at t = 0-1.0s, WFD(J=' ,str1,')' '; N = '
,str2]);
     title(['Case III - PSD at t = 0-1.0s, WFD (N=' ,str2,')']);
     end
%...
%... read the stopwatch timer
     tcpu=toc;

 nt=length(yout);
 nt0=length(x_new);
 z=zout((nt-nt0+1):(nt));
 y=yout((nt-nt0+1):(nt));
 for i=1:length(y)
     yexact(i) = pbe_exact01(z(i),1);
 end
 ydata=yexact;
 y06=y';
 y06(1)=0;

% %%%%%% error calculation %%%%%%%
 err = (y06-ydata);
 ydev=err.^2;
 sse=sum(ydev);
 avg_error=sqrt(sse/nz)
 max_error=sqrt(max(ydev))
 %figure(2); plot(z,err); xlabel('L, Dimensionless Size'); ylabel('(model-
analytic)')
```

```
 %% save data
%  ywfd=y06;
%  save case2_modif z ywfd
```

```
%pbe05_adaptive_main.m
%... Adaptive grid solution to PBE equation - Case III(using ode15s)
%... initial condition was modified
     %close all
     clear all
%...
%... start a stopwatch timer
     tic
%...
%... set global variables
     global G B Gt;
     global z0 zL nz D1;
%...
%... spatial grid
     z0=0.0;
     zL=1.0;
     J=9;
     nz=2^J+1;
     dz=(zL-z0)/(nz-1);
     z=[z0:dz:zL]';
%...
%... initial conditions
     for i=1:nz,
       x(i,1) = seed03(z(i),0);
     end;
%...
%... parameters of the adaptive grid
     npdes=1;
     nzmax=nz;
     alpha=1;
     beta=100;
     tolz=0.05;
     bound=1.1;
     imesh=0;
     ilim=0;
%... model parameter
     %B = -2.14e12.*z.^3 + 5.09e9.*z.^2   - 3.07e6.*z  + 640;
     %G = 1.08e-10.*z.^3 - 2.29e-10.*z.^2 - 3.2e-11.*z + 1.6975e-10;
     G=2*1.04414e-10;
     %Gt = 5.22e-22.*t.^3 -4.54e-18.*t.^2 - 1.34e-14.*t + 1.69e-10;
%... refine the initial grid
%...

[z_new,nz_new,ier,tolz_new]=agereg(z,x,npdes,nzmax,alpha,beta,tolz,bound,ime
sh,ilim);
%...
%... interpolate the dependent variables
%...
     x_new=spline(z,x,z_new);
     x=x_new';
     z=z_new';
     nz=nz_new;
     tolz=tolz_new;
%...
%% differentiation matrix (convective term)
      v=x;
      D1=five_point_biased_upwind_D1(z,v);
%      [D0, D1, D2]=Basis2(J,z);
%...
%... call to ODE solver
%...
     t0=0;
```

```
     tf=3000;
     Dt=300;
     tspan=[t0 t0+Dt];
     nout=(tf-t0)/Dt+1;
     tout=t0;
     yout=x;
     zout=z;
     nzout=nz;
%...
%... initial situation
%...
     figure(2)
     subplot(2,1,1)
     plot(z,x,'k');
     ylabel('n(L,t)');
     %axis([0 1 0 1.4]);

     hold on
     subplot(2,1,2)
     plot(z,t0*ones(nz,1),'.k')
     xlabel('L, Dimensionless size');
     ylabel('t');
     axis([0 1 0 3000]);
     hold on
%      figure(2)
%      plot(t0,nz,'*k')
%      xlabel('t');
%      ylabel('nz');
%      title('Number of grid points')
%      hold on
%...
     options = odeset('RelTol',1e-3,'AbsTol',1e-3);
%%%%%%%%%%%%%%%%%%%%%%%%%%%%%%%%%%%%%%%%%%%%%%%%%%%%%%%%%%%%...
%%%%%%%%%%%%%%%%%%%%%%%%%%%%%%%%%%%%%%%%%%%%%%%%%%%%%%%%%%%%...
     for iout=2:nout
%...
%
       [t,y] = ode15s('pbe_pde05',tspan,x);
%...
       tk=t(length(t));
       tspan=[tk tk+Dt];
       x=y(length(t),:);
%...
%... refine the grid
%...

[z_new,nz_new,ier,tolz_new]=agereg(z,x,npdes,nzmax,alpha,beta,tolz,bound,ime
sh,ilim);
   pause(0.1)
%...
%... interpolate the dependent variables
%...
          x_new=spline(z,x,z_new);
          x=x_new';
          yout=[yout ; x];
%...
          z=z_new';
          nz=nz_new;
          tolz=tolz_new;
          zout=[zout ; z];
          nzout=[nzout ; nz];
          tout=[tout ; tk];
%...
          figure(2)
          subplot(2,1,1)
          plot(z,x,'k');
%...
          subplot(2,1,2)
```

```
          plot(z,tk*ones(nz_new,1),'.k')
          %figure(2)
          %plot(tk,nz_new,'*k');
%...
%... compute new differentiation matrices
%% matrix recomputation
     D1=five_point_biased_upwind_D1(z,v);

%%
%...
     str1=num2str(J);
     str2=num2str(nz);
     subplot(2,1,1)
     title(['Case III - PSD at t = 0-3000s, WFD (N=' ,str2,')']);
     end
%...
%... read the stopwatch timer
     tcpu=toc;

 y06=y';
 y06(1)=0;
```

## 2. *Main codes for calculation of differentiation matrices*

```
% Constructing the basis functions using wavelet-collocation method
% the special axial is normalised into [0,1]
function [D0,D1,D2]=Basis1(n1,L,M)

 %n1: level of wavelet (can be from 3-10 or more)
 %L: support length of scaling function (default = 6)
 %choosing 2*M points at each boundary

hn1=1/2^n1;
hn2=hn1/2;
x1=0:hn1:1;
dim=length(x1);
a=zeros(L-1,2*M);b=zeros(L-1,2*M);
D0=zeros(dim,dim); D1=zeros(dim,dim); D2=zeros(dim,dim);

%constructing polynomials P1, P2 of degree 2*M-1 at each boundary
for k = 1:L-1
    xs = x1(k)+hn2; %start
    xe = x1(dim-L+k)+hn2; %end
    for j=1:2*M
        aa=1; bb=1;
        for i=1:2*M
            if i~=j
                aa=aa*(xs-x1(i))/(x1(j)-x1(i)); %interpolation at left end
                bb=bb*(xe-x1(dim-L+i))/(x1(dim-L+j)-x1(dim-L+i));
            end
        end
        a(k,j)=aa;  %dimension a(5,6), b(5,6)
        b(k,j)=bb;
    end
end

%Calculating basis function D0,D1(first derivative) and D2(second
%derivative) with dimension dim*dim

for m=1:dim
    for n=1:dim
        D0(m,n)=theta0(m-n,L);
        D1(m,n)=theta1(m-n,L);
        D2(m,n)=theta2(m-n,L);
        if (n>=1 & n<=2*M)
```

```
            for k=1:L-1
            D0(m,n)=D0(m,n)+a(k,n)*theta0(m-k+5,L);
            D1(m,n)=D1(m,n)+a(k,n)*theta1(m-k+5,L);
            D2(m,n)=D2(m,n)+a(k,n)*theta2(m-k+5,L);
            end
        elseif (n>=dim-2*M+1 & n<=dim)
            for k=1:L-1
            D0(m,n)=D0(m,n)+b(k,n+2*M-dim)*theta0(m-k-dim,L);
            D1(m,n)=D1(m,n)+b(k,n+2*M-dim)*theta1(m-k-dim,L);
            D2(m,n)=D2(m,n)+b(k,n+2*M-dim)*theta2(m-k-dim,L);
            end
        end
    end
end
D1=2^n1*D1;
D2=2^(2*n1)*D2;
```

```
function th0 = theta0(k,D)
%Define the function for computing theta

if nargin < 2
    D  = 6;
end

if abs(k) <= 0
    th0 = 1;
else
    th0 = 0;
end
```

```
function th1 = theta1(k,D)
%Define the function for computing the first derivate of theta

if nargin < 2
    D  = 6;
end

t1=[0 0.0003 0.0146 -0.1452 0.7452 0 -0.7452 0.1452 -0.0146 -0.0003 0];

if abs(k) <= D-1
    th1 = t1(k+D);
else
    th1 = 0;
end
```

```
function th2 = theta2(k,D)
%Define the function for computing the second derivate of theta

if nargin < 2
    D  = 6;
end

t2=[0 0.0054 0.1143 -0.8762 3.3905 -5.2679 3.3905 -0.8762 0.1143 0.0054 0];

if abs(k) <= D-1
    th2 = t2(k+D);
else
    th2 = 0;
end
```

```
function [D]=five_point_biased_upwind_D1(z,v)
      m=1;
      ns=5;
%...
%...  sparse discretization matrix
      n = length(z);
      D = sparse(n,n);

%...
%...     (1)  finite difference approximation for positive v
```

```
              if v > 0
%...
%...             boundary points
                 zs=z(1:ns);
                 for i=1:3,
                   zd=z(i);
                   [w]=weights(zd,zs,ns,m);
                   D(i,1:ns)=w(1:ns,m+1)';
                 end;
%...
%...             interior points
                 for i=4:n-1,
                 zs=z(i-3:i+1);
                 zd=z(i);
                 [w]=weights(zd,zs,ns,m);
                 D(i,i-3:i+1)=w(1:ns,m+1)';
                 end;
%...
%...             boundary point
                 zs=z(n-ns+1:n);
                 zd=z(n);
                 [w]=weights(zd,zs,ns,m);
                 D(n,n-ns+1:n)=w(1:ns,m+1)';
              end;
%...
%...     (2)  finite difference approximation for negative v
              if v < 0
%...
%...             boundary point
                 zs=z(1:ns);
                 zd=z(1);
                 [w]=weights(zd,zs,ns,m);
                 D(1,1:ns)=w(1:ns,m+1)';
%...
%...             interior points
                 for i=2:n-3,
                   zs=z(i-1:i+3);
                   zd=z(i);
                   [w]=weights(zd,zs,ns,m);
                   D(i,i-1:i+3)=w(1:ns,m+1)';
                 end;
%...
%...            boundary points
                zs=z(n-ns+1:n);
                for i=3:-1:1,
                  zd=z(n-i+1);
                  [w]=weights(zd,zs,ns,m);
                  D(n-i+1,n-4:n)=w(1:ns,m+1)';
                end;
              end;
```

## *3. Main scripts for simulation in Chapter 3*

```
% run_batchMAP01.m
clear all;
global cs dc0 Ls0 dens S fv F g kg b j kb i KR WS0
tspan=0:10:6000;
cs=0.1243;      % kg solute/kg solvent
dc0=0.0150;     % kg solute/kg solvent
Ls0=550e-6;     % m
dens=2660;      % kg/m3
S=25.46*1;        % kg H20
fv=0.525;       % vol shape factor
```

```
F=7.0;          % surface to vol shape factors
g=1.5;          % growth order
kg=5.0e-5;      % growth constant, m/[s (kg/kg)^g]
b=3.0;          % nucleation order
j=1.0;          % exponent magma density
kb=1e11*1;        % nucleation constant, no/[kg s (kg/kg)^b (kg/kg)^j]
i=b/g;          % relative order
KR=4e19;        % relative nucleation rate constant
WS0=3.92e-4*S*1;          % kg seed crystals
%
N0=WS0/(fv*dens*Ls0^3); % number of seeds
MT0=WS0/S;              % mass of seed crystals per kg solvent
VT0=MT0/(dens*fv);      % total vol of seeds per kg solvent
AT0=F*WS0/(dens*Ls0*S); % total surface area of crystals per kg solvent
%
% Initial Condition at t = 0
y0=[N0 Ls0 AT0 VT0 dc0];
%
% Intergration
tic
[t,y]=ode15s(@batchMAP01,tspan,y0);
%
% Post-processing data
delc=y(:,5);            % supersaturation (same as dc)
W=WS0+(dc0-delc)*S;     % mass of solid deposited
AT=AT0.*(W./WS0).^(2/3);% average surface area of crystals
MT=MT0.*(W/WS0);         % suspension density
L=Ls0.*(W./WS0).^(1/3); % average size of crystals
nn=y(:,1)./(L*S);       % no/ m.kg of solvent
mc=y(:,4).*fv*dens;     % Total Mass of Crystals per kg solvent
G=kg.*delc.^b;
Bb=kb*MT.*delc.^b;
Br=KR*MT.*G.^2;
A=Br./(G.*MT);
%plot(L,G);
toc
%
% [A,H1,H2]=plotyy(t,delc,t,G);
% xlabel('time [s]')
% set(H2,'LineStyle','--')
% set(get(A(1),'Ylabel'),'String','\Deltac [kg/kg solvent]')
% set(get(A(2),'Ylabel'),'String','G [m/s]')
% title('Case III - Supersaturation and Growth profiles')

% [A,H1,H2]=plotyy(t,nn,t,Bb);
% xlabel('time [s]')
% set(H2,'LineStyle','--')
% set(get(A(1),'Ylabel'),'String','Total crystal [no/m kg solvent]')
% set(get(A(2),'Ylabel'),'String','B [no/kg solvent s]')
% title('Case III - Total crystal and Nucletion rate')

%Plotting
subplot(2,2,1); plot(t,nn);title('Total Number'); ylabel('no/m.kg solvent')
hold on
subplot(2,2,2); plot(t,L);title('Average size'); ylabel('m')
hold on
subplot(2,2,3); plot(t,mc);title('Suspension density'); xlabel('time [s]');
ylabel('kg crystal/kg solvent')
hold on
subplot(2,2,4); plot(t,delc);title('Supersaturation'); xlabel('time [s]');
ylabel('kg/kg solvent')
hold on

% subplot(2,2,1); plot(t,nn,'b:'); hold on
% subplot(2,2,2); plot(t,L,'b:'); hold on
% subplot(2,2,3); plot(t,mc,'b:'); hold on
% subplot(2,2,4); plot(t,delc,'b:'); hold on
%
```

```
% subplot(2,2,1); plot(t,nn,'b--'); hold on
% subplot(2,2,2); plot(t,L,'b--'); hold on
% subplot(2,2,3); plot(t,mc,'b--'); hold on
% subplot(2,2,4); plot(t,delc,'b--'); hold on
```

```
% @main_tavare_batch
clear; clc
delt=1;         % seconds
tfinal=10000;
tspan=0:delt:tfinal;

S=200;          % kg
Ca0=1*1e-3;       %kmol/kg
Cb0=Ca0;       %kmol/kg
Cc0=0;
m00=0;
m10=m00;
m20=m00;
m30=m00;
L0=0;
y0=[m00 m10 m20 m30 Ca0*S Cb0*S Cc0*S L0];

% Integration
% options = odeset('RelTol',1e-06,'AbsTol',1e-3,'MaxStep',1e-3);
tic
[t,y]=ode15s(@tavare_batch,tspan,y0)
toc

CA=y(:,5);              % Conc. of A in kmol
CC=y(:,7);              % Conc. of C in kmol

kv=0.52;                % shape factor
Rho_c=2000;             % Crystal density (kg/m3)

mc=y(2:end,4).*kv*Rho_c; %Total Mass of Crystals
NT=y(2:end,1);           % Total Number of Particles
%Lc=y(2:end,end);
%plot(t(2:end),Lc,'r');title('Average Length of Crystals'); ylabel('m');
xlabel('seconds')
subplot(2,2,1)
plot(t,CA,'r'); title('Mole of A');ylabel('kmol');
subplot(2,2,2)
plot(t,CC,'r'); title('Mole of C');ylabel('kmol');
subplot(2,2,3)
plot(t(2:end),NT,'r'); title('Total Number of
Crystal');ylabel('no.');xlabel('seconds')
subplot(2,2,4)
plot(t(2:end),mc,'r'); title('Total Mass of
Crystal');ylabel('kg');xlabel('seconds')
nA=real(y(end,5));
nC=real(y(end,7));
Numb=real(y(end,1));
Mass=real(mc(end));
LC=real(y(end,8));
yf=[nA nC Mass]
LC
Numb
```

```
function dzdt=tavare_batch(t,z)
% batch crystalliser
%% Variable
m0=z(1);      % no./kg
m1=z(2);       % m/kg
m2=z(3);       % m2/kg
m3=z(4);       % m3/kg
Ca=z(5);       % kmol/kg
Cb=z(6);       % kmol/kg
Cc=z(7);       % kmol/kg
```

```
L=z(8);             % m

%% Data
sat_time=1000;
Mc=100;                 % molecular weight (kg/kmol)
Ccs=1e-4;               % kmol/kg
S=200;                 % kg
Rho_c=2000;             % kg/m3
Beta=1.0;
LamdaD=2e-7;            % m
ka=3.68;
kv=0.52;
%tau=1e4;               % seconds
k=1e-1;                % kg/kmol.s
g=1.5;
kg=1*7.9e-8;             % m/s(mol/kg)^-g
b=4.5;
kb=1*3.1e10;             % no/s.kg (mol/kg)^-b [kb=3.1e10]
% d=1.5;
% kd=7.9e-8;             % m/s(mol/kg)^d
% r=3;
% kR=6.4e31;             % no/s.kg.(m/s)^1
% Rho=1000;           % kg/m3
%% Operating condition
Ca0=1*1e-3;       % kmol/kg
Cb0=Ca0;

%% Model equations
% kinetics
rc=k*Ca*Cb;             % kg kmol/s

% Nucleation and Growth
Bn=kb*S*(Cc/S*1000-Ccs*1000)^b;       % no./s
G=kg*(Cc/S*1000-Ccs*1000)^g;        % m/s
% alpha
alpha = (kv*Rho_c/Mc)*(3*m2*G);     % kmol/s

% mass
%mass=V*Rho;
if Cc<=Ccs*S;
    dzdt(1)=0;
else
    dzdt(1)=Bn;
end
dzdt(2)=m0*G;
dzdt(3)=2*m1*G;
dzdt(4)=3*m2*G;

%Component mass balance
dzdt(5)=- rc/S;
dzdt(6)=- rc/S;
dzdt(7)=rc/S - alpha;
dzdt(8)=G;

% Transpose
dzdt=dzdt'
```

## 4. *Main codes for kinetics calculations in Chapter 7*

```
% run_kinetic2.m
clear; clc
k0=[0.0008 40 1];
constants=fminsearch('kinetic2',k0)
load set103 % changeable
y0=delC(1);
[t,y]=ode23(@sb_rx,time,y0,[],constants)
SSE=(sum(y-delC).^2);
```

```
function dDelCdt=sb_rx(t,y,k)
w0=2/1000; % seed amount (kg)
S0=305.13; % initial solution (g)
F=7;
rhoC=1803;
L0avg=430/1e6; % seed size (m)
delC0=0.019085; % initial delta C (in kg/kg solution)
if t<=660
    S=(S0+(0.032707*t))/1000;
else
    S=326.7166/1000;
end

Mt0=w0/S;
At0=F*w0/(rhoC*L0avg*S);
w=w0+((delC0-y)*S);
Mt=Mt0*(w/w0);
At=At0*(w/w0)^(2/3);
r=1;
b=2.6;
g=1.8;
reaction = k(1)*(delC0-y)^(r);
if t<=660
    dDelCdt=(reaction*0.115)-((k(2)*Mt*y^(b)) + (k(3)*At*y^(g)));
else
    dDelCdt=-((k(2)*Mt*y^(b)) + (k(3)*At*y^(g)));
end
```

```
function min=kinetic1(k)
load set103 % changeable
y0=delC(1);
[t,y]=ode23(@sb_rx,time,y0,[],k)
plot(t,y,time,delC,'ro')
xlabel('time [seconds]')
ylabel('desupersaturation [kg/kg solution]')
grid off
pause(.05)
min=(sum(y-delC).^2);
```

# C. Research Proposal - June 2008

# *A Further Investigation on Mono Ammonium Phosphate (MAP) Crystallisation*

**Johan Utomo**

A research collaboration between

**Curtin University of Technology**

and

**University of Hyogo**

**June 2008**

# *Backgrounds*

Mono and di- ammonium phosphate are important commodities in fertiliser and chemical industry. Mono ammonium phosphate (MAP) and di-ammonium phosphate (DAP) are known as fire retardant materials. As fertiliser, they are the most popular source of phosphorous and the most commercially produced in the world. The United States produced more than 10 million tonnes of DAP and 5.3 million tonnes of MAP in 2004. WMC Fertilizers in Australia produces about 1 million tonnes MAP and DAP annually. They are made by reaction between ammonia gas and impure phosphoric acid in a pre-neutraliser reactor at high temperature (110$^oC$) before sent to granulator. The equations for the neutralisation reaction between ammonia and phosphoric acid are as follows:

$$NH_3 + H_3PO_4 \rightarrow NH_4H_2PO_4 \text{ (MAP)}$$

$$NH_3 + NH_4H_2PO_4 \rightarrow (NH_4)_2HPO_4 \text{ (DAP)}$$

$$NH_3 + (NH_4)_2HPO_4 \rightarrow (NH_4)_3PO_4 \text{ (TAP)}$$

MAP is produced when molar ratio of nitrogen to phosphorous (N/P) is 1.0 and DAP when is 2.0.

In industry, this process leads to some challenges and causes process inefficiencies due to high recycle ratio in granulation process, the fluidity of the slurry and uncontrolled product size distribution which further trigger a domino effect lowers the downstream units' efficiency and produces off specification product.

Although these commodity are commercially produced and matured in research some challenges in the crystallisation kinetics, solubility are still remain and yet not been addressed. The need of MAP crystallization models in order to predict, design and optimise the process is critical. Therefore recently, some works in MAP reactive crystallization using phosphoric acid, and using MAP saturated have been studied. After that, seeded MAP reactive crystallization also has been investigated by analysing several variables. To make it content, both non-seeded and seeded batch cooling crystallization have been carried. Some crystallization kinetics have successfully deduced from these experiments. Due to time limitation and scope of the previous work, an extension for new research can be done in several areas such as seeded batch cooling crystallization in higher scale and wider operational range, anti-solvent crystallization and impurity/additive effect on crystal growth.

## *Research Opportunities*

1. **Seeded Batch Cooling Crystallisation**
   A higher scale up to 2-4 litre crystalliser volume can be used to validate previous work. The temperature and mixing in a wider operation range can be employed to study their effects on nucleation and crystal growth. The dynamic CSD measurement data can be gathered as capacity has been increased. Furthermore, MAP as solute can be changed with another solute such as DAP or KDP.
2. **Investigation of Anti-solvent Addition in Batch Cooling Crystallization**
   Additional solvents such as ethanol, 1-propanol, 2-propanol can be utilised to study different metastable zone generated. Variation of solvent amount per water as intial solvent may cause different effect on growth kinetics. Nucleation kinetics can be studied by performing non-seeded while seeded crystallization may study the growth kinetics.
3. **Investigation of Impurity Effect in Seeded Batch Cooling Crystallisation**
   Some impurities which are found in industrial application such as Al(III), Ca(II), Fe(III) and Mg(III) may alter the kinetics and crystal habit. Seeded batch operation mode should be employed to investigate the effects of individual and collective impurity at a very low concentration. Furthermore, higher concentration of impurities which are commonly found in plant phosphoric acid should be studied by using artificial high impurity phosphoric acid. Finally, EDTA and borates as chilating agent are also applied as additive and its effects on crystal growth will be observed.

## *Research Objectives*

1. First experiment tries to study the effect of a wider range of temperature and mixing intensity in a higher scale to validate the previous work.
2. Second experiment challenges us to obtain new insights of the metastable zone by adding an anti-solvent / additive in order to change the system solubility.
3. Third experiment tries to clarify the effect of impurities both in lower concentration and in typical concentration of plant phosphoric acid to the crystal growth, kinetics and crystal habit as well.

## *Significances*

1. More insight can be compiled in order to comprehend the crystallization of mono and/or di-ammonium phosphate.
2. A clear and practical solubility and metastable zone information can be obtained.
3. Reliable crystallization kinetics deduced are important for modelling, designing and controlling purposes.
4. Economical impact follows the improvement of process efficiency, product quality and operational stability.

## *Experiment*

| Exp | Controlled | Independent | Dependent |
|---|---|---|---|
| 1a | Seed | 20/ 30/ 40/ 50 degC | Cond, CSD, time |
| 1b | Seed | 200/300/400/500/600 RPM | Cond, CSD, time |
| 1c | T and RPM | 30% Csc/ 50%/ 100%/ 200% Csc | Cond, CSD, time |
| 2a | Seed; T and RPM | Alcohols: EtOH, 1-PrOH, 2-PrOH<br>Conc: 5%/10%/15% (g/g water) | Cond, CSD, time |
| 2b | NS; T, C and RPM | Alcohols: EtOH, 1-PrOH, 2-PrOH | Cond, CSD, time |
| 3a | Seed, T, RPM | Al (III), Fe (III), Mg (II), and Ca (II) | Cond, CSD, time |
| 3b | NS, T, RPM | PA set 1, set 2, set 3 and Set 4 | pH, time, CSD |
| 3c | Seed, T, RPM | EDTA, borates | Cond, CSD, time |

## *Timeline*

Total estimated time for planned experiments is **5-7 months**. The first experiment is expected to be finish within two month as the experimental setup is ready to use. The second and the third are expected to be carried within 1-2 months for each and one additional month is prepared as contingency time. These experiments are independent therefore can be conducted separately.

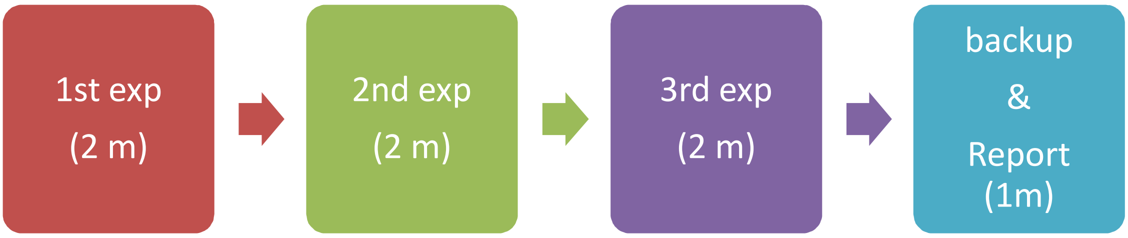

## *Materials and Equipments*

- MAP crystal (98.5 wt%-solid)
- DAP crystal (98.5 wt%-solid)
- Phosphoric acid solution, 40 wt%
- Ammonia solution, 28 wt%
- Ethanol, 99.5 vol%
- Acetone, 99 vol%
- NaOH standard solution 1 M
- HCl standard solution 1 M
- 1-propanol solution
- 2-propanol solution
- 300-ml jacketed vessel
- 500-ml jacketed vessel
- Multi-channel closure (glass and flexi-glass)
- Thermocouple
- Water bath and T controller
- pH meter and pH tube pump (T adjustment probe)
- Conductivity probe and meter
- Data logger
- Turbine impeller
- Stirring motor
- 2 additional tube pumps
- Filter and vacuum pump

# *Final remarks*

- An extension of previous work in regards to a wider operational range, anti-solvent/addition and impurities effect is important and feasible to be conducted within 7 months period.
- A study in seeded batch cooling crystallisation in a higher scale may add a vital value for model validation and kinetics determination.
- Anti-solvent crystallisation experiment is valuable in order get additional information on metastable zone.
- Impurity (as common in industry) effects may significantly contribute to the crystallisation mechanisms, particularly crystal growth and habit.